The European Academy of Wind Energy

Durham University

Book of Abstracts

5th PhD SEMINAR ON WIND ENERGY IN EUROPE

Durham University, UK

30th September and 1st October

Organized by Durham University for

European Academy of Wind Energy (EAWE)

EPSRC Pioneering research and skills

one NorthEast
The Development Agency for the North East of England

narec


The European Academy of Wind Energy


Durham
University

The European Academy of Wind Energy

Durham University

Book of Abstracts

5th PhD SEMINAR ON WIND ENERGY IN EUROPE

Durham University, UK

30th September and 1st October

Organized by Durham University for

European Academy of Wind Energy (EAWE)

Durham 2009


The European Academy of Wind Energy


Durham
University

The European Academy of Wind Energy

EAWE Steering Committee

President:
Prof. Dr. Ir. G. A. M. van Kuik
University of Delft, The Netherlands

Vice President:
Mr. Felix Avia Aranda
CENER, Spain

Secretary:
Maren Wagner

Local organising Committee

Chair:
Prof. Peter J. Tavner
Durham University, UK

Editors:
Mr. Simon Blake
Durham University, UK

Mr. Payam Jamshidi
University of Manchester, UK

1st Edition, Durham, Durham University, 2009

Printed: 100 Copies
Press date: September 2009


The European Academy of Wind Energy


Durham
University

TABLE OF CONTENTS

SESSION 1

Mitigation of Aerodynamic and Hydrodynamic Induced Loads of Offshore Wind Turbines……3
Tim Fischer; *University of Stuttgart*

Floating Offshore Wind Turbines – 3D hydrodynamics coupled to an advanced aero-elastic code……6
G. K. V. Ramachandran, J. N. Sorensen, J. J. Jensen, H. Bredmose; *Technical University of Denmark*

Quasi-3D aerodynamic code for analyzing dynamic flap and sensor response……...10
Néstor Ramos Garcia; *Technical University of Denmark*

Quasi-simultaneous interaction for prediction of aerodynamic flow over wind turbine blades……14
H. A. Bijleveld, A.E.P. Veldman; *University of Groningen*

Analysis and Design of Wing Tips……..18
Jacob Borbye, Jens Nørkær Sørensen, Morten Brons; *Technical University of Denmark*

A Dynamical Approach to Wind Power Generation……22
Patrick Milan, Matthias Wächter, Joachim Peinke; *University of Oldenburg*

SESSION 2A

Wind power prediction errors of a shortest-term forecast of the total German wind power generation……..29
J. Dobschinski, A. Wessel, B. Lange ; *ISET, Kassel*

Development and characterisation of the sphere anemometer……33
H. Heißelmann, M. Hölling, J. Peinke; *University of Oldenburg and ForWind*

Characterization of high-frequency atmospheric turbulence……37
A. Morales, M. Wachter, J. Peinke; *University of Oldenburg and ForWind*

Stochastic data analysis for in situ damage analysis……41
Philip Rinn, Joachim Peinke; *University of Oldenburg and ForWind*

SESSION 2B

Fatigue Strength of Welded Components of Support Structures of Wind Energy Converters in the VHCF Regime……47
P. Schaumann, S. Steppler; *Liebniz Universitaet Hannover and ForWind*

Influence of Manufacturing Aspects on Fatigue Assessment……...51
P. Schaumann, M. Mickley; *Liebniz Universitaet Hannover and ForWind*

Reliability Assessment and Reliability-Based Inspection and Maintenance of Offshore Wind Turbines……...56
Jose G. Rangel-Ramirez, John D. Sørensen; *Aalborg University*

Risk-based operation and maintenance of offshore wind turbines……...61
Jannie Jessen Nielsen, John Dalsgaard Sørensen; *Aalborg University*

SESSION 3

Condition Monitoring of Wind Turbines……67
Christopher J. Crabtree, Peter J. Tavner; *Durham University*

Systems Engineering based Tero-technology: A methodology and applications within wind power system……..71
Idris El-Thalji; *Vaxjo University*

Analysis of wind turbine data with a view towards load monitoring……...72
Claudia Hofemann, Herman Frederik Veltkamp, Gerard van Bussel; *Technical University, Delft*

Wake Skew Angle Variation with Rotor Thrust for Wind Turbines in Yaw Based on the MEXICO Experiment……75
Daniel Micallef, Carlos S. Ferreira, Tonio Sant; *Technical University, Delft*

Details of a Medium Scale Wind Turbine Based on the Brushless Doubly-Fed Machine……79
Thomas Logan, Joseph Warrington, Shiyi Shao, Richard McMahon; *Cambridge University*

Modeling and Simulation of Long Time Behaviour of Alpha Ventus Wind Farm and Coupling to WCMS……..84
Hui Guo, Z. A. Styczynski; *Otto von Guericke University of Magdeburg*

SESSION 4A

What Does a Floating Offshore Wind Turbine Look Like?.....90
Karl Merz; *Technical University of Norway*

Ensuring maximum energy capture by wind turbines during below rated operation……..97
A. Chatzopoulos, W. E. Leithead; *University of Strathclyde*

Power Limitation at high wind speeds for a variable speed stall-regulated fixed pitch wind turbine……101
N. Rosmin, S. J. Watson, M. Thomson; *Loughborough University*

Active Flow Control for Noise Reduction and Performance Improvement of Future Generation Wind Turbines……105
Thorsten Lutz, Alexander Wolf; *Stuttgart University*

Extreme Response for Wind Turbines……....110
Henrik Stensgaard Toft, John Dalsgaard Sørensen; *Aalborg University*

SESSION 4B

A Study of Aerofoil Geometries on Post-stall Performance at Low Reynolds Number……..116
Supakit Worasinchai, Grant Ingram, Rob Dominy; *Durham University*

Optimisation design of wind turbine blades based on CHC algorithm……120
Long Wang, Tongguang Wang; *Nanjing University*

Dynamic Lift Measurement under Turbulent Conditions……..125
Jörge Schneemann, Pascal Knebel, Michael Hölling, Joachim Peinke; *University of Oldenburg and ForWind*

A CFD Investigation of the Near-Blade Local Flow Angle……130
Sugoi Gomez-Iradi, George N. Barakos, Xavier Munduate; *University of Liverpool*

SESSION 5

Modal Analysis and Optimization of a Tubular Tower……142
Ruitao Peng, Xiongwei Liu; *University of Central Lancashire*

A Novel Floating Offshore Wind Turbine Concept……...146
Luca Vita; *Technical University of Denmark*

Development of Design Methods and Requirements of Offshore Wind Turbines with Complex Support Structures……..……..150
Daniel Kaufer; *University of Stuttgart*

Advanced Aerodynamic and Aero-Elastic Analysis of Wind Turbines with coupled MBS/CFD……153
Denis Matha; *University of Stuttgart*

Urban Wind Energy……155
Christina Beller; *Technical University of Denmark*

Computational Fluid Dynamics (CFD) Modelling of Wind Flow in and Around Forest Canopies……..159
Scott Wylie, Simon Watson; *Loughborough University*

SESSION 6A

Compensating gear plays in the pitch actuation system of a wind turbine...165
Jungchul Choi; *ISET, Kassel*

Primary and Secondary Frequency Control with Wind Farms……169
Alejandro J. Gesino; *ISET, Kassel*

Hybrid HVDC Transmission Systems for Offshore Wind Farms……...173
Raymundo E. Torres, Tore Underland, Marta Molinas;
Norwegian University of Science and Technology

Numerical study of the performance of rooftop size VAWTs……177
S. Wang, L. Ma, D. B. Ingham, M. Pourkashanian, Z. Tao
University of Leeds and Beijing University

SESSION 6B

Direct Numerical Simulations of a Heaving Aerofoil Using Spectral/HP Elements Method……183
W.Medjroubi, B.Stoevesandt, J.Peinke;
University of Oldenburg and ForWind

Structural Design of Large Future Wind Turbine Blades under Combined Loading……188
Zuzana Andrlová, Kim Branner; *Technical University of Denmark, Riso*

A Case Study of a 10kW Horizontal Axis Wind Turbine Blade Design……..192
Xinzi Tang, Xiongwei Liu; *University of Central Lancashire*

Wind turbine blade vibration at standstill conditions……197
Witold Skrzypinski, Mac Gaunaa; *Technical University of Denmark, Riso*

SESSION 7

Nonlinear Model Predictive Control of Wind Turbines……..203
L. C. Henriksen, A. N. K. Poulsen; *Technical University of Denmark*

Data-driven control for wind turbines with smart rotors……206
Gijs van der Veen, Jan-Willem van Wingerden, Michael Verhaegen; *Delft University of Technology*

Optimisation of Wind Turbine Rotor Using Cost of Energy as a Parameter and the effects of the Weibull Distribution……..……209
T. S. Yeow, A. Cuerva, J. Alvarez, A.Munuera; *Universidad Politecnica de Madrid*

Wind farm – fuel cell hybrid energy system for reducing power fluctuations in wind farms……..……216
J. E. Villena-Lapaz, A. Vigueras-Roderiguez, E. Gómez-Lázaro, J. A. Fuentes-Moreno, A. Molina-Garcia; *Albacete Science and Technology Park*

Energy Preservation in the Numerical Calculation of Wind Turbine Wakes.223
B. Sanderse; *Energy Research Centre of the Netherlands*

SESSION 1

Wednesday, 30.09.2009

10:00AM

Mitigation of Aerodynamic and Hydrodynamic Induced Loads of Offshore Wind Turbines

Tim Fischer

Endowed Chair of Wind Energy (SWE) at the Institute of Aircraft Design, Universität Stuttgart

Allmandring 5b, 70569 Stuttgart, Germany, tim.fischer@ifb.uni-stuttgart.de

ABSTRACT

The support structure is a major cost item for large and/or deep-water offshore wind turbines. Optimisation through integrated design of the rotor-nacelle-assembly and the support structure is a powerful means of reducing the cost.

Within an integrated approach, the characteristics and the control of the turbine are used to simultaneously reduce aerodynamic and hydrodynamic loads especially with respect to fatigue. Furthermore turbine control might be used for compensation of variations in the site conditions within the wind farm cluster, resulting in a different fundamental eigenfrequency of the structure.

KEYWORDS

Offshore, Loads, Mitigation, Control, Damping, Support Structure, Integrated Design

1 INTRODUCTION

Since support structures are one of the main cost drivers offshore and since offshore other rules apply with regards to design and site conditions, different methodologies have to be developed to mitigate the loads on the support structure and therefore to reduce the associated component costs. Until now, only a few offshore-specific turbine types are available on the market and most of them do not include control algorithms for support structure load mitigation adapted to offshore conditions. This enables high potential of structural optimisation by means of offshore-specific controls in the integrated design process of support structures.

2 PROJECT DESCRIPTION

Reduction of the external wind and wave loads and of the associated dynamic response is, beside optimised manufacturing and installation logistics, an obvious way to achieve more

cost-effective design. In the work presented here this is aimed for by integrating the design of the rotor-nacelle-assembly (RNA) and support structure in the design process. Hence, the RNA is considered as an active element in mitigating the loads on the support structure. For support structure load mitigation, different concepts are studied and are distinguished at three different levels as seen in Figure 1 for some already studied examples. The goal is to identify a suitable selection of options to finally obtain an optimised offshore wind turbine design.

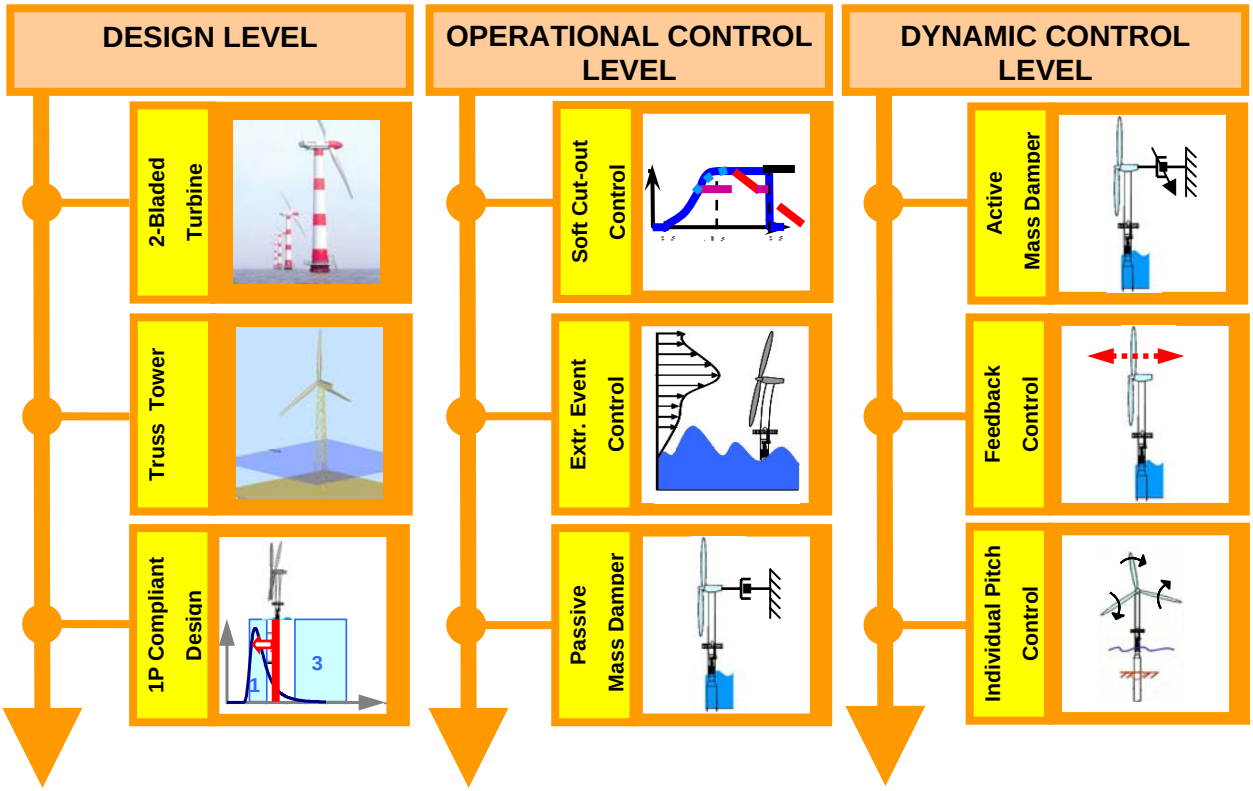

Figure 1: Levels and possible implementations of load mitigation

Since offshore different design needs are present, one might think about offshore-specific design solutions (see design level in Figure 1). These can range from large turbines with a 2-bladed downwind rotor or light truss tower solutions. As noise restrictions are not as limited as for onshore locations, a higher tip-speed ratio and turbines with higher specific rating are possible. Furthermore, especially for variable site conditions, it might be a promising idea to consider turbines with adjustable operational characteristics able to compensate critical site variations like changing eigenfrequency ranges. If the turbine characteristics can be adapted with the aid of, for example, shifting the rated rotational speed, the frequency limitation like the 1P can be reduced or even eliminated.

On the operational control level, the need for extreme event control is very important, as these loads are very often design drivers, at least for monopile-like structures in deep water.

However, other strategies for optimised turbine operations and related lower support structure loads may be worth discussing, such as extending the cut-out wind speed limit, applying a peak shaver or a passive tower mass damper device.

Finally, on the third level there is a significant potential in using advanced and adapted dynamic control concepts, such as active/hybrid tower mass damper, torque control or pitch control. The latter can either be implemented as active collective pitch control where the rotor acts as an active damper element as a so-called tower feedback controller. Or it can be used as individual pitch control to counteract sidewise vibrations, for example coming from wind-wave-misalignment.

3 PRESENT RESULTS AND OUTLOOK

Some of the above mentioned load mitigation concepts have already been studied and the results were published. For first results and an outlook on upcoming work, please see the bibliography below.

Acknowledgements

The presented work was funded by the Commission of the European Communities, Research Directorate-General within the scope of the Integrated Project "UpWind – Integrated Wind Turbine Design" (Project No. 019945 (SES6)).

UpWind

BIBLIOGRAPHY

[1] Fischer, T., Rainey, P., Bossanyi, E. and Kühn, M.: Optimisation Potential for Monopile Support Structures using Offshore-Specific Wind Turbine Controls, EOW, Stockholm, 2009

[2] Long, H., Fischer, T. and Moe, G.: Design Methodology and Optimisation of Lattice Structures for Offshore Wind Turbines in 35m Water, EWEC, Marseille, 2009

[3] Fischer, T. and Kühn, M.: Site Sensitive Support Structure and Machine Design for Offshore Wind Farms, EWEC, Marseille, 2009

[4] Fischer, T., Tono, A., Andersen, U. and Kühn, M.: Integrated Design of Offshore Wind Turbines for Compensation of Site Variability, DEWEK, Bremen, 2008

[5] Fischer, T., Kühn, M. and Passon, P.: Load mitigation of aerodynamically and hydrodynamically induced loads of offshore wind turbines, EWEC, Milan, 2007

[6] Fischer, T., Passon, P. and Kühn, M.: Control requirements of load mitigation of aerodynamic and hydrodynamic loads of offshore wind turbines, DEWEK, Bremen, 2006

Floating Offshore Wind Turbines – 3D hydrodynamics coupled to an advanced aero-elastic code

G. K. V. Ramachandran, J. N. Sørensen, J. J. Jensen and H. Bredmose

Fluid Mechanics Section, Dept. of Mechanical Engng., Technical University of Denmark

ABSTRACT

This paper discusses options for floating offshore wind turbines. Based on a literature review and for different selected environmental conditions, we concentrate on a Tension Leg Platform configuration. The paper describes the development of a mathematical model which takes the 3D hydrodynamic loads into account of and couples them to an advanced aero-elastic code. The goal of the overall study is to compute loads and responses on the wind turbine and its platform.

KEYWORDS

Floating offshore wind turbine; 3D hydrodynamics; aero-elasticity

1 INTRODUCTION

Wind energy is one of the solutions to the energy crisis faced by the world. Technology of conventional wind turbines attained the maturity in the last decade and the unit size of onshore wind turbine seems to have reached its saturation level. Scarcity in available land to tap wind potential has lead to the need of exploring the potential availability of offshore locations. Present technologies, which are bottom fixed concepts, are only suitable for shallow depths and cannot be used for deep water. However, the majority of the offshore potential is available in deep waters. This lead the way to think different options for tapping deep water wind potential. Recent studies have already suggested a range of configurations suitable for deep water floating wind turbines. In this paper, we consider one of these configurations, viz. the Tension Leg Platform (TLP). The first steps in the formulation of a mathematical model for the structural dynamics with 3D hydrodynamic loads are discussed.

2 CONFIGURATIONS

2.1 Classification

Different types of configurations have been suggested by many researchers. Based on static stability, the configurations are classified as ballast, mooring lines and buoyancy types [1]. Each type has its own advantages and disadvantages.

2.2 Location, wave climate and wind climate

For the present study, the North Sea in the coastal part of Norway has been chosen. The selected location is shown in Figure 1. Water depth in this location is of magnitude 200 m.

Representative parameters for the wave climate are shown in Table 1. These are based on the data in Figure 2 for the annual wave climate of the North Sea [2].

Annual average wind speed at 100 m height for the proposed location is about 8 to 10 m/s. Predominant wind direction is West and South – West [2].

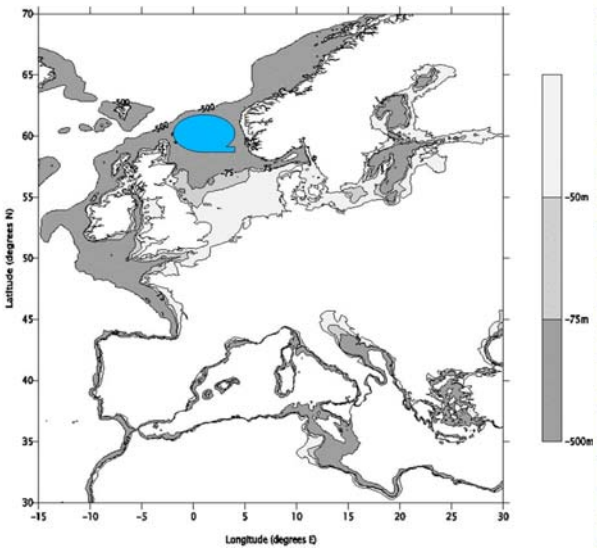

Figure 1: Proposed location showing water depth variation

Percentage of occurrence of wave height (m) in rows versus mean wave period (s) in columns

	lower	03	04	05	06	07	08	09	10	11	12	13	14	15	16	
lower	upper	04	05	06	07	08	09	10	11	12	13	14	15	16	17	total
00	01	0	0.1	0.2	0.3	0.1	0.0	0.0	0	0	0	0	0	0	0	0.7
01	02	0	0.1	2.5	8.3	4.9	1.0	0.1	0.0	0.0	0.0	0	0	0	0	17.0
02	03	0	0	0.3	6.5	12.3	5.8	1.1	0.2	0.0	0.0	0	0	0	0	26.3
03	04	0	0	0	0.5	6.6	9.9	3.6	0.5	0.1	0.0	0.0	0	0	0	21.5
04	05	0	0	0	0.0	0.7	5.9	6.4	1.7	0.2	0.0	0.0	0	0	0	15.0
05	06	0	0	0	0	0.0	0.9	4.8	2.7	0.5	0.0	0.0	0	0	0	8.9
06	07	0	0	0	0	0	0.1	1.4	2.8	0.8	0.2	0.0	0.0	0	0	5.3
07	08	0	0	0	0	0	0.0	0.1	1.3	1.2	0.2	0.0	0.0	0	0	2.8
08	09	0	0	0	0	0	0	0.0	0.2	0.9	0.2	0.0	0.0	0	0	1.3
09	10	0	0	0	0	0	0	0	0.0	0.3	0.3	0.0	0.0	0	0	0.6
10	11	0	0	0	0	0	0	0	0.0	0.1	0.2	0.1	0.0	0	0	0.4
11	12	0	0	0	0	0	0	0	0	0.0	0.1	0.1	0.0	0	0	0.1
12	13	0	0	0	0	0	0	0	0	0	0.0	0.1	0.0	0	0	0.1
13	14	0	0	0	0	0	0	0	0	0	0	0.0	0.0	0	0	0.0
14	15	0	0	0	0	0	0	0	0	0	0	0.0	0.0	0	0	0.0
15	16	0	0	0	0	0	0	0	0	0	0	0	0.0	0.0	0	0.0
16	17	0	0	0	0	0	0	0	0	0	0	0	0	0	0	0.0
total		0.0	0.1	3.0	15.6	24.9	23.6	17.7	9.5	4.0	1.2	0.3	0.1	0.0	0.0	100.0

Figure 2: North Sea – Annual Wave Climate

Table 1: North Sea Wave Climate

Parameter	Value
Significant wave height	7 m
Peak period	10 s
Water depth	200 m

2.3 Present configuration

Based on the literature, it has been observed that the platform motion will induce higher loading to the blade root and to the tower. This leads to higher fatigue damage. An optimum configuration should have smallest possible wave loading to minimise response motions induced on the turbine because of the platform movement. Based on knowledge from earlier studies, a Tension Leg Platform (TLP) has been chosen. This is one of the most stable platforms which have a relatively small impact on the turbine dynamics [1]. The configuration is shown in Figure 3.

2.4 Simplified model for initial studies

Noting the characteristics of TLP as soft in surge and sway motions, extremely stiff in rotational modes, ie., pitch and roll and limited heave and pitch motions, the system is initially

modelled in terms of a three mass model, where the rotor, nacelle, tower and floater are connected through corresponding springs and dampers. The simplified model is shown in Figure 4.

The sway and yaw motions are excited by cross coupling mechanisms of the wind turbine. The natural frequencies are either in a very low frequency region or in a high frequency region [3]. In these regions, there is little energy in the ocean spectra.

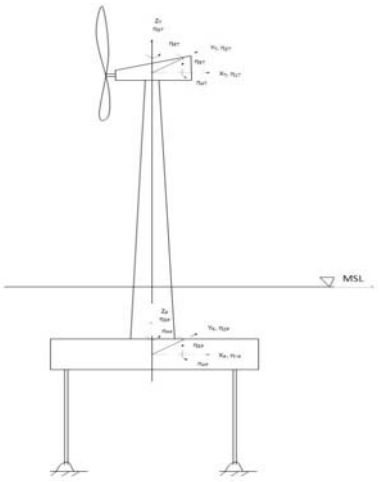

Figure 3: Proposed configuration (TLP)

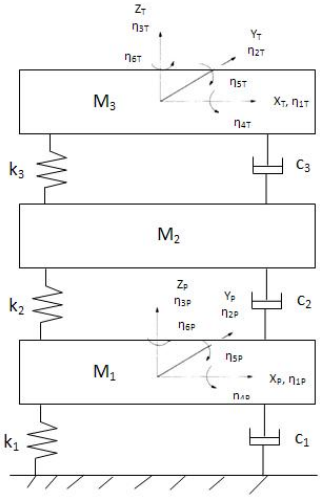

Figure 4: Simplified three mass system

For the initial computations, linear wave theory is assumed and the wave loads are calculated using Morison's equation, which is shown below:

$$F = C_M \rho A \dot{U} + C_D \frac{1}{2} \rho D |U| U \tag{1}$$

The displacement transformation from blade coordinate system to platform coordinate system is shown below [4]:

$$\mathbf{x} = \begin{Bmatrix} x \\ y \\ z \\ 1 \end{Bmatrix} = \begin{pmatrix} \cos\eta_{5P} & 0 & \sin\eta_{5P} & \eta_{1P} + R\sin\eta_{5P} \\ 0 & 1 & 0 & 0 \\ -\sin\eta_{5P} & 0 & \cos\eta_{5P} & \eta_{3P} + R\cos\eta_{5P} \\ 0 & 0 & 0 & 1 \end{pmatrix} \begin{Bmatrix} x_f \\ y_f \\ z_f \\ 1 \end{Bmatrix} = \mathbf{T}_\varphi \mathbf{x_f} \tag{2}$$

$$\mathbf{x}_f = \begin{Bmatrix} x_f \\ y_f \\ z_f \\ 1 \end{Bmatrix} = \begin{pmatrix} 1 & 0 & 0 & 0 \\ 0 & \cos\eta_{4T} & -\sin\eta_{4T} & 0 \\ 0 & \sin\eta_{4T} & \cos\eta_{4T} & 0 \\ 0 & 0 & 0 & 1 \end{pmatrix} \begin{Bmatrix} x_w \\ y_w \\ z_w \\ 1 \end{Bmatrix} = \mathbf{T}_\theta \mathbf{x}_w \tag{3}$$

$$\mathbf{x} = \mathbf{T}_\varphi \mathbf{T}_\theta \mathbf{x}_w \tag{4}$$

3 ANALYSIS APPROACH

The basis for the analysis is the wave load procedure taking into account the inertia and drag forces from the waves acting on the floater and the mooring system and eventually a full, well-proven, aerodynamic code for the wind-generated loads on the tower and blades. The two procedures will be coupled together in the time-domain and an effective stochastic procedure, the First Order Reliability Method (FORM), will be applied to derive extreme values and fatigue estimates for the total system. The feasibility of different configurations will thereby be evaluated. A sketch of the analysis procedure is shown in Figure 5.

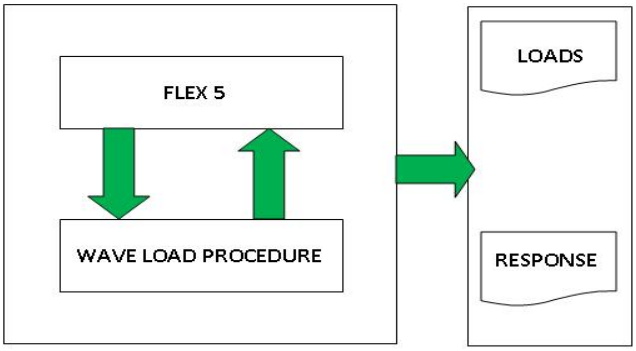

Figure 5: Schematic of analysis procedure

4 CONCLUSIONS

From the literature review and as per our analysis, a Tension Leg Platform configuration would be suitable for deep water environment. Considering this as basis, a mathematical model is under development which takes into account of the three dimensional wave field and couples with the aero-elastic code in order to estimate the loads and response on wind turbine and platform.

REFERENCES

[1] S. Butterfield, W. Musial, J. Jonkman and P. Sclavounos : Engineering Challenges for Floating Offshore Wind Turbines ; *2005 Copenhagen Offshore Wind Conference Copenhagen, Denmark, October 26–28, 2005.*

[2] http://www.waveclimate.com

[3] K. H. Lee, P. Sclavounos and E. Wayman: Floating Wind Turbines: 20th Workshop on Water Waves and Floating Bodies – Spitsbergen, Norway – May 29 to June 1, 2005.

[4] H. Suzuki and A. Sato: Load on Turbine Blade Induced by Motion of Floating Platform and Design Requirement for the Platform: Proceedings of the 26th International Conference on Offshore Mechanics and Arctic Engineering OMAE2007, June 10-15, 2007, San Diego, California, USA.

ACKNOWLEDGEMENT

The research is funded by Statkraft, Norway, through the Ocean Energy Research Programme. This support is greatly appreciated.

Quasi-3D aerodynamic code for analyzing dynamic flap and sensor response

Néstor Ramos García[1]

1) Department of Mechanical Engineering, Fluid Mechanics Section, DTU, Denmark

ABSTRACT

In the paper we present a 2D version of a quasi-3D aerodynamic code that is under development. The code is based on viscous-inviscid interaction using strong coupling between the two parts. The inviscid part is modeled using a panel method whereas the viscous part is represented by the boundary layer equations put into integral form and with extensions for 3-D rotational effects. The purpose of the code is to include a flapping trailing edge as well as rotational effects in the aerodynamic analysis. So far a 2D version of the code has been developed. The 2D code is validated against measurements of performance data for various NACA 63-xxx airfoils.

KEYWORDS

Moving flap, viscous-inviscid interaction, panel method, quasi 3-D integral boundary layer.

INTRODUCTION

In this project a fast and efficient quasi-3D aerodynamic code is being developed to analyze the local aerodynamic behaviour of an airfoil section of a wind turbine with a moving trailing edge flap and the associated sensor response. The inviscid calculations are carried on using an unsteady potential flow panel method. The viscous flow is calculated using a quasi 3-D integral boundary layer equations. Simulations will be carried out for flows around an airfoil with a moving trailing edge for both static and rotating blade. These calculations will provide guidelines for designing and evaluating the Adaptative Trailing Edge Flap (ATEF) system on a wind turbine. See figure 1.

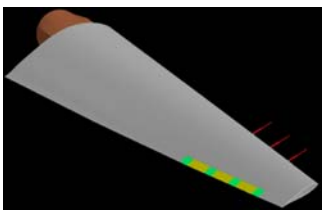

Figure1: Wing with trailing edge flaps and pitot tubes

1 VISCOUS & INVISCID FLOW SOLVERS

1.1 Inviscid Solver

The unsteady panel method solver has been implemented with a uniform source distribution and a parabolic vortex distribution placed in the panel elements [1,2]. The near wake is represented with uniformly vorticity distributed panel elements and the far wake is represented by point vortices.

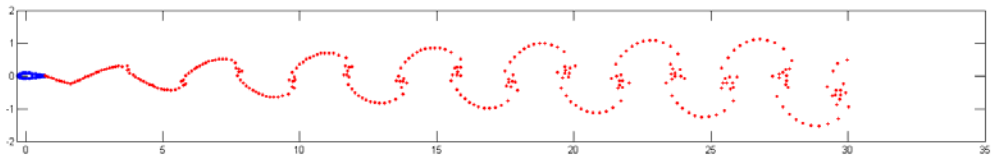

Figure 1. Downstream convection of point vortices from a sinusoidally pitching NACA0010

1.2 Viscous Solver

In order to solve the von Kármán integral relation for the laminar case Thwaites method has been implemented. An extension of Thwaites' method for 3D-flow is being tested at the moment. [3]

An integral boundary layer solver based on the standard boundary layer integral momentum and kinetic energy shape parameter equations has been implemented for the turbulent case. Following Drela's model [4], turbulent closure equations are implemented. These relations are derived using the skin-friction and velocity profile formulas of Swafford.

The laminar-turbulent transition prediction is obtained using a spatial-amplification theory based on the Orr-Sommerfeld equation, commonly known as the n^9 method [5]. Transition will occur when the most unstable Tollmien-Schlichting wave in the boundary layer has grown bigger than some factor.

1.3 Viscous-inviscid interaction

The viscous-inviscid interaction is based on the assumption of an equivalent inviscid flow, where the effects of a real flow can be added. In order to displace the dividing streamline outwards the required distance δ* from the surface, the mass flow injected normal to the wall in the equivalent inviscid flow is chosen to be equal to the streamwise rate of change of the mass flow deficit [6].

2 RESULTS

First we compare computations with similar computations employing the Xfoil code. In Figure 2a we observe how the inviscid computations are in perfect accordance with Xfoil inviscid computations. In Figure 2b, computations using viscous-inviscid interaction are shown, we observe that for a flow about to separate, 9 degrees of angle of attack, the agreement between both curves is perfect. As the flow separation area increases, a small reduction of the upper C_p curve is observed in our computations in comparison with Xfoil. (High angle of attack, α=18, Figure 2c). The Reynolds number for both viscous computations is 3e6.

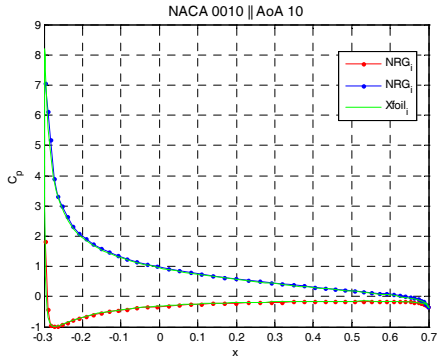

Figure 2a

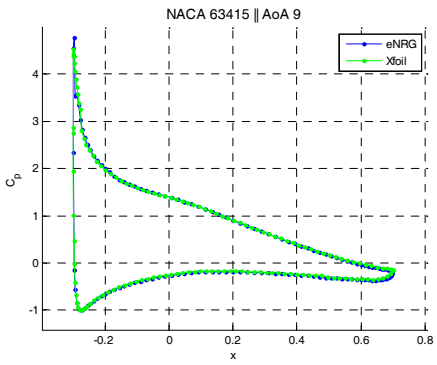

Figure 2b

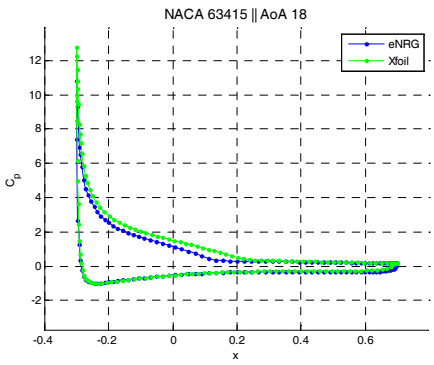

Figure 2c

In Figure 3 computed CL curves are shown for the NACA airfoils 63415 and 63418, a common series in the wind turbines blades industry. Good agreement is obtained for attached flow conditions. After the separation point is reached, the computed C_L curve stalls too early and continues to grow smoothly, while Xfoil and the 2D experimental data [7] stalls later and decreases gradually.

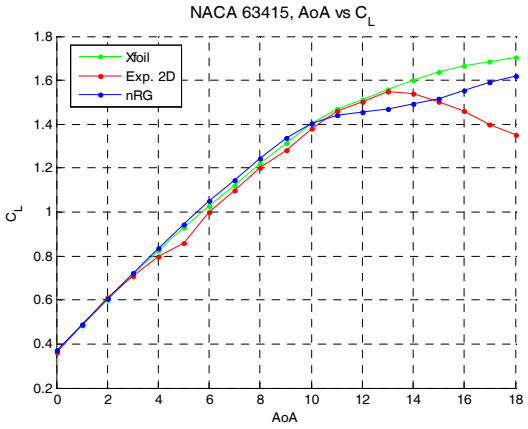

Figure 3a

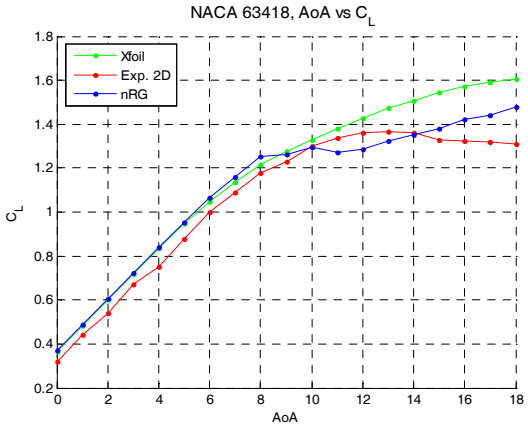

Figure 3b

3 CONCLUSIONS

A 2D version of a quasi-3D aerodynamic code has been presented. Future work will concentrate on the separation model and the derivation of a set of turbulent quasi three dimensional closure equations.

BIBLIOGRAPHY

[1] B.C. Basu and G.J. Hancock. The unsteady motion of a two-dimensional aerofoil. *J. Fluid Mech. (1978), vol. 87, part1, pp. 159-178.*

[2] *J. Nørkær Sørensen.* Three level, viscous-inviscid interaction technique for the prediction of separated flow past a rotating wing. PhD Thesis, Department of Fluid Mechanics, Technical University of Denmark.

[3] B. Thwaites. Approximate calculation of the laminar boundary layer. *The aeronautical Quarterly, Volume 1, Part II : 245-280.*

[4] M. Drela and M.B. Giles. Viscous-Inviscid Analysis of transonic and low Reynolds number airfoils. *AIAA Journal, Vol. 25, No.10, pp. 1347-1355.*

[5] C. Gleyzes, Jr. Cousteix, J.L. Bonnet. Theoretical and Experimental Study of Low Reynolds Number Transitional Separation Bubbles. *Conference on Low Reynolds number aerodynamics, 1985.*

[6] M.J. Lighthill. On displacement thicknes s. *J. Fluid Mech.*

[7] Franck Bertagnolio, Niels Sørensen, Jeppe Johansen and Peter Fuglsang. Wind Turbine Airfoil Catalogue. *Risø National Laboratory , Roskilde, Denmark, August 2001.*

Quasi-simultaneous interaction for prediction of aerodynamic flow over wind turbine blades

H.A. Bijleveld[1)], A.E.P. Veldman[2)]

[1)] Energy research Centre of the Netherlands; University of Groningen

[2)] University of Groningen

The Netherlands

ABSTRACT

A numerical simulation method for an accurate and fast prediction of the aerodynamic behaviour of wind turbine blades (RotorFlow) is currently under development. In this method, the total flow field around a blade is split into an inviscid external flow – to be solved with a potential flow solver – and a viscous boundary layer where integral boundary-layer equations are used. At the edge of the flow domains, both flows are coupled via an interaction formulation. The quasi-simultaneous interaction law will be used which has proven to be successful in 2D. A formulation for the 3D flow over rotating blades is now being developed.

KEYWORDS

Wind turbine blades, boundary layer, viscous-inviscid interaction, quasi-simultaneous coupling

1 INTRODUCTION

The current trend in wind turbine design is toward larger rotor blades. This brings challenges for the structural design as more and more material is involved and the blades become more flexible which is a challenge from a (aero)dynamic viewpoint. Safety factors – to compensate for uncertainties during design - should be as low as possible to avoid the use of unnecessary material. Besides, for optimisation purposes, design methods need to be fast.

Therefore, an accurate and fast prediction of the aerodynamic behaviour of a blade is needed. Current methods that are fast in the prediction use crude models like BEM (Blade Element Momentum). For an accurate prediction of the flow, full Navier-Stokes equations need to be solved which requires huge computational efforts.

2 ROTORFLOW

A method that is low in computational effort, but with a more detailed solution than the BEM methods is pursued in the project RotorFlow of ECN. In this method, the whole flow field is split into two flow domains: an inviscid external domain and a small viscous boundary layer

at the surface of the blade. An interaction between the domains ensures a continuous solution between the two domains.

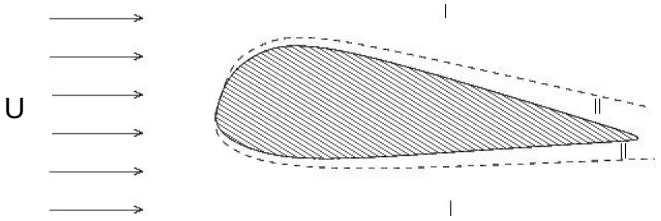

Figure 1: The flow domains. I: inviscid external flow; II: viscous boundary layer, dashed line: viscous-inviscid interaction, U: the undisturbed free-stream velocity (=wind).

Figure 1 shows the flow domain over an airfoil. The dashed line indicates the edge between the two domains. This is where a viscous-inviscid interaction is present. Region I is the inviscid external flow that can be calculated with a potential flow panel method. Region II is the viscous boundary layer where the quantities of the boundary layer are obtained with an integral boundary-layer calculation. The flow variables that are of interest at the edge of the two domains are the velocity vector ($\mathbf{u_e} = (u_e,v_e,w_e)^T$) and the boundary-layer displacement thickness: δ^* (see Figure 2).

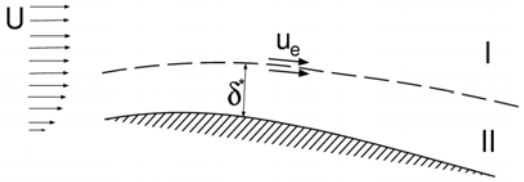

Figure 2: Variables u_e and δ^* in the flow domains.

3 VISCOUS-INVISCID INTERACTION

The viscous-inviscid interaction (VII) can be performed in several ways. Four main methods can be distinguished. Figure 3 shows them graphically and they are discussed in detail in the following section.

3.1 Main groups of interaction methods

In the direct method (see Figure 3a), the external flow prescribes the velocity on the boundary layer. The boundary layer gives the displacement thickness to the external flow. The method is unable to handle separated flows.

In the inverse method (Figure 3b), the boundary layer imposes the velocity onto the external flow. It can handle separated flows, but converges slow.

Simultaneously solving the external and boundary-layer flow converges faster, but is complex in software terms and lacks flexibility in flow modelling.

The complicated software of the simultaneous method is avoided by solving the boundary layer together with an approximated external flow and subsequently calculating the complete

external flow. The approximation is given by an interaction law. This idea was introduced by Veldman [1] and is drawn in Figure 3d. It turns out to be a powerful method that is comparable to the direct method but able to calculate separated flows.

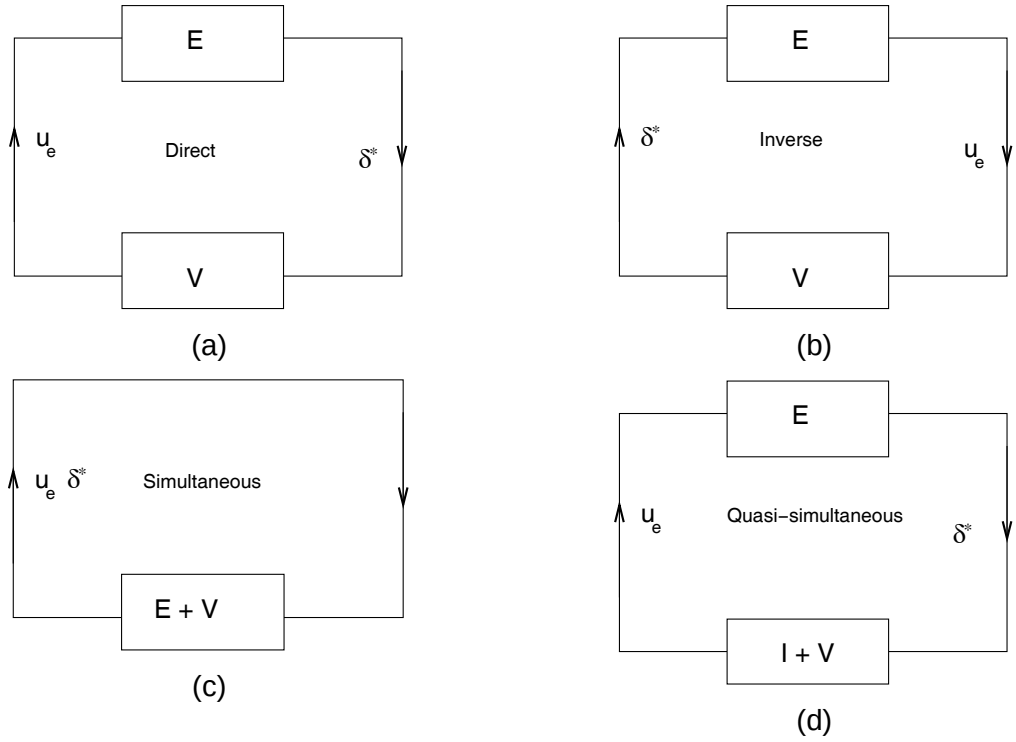

Figure 3: Schematic of four main interaction methods: E = external flow equations, V = boundary-layer equations, I = interaction law:

$$\begin{cases} u_e = E[\delta^*] \\ u_e = V[\delta^*] \end{cases}$$

a) direct method b) inverse method c) simultaneous method d) quasi-simultaneous method.

3.2 Quasi-simultaneous interaction method

The main challenge of the quasi-simultaneous interaction method is the formulation of the interaction law. Thin-airfoil theory gives a useful approximation of the external flow and is therefore used as basis for the interaction law.

The complete flow field is computed by iteratively solving the external flow and the boundary layer with the interaction law, see Figure 3d. Mathematically, this can be written as:

$$(I - E)\delta^{*(n)} = (I - V)\delta^{*(n-1)}. \quad (1)$$

In this formula, *I* is the interaction law; *V* are the viscous boundary-layer equations, *E* represents the external flow equations and *n* the iteration number. If convergence is achieved, then:

$$(E - V)\delta^* = 0, \quad (2)$$

which shows that the formulation of the interaction law is not influencing the final solution.

In 2D applications, the interaction law with only non-zero terms on the diagonal of *I* turns out to be the most robust [2]. Figure 4 shows a lift polar for the NACA0012 airfoil. It shows that

the calculations performed with the viscous method following the quasi-simultaneous approach agree very well with the experimental data even in the region around maximum lift. The calculations turn out to be robust and take only seconds on an average PC. Due to the good results in the stall region, a wide variety of wind scenarios on wind turbine blades should be possible to be analysed with ROTORFLOW.

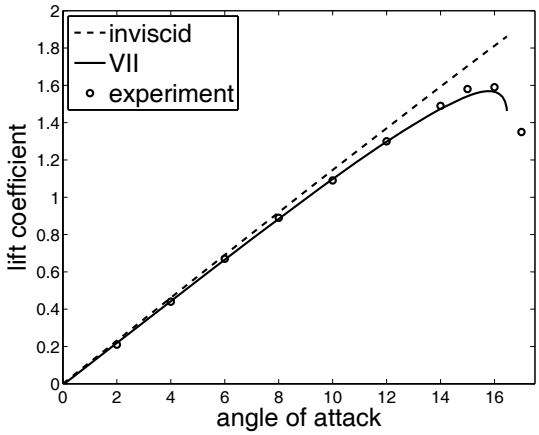

Figure 4: Lift polar for NACA0012 airfoil: viscous-inviscid (VII) calculation versus experiment [3].

Applications of a three-dimensional interaction law for quasi-simultaneous interaction methods hardly exist. This PhD project focuses on the formulation and derivation of a 3D interaction law to be used for the simulation of unsteady aerodynamic flow over wind turbine blades.

4 CONCLUSION

For a fast and accurate aerodynamic design code, where the flow field is split into a viscous and inviscid part, a three-dimensional quasi-simultaneous interaction method will be developed for use in applications for wind turbine blades. Results in 2D applications suggest this to be an accurate and robust interaction method.

BIBLIOGRAPHY

[1] Veldman, A.E.P.: New, quasi-simultaneous method to calculate interacting boundary layers, AIAA J. 19:79-85, 1981

[2] Coenen, E.G.M.: Viscous-Inviscid Interaction with the Quasi-Simultaneous Method for 2D and 3D Aerodynamic Flow, PhD thesis, Rijksuniversiteit Groningen, the Netherlands, 2001

[3] Veldman, A.E.P.: Quasi-Simultaneous Viscous-Inviscid Interaction for Transonic Airfoil Flow, AIAA-2005-4801, 4th AIAA Theoretical Fluid Mechanics Meeting Toronto, June 6-9, 2005

Analysis and Design of Wing Tips

Jakob Borbye[1)], Jens Nørkær Sørensen[1),] Morten Brøns[2)]

1) Department of Mechanical Engineering

2) Department of Mathematics

Technical University of Denmark, DK-2800 Lyngby, Denmark

ABSTRACT

An approach for design of blade tips of rotors of horizontal axis wind turbines (HAWT) is presented. A lifting line, free wake method is employed as preliminary optimization tool. This is subsequently combined with Reynolds averaged Navier-Stokes (RANS) computations, and an approach to evaluation of the RANS results based on critical point theory is suggested. The method is currently being implemented, and no computation result are presently available.

KEYWORDS

Wing tip, winglet, topology, design, optimization

1 INTRODUCTION

The main instrument in maximizing the power output of a HAWT is to increase the rotor diameter, but in some cases this approach is restricted due to e.g. siting constraints, limitations in tip speed ratio or transportation issues. In order to maximize power production it is in all cases of importance to maximize the wind turbine power coefficient, $C_{p.}$

The design of the blade tips is important due to the high power contribution from the outer sections of the blade and the large amount of trailing vorticity in the tip region (the tip vortex), which dominates the near wake and the generation of aerodynamic noise. The flow in the tip region is complex and highly three-dimensional, thus rendering standard HAWT design tools like the blade element momentum (BEM) method unable to satisfactory predict the loads[1].

In aeronautics various wing tip devices, most notably winglets, have been extensively studied and applied in practice for non-rotating wings. The underlying idea for these devices is to minimize the total drag on the blade[2], through reduction of the induced drag originating from the finite wing aspect ratio as described in lifting line theory by Prandtl[3] and Munk[4]. It was however first after the work of Whitcomb[5], that winglets were adopted in practice. Kroo[6] has given a thorough review of the design ideas to reduce induced drag.

The same ideas can with only minor modifications be applied to HAWT rotors. As pointed out by Gaunaa and Johansen[7,] an analogy exist between a non-rotating wing with finite aspect

ratio and a rotor with a finite number of blades. The limiting cases for the efficiencies are the infinite aspect ratio case and the infinite number of blades case, which are described by 2D lifting line and actuator disk theory. Thus any beneficial effects of tip modifications will be due to a reduction of tip loss effects. It is important to consider the viscous effects, to quantify the degree to which reduction of induced drag is offset by the increase in parasitic drag due to the changed tip geometry. For HAWT blades tip devices like MIE tip vanes[8] and various winglet configurations [7,9,10] have been investigated numerically, results all reporting performance increases, but also pointing out the need for better validation of the results, and analysis of the structural implications of HAWT tip devices.

2 DESIGN OF WING TIPS

Optimization of a wing tip geometry is difficult for several reasons. The design space is very large and complex, and the objective function will likely contain multiple local minima.

In the design phase a the free wake lifting line method (LLFW) by Gaunaa and Johansen[7] will be used. Each rotor blade is represented by a line vortex, with the lift force on a blade element given by the Kutta-Joukowski law:

$$\boldsymbol{L} = \Delta s \ \rho \ \boldsymbol{V}_{rel} \times \boldsymbol{\Gamma} \tag{1}$$

where $\boldsymbol{L}$ is the lift force on a vortex segment of length Δs and a bound circulation $\boldsymbol{\Gamma}$, subject to a relative velocity of $\boldsymbol{V}_{\text{rel}}$. At each section of the blade vorticity trails into the wake, such that $\Gamma_{trail} = d\Gamma_{bound} / ds$ according to the Helmholtz vortex laws[11]. This is the simplest possible rotor model which takes tip effects into account, and it has the advantage of excluding details concerning airfoil shape, which makes it suitable for optimization. The method, however, is not able to predict parasite drag, which must be neglected or modelled separately.

Only the near wake is modelled as a free wake, whereas the intermediate wake is modelled with helical vortices, and the far wake with a semi-infinite vortex tube. This is due to the inherent instability of the free wake methods, and due to the computational cost involved.

For a planar rotor with straight blades the design problem is reduced to determination of the optimal circulation distribution $\Gamma(r)$, and has been solved analytically for the number of blades N=2,4 by Goldstein[12] and later for any N by Okulov and Sørensen[13]. In the general case, where both the blade geometry circulation distribution is unknown, the problem must be solved solved through optimization, as in[1].

Particularly simple and promising configurations will be chosen for detailed investigation and validation with CFD, and to investigate the parasite drag. For these computations EllipSys3D [14,15] will be used. EllipSys3D is a multi-block finite volume code developed to solve the incompressible Reynolds averaged Navier-Stokes (RANS) equations in general curvilinear coordinates.

3 TOPOLOGICAL ANALYSIS OF TIP FLOWS

Say that a set of promising designs have been found, and refined by viscous computations with CFD. Can one assess whether a given design is close to being optimal, based on the CFD result? The existence and location of the trailing vortices, attachment and separation regions, transition regions, can contain important information on the performance of the design. Shimitzu et al.[8] provides a good example on this approach.

What topological analysis essentially does is to determine and describe these qualitative flow features in an objective and systematic way. The concept is believed to be useful both when the desired topology Is known a priori, and in cases where topology information is correlated to the actual performance, to hopefully uncover new insights about the flow.

All the aforementioned flow features are closely linked to the skin friction field of the blade surface. Surana et. al. [16,17] shows that in an incompressible flow, knowledge of skin friction field and pressure field on a surface is enough to uniquely determine the local behaviour of the velocity field close to the surface.

Topological analysis uses the concept of critical points, zeroes, of the skin friction field. Each of these critical points have a certain type which define the local dynamics of the flow. This type can be found by local series expansion and transformation of the vector field, following Perry et al.[18] and Hartnack[19]. The topology of the flow is defined by the critical points, and their connectivity, and can be represented as a directed graph. Physically, the connectors are the attachment, separation lines and vortex centres of the flow.

As part of the project a post processing tool is being developed which receives the discrete surface solution for the skin friction field as input, and does the following:

a) Create a bi-cubic spline representation of the geometry and the surface quantities.

b) Determine the location and type of the critical points of the skin friction field

c) Through an integration procedure, establish the connectivity between the critical points, and construct the topology graph.

These tools can be used to categorize results into groups of topologically equivalent flows.

It is expected that the correlation of this information with the integral forces and moments of the simulations can give rise to new insights into which tip flow features are of the largest importance for performance.

4 CONCLUSIONS

A design approach combining already applied methods with ideas from topological methods has been outlined. It is expected that this approach will lead to a more detailed understanding of the viscous phenomena occurring at the tip, and their role in performance of the design. At this point results are available.

5 BIBLIOGRAPHY

[1] Hjort, S., Laursen, J., Enevoldsen, P.B., “Aerodynamic Winglet Optimization”, Proc. of EWEC 2008, Brussels

[2] Maughmer, M. D., “The Design of Winglets for High-Performance Sailplanes” AIAA Paper 2001-2406

[3] Prandtl, L., "Theory of Lifting Surfaces" NACA Report TN-9 1920

[4] Munk, M. , “The Minimum Induced Drag of Aerofoils” NACA Report TR- 121, 1923.

[5] Whitcomb, R., “A design approach and selected wind tunnel results at high subsonic speeds for wing-tip mounted winglets”

[6] NASA TN D-8260 1976.

[7] Kroo, I: “Drag due to lift: Concepts for prediction and reduction”, Ann. Rev. Fluid Mech. 33, 587–617, 2001

[8] Gaunaa, M. and Johansen, J., “Determination of the Maximum aerodynamic efficiency of wind turbine rotors with winglets”, Proc. of EWEC 2008, Denmark.

[9] Y. Shimizu, E. Ismaili, Y. Kamada and T. Maeda, “Rotor Configuration Effects on the Performance of a HAWT With Tip-Mounted Mie-Type Vanes”

[10] H. Imamura, Y. Hasegawa, K. Kikuyama, “Numerical Analysis of the Horizontal Axis Wind Turbine with Winglets”, JSME International Journal, Series B, 41,170-176, 1998

[11] J. Johansen and N.N. Sørensen, “Aerodynamic investigation of Winglets on Wind Turbine Blades using CFD”, Risø-R-1543(EN), Risø National Laboratory, Feb. 2006.

[12] Helmholtz, H.: Über die Integrale der hydromechanischen Gleichung, welche den Wirbelbewegungen entsprechen, Crelles J. 55, 1858

[13] Goldstein, S., "On the Vortex Theory of Screw Propellers", Proc. Royal Soc. (A) 123

[14] V. Okulov, J. Sørensen, "Refined Betz Limit for Rotors with a Finite Number of Blades", Wind Energ. 2008; 11:415–426

[15] Michelsen JA “Block structured Multigrid solution of 2D and 3D elliptic PDE's.” Technical Report AFM 94-06, Technical University of Denmark, 1994.

[16] Sørensen NN “General Purpose Flow Solver Applied to Flow over Hills.” Risø-R-827-(EN), Risø National Laboratory, Roskilde, Denmark, June 1995.

[17] A. Surana, O. Grunberg, & G. Haller, ”Exact theory of three-dimensional flow separation. Part I. Steady separation”, J. Fluid. Mech., 564 (2006) 57-103.

[18] A. Surana, G. Jacobs, O. Grunberg, & G. Haller, “Exact theory of three-dimensional fixed unsteady separation”, Phys. Fluids. 20 (2008) 107101 (1-22)

[19] M.S. Chong, A.E. Perry & B.J. Cantwell, "A general classification of three dimensional flow fields." Phys. Fluids A 2(5), pp.765-777, 1990

[20] J. N. Hartnack, “Structural changes in Incompressible Flow Patterns”, Ph.D.-thesis, Technical University of Denmark, August 1999

A Dynamical Approach to Wind Power Generation

Patrick Milan, Matthias Wächter, Joachim Peinke

ForWind Center for Wind Energy Research, University of Oldenburg, Germany

ABSTRACT

We introduce the concept of power performance for a WEC (Wind Energy Converter) as the relation between the wind input and the electrical output. The performance test is applied to measurement data for the wind speed u(t) and the power output P(t), which is usually handled after the international procedure IEC 61400-12-1 [1]. We propose a new approach called the dynamical approach to characterize the extraction process u(t)→P(t) as the dynamical response of the WEC to wind fluctuations. As a first application of this procedure, the power performance of any WEC can be quantified and monitored over time. The quantification of the dynamics also allows for a simple modeling of the WEC so as to predict the power production at different times or locations.

KEYWORDS

energy extraction dynamics, dynamical approach, power curve, power forecasting

1 INTRODUCTION

The power performance of a WEC is usually characterized by a power curve P(u). The wind displays complex statistics such as turbulence, non-stationarity and intermittency (wind gust), whose effects are highly simplified in the IEC procedure. However, the extraction process appears to be a highly dynamical process, as seen in figure 1. The dynamical approach is a simplification of the overall WEC dynamics, as it correlates the wind speed u(t) and the electrical power output P(t), regardless of the intermediate steps of the energy extraction.

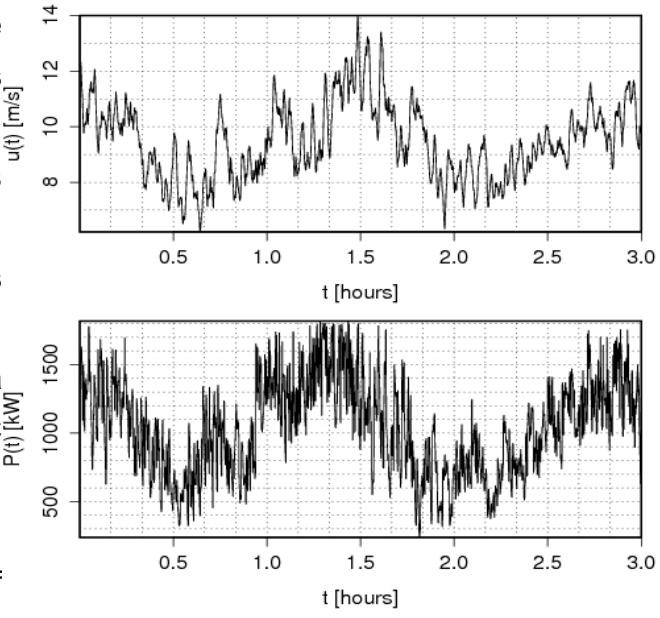

Figure 1: 1Hz measurements of wind speed u(t) (upper figure) and power output P(t) (lower figure) simultaneously for a multi-MW class WEC.

2 DYNAMICAL (LANGEVIN) POWER CURVE

The WEC responds to the wind u(t) by adjusting to the corresponding power P(t). Ideally, the power curve P(u(t)) gives P(t) knowing u(t). But as u(t) fluctuates around a mean value, P(t) fluctuates around the power curve P(u(t)). P(u) hence represents the stable, attractive dynamics of the extraction process, around which P(t) fluctuates. P(u) is labelled $P_L(u)$ here to emphasize that the power curve represents the stable fixed points of the dynamics (L stands for Langevin as we are in the formalism of the Langevin equation). A representation of this dynamical concept is given in figure 2.

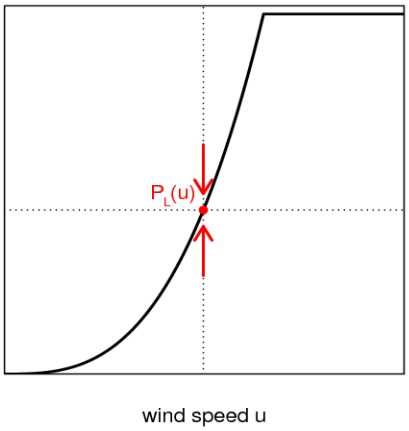

Figure 2: Dynamical approach

$$\frac{dP(t)}{dt} = -|\alpha|\{P(t) - P_L(u(t))\} + \sqrt{\beta}\cdot\Gamma(t) \qquad (1)$$

This dynamical concept can be modeled by a stochastic differential equation for P(t) [2]:

where Γ(t) is a delta-correlated Gaussian noise with mean value Γ(t) = 0 and correlation function $<\Gamma(t_1)\Gamma(t_2)> = 2\,\delta(t_2-t_1)$. α represents the intensity of the attraction (drift) towards the power curve $P_L(u)$, while β quantifies the random fluctuations around $P_L(u)$. This equation models the power output P(t) of a WEC for incoming wind speed u(t). The WEC is characterized by the parameters α, β and $P_L(u)$. Applications of this model are presented in section 3.

Modeling a WEC using equation (1) requires to know α, β and $P_L(u)$, which should be computed from measurement data. Equation (1) can be further generalized by introducing the terms $D^{(1)}(P;u)$ and $D^{(2)}(P;u)$ that will be computed from u(t) and P(t). Equation (1) then becomes the Langevin equation [3], [4]:

$$\frac{dP(t)}{dt} = D^{(1)}(P;u) + \sqrt{D^{(2)}(P;u)}\cdot\Gamma(t) \qquad (2)$$

$D^{(n)}(P;u)$ are computed from measurement data as follows:

$$D^{(n)}(P;u) = \frac{1}{n!}\lim_{\tau\to 0}\frac{1}{\tau} < [P(t+\tau) - P(t)]^n > |_{P(t)=P\ ,\ u(t)=u} \qquad (3)$$

$D^{(1)}(P;u)$ is called the drift field and $D^{(2)}(P;u)$ the diffusion field. The drift field $D^{(1)}(P;u)$ accounts for the dynamical relaxation of the WEC towards stable power values $P_L(u)$, while $D^{(2)}(P;u)$ deals with the fluctuations of P(t) [3], [4]. A visualization of the drift field is displayed in figure 3. The regions where $D^{(1)}(P;u) = 0$ correspond to $P(t) = P_L(u(t))$ in equation (1). They represent the attractive dynamics of the WEC. These are the values of P where the WEC is in a stable

dynamical situation for given u. The Langevin power curve $P_L(u)$ represents the attractive dynamics of the extraction process. A representation of $P_L(u)$ is given in figure 3.

One can see in figure 3 that multiple values of the power output are possible for equal wind speed. This indicates multi-stable behaviors of the WEC at specific wind speeds. This is observed in the regions 3m/s < u < 6m/s and 13m/s < u < 14m/s where the WEC alternates between different control strategies of the pitch control system. This illustrates the ability of the Langevin power curve $P_L(u)$ to characterize the dynamics and the resulting power performance of the WEC. As such, it is a relevant tool for performance monitoring, as modifications in time of $P_L(u)$ indicate changes in the extraction process.

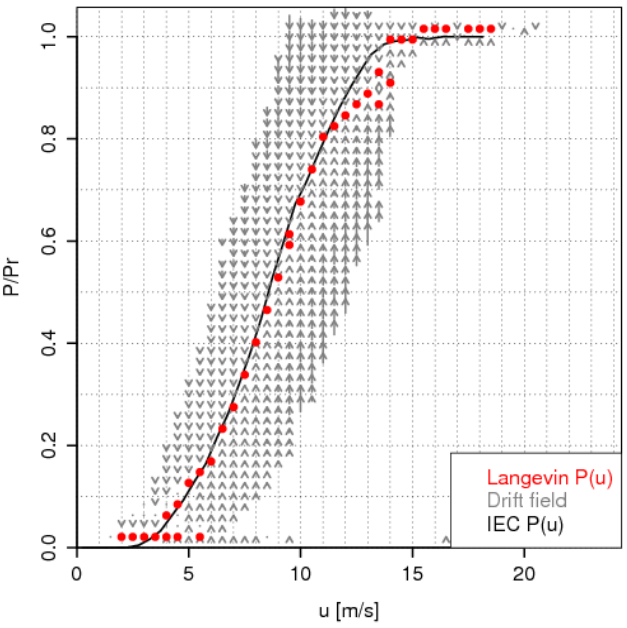

Figure 3: Drift field $D^{(1)}(P;u)$ measured on a multi-MW class WEC. The grey arrows indicate the direction of the dynamics and the intensity of the attraction (length of the arrows), while the attractive values $P_L(u)$ of the drift (the Langevin power curve) are represented by red dots. $P_{IEC}(u)$ is given by the black line. The power output P was normalized by its rated value P_r.

3 POWER PREDICTION

Although $P_L(u)$ is based on the Langevin equation (2), it is obtained without solving equation (2) but by computing equation (3) only (for n=1). For power prediction, the Langevin equation (2) can be solved to model the power output $P_{mod}(t)$ of the WEC. When a particular WEC is characterized by computing the drift field $D^{(1)}(P;u)$ and the diffusion field $D^{(2)}(P;u)$, it becomes possible to model its behavior under any other wind condition. Any WEC that was characterized at any geographic location can potentially be modeled numerically at another location where the wind was measured, so as to select the most efficient wind location before installing the WEC.

The prediction model for $P_{mod}(t)$ was applied to a WEC and was compared to the (real) measured power output P(t). For this example, the model was not applied with the Langevin equation (2), but with its simplified version (1). An illustration is given in figure 4 for a

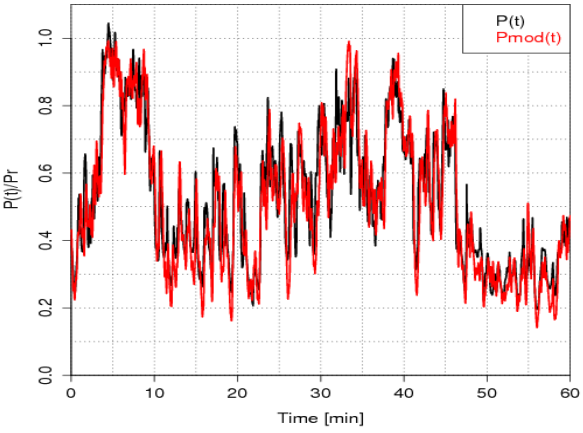

simulation of one hour, to show the accuracy of the prediction model.

Figure 4: Comparison of original power output P(t) (black in background) and simulated power output $P_{mod}(t)$ (red in front) for one hour for a multi-MW class WEC.

It is important to note that the architecture of the model makes it stable, in the sense that it cannot diverge. In case the model deviates for a particularly extreme wind condition, it will readjust naturally. To quantify the accuracy of the model, we can compare the statistics of P(t) and $P_{mod}(t)$. Results are displayed in table 1 for predictions of 24 hours and 2 weeks.

Prediction duration		$\frac{<P(t)>}{<P_{mod}(t)>}$ $\sqrt{\frac{<P(t)^2>}{<P_{mod}(t)^2>}}$
24 hours	101.30%	107.60%
2 weeks	96.00%	108.60%

Table 1: Comparison of measured power output P(t) with modeled power output $P_{mod}(t)$.

We can see in table 1 that the prediction model gives a good description of the power output P(t) of the WEC in terms of quantity (mean value) and quality (fluctuations). While the prediction model is still under development, its results are encouraging.

4 CONCLUSION

The concept of the dynamical approach is based on the short-time dynamics of the WEC. The Langevin power curve characterizes the power performance of the WEC, and may be

used as a monitoring tool. As a second application of this approach, the Langevin equation allows to reproduce the dynamical behavior of any WEC to any incoming wind through its power output. This prediction model can help to estimate the wind energy potential of any characterized WEC before it is built using local wind measurement. It can predict high-frequency power output in terms of quantity, stability and availability. In addition, an integration of wind forecast models is being developed, towards a prediction of power production several days in advance for any WEC being monitored.

BIBLIOGRAPHY

[1] IEC, “Wind Turbine Generator Systems, Part 12: Wind turbine power performance testing,” International Standard 61400-12-1, International Electrotechnical Commission, 2005.

[2] Gottschall, J. and Peinke, J., “How to improve the estimation of power curves for wind turbines,” Environmental Research Letters, Vol. 3, No. 1, 2008, pp. 015005 (7pp).

[3] Anahua, E., Barth, S., and Peinke, J., “Markovian power curves for wind turbines,” Wind Energy, Vol. 11, No. 3, 2008, pp. 219–232.

[4] Gottschall, J. and Peinke, J., “Stochastic modelling of a wind turbine’s power output with special respect to turbulent dynamics,” J Phys: Conf Ser, Vol. 75, 2007, pp. 012045.

Wish for the presentation of this paper: ORAL PRESENTATION + POSTER

SESSION 2 – PART A

Wednesday, 30.09.2009

11:30AM

Wind power prediction errors of a shortest-term forecast of the total German wind power generation

J. Dobschinski, A.Wessel, B.Lange

ISET e.V., Königstor 59, 34119 Kassel, Germany

ABSTRACT

In electricity systems with large penetration of wind power, the limited predictability of the wind power generation leads to an increase in reserve requirements. The present study concentrates on the reduction of large forecast errors of the German wind power generation by using advanced shortest-term predictions. The aim is to estimate the maximum remaining uncertainty after latest possible trading on the intraday market.

KEYWORDS

Wind power forecasting, shortest-term forecasts, reduction of extreme forecast errors, wind power induced reserve requirements,

1 INTRODUCTION

In 2009 about 24 GW of installed wind power capacity have to be integrated as a must-run unit into the German power supply system. Due to the fluctuating nature of wind power the electricity supplier require accurate and reliable forecasts of the electricity generated by wind turbines for the next hours to days ahead. In addition to power station outage and stochastic load variability the limited predictability of the wind power generation leads to an increase in reserve requirements. Hence, improved accuracy of wind power forecasts do not only lead to higher grid reliability but also to attractive cost savings concerning the allocation of control reserve.

Concerning the allocation of control and reserve power induced by wind power forecast errors, the tails of the historical observed forecast errors and especially the maximum errors play the major role.

In this study a case study has been performed to compare the forecast errors of shortest-term wind power prediction systems with a focus on the largest error. The following two forecasts have been compared concerning their global performance and their error distributions:

a) ISET advanced shortest-term forecast system [1]

b) persistence approach

2 SZENARIO

The case study is based on a total wind power generation capacity of the German transmission grid with a capacity of about 23 GW. The covered time period range from January to May 2008. With regard to the estimation of the maximum remaining forecast uncertainty after latest possible trading on the intraday market, forecasts with horizons of 4 hours has been investigated.

The ISET advanced shortest-term forecast system is based on individual forecasts of 62 reference wind farms distributed over Germany using artificial neural networks and a final up-scaling procedure performed by the ISET online-model [2]. The persistence forecast has been calculated out of the final power time series of the total German power generation which is based on the measurements of the 62 reference wind farms and the ISET online-model.

3 RESULTS

The resulting forecast errors are visible in figure 1. There is also a plot in semi-logarithmic format being more suitable for analysing the tails of the distribution. It is visible that the distribution based on the persistence forecast is much broader which reflects, that the global performance of the persistence approach is inferior to the advanced forecast.

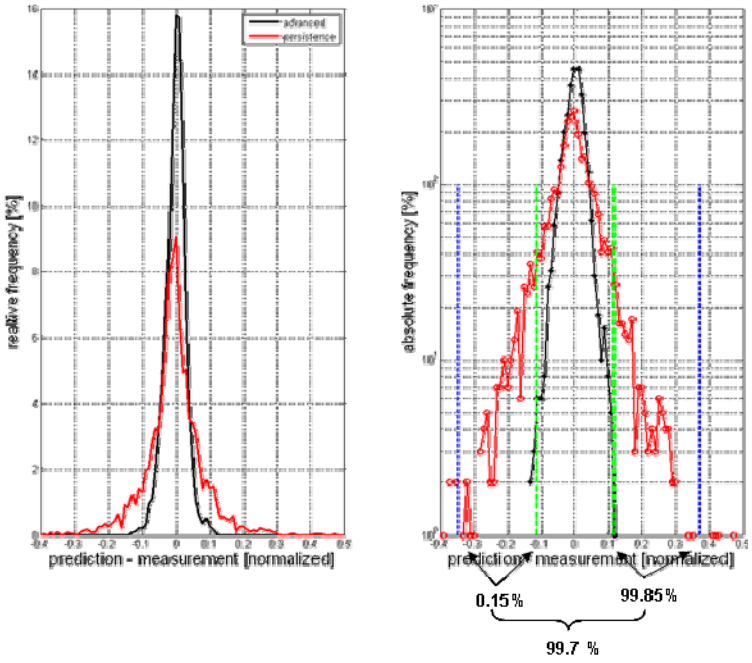

Figure 1: Distribution of forecast errors (normalized on capacity) with respect to the relative frequency (left) and the absolute frequency (right) in semi-logarithmic format. The green (advanced) and blue (persistence) line corresponds to the 99.7 % error interval based on the 0.15% and 99.85 % percentile

Table 1: PERFORMANCE PARAMTERS CONCERNING THE ADVANCED SHORTEST-TERM FORECASTS AND THE PERSISTENCE APPROACH

Advanced system:	Persistence:
nRMSE = 3.11 %	nRMSE = 8.19 %
nMAE = 2.37 %	nMAE = 5.66 %

The global accuracy is represented by the root mean square error normalized on capacity (nRMSE) and the mean absolute error (MAE) and is given in table 1. It is obvious that also for the largest errors (positive and negative) the persistence forecast shows significant larger values. The coloured lines show as an example the (static) 99.7 % error interval [3] which is significantly smaller in the case of the advanced system.

The tails of the distribution show the extreme forecast errors. Figure 2 shows a global overview of the percentiles as well as a close-up of the tails in the range of 0-1% and 99-100%. It is apparent that the advanced model shows a better performance, which is further increasing for the highest errors.

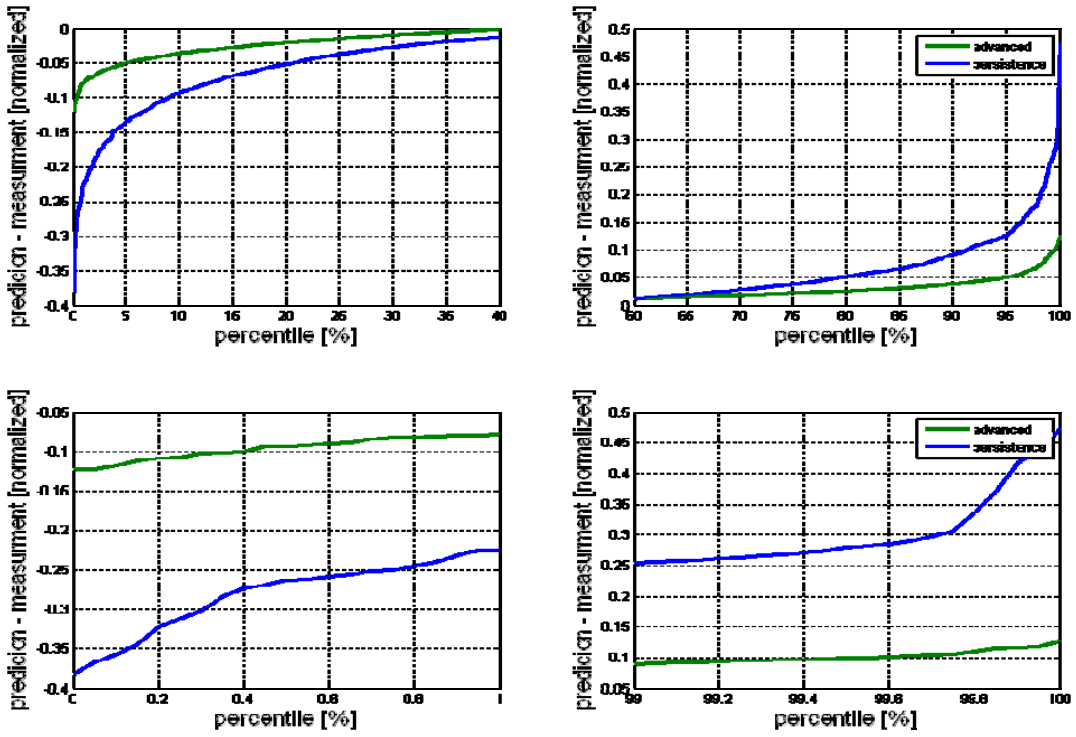

Figure 2: Forecast errors versus percentiles of the error distributions. On top there is a global overview showing the percentiles ranging from 0% to 40% (left) and 60% to 100% (right). The lower plots represent the larger errors in more detail: 0% to 1% (left) and 99% to 100% (right).

4 CONCLUSION

The ISET advanced (and optimized) shortest-term forecast shows an improvement in the RMSE compared to persistence of about 62% for a 4 hour wind power forecast for Germany during the selected test period. The investigation of the error distribution with special focus on the largest errors has revealed that not only the global forecast quality is improved by using the advanced forecast but that also large errors are significantly reduced. Concerning the maximal errors the advanced shortest-term forecast leads to an improvement exceeding 65 % compared to the persistence approach.

In the following steps of this work the control and reserve requirements induced by wind power forecast errors will be investigated with a focus on the potential of using shortest-term forecasts for reducing the minute reserve power. Nowadays the estimation of the part of reserve requirement induced by wind power depends only on the global uncertainty of the used wind power forecast while the meteorological and hence the forecast uncertainty can be temporally resolved in more detail. Therefore the capability of dynamic prediction intervals to further reduce the wind power induced reserve requirements will be evaluated

BIBLIOGRAPHY

[1] Wessel et al.: “Improving short-term forecast with online wind measurements”, Proceeding, DEWEK, Bremen, 2008www.ewea.org.

[2] Biermann et al. : ”Entwicklung eines Rechenmodells zur Windleistungsprognose für das Gebiet des deutschen Verbundnetzes”, Abschlußbericht BMU Forschungsvorhaben, ISET, 2005

[3] Dobschinski et al.: „Estimation of wind power prediction intervals using stochastic methods and artificial intelligence model ensembles“, Proceeding, DEWEK, Bremen, 2008

Development and characterisation of the sphere anemometer

Heißelmann H[1)], Hölling M[1)], Peinke J[1)]

[1)] ForWind – University of Oldenburg

ABSTRACT

The widely spread cup anemometers show a tendency to overestimate the mean flow velocity due to its moment of inertia when exploited to turbulent flow conditions as present in natural wind fields. We present the newly developed sphere anemometer as a simple and robust alternative to cup anemometry which uses a light pointer in order to detect the velocity-dependent deflection of a sphere and its support. A 2D-calibration function was obtained allowing for the simultaneous determination of wind speed an direction. Furthermore, comparative investigations of the dynamic behaviour under turbulent conditions were performed with cup anemometer and sphere anemometer.

KEYWORDS

anemometer, wind speed, measurement, direction, sensor, gust

1 INTRODUCTION

In times of growing energy demand, the importance of wind energy is rapidly increasing and so is the need for accurate wind speed and direction measurements. The widely spread cup anemometers are only capable of detecting wind speeds with a comparably low temporal resolution (~1 Hz) while over-estimating the wind speed under turbulent conditions (over-speeding) **Error! Reference source not found.**. Since the higher-resolving ultra-sonic anemometers are rather easily damaged, the sphere anemometer was developed as a simple and robust alternative at the University of Oldenburg.

2 THE SPHERE ANEMOMETER

2.1 Measuring principle

The sphere anemometer makes use of the total drag force F acting on a flexible tube (F_t) and a sphere (F_s) mounted atop of it. The velocity-dependent drag force causes a deflection s of the tip of the tube (see fig. 1, left), which is given by

$$s = \frac{l^3}{E\ J}\ \left(\frac{F_s}{3}\ \frac{F_t}{8}\right), \qquad (1)$$

where *l* is the tube length, *E* is the tube's elasticity modulus and *J* is the tubes second moment of area. F_s and F_t denote the drag forces acting on the sphere and the tube, respectively. According to the general expression of the drag force

$$F = \frac{1}{2} \quad A \, c_d \, v^2 \tag{2}$$

with fluid density , cross-section *A*, fluid velocity *v* and *Re*-dependent drag coefficient $c_d = c_d \; Re$ the displacement *s* is proportional to *v* and c_d

$$s \quad c_d \, v^2 . \tag{3}$$

2.2 Anemometer set-up

The measuring principle described above was realised by mounting a fibreglass tube of 8 mm diameter to a streamlined case and by fixing a light sphere of 7 cm diameter to its tip. The choice of the sphere and tube dimensions is motivated by the fact, that their respective drag coefficients can be considered constant for Reynolds numbers between 800 and 200,000 **Error! Reference source not found.Error! Reference source not found.**, equal to velocities between 0.3 m/s and 42 m/s. For this range the displacement of the tube is only proportional to the velocity squared, which results in a square-root-function

$$v = m \quad \overline{s} \tag{4}$$

and allows for a very convenient calibration of the sphere anemometer.

The displacement of the tip is detected by means of a light pointer, known from atomic force microscopes. For this purpose a laser diode is mounted on top of the tube and aimed on a two-dimensional position sensitive detector (2D-PSD) at the bottom of the measurement unit as sketched in figure 1, right.

The deflection of the tube causes a displacement of the laser spot on the 2D-PSD and a change of the output signals U_x and U_y. Via calibration, this allows for the simultaneous measurement of wind speed and direction.

3 WIND TUNNEL MEASUREMENTS

3.1 Sensor calibration

One major constraint to the accurate wind speed and direction measurement is the existence of an unambiguous two-dimensional calibration function. This feature of the new sphere anemometer was examined in wind tunnel experiments at the University of Oldenburg. In order to obtain a two-dimensional calibration function, the sphere anemometer was placed on a turntable (see fig. 2,left) and the output signals U_x and U_y were recorded at wind speeds from 0 m/s to 20 m/s. The angle of attack (AoA) was varied between 0° and 350° in 10° steps by a stepping motor. In figure 2 (right) the *x*-component of the PSD-output U_x was plotted against its *y*-component U_y representing the light spot position on the 2D-PSD. It is easily seen that the plot of the 2D-calibration shows no overlapping or crossing of calibration functions for subsequent angles of attack. Furthermore, a system of concentrical rings is observed with each ring corresponding to one velocity. The unambiguity of the 2D-calibration allows for the calculation of the wind speed and direction from the high-resolved measurement data recorded with the sphere anemometer.

3.2 Measurements of gusty wind

Since an exact calibration function of the sphere anemometer could be obtained, the next step in the sensor development was the comparison to state-of-the-art cup anemometry. Therefore, both anemometers were exploited to artificial wind gusts of approximately 1.3 Hz which were produced by a motor-driven gust generator in the wind tunnel. Furthermore, a high-resolving hot-wire anemometer served as a reference.

Two-second excerpts of the recorded data are displayed in figure 3. While the effect of over-speeding is observed clearly in the cup anemometer data (blue), the sphere anemometer (red) is able to resolve the fast wind speed fluctuations up to its natural frequency **Error! Reference source not found.** and does not exhibit any over-speeding. However, the comparison of the sphere anemometer data with hot-wire data shows slight deviations as regards the peak velocities, which are caused by the different sensor dimensions (sphere anemometer: 7 cm vs. hot-wire: 0.5 cm).

4 CONCLUSIONS

This paper presents the newly developed sphere anemometer as a simple and robust alternative to cup anemometry. In wind tunnel experiments a two-dimensional calibration function for the anemometer was obtained which allows for the simultaneous measurement of wind speed and direction using only one sensor. Furthermore, laboratory experiments under turbulent wind conditions showed that the sphere anemometer provides a higher temporal resolution than cup anemometers while it does not exhibit any over-speeding. In contrast to cup anemometers it has no wearing parts.

BIBLIOGRAPHY

[1] Tritton, D.J.: Physical Fluid Dynamics, Oxford Science Publications, 2nd Ed. 1988

[2] Böswirth, L.: Technische Strömungslehre, Vieweg, 7th Ed. 2007

[3] Westermann, D.: Overspeeding - über das eigentümliche Tiefpassverhalten von Schalensternanemometern, DEWI Magazin, 9:56–63 1996.

[4] Heißelmann, H.; et. al.: Sphere anemometer - A possible alternative to cup anemometry, EWEC Conference Proceedings, 2008

Characterization of high-frequency atmospheric turbulence.

A. Morales, M. Wächter, J. Peinke

ForWind- University of Oldenburg, Germany.,

ABSTRACT

We propose a general statistical framework for the characterization of wind turbulence from where different statistical approaches can be understood and further developed.

We consider not only the usual low order statistical description, but also higher order two-point statistics at different time scales and their corresponding probability density functions (PDFs). Finally we also present an outlook on a novel approach based in the use of n-point statistics in order to generate artificial high frequency wind time series which can be coupled to the output of forecast models in order to give a high frequency wind prediction.

KEYWORDS

Wind turbulence, wind speed increments, intermittency, high-frequency wind forecasting.

1 INTRODUCTION

Atmospheric wind is not only the source of energy for Wind Energy Converters (WECs), but also the source of mechanical loads which limit the life time of the machines and constrain their operation. In particular wind turbulence leads to power fluctuations, fatigue and extreme loads on WECs. Therefore a thorough description and characterization of wind turbulence is crucial for a reliable design and efficient operation of WECs. Currently there are several approaches, for the statistical or even deterministic characterization of turbulence and corresponding extreme events as gusts (see e.g. IEC Norm [1]). We think it is important to show the scope of each type of statistics in a general but clear way, in order to understand and interpret properly the used characterization of the atmospheric turbulence. With that aim we have been worked in a general statistical framework for the characterization of wind turbulence from where different statistical approaches can be understood and further developed. In this small contribution we show schematically the main points of this framework. We present it in a way that with every step more statistical information for the description of the wind turbulence is taken into account. We then end with an outlook on the use of n-point statistics which, at the same time, gives the basis for the generation of the high frequency wind time series. The generation of realistic (at least in a statistical sense) high frequency wind time series can be later coupled to a dynamical approach for the calculation of power curves [2], enabling the forecast of high frequency power fluctuations. This last part is under development and the future steps to be followed will be presented.

For illustration purposes we use wind data of the research platform FINO I (with sample rate 1hz, 1 month data) and onshore data from the Growian (2.5hz, 32hours) experiment.

2 WIND TURBULENCE CHARACTERIZATION FRAMEWORK

2.1 One-point statistics

It is common in the wind energy community to define fluctuations around 10-minute mean wind speed as:

$$u(t) = \langle u \rangle_T + u'(t)_{\langle u \rangle_T}. \tag{1}$$

Typical statistics of these fluctuations are shown in Figure1. In order to characterize the strength of the turbulence in this context the so-called turbulence intensity (TI) is defined as:

$$I = \frac{\sqrt{\langle u'^2 \rangle}}{\langle u \rangle_T} = \frac{\sigma_{u'}}{\langle u \rangle_{10min}}. \tag{2}$$

Where the standard deviation is defined over each 10-minute time span. That would correspond to standard deviations of each of the distributions in Fig. 1(a). The superposition of Gaussian distributions with different standard deviations (and for a given bin of mean speed that means also for different TIs) lead to the intermittent distribution in Fig.1(b). The fact that when, normalized by their corresponding 10-minute standard deviations, Gaussian statistics are recovered (see Fig. (c)) supports the argument that fluctuations defined through eq. (1) follow Gaussian statistics within 10-minute time spans. However some deviations principally at extreme values are observed.

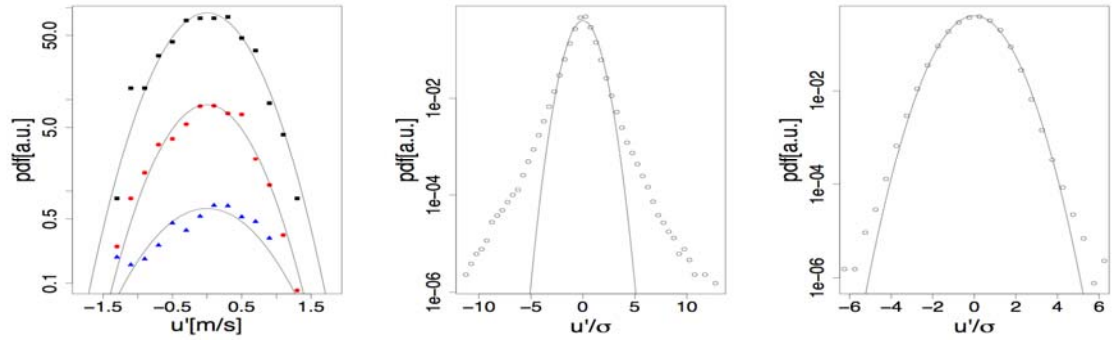

Figure 1: u´ PDFs. (a) For three single 10-minute spans. (b) For a 20-day data set. (c) Same as (b) but u´ are normalized by single 10-minute standard deviations. Lines represent Gaussian PDFs.

2.1 Two-Point 2nd Order Statistics.

The information of the fluctuations (u') PDFs by itself, does not show how the fluctuations reach that distribution in time. Thus several different time-series may exhibit the very same PDFs and still look very different (e.g., Fig. 2). Therefore it is necessary to study two-point statistics in order to grasp more information from the turbulent signal and enhance the characterization of turbulence. The autocorrelation function is an example of two-point statistics:

$$R_{u'u'}(\tau) = \langle (u'(t+\tau)u'(t)) \rangle \tag{3}$$

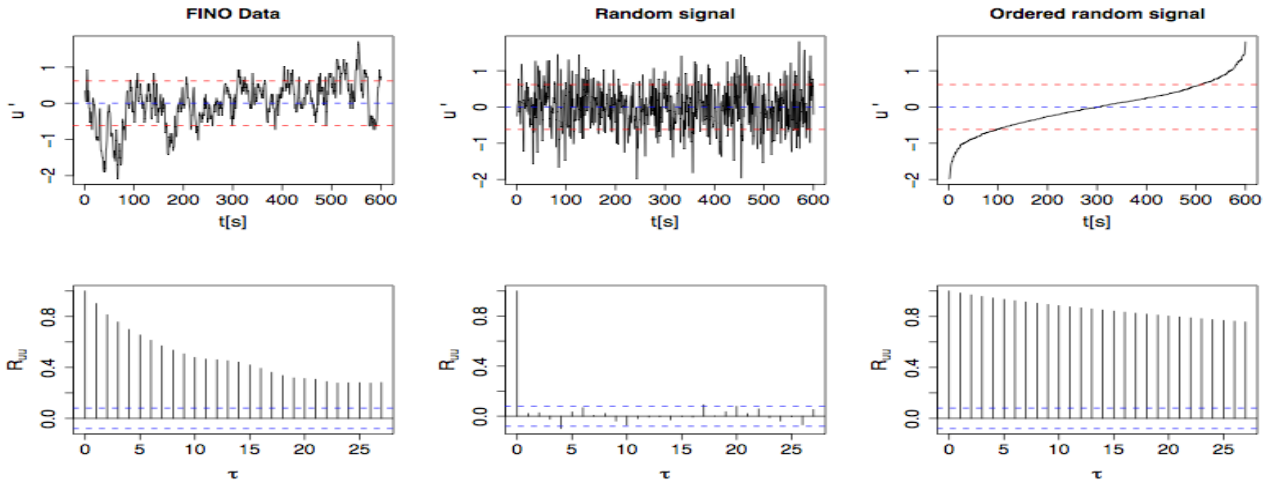

Figure 2: Top different time series with the same standard deviation and Gaussian distribution. Down the corresponding autocorrelation functions.

As seen in Fig 2. this statistical tool already provide useful information in order to distinguish between the signals. The three time series follow closely the same Gaussian distribution.

2.2 Higher Order Two-Point Statistic

The information gathered by the autocorrelation and its Fourier transformation just reflect 2nd order two-point statistics. For studying wind fluctuations in a more general way we define wind speed increments:

$$\delta u(t,\tau) = u(t+\tau) - u(t). \tag{4}$$

The increments are wind speed differences over a given scale, enabling the study of wind fluctuations against the evolution of that scale (temporal or spatial). The moments of the increments are called structure functions and well studied in laboratory turbulence.

$$\langle \delta u(t,\tau)^n \rangle \tag{5}$$

Note that when n=2, namely the second order structure function, a relationship between this and the autocorrelation function exists (compare equations (3) and (5)). However no further information of higher order structure functions is contained in the autocorrelation function (or spectral density function). On the other hand, increment PDFs contain information of all orders. The PDFs clearly show a peak around the mean value and so-called heavy tails (intermittency). For the fits in Fig. (3) and characterization of such PDFs we use the well established description of Castaing [3] for laboratory turbulence. It models the turbulent PDFs, depending mainly on the so-called form (shape) parameter λ. This form parameter is strongly related with the flatness of the distribution. Fig. 4 shows the values of the form parameter against the scale tau for two data sets of wind. The conditioned data from FINO and the Growian data set share more or less the same turbulence intensity and the same mean wind speed.
Despite of this fact, for small and large scales the shape parameter is clearly different, indicating a site dependent relationship. Thus these site differences would not be characterize only by means of the turbulence intensity or even lower two-point statistics.

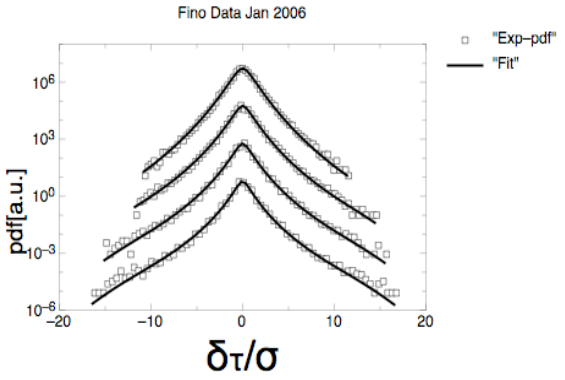

Figure 3: Increment PDFs and respective fits according to Castaing's formula. The PDFs are shifted. From bottom to top tau=2,4,10,60s.

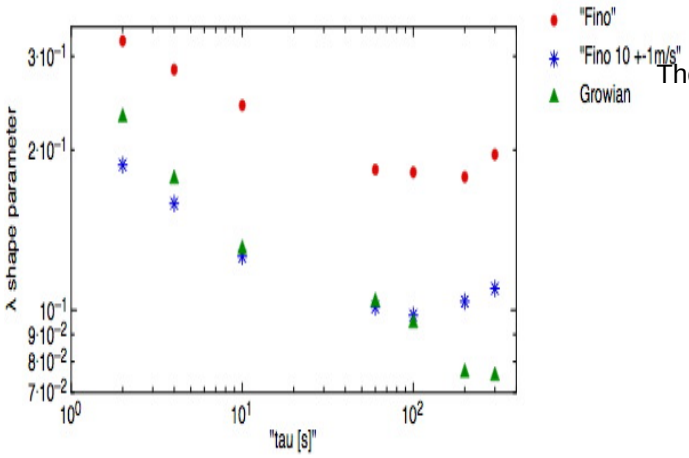

Figure 4: Shape parameter according to Castaing's formula Vs scale tau. Dots: Fino Data Stars: conditioned Fino data (10+-1m/s). Triangles Growian data.

2.4 Outlook

In the future we will work in the use of n-point statistics to both, characterize wind situations and generate high-frequency wind signals. The generation of high-frequency wind time series is intended to be used together with a low-frequency wind forecast. The idea here is to give a "high-frequency" wind forecast to be used as an input of a dynamical method for the calculation of WECs power [4]. Thus giving a high-frequency power forecast.

The following steps are being followed:

- Acquisition of the low-frequency wind forecast from Weather Research and Forecasting (WRF) model.
- Statistical analysis of the WRF forecast for 1 hour and 10 minute outputs.
- Review of Nawroth's multi-scale reconstruction technique of time series.
- In the context of the above technique, analysis of Markovian properties of wind increment time series.

3 CONCLUSIONS

The statistical characterization of wind turbulence was briefly studied. Showing the usefulness and limitations of every order and type of statistics. The use of high order two-point statistics was introduced in order to improve the characterization of wind turbulence. Remarkably the only extra parameter needed is the so-called shape parameter. The next step is to study n-point statistics and its applications.

BIBLIOGRAPHY

[1] IEC 61400-1, Ed. 3, Windturbines – Part 1 : Design requirements, International Electric Commission

[2] Gottschall, J. and Peinke, J., How to improve the esimation of power curves for wind turbines. *Envionmental Research Letters*, Vol. 3. No.1. 2008, pp. 015005 (7pp).

[3] Castaing B, e,a. 1990 Phys D 46 177-200.

[4] A. P. Nawroth, J. Peinke, *Multiscale reconstruction of time series*, Physics Letters A 360 (2006) 234-237.

allan.morales@uni-oldenburg.de

Stochastic data analysis for in situ damage analysis

Philip Rinn[1)], Joachim Peinke[1)]

[1)] ForWind - Center for Wind Energy Research
and Carl-von-Ossietzky University of Oldenburg
26111 Oldenburg, Germany

ABSTRACT

In wind energy detecting damages becomes more and more important especially offshore. We present a new application for the reconstruction of a Langevin equation from real data. In contrast to other damage analysis tools we separate the deterministic and the stochastic part of the system and show a change in the determinism of the system. From data sets of damaged and undamaged beam structures in turbulent air inflow the drift coefficient, which is the deterministic part, is reconstructed. We show that the slope of the drift changes with increasing damage.

KEYWORDS

Stochastic analysis, Langevin equation, damage analysis

1 INTRODUCTION

Nowadays most damage detection systems search for changes in eigenfrequencies to detect damages [1]. One drawback of this approach is that noisy excitation of the structure makes it harder to detect changes reliably, because peaks in the frequency spectrum are broadened due to the noise and changes can't be detected precisely. Our approach is to look at the dynamical behaviour of the system and to analyse damages due to it's changing of the systems dynamics. With methods from stochastic data analysis we cut off the stochastic part and analysed the deterministic part of the system only. Doing so we get rid of the overlying noise and analyse only the determinism of the system.

2 EXPERIMENTAL SETUP

As a model of a one-sided fixed beam structure the sphere anemometer [2] was used to acquire data. The sphere anemometer (cf. figure 1) is based on the light pointer principle. A

laser diode in the top of the anemometer is aimed onto a two dimensional position sensitive detector (2D-PSD), so the deflection of the tube can be measured in the horizontal *xy*-plane.

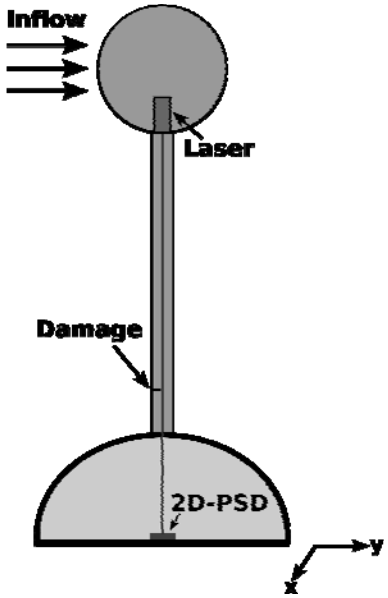

Figure 1: Schema of the sphere anemometer

For our measurements two steel tubes were prepared, the dynamical behaviour of one tube was changed in two steps, the other tube was undamaged. In the first step the tube was heated and cooled down fast and in the second step the cube was cut at a length of 40 % of it's circumference. The measurements were done in the wind tunnel of the University of Oldenburg. With a motor driven gust generator turbulent inflow conditions were achieved.
For five different wind speeds (7 m/s, 10 m/s, 15 m/s, 17 m/s and 20 m/s) time series of ten minutes length with a sampling rate of \$30\,\$kHz were recorded. From the measured data the deflection of the tube in *x*- and *y*-direction was calculated.

3 ANALYSIS

A wide range of dynamic systems can be described by a stochastic differential equation, the Langevin equation (1). The time derivative of the system trajectory $X(t)$ can be expressed as a sum of a deterministic part $D^{(1)}$ and the product of a stochastic force $\Gamma(t)$ and a weight coefficient $D^{(2)}$. The stochastic force $\Gamma(t)$ is δ-correlated Gaussian white noise.
For stationary continuous Markov processes Siegert et al. [3] and Friedrich et al. [4] developed a method to reconstruct drift $D^{(1)}$ (eqn. (2)) and diffusion $D^{(2)}$ (eqn. (3)) directly from measured data.

$$\dot{X}(t) = D^{(1)}(X(t),t) + \sqrt{D^{(2)}(X(t),t)}\,\Gamma(t) \quad \text{with} \tag{1}$$

$$D^{(1)}(x,t) = \lim_{\tau\to 0}\frac{1}{\tau}\langle (X(t+\tau)-x)\rangle|_{X(t)=x} \tag{2}$$

$$D^{(2)}(x,t) = \frac{1}{2}\lim_{\tau\to 0}\frac{1}{\tau}\langle (X(t+\tau)-x)^2\rangle|_{X(t)=x} \tag{3}$$

Equation (1) should be interpreted in the way that for every time t_i where the system meets an arbitrary but fixed point x in phase space, $X(t_i+\tau)$ is defined by the deterministic function $D^{(1)}(x)$ and the stochastic function $\sqrt{D^{(2)}(x)}\,\Gamma(t_i)$. Both, $D^{(1)}(x)$ and $D^{(2)}(x)$ are constant for fixed x.

From Equations (2) and (3) one can integrate drift and diffusion numerically over small intervals. If the system is at time t in the state $x = X(t)$ the drift can be calculated for small τ by averaging over the difference of the system state at $t+\tau$ and the state at t. The average has to be taken over the whole ensemble or in the stationary case over all $t = t_i$ with $X(t_i) = x$. Diffusion can be calculated analogously.

To analyse the dynamical behaviour only the deterministic part of the Langevin equation is needed. The x- and y-coordinates of the deflection of the tube span the phase space which was cut into 40 equidistant bins in each direction. The drift was calculated for each bin resulting in two 40x40 matrices.

Figure 2 shows on the left side a cut in x-direction through the drift for the main flow direction (y-direction) at 15 m/s. The slope of the heated tube is 17 % bigger than of the undamaged while the slope of the cut tube is 75 % smaller. The big errors in the outermost bins are due to the small number of events in these bins as large deflections are not so frequent as small.

The change of the slope can be made plausible when one interprets the drift as an indicator how fast the tube returns to its position of rest. A decreasing restoring force then results in a decreasing slope of the drift. The cut in the tube is a decrease of it's stiffness so the slope of the drift should be significantly smaller, in the second case the stiffness increases when hardening steel so the slope should be bigger in this case.

On the right side of figure 2 the frequency spectrum of the deflection in y-direction is shown, the first eigenfrequency of the sphere anemometer is very pronounced. The peaks are quite broad due to the noisy excitation and it is impossible to detect a shift in the eigenfrequency for the heated tube, although the peak is broadened. The shift in frequency for cut tube is clearly measurable, it is 10 %.

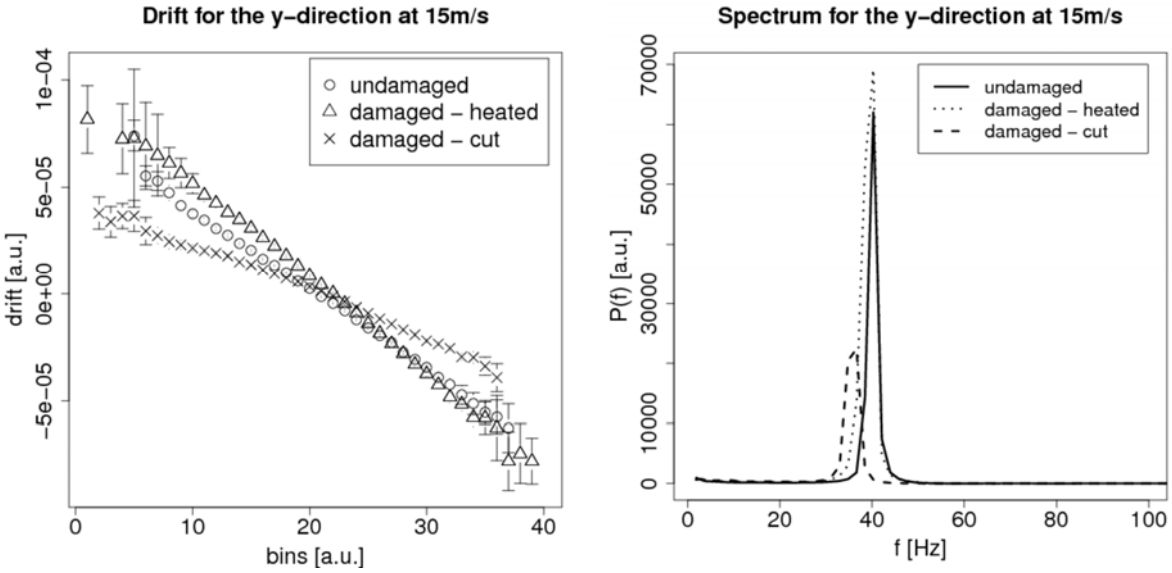

Figure 2: Cut in *x*-direction through the drift (left) and spectrum (right) for the main flow direction

4 CONCLUSIONS

We showed that analysing the deflection of a tube by means of drift can be fruitful for damage analysis. The slope of the drift is a sensitive indicator of the restoring force and thus the damage. While for the heated tube no shift in the first eigenfrequency could be detected our method showed a increase of the slope of the drift. This shows the capability of our method quite well and more data has to be acquired to find a threshold at which a damage can be detected, to determine whether the kind of damage can be analysed and to see how much data is needed to reliably calculate the drift. In this work the mean wind speed was constant in free field this is not the case. Further investigations must be done in this area.

BIBLIOGRAPHY

[1] Volkmer, P.: Zustandsüberwachung sichert höhere Verfügbarkeit, Erneuerbare Energien, 2005.

[2] Heißelmann, H.: Optimierung des Kugelanemometers für die Messung zwei-dimensionaler Strömungen, Diplomarbeit; Oldenburg, 2008.

[3] Siegert, S.; et al.: Analysis of data sets of stochastic systems, Phys. Lett. A, 1998.

[4] Friedrich, R.; et al.: Extracting model equations from experimental data, Phys. Lett. A, 2000.

SESSION 2 – PART B

Wednesday, 30.09.2009

11:30AM

Fatigue Strength of Welded Components of Support Structures of Wind Energy Converters in the VHCF Regime

Schaumann, P.[1)], Steppeler, S.[1)]

[1)] Institute for Steel Construction, Leibniz Universitaet Hannover, Germany

ForWind Center of Wind Energy Research

ABSTRACT

Welded components in wind energy converters may be exposed to more than 10^9 load cycles during their design life. However, experimental results beyond 10^7 are limited. Due to residual stresses welded joints have decreasing fatigue strength with increasing number of cycles in the very high cycle fatigue regime. This paper shows the importance of the planned systematic experimental and numerical investigations. Aim of the planned research activities is to contribute to a reliable prediction of the fatigue behaviour of welded steel structures in the very high cycle fatigue regime.

KEYWORDS

Wind energy converter, support structures, welded joints, residual stresses, fatigue strength, VHCF, fatigue tests

1 INTRODUCTION

Support structures of offshore wind energy converters are designed for a lifetime of about 20 years. They are exposed to high dynamic loads caused by wind, waves and operation and have to resist about 10^9 load cycles. Therefore, fatigue resistance becomes relevant for providing secure service time and economic design. As a result of growing turbine capacity and adverse offshore conditions welded components which are involved in the load transfer need to be checked for fatigue in detail.

2 FATIGUE STRENGTH OF WELDED STRUCTURES OF WIND ENERGY CONVERTERS

2.1 Fatigue strength

In common design rules, fatigue strength curves (Woehler or SN-curves) based on fatigue tests provide a basis for the fatigue assessment. SN-curves are subdivided in different areas: low cycle fatigue (LCF), high cycle fatigue (HCF) and very high cycle fatigue (VHCF), like shown in Figure 1. In the range of valid standards for steel structures like Eurocode 3 [1] or

IIW [2] the transition region of the constant amplitude fatigue limit is defined at $5 \cdot 10^6$ respectively 10^7 load cycles. Stress variation ranging lower than the Cut-Off-Limit of 10^8 load cycles are declared as not damage relevant. Beyond this point the SN-curve is assumed to be a horizontal asymptote. It is considered that there is infinite fatigue life. But several investigations on unwelded and welded components have shown that the fatigue strength is still decreasing with increasing numbers of cycles [5] [6]. In offshore regulations like GL [3] and DNV [4] the Cut-Off-Limit of 10^8 load cycles is not considered, there is finite fatigue life. It is assumed that the SN-curve follows the slope of the HCF regime.

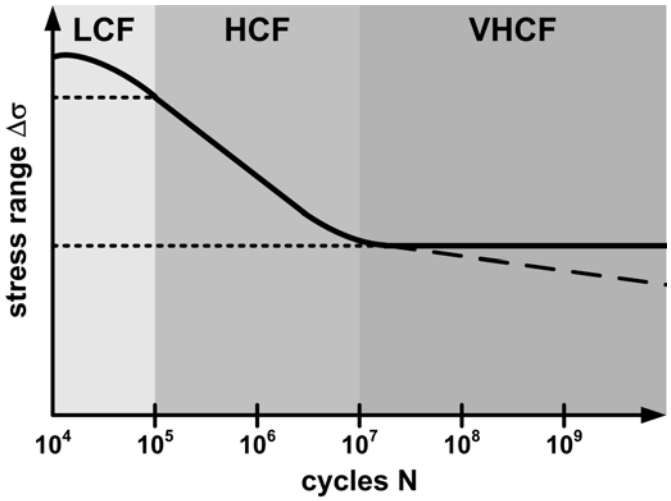

Figure 1: Areas of SN-curves

2.2 Welded Joints

In the field of engineering welded joints are often used, whereas welded steel structures have a large percentage. Welding is a cost saving, fast and efficient joining technique. Many welded steel structures are exposed to cyclic loading and have to resist more than 10^7 load cycles. Besides the static ultimate limit state analysis the fatigue resistance has to be checked. In general, welded joints have representative medium or strong notches. Welded joints belong to the fatigue critical details of constructions. The crack initiation is often located at weld transition or seam root.

The fatigue resistance highly depends on the inhomogeneity of the material. The properties of base and weld metal and the heat affected zone are different. Caused by the locally concentrated input of heat during the welding process high residual stresses or distortions may occur while cooling down. It is a fact that high residual tensile stresses essentially reduce the fatigue life of welded joints. Worst case scenario is that the maximum tensile stresses coincide with the fatigue critical area of the weld seam.

2.3 Fatigue Tests

The areas of LCF and HCF of welded joints are well covered by fatigue tests. But the course of the SN-curve in the VHCF area is still subject of research. Especially the existence of an

endurance limit is strongly discussed. As illustrated in Figure 2, only a small number of experimentally verified results in VHCF regime up to 10^8 load cycles exists. This can be attributed to limited possibilities in testing. To obtain experimental data in the area of VHCF ($N > 10^7$) testing machines with high frequencies are necessary.

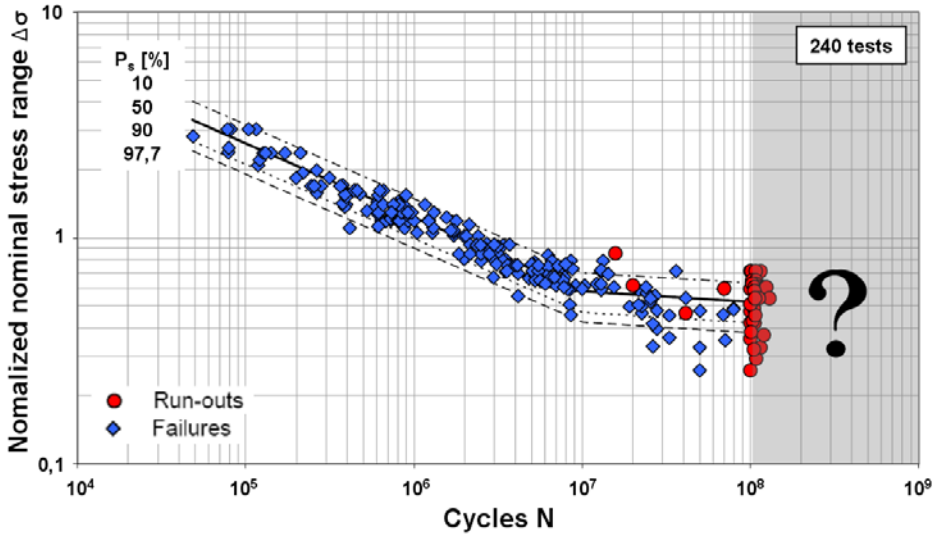

Figure 2: Overview of normalized fatigue tests of welded joints from [3]

There are various options in testing to reach a high number of cycles in a reasonable period of time. Servo-hydraulic fatigue testing machines reach maximum frequencies of 20 Hz, which is not practicable. Resonance testing machines run at maximum frequencies of 300 Hz. This is a more acceptable period of time. Ultrasonic testing machines work with maximum frequencies of 40 kHz. But in case of welded components ultrasonic testing is not practicable, because the production of small non-distorted specimens [6] is difficult.

3 PLANNED RESEARCH ACTIVITIES

With regard to high dynamic loadings of support structures of offshore wind energy converters ($N > 10^9$) the course of the SN-curve of welded components in the VHCF regime becomes relevant. Aim of the planned research activities is to contribute to a reliable prediction of the fatigue behaviour of welded steel structures in VHCF. Here the application of existing fatigue life prediction methods has to be proofed and developed if necessary.

Until now, basically unwelded metals with macroscopic homogeneous structures of unnotched components were investigated in the VHCF regime. Like shown before, the experimental data of welded joints beyond 10^7 is limited. There is the need of experimental and numerical investigations of fatigue behaviour of metallic structures with inhomogeneous material structure caused by the joining technique.

In order to extend the state of knowledge of fatigue strength of welded joints in the VHCF regime ($N > 10^7$) fatigue tests will be performed systematically. Therefore, a new magnetic resonance testing machine with frequencies up to 400 Hz was developed [8]. One test with 10^9 cycles takes about 30 days. Currently, this testing machine is approved.

Furthermore, the influence of residual stresses on the fatigue strength especially in the VHCF regime will be investigated. There is no final clarity how the residual stresses behave under a high number of cycles with low stress amplitudes. In order to get results of the damage development of the specimens, the temporal changes of measuring values of the testing machine and the residual stresses shall be measured. The time-dependent behaviour of the residual stresses will be observed with X-ray diffraction.

Numerical models in macro scale will be applied to define the testing parameters and to classify the experimental results. The numerical models will be fit and verified with the measuring values.

The investigations focus on the analysis of damage mechanisms and the development of damage models in macro scale for predicting the life time reliably.

4 CONCLUSIONS

This paper presents the background of planned experimental and numerical investigations on welded joints in the VHCF regime. The purpose is the extension of the state of knowledge in this field. The aim is to contribute to a reliable prediction of the fatigue behaviour of welded steel structures in VHCF.

BIBLIOGRAPHY

[1] Eurocode 3: Design of Steel Constructions, Part 1. Beuth-Verlag, Berlin (1993).

[2] Hobbacher, A. (Ed): Recommendations for Fatigue Design of Welded Joints and Components. IIW-Document XIII-1965-03 / XV-1127-03, Paris, France 2003.

[3] Germanischer LIoyd WindEnergie GmbH: Rules and Guidelines IV Industrial Services – Guideline for the Certification of Offshore Wind Turbines. Edition 2005.

[4] Offshore Standard DNV-OS-J101: Design of Offshore Wind Turbine Structures. Det Norske Veritas, June, 2004.

[5] Berger, C.; Pyttel, B.; Schwerdt, D.: Beyond HCF – Is there a fatigue limit? Materialwissenschaften und Werkstofftechnik, 2008, 39, No. 10.

[6] Sonsino, C.M.: Course of SN-curves especially in the high-cycle fatigue regime with regard to component design and safty. International Journal of Fatigue 29 (2007).

[7] Sonsino, C.M.; Maddox, S.J.; Haagensen, P.:A Short Study on the Form of the SN-Curves for Welded Details in the High-Cycle-Fatigue Regime. IIW-Doc. No. XIII-2045-05 (2005).

[8] Schaumann, P.; Keindorf, C.; Alt, A.: High frequency fatigue tests on welded joints applying a lately developed magnetic resonance testing machine (Hochfrequente Ermüdungstests an Schweißverbindungen mit einem neu entwickelten Magnetresonanzprüfrahmen). Große Schweißtechnische Tagung, 17.-19.09.2008, Dresden, 2008. (in German)

Influence of Manufacturing Aspects on Fatigue Assessment

Schaumann, P., Mickley, M.

[1)] Institute for Steel Construction, Leibniz Universitaet Hannover, Germany

ForWind Center of Wind Energy Research

ABSTRACT

Within the optimisation process of offshore wind turbine one essential part is the support structure. About 45% of the total costs are required for the fabrication and installation of the support structures. This percentage shows the high potential for decreasing investment cost of offshore wind farms by improving fabrication methods in the future. For jacket structures welded connections are not only the most time consuming working stage for the assembly but also critical details concerning the ultimate and fatigue limit state in design. Against the conventional approach in structural engineering these investigations focus on the already completed structure for getting more information about the influence of manufacturing proceedings on the qualities of the structures. This paper describes the choice of suitable measurement methods, first attempts for their integration in the manufacturing process and the interpretation of measurement data for further proceedings e.g. numerical investigations of the imperfect model.

KEYWORDS

Support structures of offshore wind energy converters, optimisation of design and fabrication, Reverse Engineering, geometrical imperfections, interpretation of laser scan measurement data

1 RESEARCH WITHIN THE GERMAN TEST FIELD “ALPHA VENTUS”

At the German test field “alpha ventus” twelve turbines are being installed in 30 meter water depth at the moment. The improvement and cost-cutting of manufacturing and design becomes more important since thousands of offshore wind energy converters are planned in the North and Baltic Sea in the next years. The German Federal Ministry for the Environment, Nature Conservation and Nuclear Safety (BMU) is funding “alpha ventus” with the research initiative RAVE. Priority objective of the RAVE-project GIGAWIND alpha ventus is cost reduction for support structures of offshore wind turbines, which includes towers, different types of substructures and foundations. This can be divided in designing lighter support structures on the one hand (material cost) and in optimising the design process on

the other hand (personnel cost). Because of the interdisciplinary orientation of the project all civil engineering specialisations are involved within different particular projects. This paper deals with the influence of manufacturing aspects on fatigue assessment which is content of one particular project.

2 WELDED JOINTS AS CRITICAL CONSTRUCTION DETAILS

The currently applied structural and fatigue assessment of support structures for Offshore Wind Turbines is based on common design rules. Normally, constructions in structural engineering are treated as limited, single structures. This means for instance that varying aspects of manufacturing are considered by high safety factors. For manufacturers a change to serial production of support structures is necessary to accommodate the high demand and to stay competitive on the international market. Series production means the chance to improve the quality of the products by a systematic development of facilities accompanying quality management system. But these positive effects are not considered in design standards so far and may result in conservatively designed structures. For this reason, parameters like geometry tolerances and aspects of welding like distortions were measured parallel to the manufacturing to get more information about their development during the production process.

2.1 Geometrical Imperfections

In many cases fatigue assessment is design driver for offshore structures [2] [3]. In particular welded tubular joints are critical details of the investigated jacket structures. Their load bearing characteristics and with it their fatigue resistance significantly depend on geometry. Variations of the planned, perfect shape to the real state of construction are hard to consider during the stage of design. These variations, also referred to as geometrical imperfections, are

- variations of shape, e.g. through buckling or circular runout
- variations of thickness
- axis offset, eccentricity
- geometrical irregularities caused by welds → geometrical notch effect

As one step of evaluation, these exemplified metrological investigations of real existing imperfections can be compared with the tolerances according to standards.

2.2 Purpose and Motivation of Reverse Engineering

In contrast to the design process where details are constructed at the drawing board and then are fabricated, these investigations take the reverse way of regarding the already completed structure [6], see also Figure 1. Parameters like geometry tolerances and aspects

of welding like distortions are surveyed parallel to the manufacturing to get more information about their development during the production process and possible influences on the design. At first the focus is on the choice of suitable measurement techniques and planning and coordinating of the field campaign at the fabrication shop.

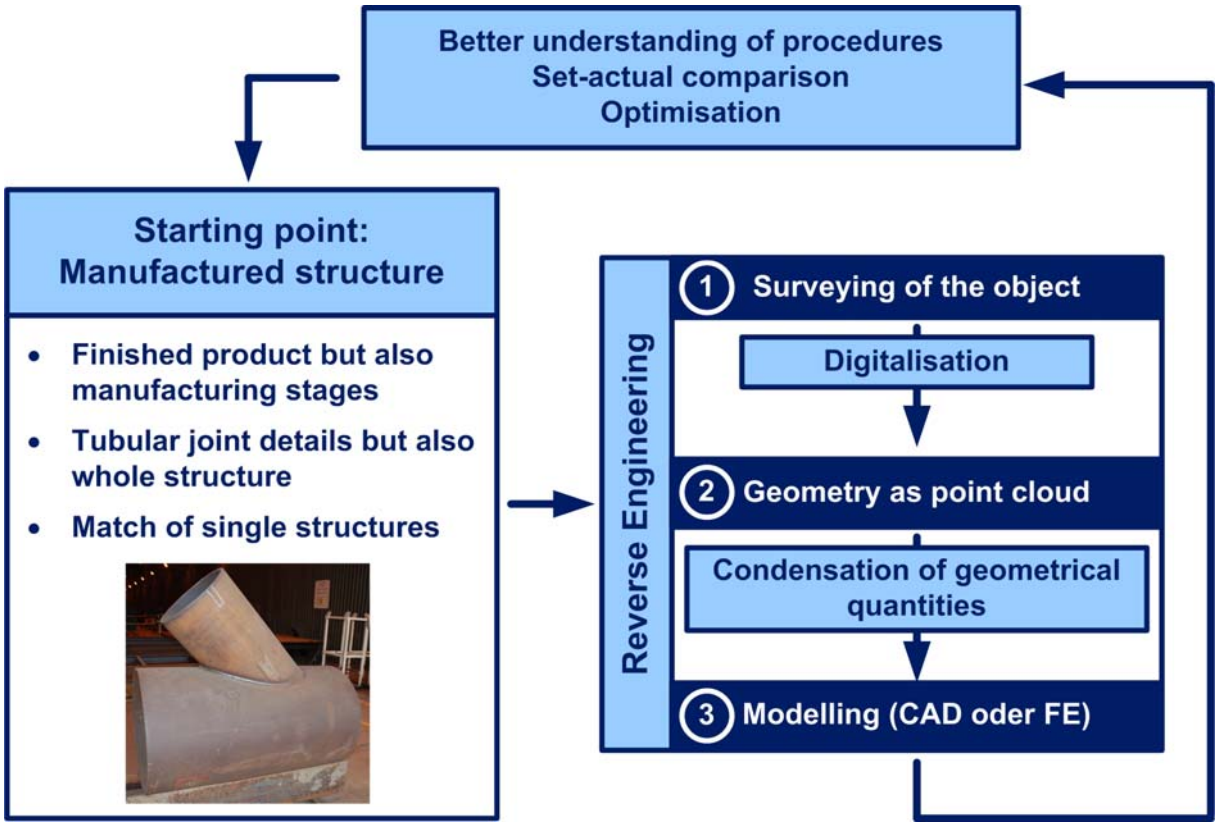

Figure 1: Application of Reverse Engineering

Afterwards methods have to be developed for interpreting and editing the measurement data for further analyses. These might be FE-analyses which base on the imperfect model.

2.3 Laser scanning for Measuring

After discussing different measurement methods, the parallel application of two techniques laser scanning and tachymetry are favoured as fast and most practicable. The preparation is easy and the net measurement time is short. Both techniques were applied during two separate field campaigns. Laser scanning is used in the field campaign of the Leibniz Universitaet Hannover and is described in this paper. At this, the Institute for Steel Construction has been supported by the Institute for Geodesy, Leibniz Universitaet Hannover. Tachymetry is applied by Fraunhofer-IWES.

Laser scanning describes a method where a surface is sampled or scanned using laser technology. The purpose of laser scanning is usually to generate a 3D point cloud which represents the surface of the subject. Then these points can be used to extrapolate the shape of the subject [4][5].

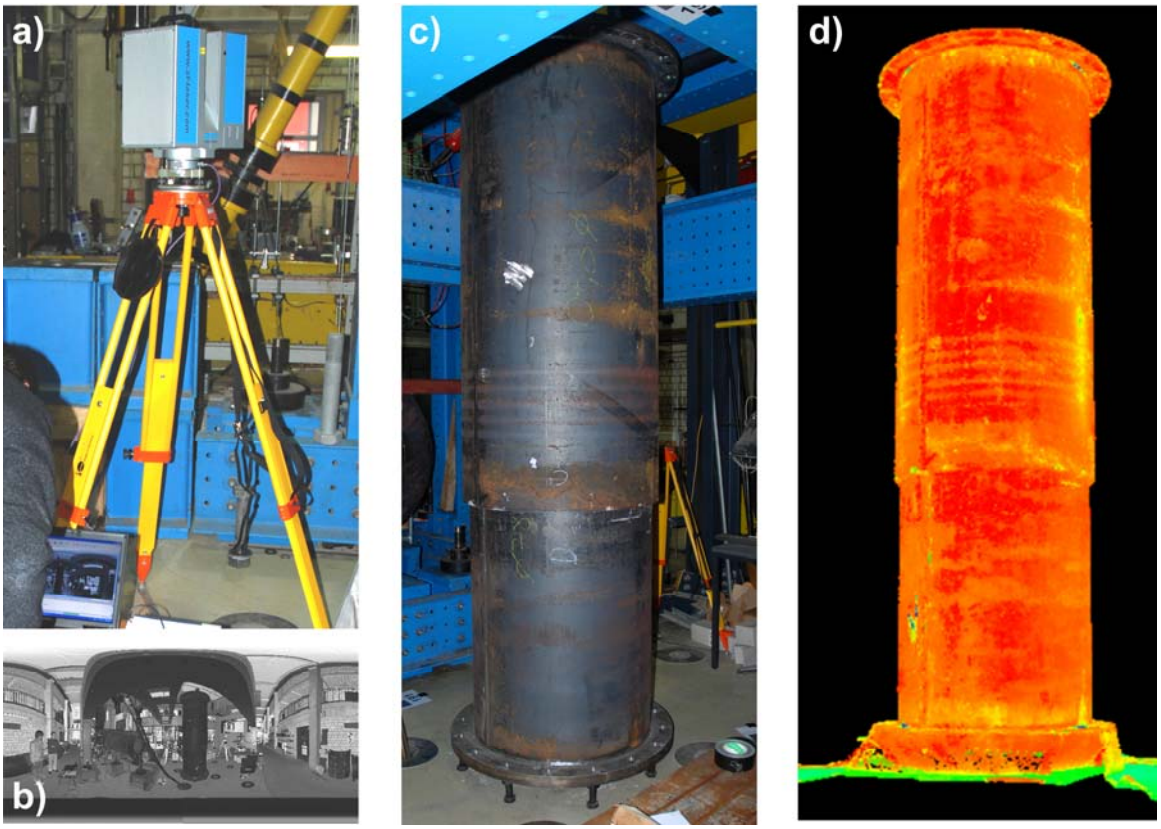

Figure 2 **a)** **Laser scanner Z+F Imager 5006 by Zoller + Froehlich on tripod with computational equipment and laser scan recording**
b) **Laser scan recording of one viewpoint**
c) **Specimen at the testing laboratory of the Institute for Steel Construction**
d) **Digital 3D-model as point cloud**

2.4 Test recording at the testing facilities of the Institute for Steel Construction

For trying laser scanning and the interpretation of the measurement data, test recordings were carried out on a large, tubular test specimen at the laboratory of the Institute for Steel Construction. Figure 2 shows details about the laser scanner, the recorded test specimen and the measurement result. Critical steps of the total proceedings could be identified and the practicability could be proved.

3 ACTUAL STATE OF AFFAIRS

In April this year the field campaign was arranged at a steelwork company in Scotland. Exemplified measurements of welded X-bracings and K-Joints at different production stages, like tack welded and afterwards welded, were arranged. At the moment the measurement data is interpreted and editing for further numerical investigations. Because of the high amount of points this step is very time-consuming. Algorithms have to be developed to reduce the data without influencing the accuracy of the measurements.

4 CONCLUSION AND OUTLOOK

These exemplified measurements signify the potential of integrating modern measurement techniques into the manufacturing process. At the beginning of mass manufacturing of large steel structures this means a great chance for improving quality and decreasing costs. For these developments the automotive industry might be a model. Further investigations of fast and efficient algorithms are needed for an efficient realisation of these measurement systems to check the effect of manufacturing imperfections on structures continuously.

BIBLIOGRAPHY

[1] Schaumann, P.; Mickley, M.; Neuner, H.: Influence of Production Aspects on Fatigue Assessment at Series Production (Einfluss fertigungstechnischer Aspekte auf die Lebensdaueranalyse bei Großserienfertigung), in: Ganzheitliches Dimensionierungs-konzept fuer OWEA-Tragstrukturen im Offshore-Testfeld alpha ventus, GIGAWIND alpha ventus Jahresbericht 2008, www.gigawind.de, 2009, p. 11-20 (in German)

[2] Schaumann, P.; Wilke, F.: Enhanced Structural Design for Offshore Wind Turbines, XICAT 2006, Xi'an International Conference of Architecture und Technology, Xi'an, China, 2006

[3] Schaumann, P.; Böker, C.: Fatigue loading from heavy seas of lattice offshore structures (Ermüdungsbeanspruchung aus Seegang bei aufgelösten Tragstrukturen), Stahlbau (76), Heft 9, S. 620-626, Ernst & Sohn, 2007 (in German)

[4] Kutterer, H.; Pfaffenholz, J.-A.; Veenegeerts, H.: Kinematisches terrestrisches Laser scanning, Zeitschrift für Vermessungswesen 134, Heft 2, S.79-87, 2009

[5] Teutsch, C.: Model-based Analysis and Evaluation of Points Sets from Optical 3D Laser Scanners, Magdeburger Schriften zur Visualisierung, Dissertation, Shaker Verlag, 2007

[6] Raja, V.; Fernandes, K.J.: Reverse Engineering – An Industrial Perspective, Springer-Verlag London, 2008

- Oral presentation only

Reliability Assessment and Reliability-Based Inspection and Maintenance of Offshore Wind Turbines

José G. Rangel-Ramírez[1)], John D. Sørensen[1),2)]

[1)] Aalborg University, Denmark, [2)] RISØ-DTU, Denmark.

ABSTRACT

Probabilistic methodologies represent an important tool to identify the suitable strategy to inspect and deal with the deterioration in structures such as offshore wind turbines (OWT). Reliability based methods such as Risk Based Inspection (RBI) planning may represent a proper methodology to optimize inspection and maintenance (I&M) efforts, entailing to a suitable life-cycle performance without neglecting the economical aspect. Moreover, the integration of condition monitoring information (CMI) can be done through probabilistic inference. In this work, a reliability-based I&M planning OWT is presented where CMI may be incorporated. This framework is addressing to fatigue prone details in support structures for OWT. As part of the results, the life-cycle reliabilities and optimal inspection times are calculated. The influence on inspection times resulting from wind farm location of OWT and data updating is illustrated.

KEYWORDS

Reliability, inspection and maintenance, condition monitoring, fatigue failure, wake turbulence.

1 INTRODUCTION

Risk-Based Inspection planning, understood as an application of Bayesian decision analysis, has been extensively applied in the oil and gas (O&G) industry, see [1], [2] and [3]. The aim is to identify the optimal I&M strategy to "control" of deterioration in the structure, taking into account economical aspects. Unlike other structures with significant consequences of failure, OWTs allow due to their low risk to society, the use of cost-benefit analyses associated to a minimum reliability level. The offshore wind resources have been monitored since the beginning of the 1990's. This information can be integrated into the RBI approach. Site conditions such as deep water depths, waves and turbulence in wind farms, affect detrimentally the life-cycle performance of OWT. At deeper water locations, jacket and tripod type support structures can be expected to be uses in the coming years, making it relevant to investigate the effect of inspection during operation.

It this work is considered RBI planning optimization for fatigue prone details in jacket and tripod types of OWT support structures. Representative limit state equations for ultimate structural fatigue failure using both linear and bilinear SN-curves and for single and wind farm location. The increase of turbulence in wind farms is taken into account using a code-based turbulence model. It is also described how CMI can be integrated into a RBI format.

2 INSPECTION PLANNING AND CONDITION MONITORING

The I&M planning strategies should attain the minimization of overall service life costs while a minimum reliability level for the establish risk acceptance criteria should be achieved. Due to the nature of degradation processes at offshore sites, a probabilistic approach can be a rational tool to deal with a deterioration process where probabilistic and statistical models

can be formulated for prediction including the uncertainties coming from external agents, model uncertainties, human-actions and internal processes.
The decision process can be summarized as follows. The structure is initially designed with dimensions and materials determined according to optimal design parameters $z=(z_1,z_2,...,z_n)$, taking into account code and practical requirements. The installed structure will be affected by external agents, modelled by future random states of nature X_o. Monitoring activities "e" at the times $t=(t_1,t_2,...,t_n)$, including inspection and analyzing actions which result in inspection results "S" that are obtained depending on inspection quality modelled by $q=(q_1,q_2,...,q_n)$. Based on these monitoring results, mitigation alternatives will be considered regarding a fixed or adapting mitigation policy d(S). When these mitigation actions have been done a state of nature X_i will be the beginning of new random outcomes due to the external exposure and damage process. The total service life costs $C_T(z,e,S,d(S),X_i)$ can be optimized by minimizing the expect value of the total costs C_T:

$$\min \mathrm{E}[C_T(z,e,d(S),X_i)] = C_I(z) + \mathrm{E}[C_{Insp}(z,e,d(S),X_i)] + \mathrm{E}[C_{Rep}(z,e,d(S),X_i)] + \mathrm{E}[C_F(z,e,d(S),X_i)] \quad (1)$$

$$z_i^{min} \le z_i \le z_i^{max}, \qquad i = 1,2,...,N$$

$$\Delta P_{F,t}(t,z,e,d(S)) \le \Delta P_F^{max}, \quad t = 1,2,....,T_L$$

T_L is the service life, C_I is the initial costs, $E[C_{Insp}]$ is the expected inspection costs, $E[C_{Rep}]$ is the expected repair costs and $E[C_F]$ is the expected failure costs. Equation (1) is constrained by limits on design parameters and that the annual probability of failure $\Delta P_{F,t}$ has to be less than ΔP_F^{max} at all times, assuring a maximum annual risk-state. The *n* inspections are performed at times t_i, $i=1,\ldots,n$ where $t_o \le t_1,t_2,... .,t_n \le T_L$.
Due to the desire to increase the efficiency and competitiveness of wind industry in compliance with safety standards and requirements, surveillance systems have been developed. External measurements for offshore wind farms have been carried out since the beginning of the 1990's, see [4] and [5], having as main objectives to obtain project-related, long- and short-term data. For CMI, high reliability components are only considered in this work within a RBI framework. For these components, the surveillance activities could be divided in CMS and inspection activities. The inclusion of these data can be achieved through updating of variable and inference of data.

The RBI methodology is concerned with updating using events at the moment of finding the suitable inspection and maintenance strategy. At updating, a limit state function $g(x_1,x_2,\ldots,x_i)$ is formulated as a function of *i* stochastic variables and an event function $h(x_i,x_2,\ldots,x_i)$ representing the new information, is considered jointly. The conditional probability of failure is denoted by $P(g(x_1,\ldots,x_i)\le 0|h(x_1,\ldots,x_i)\le 0)$. In RBI, the limit state function could be related to fatigue failure and the event function can be the no-detection-of-cracks at the inspection. Bayesian statistical methods can be used to update the density functions $f_{xi}(x_i,q_i)$ of stochastic variables x_i considering the vector of the distribution parameters q_i as uncertain.

3 PROBABILISTIC MODEL

The probabilistic models for assessing the fatigue failure life based on SN-curves and fracture mechanics (FM) model are briefly mentioned. For RBI planning the FM model is usually calibrated to result in the same reliability level as the code-based SN model. To evaluate the fatigue life is used the probabilistic model for fatigue failure described in [6], [7] and [8]. For the free flow ambient turbulence conditions and the assessment of the SN-fatigue life, the design equation is written:

$$G(z) = 1 - \frac{\nu \cdot FDF \cdot T_L}{K_C} \int_{U_{in}}^{U_{out}} D_L(m;\sigma_{\Delta\sigma}(U)) \cdot f_U(U)\, dU = 0 \quad (2)$$

where D_L stand for the accumulated damage for a linear and bi-linear SN-curve, ν is the total number of fatigue load cycles per year, FDF is the fatigue design factor ($FDF=T_F/T_L$), K_C is the characteristic value of *K*, U_{in} and U_{out} are the cut-in and -out wind speed, $f_U(U)$ is the density function of mean wind speed *U*. $\sigma_{\Delta\sigma}(U)$ is the standard deviation at mean wind speed *U*. The corresponding limit state equation is written:

$$g(t) = \Delta - \frac{\nu \cdot t}{K} \int_{U_{in}}^{U_{out}} \int_{0}^{\infty} (X_W \cdot X_{SCF})^m \cdot D_L\left(m; \alpha_{\Delta\sigma}(U) \frac{\sigma_u(U)}{z}\right) \cdot f_{\sigma_u}(\sigma_u \mid U) \cdot f_U(U)\, d\sigma_u\, dU \quad (3)$$

where Δ is a stochastic variable modeling the uncertainty related to the Miner rule for damage accumulation, *t* is the life time in years, X_W is the model uncertainty related to wind load effects, X_{SCF} is the model uncertainty related to local stress analysis. The assessing of the fatigue failure life based on FM-approach is described in [8].

4 APPLICATION EXAMPLES

A steel jacket support structure of an OWT is considered. The OWTs are assumed to have an expected lifetime equal to 20 years and design fatigue life times (T_F) of 40, 50 and 60 years. For the Influence coefficient the mudline bending moment for a pitch controlled wind turbine is used as a representative function in the support structure and/or transition node. SN-Linear (L) and bilinear (BL) curves will be considered for In-wind farm location (IWF) and single/alone (S) OWT. The design value "*z*" for each case is shown in table 1. In figures 1 and 2 are shown the results of the assessment of the reliability with SN- and FM-approach. The reliability indices β and Δβ are related to the cumulative probability of failure (P_F) and the annual probability (ΔP_F) of failure. The results in table 1 show that the design values for cases IWF are larger than the ones for free flow turbulence. This is due to the additional accumulation of fatigue from wake turbulence. For all cases the FM model is calibrated considering the reliability indices in the interval from 10 to 20 years (figure 2) and their respective inspection in this interval. There will be inspections in the remaining part of the lifetime that were not included.

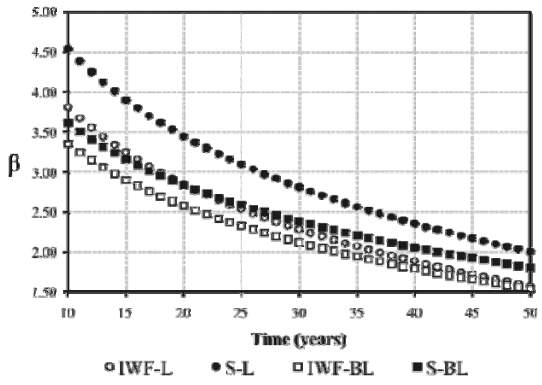

Figure 1. Reliability indices for SN-approach corresponding to an cumulative probability of failure of case A with T_F=50 years.

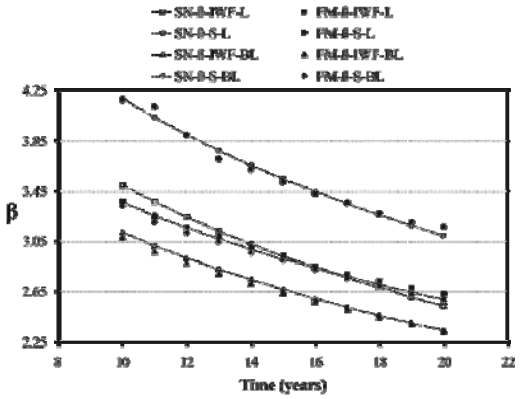

Fig 2. Reliability indices for SN- and calibrated FM-approach corresponding to the cumulative probability of failure of case A with T_F=40 years.

In Figure 1 and 2 are shown the resulting life-cycle assessment of reliability with SN and FM approach. In table 1, inspection times are shown determined with a maximum acceptable annual probability of failure equal to 1.0×10^{-4}. Comparing the first inspection time, slightly earlier inspections are needed in wind farm sites due to the increase of fatigue coming from wake turbulence even though the design parameter *z* is larger. As expected lower uncertainty for the model uncertainties implies that the first inspection will come (significantly) later. It is noted that in all four cases the design parameter z is determined by deterministic design such that the code-based design criteria is exactly satisfied.

Table 1.Inspection times corresponding ΔP_F^{max}=1x10^{-4} and z-design parameter

T_F	CASE	z	Inspection times (year)
40	IWF - L	0.4939	9
	S - L	0.4309	17
	IWF - BL	0.3841	6
	S - BL	0.3306	8
50	IWF - L	0.5321	12
	S - L	0.4642	--
	IWF - BL	0.4049	9
	S - BL	0.3482	11
60	IWF - L	0.5654	18
	S - L	0.4934	--
	IWF - BL	0.4253	11
	S - BL	0.3657	15

5 CONCLUSIONS

The approach represents a viable method to obtain reliability based inspection and maintenance plans for fatigue critical details in offshore wind turbines, especially details in the tower and the support structure. The use of the RBI framework for wind farms may potentially be beneficial for optimizing the inspection and maintenance efforts, generating inspection plans assuring fulfillment of acceptance criteria for the whole wind farm. Furthermore, the approach could also be applied as a decision tool for estimating the consequences of a possible service life extension. In this paper is described the integration of CMI using Bayesian updating. Besides of being applied to high reliability components, this approach for updating within a RBI framework may be also used on different components with lower reliability levels having the proper limit state equations relating the real-time information coming from the measuring devices for different components.

ACKNOWLEDGEMENTS

The financial support from the Mexican National Council of Science and Technology (CONACYT) is greatly appreciated.

BIBLIOGRAPHY

[1] Faber, M.H., Engelund, S., Sørensen, J.D., and Bloch, A., Simplified and Generic Risk-based Inspection Planning, 2000, Proc. Int. Conf. Offshore Mech. & Arct. Eng, S&R paper 6143.

[2] Sørensen, J. D. & M.H. Faber, M.H., Generic inspection planning for steel structures, 2001, Proc. International Conference on Structural Safety and Reliability, ICOSSAR'01, USA.

[3] Moan, T., Reliability-based management of inspection, maintenance and repair of offshore structures. 2005, Structures and infrastructure Engineering, Vol.1, No.1, 33-62.

[4] Barthelmie, R., Hansen, O.F., Enevoldsen, Karen, Højstrup J., Frandsen, S., Pryor S., Larsen S., Motta M, Sanderhoff P., 2005. Ten Years of Meteorological Measurements for Offshore Wind Farms. Journal of Solar Energy Division of The American Soceity of Mechanical Engineers. May 2005, Volume 127, pp. 170-176.

[5] Frandsen S., Chacón L., Crespo A., Enevoldsen P., Gómez-Elvira R., Hernández J., Højstrup J., Manuel F., Thomsen K. and Sørensen P., 1996. Final Report on Measurements on and Modelling of Offshore Wind Farms, Risø-R-903(EN), Risø National Laboratory, Bonus Energy AS, Universidad Politecnica de Madrid, Elkraft AS, Finish Meteorological Institute.

[6] Frandsen, S., 2005. Turbulence and turbulence-generated structural loading in wind turbine clusters, Risø National Laboratory, Denmark, Report R1188.

[7] Sørensen, J.D., Frandsen, S. & Tarp-Johansen, N.J., 2007. Fatigue reliability and effective turbulence models in wind farms. Applications of Statistics and Probability in Civil Engineering -Kanda, Takada & Furuta (Eds).

[8] Rangel-Ramirez, J.G. & Sørensen, J.D. 2008. Optimal Risk-Based Inspection Planning for Offshore Wind Turbines. International Journal of Steel Structures. Volume 8(4), pp. 295-303

Risk-based operation and maintenance of offshore wind turbines

Jannie Jessen Nielsen[1)], John Dalsgaard Sørensen [1,2)]

[1)] Department of Civil Engineering, Aalborg University, Denmark

[2)] Wind Energy Division, Risø-DTU, Denmark

ABSTRACT

Operation and maintenance for offshore wind turbines is a large contributor to the total cost. Today corrective maintenance is usually used, meaning that components are repaired after they fail. The use of condition-based maintenance based on Bayesian decision theory has the potential to minimize the costs to operation and maintenance, and hereby increase the overall benefit. This paper outlines the basic concepts of condition-based maintenance.

KEYWORDS

Operation and maintenance, corrective maintenance, condition based maintenance, offshore wind turbines

1 INTRODUCTION

Costs to operation and maintenance for offshore wind turbines can be very large compared to other costs, and can be expected to increase when wind farms are placed at deeper water depths and in more harsh environments. For other offshore installations such as oil & gas installations, cost-effective procedures for risk-based inspection planning have been developed during the last 10-15 years and are used at several locations worldwide [1]. These procedures are based on pre-posterior Bayesian decision theory [2].

Maintenance activities can be divided in corrective and preventive maintenance, where the latter covers both planned and condition-based maintenance. Optimal the maintenance should be planned using a risk-based approach with pre-posterior Bayesian decision theory, as described in [3], with the use of observations from condition monitoring and inspections.

2 OPTIMAL PLANNING OF INSPECTION AND MAINTENANCE

2.1 Life Cycle Decision Model

A decision tree related to the life cycle of an engineering structure such as a wind turbine or wind farm is shown in Figure 1. The decisions taken by the decision maker (designer / owner / …) and observations of uncertain parameters that are unknown at the time of the decision are:

- At the design stage a decision on the optimal design parameters is made which in principle should maximize the total expected benefits minus costs during the whole lifetime such that safety requirements are fulfilled at any time.
- During the lifetime continuous monitoring of the wind turbines and inspections of critical components are performed. These are indicated in the box 'repeated inspection/maintenance' in Figure 1. Each box consists of: (1) a decision on times and types of inspection / monitoring for the rest of the lifetime; (2) observations from inspection / monitoring; (3) decision on eventual maintenance / repair based on the inspection / monitoring results.
- Realisation of uncertain parameters such as wind and wave climate, strengths, degradation, model uncertainties will take place during the lifetime.
- The total cost is the sum of all costs in the remaining part of the lifetime after the time of the decision.

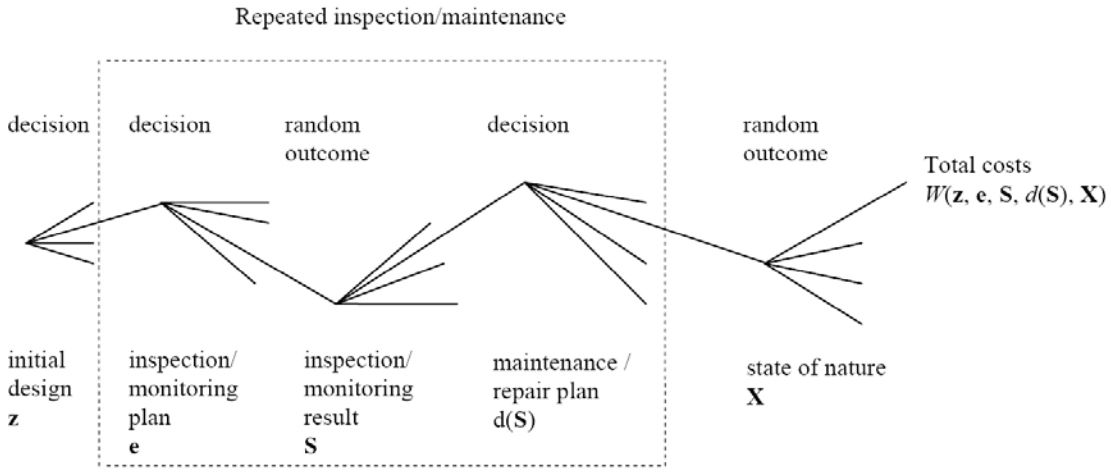

Figure 1: Decision tree for optimal operation and maintenance planning [3]

2.2 Damage and Uncertainty Modelling

Deterioration mechanisms such as fatigue, corrosion, wear and erosion are associated with significant uncertainty. Observations of the degree of damage $D(t)$ can increase the reliability of predictions using Bayesian statistical techniques as illustrated in Figure 2. Generally an inspection at time T_1 and associated maintenance/repair will decrease the uncertainty and the expected mean damage level at time T_2 will be smaller since most realizations with large damage level at time T_1 can be expected to be maintained / repaired.

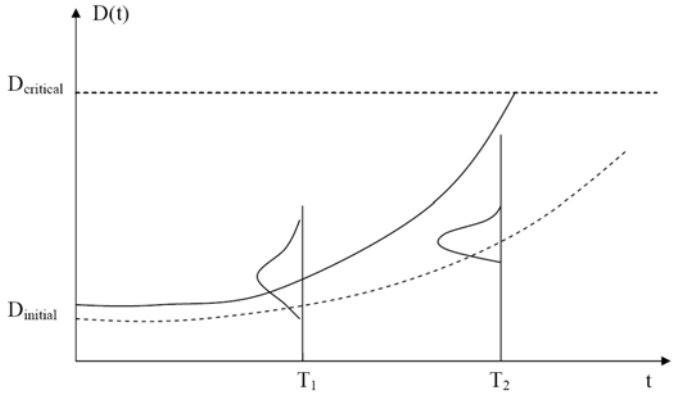

Figure 2: Damage model and updating by inspection at time T_1 [3]

2.3 Cost-Benefit Models for Optimal Decision Making

The aim is to maximize the total gain minus the costs, W, and the optimization problem can basically be written

$$\max W = B - C_I - C_{IN} - C_{REP} - C_F \quad (1)$$

where B is the benefits, C_I is the initial costs, C_{IN} is the inspection and service costs, C_{REP} is the repair and maintenance costs and C_F is the expected failure costs, and all values are functions of the design parameters, decision parameters for inspections, and decision rules for repairs.

3 COMPARISON: CORRECTIVE OR CONDITION-BASED MAINTENANCE

For corrective maintenance the costs (or lost benefit) are due to lost production, repair of damaged components and escalated damage due to failure of components. In condition-based maintenance monitoring and inspections will give an additional cost, but lost production and escalated damage is decreased. Simulation techniques can be used to determine the optimal planning for a given case. The major contributors to uncertainty should be included in the model, and are described in the following.

3.1 Uncertainties and Parameters

The weather has a major influence on several aspects within operation and maintenance of offshore wind turbines, e.g. damage accumulation, weather windows for repair, and (lost) production. The parameters in the damage model for the different components will vary due to natural variations in execution, and the model is uncertain too. When an inspection is performed, there is a probability that the damage is not found. This is described with a POD (probability of detection) curve, and in general it is easier to detect a larger damage. Also there is a possibility of false detections of damages that do not exist. When damage is detected, a decision rule determines whether a repair should be carried out. Optimal the decision rule should be based on a risk analysis for the rest of the lifetime of the component, but a simpler rule with a limit damage level might be easier to use. Dependent on the weather it might not be possible to access the wind turbine with a boat for some time, and the additional cost of a helicopter should be held against the expected cost of failure and loss of production. Often it will be less expensive to execute the repair before the component has actually failed. Of course the inspections will only have a positive effect, if the damage does not happen too abrupt to be detected during inspections.

4 CONCLUSIONS

A risk-based approach for planning of operation and maintenance of offshore wind turbines is described. Simulation techniques can be used to assess the gain of the use of condition-based maintenance compared to e.g. corrective maintenance.

5 ACKNOWLEDGEMENT

The work presented in this paper is part of the project “Reliability-based analysis applied for reduction of cost of energy for offshore wind turbines” supported by the The Danish Council for Strategic Research, grant no. 2104-08-0014. The financial support is greatly appreciated.

BIBLIOGRAPHY

[1] Moan T. Reliability-based management of inspection, maintenance and repair of offshore structures. Structure and Infrastructure Engineering 2005; 1: 33-62.

[2] Benjamin JR, Cornell CA. Probability, Statistics and Decision for Civil Engineers. McGraw-Hill: New York, NY, 1970.

[3] Sørensen JD. Framework for Risk-based Planning of Operation and Maintenance for Offshore Wind Turbines. Wind Energy 2009; 12: 493-506.

SESSION 3

Wednesday, 30.09.2009

2:30PM

Condition Monitoring of Wind Turbines

Christopher J Crabtree [1], Peter J Tavner [1]

[1] Durham University School of Engineering and Computer Sciences, UK

ABSTRACT

Condition monitoring (CM) of wind turbines (WT) is assuming greater importance as the installed capacity of wind turbines increases. This paper briefly describes a test rig for the development of CM techniques for WTs. The test rig includes features of a WT including its variable speed and torque nature, a simple gearbox, induction generator and grid connection. 'Fault-like perturbations' are applied to the rig and signals recorded and analysed. This paper gives an example of fault detection in the three phase power signal by tracking fault frequencies using a wavelet energy tracking method.

KEYWORDS

Condition monitoring, drive train, power signal,

1 INTRODUCTION

WTs are fast becoming one of the major sources of renewable energy in the UK with over 3.7GW currently installed on UK networks [1]. The move to offshore development is primarily a result of increased wind speeds, lower turbulence levels and the resulting higher capacity factor. However, these benefits lead to harsher operating conditions and a need for improved monitoring and maintenance strategies. Tavner et al. [2] have demonstrated that failures in the drive train result in large downtimes and high costs. This research aims to further the understanding of CM of WTs through the development of a test rig and the application of signal processing techniques. CM of rotating machines is well understood for large, high speed rotating machines but has not been widely investigated for wind turbines with low speed shafts and highly dynamic variations in torque and speed. The test rig allows repeatable driving conditions to be applied to the drive train. The research investigates the possibility of using the generator three phase power signal as an available and global source of drive train information.

2 CONDITION MONITORING TEST RIG

2.1 Drive Train Layout

The test rig consists of a 30kW wound rotor induction generator being driven through a two-stage gearbox by a 54kW DC motor. The driving conditions are controlled by a LabVIEW control environment which also acts as a data acquisition system sampling at 5kHz. The test rig is shown in figure 1. The test rig is fitted with two tachometers, an accelerometer on the gearbox or generator and a torque transducer and x-y displacement sensors on the high speed shaft.

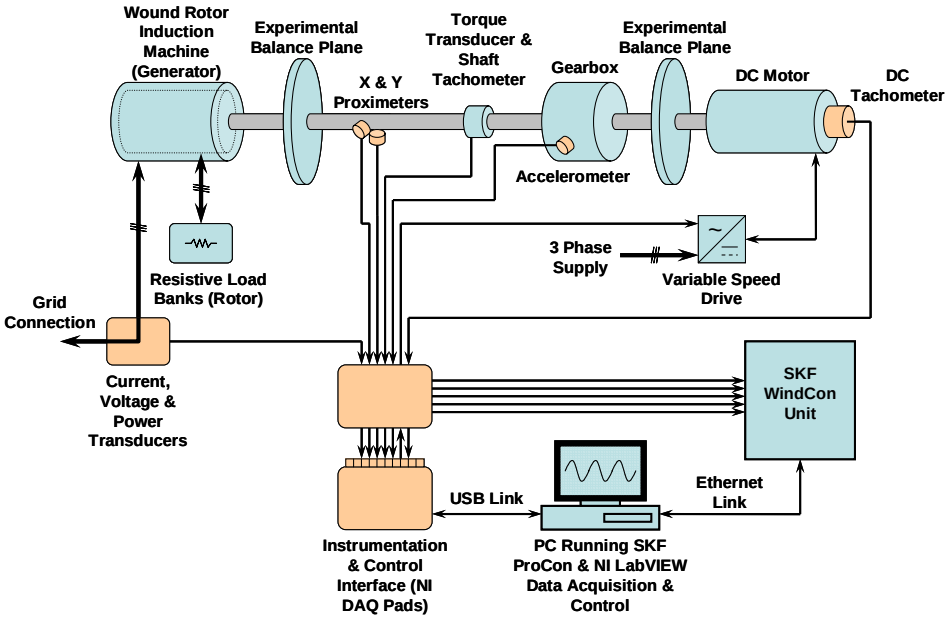

Figure 1: Durham University Condition Monitoring Test Rig

The rig is also fitted with current and voltage transducers allowing for the calculation and frequency analysis of the instantaneous three phase power signal. Resistive load banks on the rotor circuit allow electrical asymmetry to be applied to the generator and experimental balance planes are mounted on the low and high speed shafts to emulate mass unbalance.

2.2 Driving Conditions

A WT drive train is subject to highly dynamic speed and torque changes and it is important that any CM technique is capable of dealing with these. The test rig is driven using data from a detailed 2MW turbine model developed at the University of Strathclyde as part of the Supergen Wind Energy Technologies Consortium at two mean wind speeds, 7.5m/s and 15m/s, and two levels of turbulence, 6% and 20%, representative of normal and turbulent conditions offshore. An example of the 7.5m/s, 20% turbulence driving condition is given in figure 2. It can be seen that the resulting three phase power and shaft torque signals feature highly variable amplitudes over time.

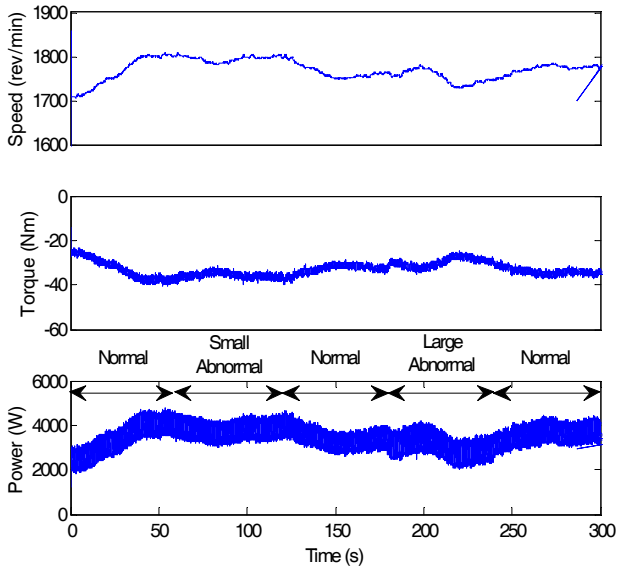

Figure 2: Example speed, torque and three phase power measurements taken from the Durham University test rig under fault testing

3 EXAMPLE RESULTS

3.1 Electrical Asymmetry of the Generator Rotor

To demonstrate the variable nature of monitoring signals the test rig was driven under wind driving conditions and asymmetry applied periodically as shown in figure 3 with different severities. The signals recorded from this test are shown in figure 2.

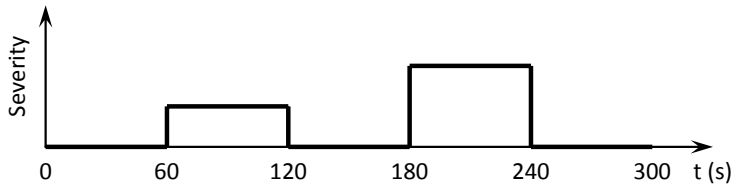

Figure 3: Electrical asymmetry applied to the generator rotor

It can be seen from figure 2 that the variable level of three phase power has masked any clear change as a result of the fault being applied and so it is necessary to track a known fault-related frequency. In this case the frequency twice slip frequency ($2sf_{se}$) was tracked as this is characteristic of an electrical asymmetry and its frequency is shown in figure 4. Using an energy tracking method based on the wavelet transform [3] developed at Durham University we can extract the energy in this frequency and this is shown in figure 5. It can be seen that the small asymmetry applied in the period 60-120s is not easily detectable however the larger asymmetry applied in the period 180-240s is clearly visible in the result.

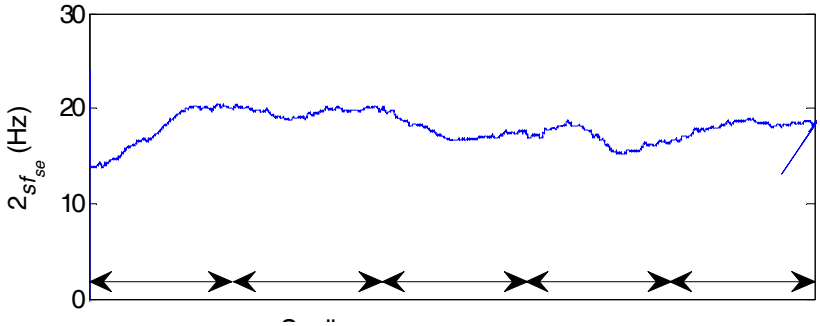

Figure 4: Value of frequency $2sf_{se}$ being tracked

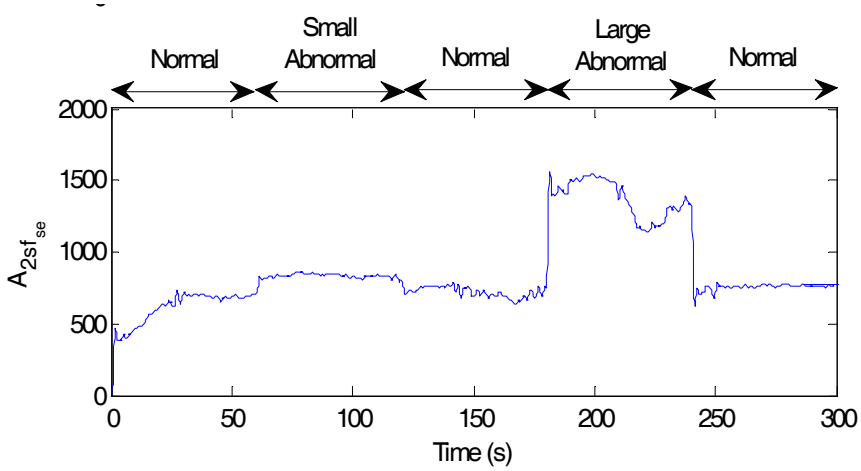

Figure 5: Energy in the frequency $2sf_{se}$ extracted using the wavelet transform

4 CONCLUSIONS

It can be seen that condition monitoring of wind turbines will play an important role in improving the reliability of the technology and that techniques will need to be developed to deal with highly dynamic signals being generated in the turbine drive train. This work has demonstrated that faults are detectable in the electrical power signal without the need for complex and expensive transducers.

Future work will aim to detect a greater range of fault conditions and to improve the quality of detection algorithms with the aid of the test rig.

BIBLIOGRAPHY

[1] BWEA UK Wind Energy Database, www.bwea.com/ukwed/index.asp

[2] Tavner PJ, van Bussel, GJW and Spinato, F. Machine and Convertor Reliabilities in Wind Turbines, 3rd International IET Conference, Power Electronics, Machines and Drives, Dublin, 2006

[3] Yang, W, Tavner, PJ, Crabtree, CJ, Wilkinson, MRW, Cost-Effective Condition Monitoring for Wind Turbines, IEEE Transactions on Industrial Electronics, In Press, 2009.

Systems Engineering based Tero-technology: A methodology and applications within wind power system

Idriss El-Thalji

School of Technology and Design,
Växjö University, SE-35195,
Växjö, Sweden. 2009

ABSTRACT

The ongoing research in Vaxjo University is currently focused on using systems engineering approach for analysis and design of operation and maintenance system and their practices within wind power system. The research work started since 2007 as a reviews for the current maintenance practices of wind power system based on researchers' perspective, and another review highlighted the practitioners'' perspective and their requirements for more cost-effective maintenance strategy. Recently, the research coupled with Swedish wind research projects to investigate the physical failures on wind turbine's gearbox and their terotechnolocial impact.

KEYWORDS

Operation & maintenance, Tero-technology, Systems Engineering, Wind power system

PAPER ABSTRACT

Inappropriate maintenance of complex technical wind power system is the main reason of increasing the cost of energy per production unit and energy losses due to unavailability and performance losses appropriate strategy and technology of maintenance has the key role to design cost-effective maintenance. This task demands long term preparations and noticeable financial investment that shortly produces measureable benefits. In this paper, systems engineering approach used for analysis and design the technical and terotechnical characteristics of operation and maintenance system and energy efficiency. The result of ongoing research work in Vaxjo University point that beside failures of technical system due to their stakeholders faults, large percentage of unavailable time and performance losses is due site and season characteristics which are not taken in designer consideration. In this paper, a developed model of analysis and design the terotechnical aspects of wind power system, particularly, the operation and maintenance system using Systems Engineering have been conceptually constructed and phased into five phases from the situational analysis consists of defining life cycle processes, stakeholders and their requirements, in addition to investigation of the physical failures classified based on site and season characteristics, that cover the Swedish wind farms' issues which are varying as onshore, offshore applications and cold climate effects, in order to achieve an optimized life cycle cost and competitive cost of energy.

Analysis of wind turbine data with a view towards load monitoring

Claudia Hofemann[1)], Herman Frederik Veltkamp[2)], Gerard van Bussel[1)]

1) TU Delft, Netherlands, 2) Vestas R&D Global Research, Netherlands

ABSTRACT

The objective of this PhD research is to develop a method to use standard signals such as rotor speed, electrical power, pitch angle, etc. for load monitoring. The proposed method will allow to reconstruct the particular mechanical loading experienced by any turbine in the field. The site specific feedback on the actual fatigue loads experienced by the turbine will make it possible to improve wind turbine design parameters and to adjust the design lifetime.

KEYWORDS

Wind turbine loads, load monitoring, neural networks, SCADA signals, load reconstruction, design parameters

1 INTRODUCTION

Due to the high costs of measurement equipment and the large effort of post-processing and evaluating the collected data, the loading of wind turbines is not generally monitored. As a consequence, very little is known about the load history for most of the many existing turbines. Besides information about energy production, operating hours, maintenance and repair activities, the turbine's performance and especially its dynamic behavior is only known from a few verification turbines. This does not necessarily reflect the real conditions at a particular site properly.

SCADA data, as signals indicating the wind speed, electrical power and the pitch angle, is available for these turbines. The objective of this PhD research is to develop a method of using these easily accessible signals to reconstruct the mechanical loading experienced by a wind turbine.

2 METHOLOGIE

The reconstruction of mechanical loads acting on wind turbines will be realised by implementing an Artificial Neural Network (ANN).

An Artificial Neural Network is a non-linear statistical data modelling tool which is self learning. During the learning phase, the system can change based on external or internal information, which is feed into the network. Thus, the network can adapt to changing external conditions, as for example different streaming conditions (free stream conditions or wake effects). Those networks are typically used to model complex relationships between in- and outputs or for pattern recognition.

Previous work as the flight leader project by ECN [1] or the work performed by Nicolai Cosack from the University of Stuttgart [2] demonstrated that ANNs are an appropriate method to perform load monitoring using only SCADA data.

Correlations between load indicators and the SCADA data will be established by training the ANN with verification data. As a second step the established relationships will be applied to another turbine of the same type located at another site.

To be able to correctly reproduce the mechanical loads seen by the turbine the relations between SCADA signals and load indicators have to be as precise as possible. To achieve an accurate description of the relationships inside the ANN, the environmental conditions as well as the turbines' operational modes as power production, parked, etc. have to be characterised beforehand [1].

To implement the network on wind turbines located at different sites a catalogue needs to be developed categorizing the environmental conditions as wind profile, turbulence intensity or temperature profiles regarding to their influence on the wind turbine's behaviour.

At ECN, a similar project, aiming to prove that the knowledge gathered via one verification turbine can be transferred to another turbine within this specific wind park, has been developed. The flight leader project, using SCADA signals as well, has shown that a reliable prediction of mechanical loads via neural networks within one wind park is possible. By now the project has been tested on two turbines of the ECN Wind Turbine Test Site Wieringermeer and shown that ANN techniques can be used for accurately estimating load indicators using only 10-minute statistics of standard SCADA parameters [1]. Whereas the flight leader project focuses on a implementation of the system within a wind park, creating the need to equip at least one wind turbine per wind farm with measuring devices, this project focuses on the development of a method allowing to reconstruct the mechanical loadings for a complete wind turbine fleet.

The ANN will be trained and verified with data obtained from verification turbines located at different sites. Afterwards, to achieve a greater topographic variance the code will be extrapolated using the commercial wind turbine fleet.
To narrow down the input feed into the ANN, only data logged by Vestas V90 wind turbines will be used. Once the approach has been implemented, the method will be applied on other turbine types to test if and under what circumstances an adoption of the network is possible.

3 CONCLUSIONS

This research projects looks into the loads of wind turbines induced by the environment.
The aim of this project is to develop a method that allows to reconstruct and to predict site specific loads without the need to equip commercial wind turbines with additional sensors.
The derived results can be used for site specific optimisation of turbine parameters, long-term operation control, and validation of design parameters. Furthermore this tool will make it possible to correlate component failures with loading.

BIBLIOGRAPHY

1

[1] Obdam, T.S.; et al.: Flight Leader Concept for Wind Farm Load Counting and Performance Assessment, European Wind Energy Conference 2009,Marseille, France, 16-19 March 2009

[2] Cosack, N.; et al.: An Approach for Fatigue Load Monitoring without Load Measurement Devices, European Wind Energy Conference 2009,Marseille, France, 16-19 March 2009

Please note that all papers should be less than 4 pages.

Please indicate whether you wish to present your paper by

- Oral presentation only
- Poster only (posters should be printed and brought to Durham by the participant)
- Both oral presentation and poster

Wake Skew Angle Variation with Rotor Thrust for Wind Turbines in Yaw Based on the MEXICO Experiment

Daniel Micallef[1)], Carlos S. Ferreira[2)], Tonio Sant[3)]

[1)] DUWIND, TUDelft, The Netherlands and University of Malta, Malta, [2)] DUWIND, TUDelft, The Netherlands, [3)] University of Malta, Malta.

ABSTRACT

The primary objective of the MEXICO (Model Experiments in Controlled Conditions) project was to generate experimental data from which the uncertainties of the computational tools employed to predict wind turbine performance and loads. Pressure sensors were used for pressure measurements while PIV was used with the major aim of tracking the tip vortex trajectory. The aerodynamic forces on the blades were derived found from the pressure measurements and were used in an inverse free wake lifting line model to compute the positions of the tip vortices. From these the wake skew angle was derived. A relationship between the skew angle and the thrust coefficient was thus drawn.

KEYWORDS

Yaw, Skew Angle, MEXICO experiment.

1 INTRODUCTION

The pressure measurements were carried out for both axial and yawed flow conditions with yaw angles of 15, 30 and 45 degrees. For the PIV measurements data was gathered for axial flow but only for the 30 degree yaw case for a single tip speed ratio. A three bladed rotor was used with a diameter of 4.5m and 0.42m hub diameter. For the blade geometry and other details the reader is referred to [1]. Pressure measurements were first validated and used to find the loads acting on the rotor. In this study, an inverse free wake model [2] was used for all of the yaw angles to obtain the skew angles. The forces were prescribed to the program and the induced velocities calculated in an iterative manner until the angle of attack converged. The wake geometry for a number rotor revolutions (depending on the tip speed ratio) was obtained from the inverse free wake model for the mentioned yaw angles for four different tip speed ratios (4.18, 5.55, 6.68 and 10) with a rotor speed of 424.5r.p.m and with wind speeds of 10, 15, 18 and 24 m/s. From the wake geometry a relationship can be obtained between the skew angle and the thrust coefficient obtained from experiment.

This relationship was also investigated by W. Haans et al. [3] by means of an experiment of a yawed rotor at TUDelft.

2 RELATIONSHIP BETWEEN SKEW ANGLE AND THRUST COEFFICIENT

2.1 Methodology

In order to obtain an estimate of the skew angle, a graphical procedure was employed. A line, oriented at an angle equal to the rotor yaw angle was constructed to be used as reference. Another line at the rotor yaw angle was constructed but this time joining the vortex cores of the wake sheet boundary. If the line cannot pass through the cores exactly, the position of the line and its length are adjusted to another position which intersects an interpolation line passing through the vortex cores. The process is repeated for all the blades for a number of revolutions determined by the numerical stability of the inverse free wake model. The midpoint of each and every line is hence determined and a line of best fit is passed through these midpoints. The angle of this line may then be found and was denoted by θ. The skew angle is then given by

$$\chi = \gamma + \theta \tag{1}$$

An example is shown in figure 1 for the 30 degree yaw and wind speed of 10m/s.

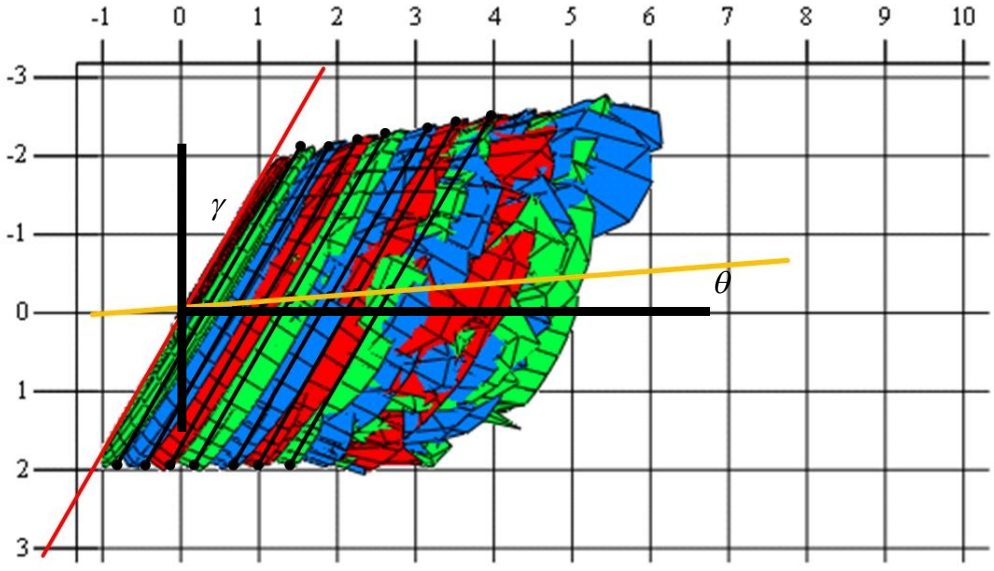

Figure 1: Wake geometry as obtained from the inverse free wake model and geometrical construction of θ.

2.2 Derivation of a linear relationship between skew angle and thrust coefficient

The skew angle was found for each yawed flow case by means of the inverse free wake code. The thrust coefficients were obtained from the MEXICO data for each test case. The thrust coefficient will vary with azimuth but an average was taken over all rotor revolutions.

The relationships between skew angle and thrust coefficients are shown in figure 2. This is consistent with the results found from Haans et al [3].These linear fits can be represented by means of the linear expression:

$$\chi_\gamma = k_1 \cdot C_T + k_2 \tag{2}$$

for $\gamma \in [15°, 30°, 45°]$. Table 1 shows the intercept and gradients for the linear fit described by eqn. (2).

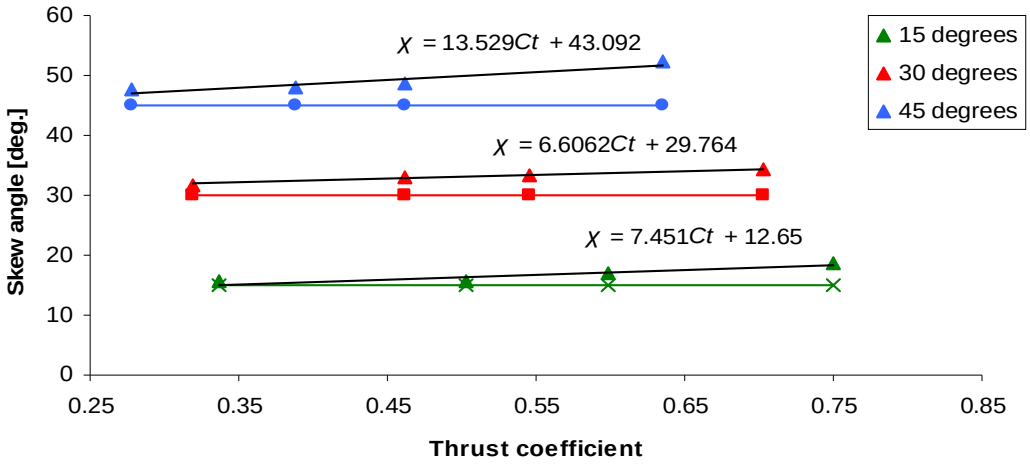

Figure 2: Skew angle against thrust coefficient for different rotor yaw angles. Coloured lines show the yaw angle while bold black lines show a linear fit for the skew angle.

Table 1: Intercept and gradients for linear fit for different yaw angles

γ [deg.]	k_1	k_2
15	13.529	43.092
30	6.6062	29.764
45	7.451	12.65

A general relationship can be found in terms of the yaw angle by considering these gradients and the intercepts. For the axial flow condition the skew angle must necessarily pass through 0. Figure 3 shows linear fits of the gradient and intercept with yaw angle. For a higher order approximation more points would be required but the MEXICO data is limited to just three yaw angles. The linear fits shown in figure 3 seem to make sense as the data points do not show too much scatter. Further investigation can however be done in future experiments with a larger number of data points. The linear equations for the gradient and intercept are also shown on figure 3. Using these equations in (2) and rounding up:

$$\chi \approx \gamma\left(0.3C_T + 1\right) \tag{3}$$

3 CONCLUSIONS

In this paper, the MEXICO experimental data was used as an input to an inverse free wake vortex model. From the wake geometry a relationship was obtained between the thrust and the skew angle. It was found that the rate of increase of the skew angle with thrust coefficient increases with rotor yaw error. This was expected since the induced velocities at high yaw angles will deflect the wake in a more pronounced manner. In future work, a PIV experiment will be performed for yawed conditions at TUDelft and more yaw angles will be considered to be able to reconstruct a higher order relationship between thrust coefficient and skew angle.

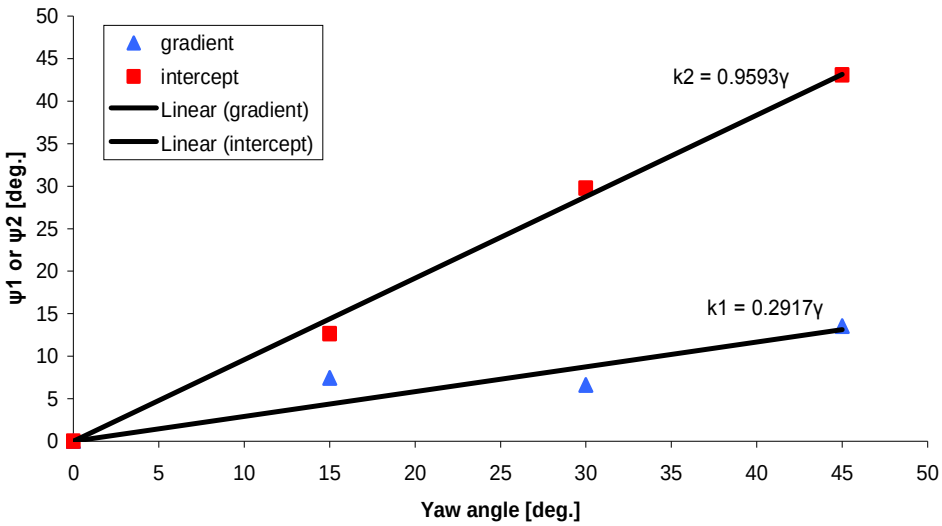

Figure 3: Linear fits for gradient and intercept quantities in terms of the yaw angle.

BIBLIOGRAPHY

[1] Model Experiments in Controlled Conditions (MEXICO) - Final Report

[2] T.Sant: Improving BEM Based Aerodynamic Models in Wind Turbine Design Codes. PhD thesis, TUDelft.

[3] W. Haans, T. Sant, G.A.M. van Kuik and G.J.W. van Bussel, Measurement of Tip Vortex Paths in the Wake of a HAWT Under Yawed Flow Conditions, Journal of Solar Energy Engineering, Vol. 127, No. 4, November 2005, pp. 456-463.

Details of a Medium Scale Wind Turbine Based on the Brushless Doubly-Fed Machine

Thomas Logan[1)], Joseph Warrington[1)], Shiyi Shao[1)], Richard McMahon[1)]

[1)] University of Cambridge, United Kingdom

ABSTRACT

This paper describes the design and implementation of a 20kW wind turbine recently installed in Cambridge with a Brushless Doubly-Fed Machine (BDFM) as its generator. The BDFM is a medium speed generator suitable for direct grid connection in which variable speed operation is possible with only a fractionally rated power converter. Details of the machine design and performance are presented along with a description of the machine controller and the system to maximise the output of the turbine.

KEYWORDS

Brushless Doubly-Fed Machine, BDFM, DFIG, Maximum Power Point Tracking

1 INTRODUCTION

The Brushless Doubly-Fed Machine (BDFM) is an electrical generator with similar properties to the Doubly-Fed Induction Generator (DFIG) in that variable speed operation is possible with a converter rated at only a fraction of the machine rating [1]. However, due to the BDFM's design the brush contacts to the rotor are eliminated, increasing machine reliability and lowering maintenance requirements. This is particularly beneficial for wind turbines located off-shore where maintenance costs are high.

This paper details a practical implementation of a 20kW BDFM-based wind turbine erected by the authors (in collaboration with Durham University) in Cambridge in March 2009. The mechanical parts of the turbine were supplied by Gazelle Wind Turbines and the BDFM was designed to replace the squirrel-cage induction machine normally used. The hub height is 13 metres and the blade swept diameter is 11 metres. It is of a free-yaw, downwind design. A photograph of the turbine as installed can be seen in Fig. 1.

Figure 1: Photograph of the wind turbine as installed in Cambridge.

2 BDFM

The BDFM employs two stator windings, which produce airgap fields of different pole numbers in order to avoid transformer coupling between them. These fields do, however, both couple to the rotor. In normal use one winding, termed the power winding (PW), is assumed to be connected to the mains, while the other, termed the control winding (CW), is fed a variable voltage at variable frequency from a bi-directional converter and sees only a certain fraction of the total power flow. Manipulation of this feed controls the power factor and rotor speed. Full details of BDFM operation (such as its equivalent circuit) can be found in [1]. Its typical electrical connection can be seen in Fig. 2.

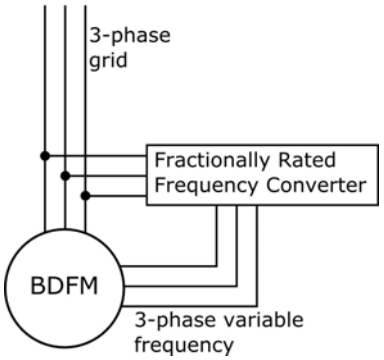

Figure 2: Typical connection of the BDFM

2.1 Design

The first step in BDFM design is to choose the appropriate pole number combination. In its normal operation the mechanical rotor speed ω_r is related to the stator winding frequencies ω_1 and ω_2 by [1]:

$$\omega_r = \frac{\omega_1 + \omega_2}{p_1 + p_2} \tag{1}$$

where p_1 and p_2 are the pole-pair numbers of the two stator windings. The pole-pair combination (and the converter size) is determined by the required deviation from the natural speed, the synchronous rotor speed when $\omega_2 = 0$. [1] shows the nominal converter rating required for an ideal BDFM is given by $S_2=|\omega_2/\omega_1|S_1$ (where S_1 is the PW apparent power), which with equation (1) shows that for a rated speed of 750rpm at 50Hz (with a gearbox ratio of 7.1:1) with a 50% rated converter the sum of the pole pairs must be six, thus a 4-pole/8-pole BDFM was chosen. With the pole-pairs chosen a design procedure based on magnetic and electrical loadings can be followed (detail to be published soon), in this case to rewind an existing 4-pole induction machine. The key dimensions of the BDFM are:

Stator bore diameter	200 mm	Stator 1 / 2 pole pairs	04/08/09
Stack length	292 mm	Stator 1 / 2 turns	176 / 336
Airgap thickness	0.65 mm	Stator 1 / 2 slot area	42% / 58%
Natural / Rated speed	500 rpm / 750 rpm	Stator 1 / 2 current rating	18.4 A / 13.7 A

2.2 Performance

BDFM performance is best summarised on an operating chart like that of the synchronous machine (with a separate chart for each operating speed) [3]. The continuous operation chart for the BDFM at 750 rpm calculated from measured machine parameters can be seen in fig.

3, in which the three ellipses are the three stator heating limits, all of which must be observed. Preliminary tests show that final winding temperatures at some points on the edge of the safe region are 120ºC or less suggesting that the area is safe but rather conservative for windings rated for 155ºC. The thermal time constant of the machine is approximately 30 minutes so for duty-cycle operation (such as the gusty wind conditions experienced by the turbine) the short-term peak output can be rather higher than suggested by the chart.

3 SYSTEM IMPLEMENTATION

The wind turbine system relies on a number of interacting systems shown in the block diagram of Fig. 4.

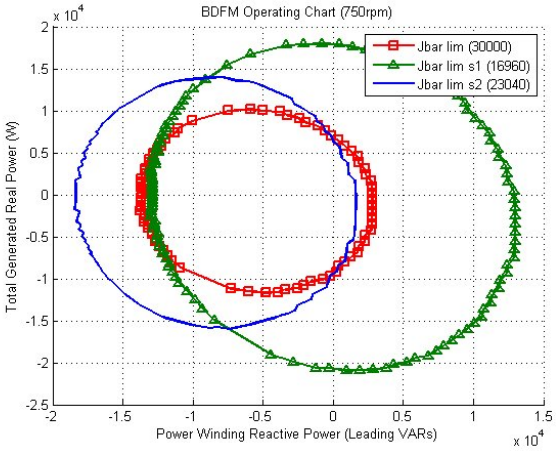

Figure 3: Operating chart for the BDFM at 750rpm

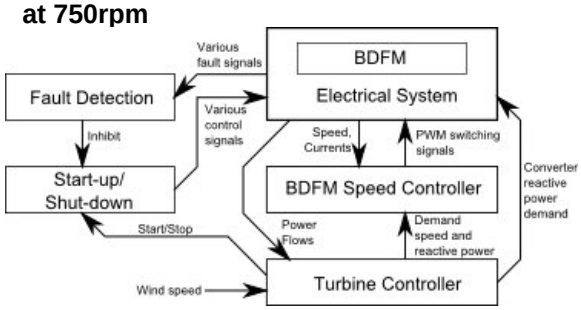

Figure 4: Block diagram of the wind turbine showing its constituent subsystems.

3.1 BDFM Speed Controller

The speed controller system manipulates the magnitude and phase of the voltage applied to the control winding to make the BDFM achieve a desired torque and speed to match the wind torque. This is achieved via a vector control scheme oriented with PW flux reference frame, in which two PI controllers manipulate quantities v_{2q} and v_{2d} to regulate the shaft speed and PW reactive power respectively in a scheme fully described in [3].

3.2 Turbine Controller

The outer stage of the turbine control system is to manage the machine speed (and so tip-speed) in order to extract the most energy from the current wind conditions and to make the turbine operate at a reasonable power factor. Speed control is achieved with a maximum power point tracking (MPPT) routine[2]. In this scheme the speed is periodically adjusted and the short-term average output power at the new speed compared with the average output power at the original speed. If the power output improves the speed is again adjusted in the

same direction, otherwise it is adjusted in the opposite direction, thus moving the rotor speed to the optimum value. This system also manages stopping the turbine in periods of low wind.

4 PERFORMANCE

Detailed high-resolution measurements of turbine performance have been available for several weeks and show the performance of the turbine and the MPPT algorithm. Some data covering the period of the 14th and 15th July 2009 is shown in figure 5. Firstly the figure shows that the wind conditions are rather poor at the site and the wind is very gusty. This is as expected because the turbine is located on an urban site chosen for its location on Engineering Department land. The spiky nature of the graph shows that for relatively small gusts of say 6m/s the turbine may output 5kW if it is properly aligned with the wind but that very often the turbine is not properly aligned.

Operation of the MPPT routine can be seen in the figure. After around 16,000 seconds the wind energy (proportional to v^3) increases, and the tracker increases the rotor speed in response and the turbine produces a larger power output. This continues until the wind speed drops, power output decreases, and eventually the blade rotation slows to the lower speed limit in response. The resulting reduction in power loss is shown in the period after 44,000 seconds. Note that ordinarily the turbine would be deactivated with such a drop in wind speed and power output, but here the effect of MPPT is being demonstrated.

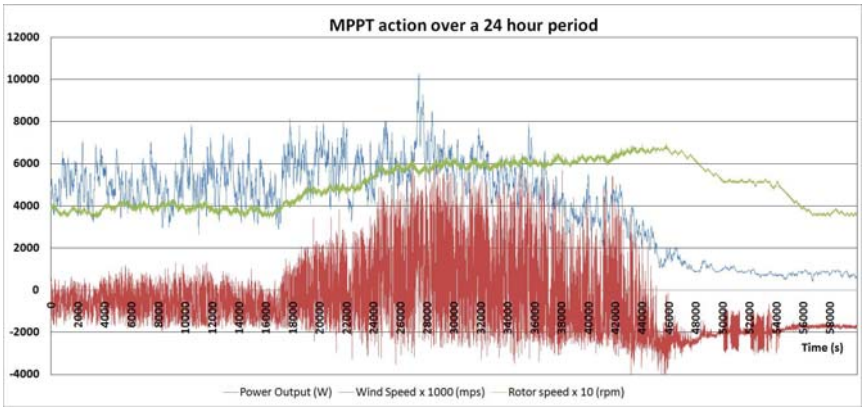

Figure 5: Operating data for the wind turbine over the period of the 14th and 15th July 2009 showing wind speed and power output

5 CONCLUSIONS

From this work we can conclude that a BDFM-based wind turbine is practical. We may also conclude that the speed control and MPPT algorithms presented work effectively. Though the siting of the turbine is not ideal, from the modest wind resource available the system is able to generate significant power. The 4/8 BDFM design works well but is larger than the 4-pole induction machine it replaces due to its high number of poles and slower speed. Future work will also consider the 2/6 BDFM, which potentially offers a higher power density.

BIBLIOGRAPHY

[1] The BDFM as a Generator in Wind Turbines, McMahon, R. A.; Wang, X.; Abdi-Jalebi, E.; Tavner, P. J.; Roberts, P. C. & Jagiela, M., 12th International Power Electronics and Motion Control Conference, 2006. EPE-PEMC 2006

[2] Practical Deployment of the Brushless Doubly-Fed Machine in a Medium Scale Wind Turbine; Logan, T., Warrington, J., Shao, S., McMahon, R.; IEEE International Conference on Power Electronics and Drive Systems 2009, PEDS 2009.

[3] Operating charts for the Brushless Doubly-Fed Machine (BDFM); T. Logan and R. McMahon; IEEE International Electric Machines and Drives Conference, 2009. IEMDC '09.

[4] Shao S. Abdi E. Barati F. McMahon R. Stator Flux oriented Vector Control for Brushless Doubly-Fed Induction Generator, IEEE Transactions on Industrial Electronics, 2009.

Modeling and Simulation of Long Time Behaviour of Alpha Ventus Wind Farm and Coupling to WCMS

H. Guo, Z. A. Styczynski

Otto-von-Guericke-University Magdeburg, Germany

ABSTRACT

This paper deals with the model development and exemplary simulation performance of long time behaviour of the first German offshore wind farm (WF) alpha ventus as well as its coupling to the Wind Farm Cluster Management System (WCMS). In order to investigate the long time behaviour of the alpha ventus a simulation model based on the characteristic power curve of the wind turbines (WT) has been developed. The dynamic characteristics of the WT are not considered in this model, since the purpose of the study is to develop and validate a model for behavior analysis of the WF on a long time scale taking into account the influence of the WCMS, and to give some relevant suggestions for an optimal integration of additional large scale offshore generation into the operation of the whole power system.

KEYWORDS

Wind farm model, long time simulation, wind farm cluster management system (WCMS)

1 INTRODUCTION

The technology of the WTs as well as the wind energy industry and market has rapidly developed in the past decades. The global installed wind energy capacity has increased significantly and the additional new large scale installations are planed in the offshore sector for the near future. The analysis of WFs behavior and its influence on the grid became an important issue, which requires the development of the appropriate simulation models. In reference [2] some different WT models have been defined. According to the analysis issues and problem to be solved the WFs can be modeled in different detail grades. Generally, the simulation issues of a WF could be divided into two types: time independent and time dependent [3]. The dynamic models, which have the maximal simulation time step up to 10 ms, are used to analyze different disturbances, e.g. faults. Static WT models have a lower detail grade than dynamic models and are usually used in the first phase of WF planning to estimate and predict the power output as well as to analyze an optimal active and reactive power control strategy. In this paper a WF model developed within the framework of the RAVE project is presented that has been designed for analysis of long time behavior of the WF.

2 MODELING OF ALPHA VENTUS WINDFARM

2.1 General

The alpha ventus wind farm is the first offshore wind farm in Germany. In this wind farm 12 wind turbine (6 Multibird M5000 and 6 REpower 5M) are planned to be installed and each of them will have 5 MW rated power. The total capacity of this wind farm will be 60 MW. Figure 1 shows the general structure of the alpha ventus wind farm.

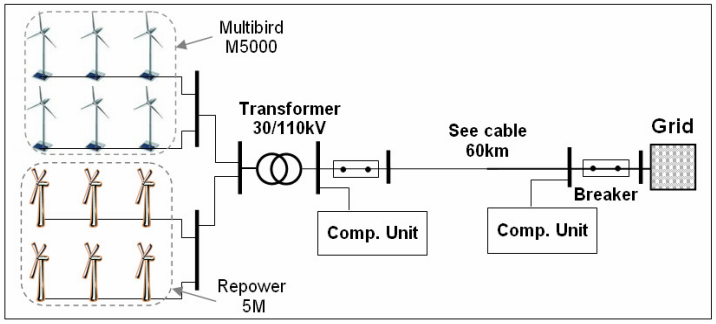

Figure 1: Wind farm structure for alpha ventus

2.2 Wind farm model

The purpose of the WF model in this paper is to provide a model that will be used to investigate the long time behaviour of the alpha ventus WF. The model should be able to calculate the WF power output based on the predicted wind profile. Furthermore, it will be able to evaluate the power losses and the voltage status taking into account the allowable operational characteristics of the WTs such as active versus reactive power capability curve or the allowable gradients of active and reactive power as well as the state of the compensation units. The WT models have been developed based on the power performance curve of the WT, which is characteristic for each different turbine typef. With such a curve, as presented in Figure 2 (left), it is possible to calculate the power output of a WT without considering all of the technical details that are relevant especially for dynamic behavior [1]. Furthermore, with this model the reactive power output of the WT can be estimated since the reactive power capability characteristic is considered, Figure 2 (right).

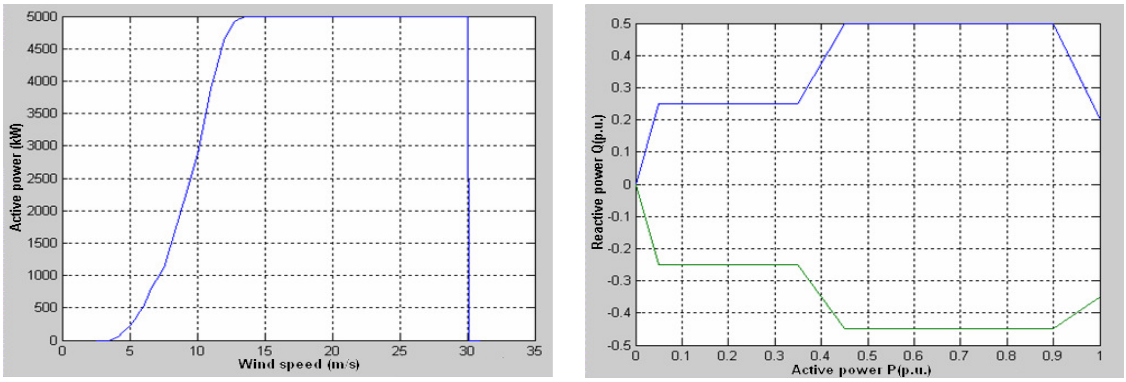

Figure 2: Exemplary power performance curve (left) and PQ-capability curve (right) of a WT

Figure 3 shows the general structure of the developed WT model with coupling to the WCMS. The WCMS role is to set an optimal point of operation (P_{REF_CM}, Q_{REF_CM}) for the wind farm. Using the mentioned WCMS reference signals and predicted wind profile as input to the WT model the active and reactive power output can be calculated. In this way different scenarios considering, e.g. daily or monthly power generation profiles, can be analyzed to gather information about the impact of the WCMS on the grid integration of an offshore wind farm and its influence on the power system operation.

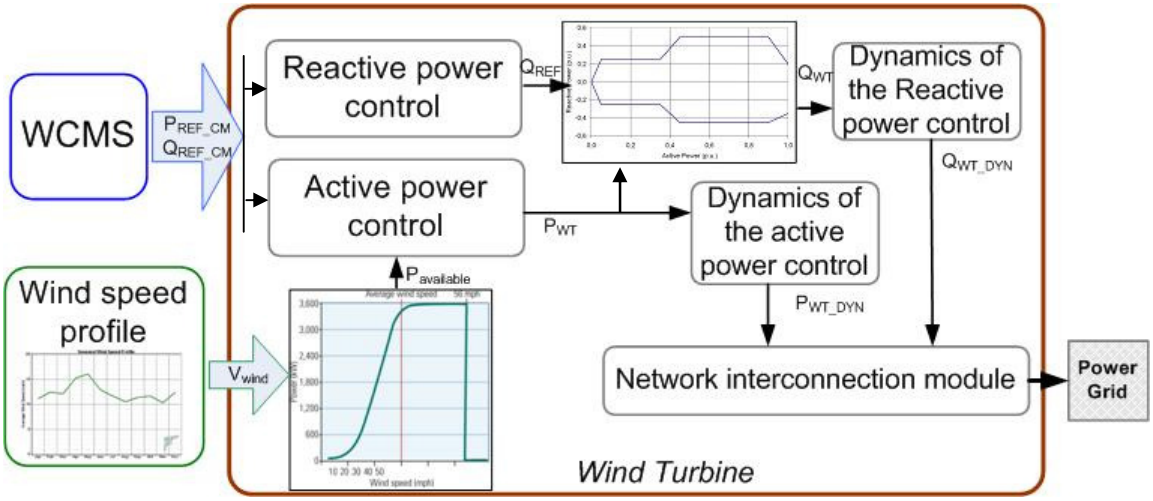

Figure 3: General structure of the wind turbine and coupling to WCMS

3 SIMULATION AND RESULTS

The wind turbine model was developed with “Var P-/Q regler” by using simulation software PSS^{TM}NETOMAC [5]. The simulation time period of 24 hours was chosen, with the simulation time step of 10 seconds. The wind farm was assumed to be operated with a power factor of 0.95 (capacitive), so that the wind farm was able to provide the power grid with reactive power. Figure 4 shows the simulation results. The wind speed in time series is used as input and it could be obtained from the wind speed prediction approach. P-request is the active power which is delivered from the WCMS. It represents the desired active power of the wind farm, and the actual active power will be limited so as not exceed the requested power. The reactive power control insures that the actual reactive output not exceed the maximum of the reactive power limit of the wind turbines. In Figure 4 the voltage of the wind farm at the low voltage side of the transformer is plotted. The aggregative control of the active-/reactive power output of the wind farm can be achieved with the WCMS. The coupling of the wind farm model with WCMS will be implemented through the exchange of information about the required power (power set points) and wind speed information (predicted), and after carrying this out the simulation results will be returned to WCMS. The power factor, the voltage level and frequency will also be observed and appropriate strategies will be applied in case some abnormal situation occurs.

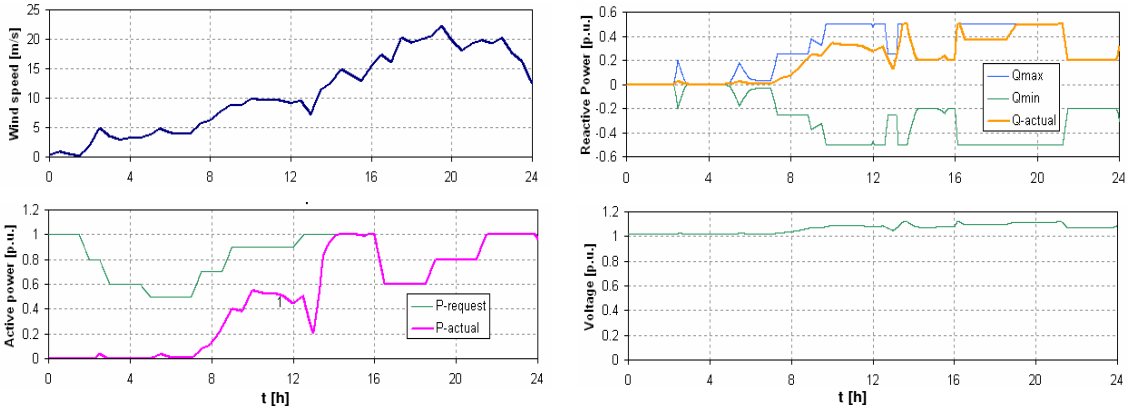

Figure 4: Simulation results of wind farm Alpha Ventus

4 CONCLUSIONS

In this paper a model for the alpha ventus offshore wind farm is described, in which the generation units are modeled with the characteristic power performance curve of the wind turbines. The simulation results show that this model is able to describe the long time behaviour of the wind farm with regard to control of wind farm power output according to requested power and the reactive power limitation in coupling with WCMS.

BIBLIOGRAPHY

Hui Guo studied electrical engineering at the Zhen Zhou University, China and then at the Otto-von-Guericke University, Germany. He graduated in 2008 with a Master of Science degree and then joined the Chair of Electric Power Networks and Renewable Energy Sources at the Otto-von-Guericke University Magdeburg, Germany as a research assistant and also a Ph.D student.

Zbigniew Antoni Styczynski became the Head and the Chair of Electric Power Networks and Renewable Energy Sources of the Faculty of Electrical Engineering and Information Technology at the Otto-von-Guericke University, Magdeburg, Germany in 1999. Since 2006 he has also been the president of the Centre of the Renewable Energy Saxonia Anhalt. His special field of interest includes electric power networks and systems, expert systems and optimization problems. He is a senior member of IEEE PES, a member of CIGRE SC C6, VDE ETG und IBN and a fellow of the Conrad Adenauer Foundation.

[1] J.F.Manwell, J.G. McGowan, A.L. Rogers.: Wind Energy Explained- Theory, Design and Application, John Wiley&Sons Ltd, September 2002.

[2] Technical Guidelines for Wind Turbines, February 2008, www.wind-fgw.de.

[3] K. Rudion Aggregated Modelling of Wind Farms. Res Electricae Magdeburgenses, Magdeburger Forum zur Elektrotechnik.

[4] www.alpha-ventus.de/index.php.

[5] https://www.energy.siemens.com/CMS/US/US_PRODUCTS/PORTFOLIO/PTIPSSOFTWARE/Pages/PSSNETOMAC.aspx.

SESSION 4 – PART A

Wednesday, 30.09.2009

4:00PM

What Does a Floating Offshore Wind Turbine Look Like?

Karl O. Merz

Technical University of Norway (NTNU), Trondheim, Norway

ABSTRACT

It is attempted, with partial success, to answer the question posed in the title of this paper. The answer, although not yet certain, appears to be: not wildly different than an onshore wind turbine which happens to be floating.

KEYWORDS

Design, floating, vertical-axis, H-rotor

1 INTRODUCTION

The obvious answer to the question posed in the title of this paper is that a floating offshore wind turbine looks more or less like an onshore wind turbine which happens to be floating. This answer is probably correct. That is to say, because the physics of the atmosphere are not drastically different between the coastline and the adjacent water, a design that is optimized for installation at the coastline will probably look similar to one that is optimized for installation on the water. So a floating offshore wind turbine is a three-bladed (or maybe two-bladed), pitch-regulated (or maybe stall-regulated, or maybe pitch-to-stall), upwind (or maybe downwind) propeller-like rotor, mounted atop a tubular (or maybe truss) tower, which extends deep into the water as a ballasted spar (or maybe is held by taut cables as a tension-leg platform, or maybe floats atop a large barge). Right?

Yes. Probably. But there is a problem: a floating version of an onshore wind turbine may not be good enough. Past studies, Table 1, indicate that the levelized cost of energy of a floating offshore wind turbine is approximately twice that of an onshore wind turbine. Too expensive. It will be difficult to convince people to pay for your turbine if, in exchange, you offer to double their energy costs.

2 COSTS

Why are floating wind turbines so expensive? Several reasons, all unavoidable. One of these is shown in Figure 1. In the mind of a structural engineer, the most fundamental representation of a wind turbine is a thrust load (from the air on the rotor) and a gravity load (from the mass of the rotor, nacelle, drivetrain, and electrical gobbledygook). In deep water, the load path to the ground is much longer, which means more structure.

Another reason that floating wind turbines are so expensive is that they are difficult to maintain and repair. A few months ago, I was at a meeting with some representatives from the Norwegian energy

karl.merz@ntnu.no

industry, who are kind enough to sponsor this research. One of the presentations at this meeting showed some very cool robots, whose job it was to attempt to keep the gangway between a ship and a wind turbine reasonably stable, so that a technician could climb aboard the turbine, and then be rescued, without too much danger. An alternative was to rappell in from a helicopter. With large wind farms, it was suggested that for operation and maintenance purposes it would be most cost-effective to have a manned, floating "base" to which turbines could be towed for maintenance.

Yet another reason that floating wind turbines are expensive is that they are out on the ocean, and so a connection to the electrical grid has to be put out there, too.

So, floating wind turbines are expensive. What can we do? They could be installed onshore, instead. But people do not like wind turbines in their backyard, or on their favorite island or beach; sometimes they get very upset. (http://www.vernkysten.no/) And if enough turbines will be installed to make any difference in global fossil fuel use, they are going to have to be *everywhere*. (See appendix.) Could some other form of renewable energy be used? In part, yes, but it turns out that the alternative sources are not widespread enough (tidal currents, geothermal), they are environmentally damaging if deployed on a massive scale (hydroelectric, biofuel), they are not available everywhere year-round (solar), or they are expensive, too, as expensive as floating wind turbines (waves and some of the others). [15] One feasible alternative is nuclear energy, if the waste and weapons problems have solutions.

Maybe now the fact that floating wind turbines are two times too expensive does not sound quite so bad, at least not bad enough to abandon the idea upfront.

3 DESIGN CONCEPTS

Costs may be unavoidable, but at least they can be minimized by selecting an optimal design. As stated before, an optimal floating wind turbine probably looks very similar to an optimal onshore wind turbine.

That "probably" in the previous sentence bothered me. How probable is "probably"? Thus began this research project.

Let's pretend that the optimal floating wind turbine (call it a "floater", for short) does not look similar to the optimal onshore wind turbine. Then, what does it look like?

1. It is a lift-based device, not a drag-based device.

2. It is not dramatic, in the sense of having any giant cowlings or wind-concentrating devices, or other enhancements that are never seen (for cost reasons) on onshore wind turbines.

3. It is a single-turbine construction. That is, any material that would be used to structurally connect one turbine with an adjacent turbine will instead be used to obtain greater keel depth, for stability.

4. It is simple and robust. It has a minimum of moving parts. To the greatest extent possible, it exchanges active systems (which require maintenance) with passive structures (which do not).

The third point, if you agree with it, suggests that indeed our pretend-optimum floater does look something like an onshore turbine, in the sense that it is a rotor mounted atop a tower.

The second point hints that we have probably seen something like our turbine before. Together, the points indicate an obvious direction for investigation: a vertical-axis wind turbine.

4 VERTICAL-AXIS CONCEPTS

Among potential rotor profiles that could be revolved around a vertical axis, two categories stand out as most rational. First is a Darrieus-type rotor, which is rational because the blades are shaped so as to carry the majority of aerodynamic and centrifugal forces in tension and compression, minimizing bending. Second is an H-rotor, which is rational because the blades are straight, and thus easy to construct. Figure 2 shows these two topologies.

In the context of a floater, a big drawback with a Darrieus design is that it is impractical to run guy cables to the tower top, above the rotor. Large on-land Darrieus turbines always have such stays, because without them there would be very severe bending loads on the shaft bearings. Half the problem could be solved with a sort of hybrid between the Darrieus and H-rotor designs, a Darrieus with a cross-arm. This is fine, except that where the rotating blades intersect the static tower at the bottom of the rotor, a non-standard bearing design would be required. It would be something like a rigid ring rotating on a track and wheel arrangement, the blades being attached to the ring. In any case, the rotating shaft loads are still partly unbalanced.

Given these problems, an H-rotor was selected for further investigation.

The H-rotor design is by no means new; a 130kW prototype was constructed at Carmarthen Bay, UK, in the 1980's. [14] This machine looked like Darth Vader's tie fighter, had blades that folded in order to regulate the power in high winds (which turned out to be unnecessary, because stall achieves the same effect), and was very, very heavy. It did, though, prove that the H-rotor concept was technically feasible. Another such turbine was installed on the Isles of Scilly, by the same consortium, also in the 1980's. [2]

More recently, H-rotor turbines have been studied by several authors ([4], [5], [8]), and probably others in industry whose results have not been published.

There are some potential advantages of an H-rotor over a propeller-like rotor which could be particularly important for a floater:

1. The vertical axis orientation allows the generator and associated components to be placed some distance (likely limited by drivetrain dynamics) down on the support tower, below the rotor.
2. For a given swept area and minimum clearance between the blades and mean water level, an H-rotor can be designed which has a lower center of gravity than a circular propeller-type rotor. (Again, this is likely limited by drivetrain dynamics.)
3. The large clearance between the blades and the tower leaves room for a truss with widely splayed legs. This type of structure is more efficient than a typical narrow, circular cylinder at reacting the large bending moments which occur as the floating structure pitches and rolls.

If you have read this far, then you know something about what I am trying to do and why. Unfortunately, since we are already bumping up against the four page limit (even though I decreased the font size), a discussion of the meat of this investigation -- the methods being used, assumptions, and so forth -- will have to wait. But they can be mentioned briefly.

5 METHODS

Simple, home-brewed versions of the blade element momentum method (BEM) are used to calculate rotor loads and output power. For horizontal-axis wind turbines, the BEM program is pretty much what is described by Burton et al. [3] It has been shown to give results almost identical to PHATAS (Version OCT-2002). [9],[10] For vertical-axis wind turbines, a double-multiple streamtube version of BEM is used, like Paraschivoiu's CARDAAV, but without dynamic stall. [13],[11] In either case, results are accurate through rated windspeed (that at which power peaks, and stall becomes significant), and inaccurate beyond. Post-stall behavior, above rated windspeed, is estimated by empirically-based trends.

In order to find the optimum design, Monte Carlo analysis is used, because the human brain (mine, at least) cannot estimate the simultaneous effects of all the relevant design parameters.

Assumptions related to airfoil coefficients are especially important, with some intuition required to fill in drag coefficient data, which is seldom published beyond the point of initial stall. Lift and drag immediately beyond stall govern the behavior of stall-regulated wind turbines above rated windspeed.

6 RESULTS

Some preliminary results are available. One aspect of the results is plotted in Figure 3. On the X axis is rotor average thrust force, which is representative of the severity of loading on the support structure. On the Y axis is shaft torque, which is representative of the severity of loading on the drivetrain. All the data points shown represent wind turbines which produce exactly the same amount of energy in a year: one could say that the aerodynamic performance of all these rotors is equal.

It is highly probable that an optimized H-rotor will place more severe loads on the drivetrain and support structure than an optimized propeller-type rotor. But a firm conclusion regarding overall system mass and cost cannot yet be drawn.

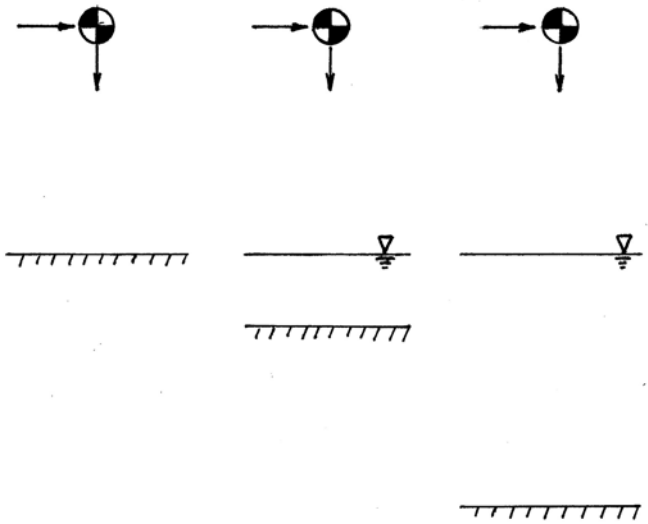

Figure 1: A highly simplified sketch of the wind turbine structural engineering problem

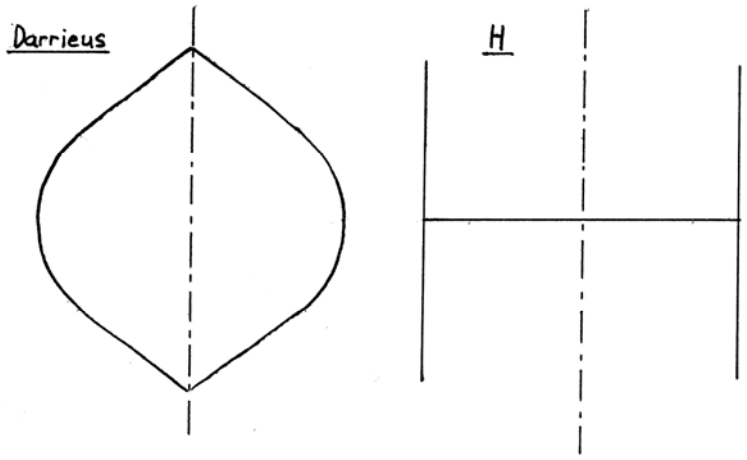

Figure 2: Shape of a Darrieus and an H rotor

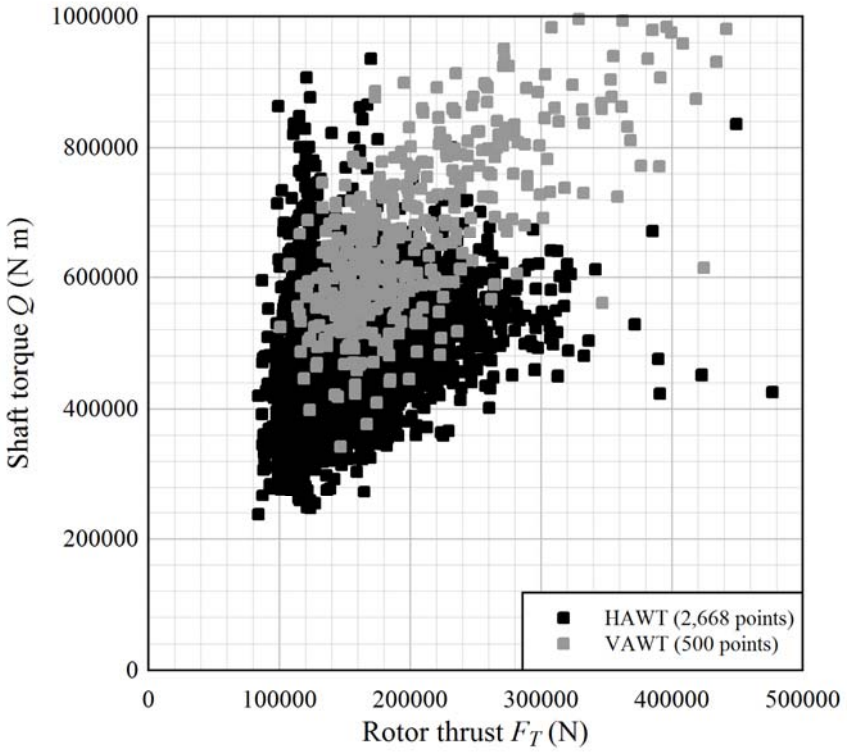

Figure 3: Preliminary results

Table 1: Costs of floaters versus turbines with other support structure types

Reference	Levelized Electricity Cost	Notes
Fulton	\$0.065-\$0.075/kWh	tension-leg platform with gravity foundation
Henderson	€0.07/kWh	three-leg shallow-water catenary-moored
Tong	6-12 p/kWh	shallow-draft spar, steel tower on concrete base
Fulton	\$0.05/kWh	fixed-foundation offshore
Pantaleo	€0.05-0.06/kWh	fixed-foundation offshore
Ackerman	2.4-6.0 p/kWh	onshore wind

BIBLIOGRAPHY

[1] Ackermann, T.; Söder, L.; ``An overview of wind energy -- status 2002''; Renewable and Sustainable Energy Reviews 6 (2002) 67-128

[2] Anderson, M.B., et al.; ``Comparison of Measured And Predicted Results for a Stall Regulated 100 kW Vertical Axis Wind Turbine''; Wind Energy Conversion 1990, Proceedings of the 12th British Wind Energy Association Conference, Norwich, UK, 27-30 March 1990, pp 335-346

[3] Burton, T., et al.; *Wind Energy Handbook*; Wiley, 2001

[4] Coton, F.N., et al.; ``The Influence of Detailed Blade Design on the Aerodynamic Performance of Straight-bladed Vertical Axis Wind Turbines''; Proc Instn Mech Engrs 210 (1996) 65-74

[5] Eriksson, S., et al.; ``Evaluation of Different Turbine Concepts for Wind Power''; Renewable and Sustainable Energy Reviews 12 (2008) 1419-1434

[6] Fulton, G.R., et al.; ``Semi-Submersible Platform and Anchor Foundation Systems for Wind Turbine Support''; NREL/SR-500-40282, National Renewable Energy Laboratory, USA, 2007

[7] Henderson, A.R., et al.; ``Feasibility study of floating wind farms in shallow offshore sites''; Wind Engineering 27 (2003) 405-418

[8] Islam, M., et al.; ``Aerodynamic Models for Darrieus-Type Straight-Bladed Vertical Axis Wind Turbines''; Renewable and Sustainable Energy Reviews 12 (2008) 1087-1109

[9] Lindenburg, C.; ``Investigation into Rotor Blade Aerodynamics -- Analysis of the stationary measurements on the UAE phase-VI rotor in the NASA-Ames wind tunnel''; ECN report ECN-C--03-025, 2003

[10] Merz, K.O.; "A Wind Turbine Rotor Aerodynamic Analysis Module for Structural Analysis Software – Quasi-Static Blade Element Momentum Method"; NTNU, Department of Civil Engineering, 2008

[11] Merz, K.O.; "BA8607 Final Project: Preliminary Concepts and Aerodynamic Analysis Methods for a Vertical-Axis Deepwater Offshore Wind Turbine"; NTNU, Department of Civil Engineering, 2009

[12] Pantaleo, A., et al.; ``Feasibility study of off-shore wind farms: an application to Puglia region''; Solar Energy 79 (2005) 321-331

[13] Paraschivoiu, I.; *Wind Turbine Design, with Emphasis on Darrieus Concept*; Polytechnic International Press, Montreál, Québec, Canada, 2002

[14] Shock, R.A.W.; ``Comparison of Variable Geometry Vertical-axis Wind Turbines with Horizontal Axis Wind Turbines''; Report ETSU-R-47, Harwell Laboratory, Oxfordshire, UK, 1990

[15] Tester, J.W., et al.; *Sustainable Energy -- Choosing Among Options*; MIT Press, 2005

[16] Tong, K.C.; ``Technical and economic aspects of a floating offshore wind farm''; Journal of Wind Engineering and Industrial Aerodynamics 74-76 (1998) 399-410

7 APPENDIX

Assume that in the future 20% of world energy will come from wind, and assume that demand corresponds to an average power of 2×10^{13} W, in line with recent predictions of global energy usage in 2020. Assuming that a typical wind turbine produces an average of one quarter of its rated power, a 4 MW rated turbine would produce an average power of 1×10^{6} W, thus:

$$\frac{(0.20)(2 \times 10^{13}\ \mathrm{W})}{1 \times 10^{6}\ \mathrm{W/turbine}} = 4,000,000\ \mathrm{turbines}$$

will be required.

A minimum separation between turbines of roughly 10 diameters is required; taking a value of 2×10^{5} m^2 per MW rated power, the land area required for windfarms would be:

$$A_{\mathrm{windfarm}} = (0.20)(2 \times 10^{13}\ \mathrm{W}) \left(\frac{2 \times 10^{5}\ \mathrm{m}^2}{(0.25)(1 \times 10^{6}\ \mathrm{W})} \right) = 3.2 \times 10^{12}\ \mathrm{m}^2$$

This is a circle 2,000 km in diameter, within which is one large (multi-MW rated) turbine per square km. A high average wind speed is implicit in the 0.25 load factor, and in practice the turbines would be spread in high-wind locations throughout the globe.

The European Academy of Wind Energy

Durham University

Ensuring maximum energy capture by wind turbines during below rated operation

A. Chatzopoulos, W.E. Leithead

University of Strathclyde, UK

ABSTRACT

The operational strategy in below rated operation of a variable speed wind turbine is frequently chosen to maximise the energy capture. To do so the operating state of the wind turbine is caused to track the maximum aerodynamic efficiency curve, the so-called Cp-max curve. Whether it does so accurately, depends on the wind turbine controller. It is sometimes claimed that the energy capture can be increased by better design of this controller. The purpose of this paper is to examine this claim. The results suggest that the energy capture is very weakly dependent on the control algorithm. There is more dependence on the choice of control strategy but even here the potential gains are limited.

KEYWORDS

wind turbine, wind power, energy capture, below rated, control

1 INTRODUCTION

The power captured by a wind turbine is mainly affected by the aerodynamic efficiency of its rotor. The way the rotor operates in order to maximize the power captured, is mainly determined by the control strategy of the wind turbine. The power coefficient is the main quantification of efficiency and depends on pitch angle, the wind speed, and the rotor speed. In the below rated operating region the rotor is regulated to achieve constant speed for the first and third operating regions, and maximization of energy capture by tracking the optimum power coefficient curve for mode two.

The aim of this paper is to present the results referring to energy capture obtained by the exhaustive assessment of the operation of a large wind turbine. Furthermore, to examine the claim that better design of a controller may increase the energy captured from the wind. Much research has been done on the hunt for new methods of control promising to maximize the energy captured by the wind turbine. Different approaches such as the one proposed in [1], presenting a complete fuzzy logic control based generation system, one component of which checks online for the desired generator speed for optimal aerodynamic efficiency. An adaptive fuzzy controller approach through identification is presented in [2] for the exploitation of maximum energy, by continuously optimizing the internal parameters and adapting them to the system. Other approaches include Nonlinear robust control as in [3] optimizing the blade pitch for a better tracking of the maximum coefficient curve, and Neural network solutions as in [4], against the fluctuations of the generator speed from Cp maximum curve.

The paper is organised as follows. Section 2, presents a detailed validation of the simulink model used for the aerodynamic efficiency analysis, against the industrially accepted software GH Bladed. Section 3, provides the detailed aerodynamic efficiency analysis and presents the results as a percentage of the total energy capture that would have been possible through an ideal operating strategy. Section 4, summarizes the paper and the conclusions of this research are drawn.

aris@eee.strath.ac.uk

2 MODEL VALIDATION

The detailed model of the Simulink simulation of the wind turbine used in this paper is thoroughly described in [5] and [6]. This simulink model that is being used for the assessment of the aerodynamic efficiency of the wind turbine is compared against Bladed. For the need of this study the wind turbine is extensively tested using the same controller but different controller gains for the tracking of the below rated Cp curve. The simulations are conducted for uniform wind speeds, as well as for turbulent wind for turbulences of 5% and 10%. Figures 3, 4 and 5 depict the normalized energy capture for the two models compared for seven different controller gains and three different averaged seeds of wind.

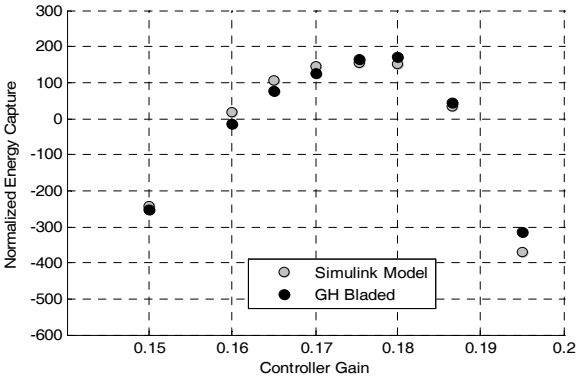

Figure 3: Comparison of Bladed Vs Simulink for different controller gains for uniform wind speed

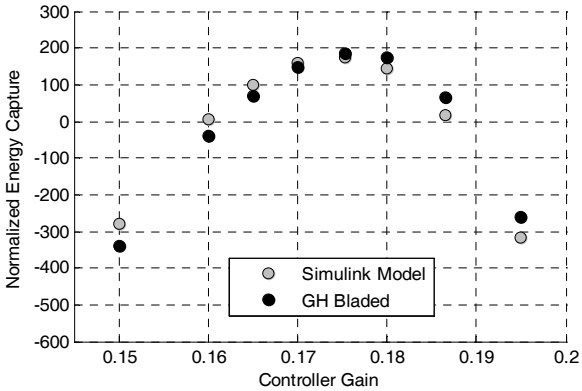

Figure 4: Comparison of Bladed Vs Simulink for different controller gains and turbulence intensity of 5%.

Each of the two models is run for wind speeds from cut-in (4m/s) to cut-out (24m/s) and for the controller gain values shown on the plots. Figures 3, 4 and 5 show a significant match of the trends of the two models. It can be inferred that the Simulink simulation model may be well used to tune the wind turbine controller and assess its energy capture.

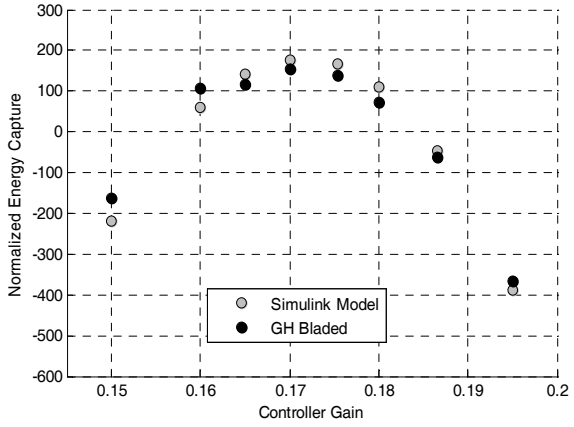

Figure 5: Comparison of Bladed Vs Simulink for different controller gains and turbulence intensity of 10%.

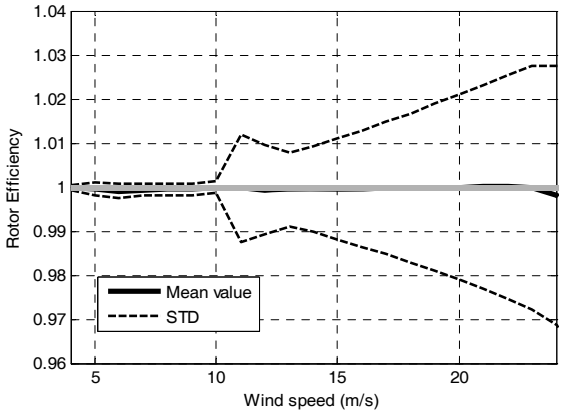

Figure 6: Efficiency for 10% turbulent wind

3 EFFICIENCY INVESTIGATION

The purpose of the efficiency analysis is to compare the actual input power going into the wind turbine with the ideal maximum input power that can theoretically be extracted from the wind. The actual input power curve is multiplied by the probability distribution function and integrated for one year for the assessment of the aerodynamic efficiency. The optimum gain for the controller is used for this assessment and full runs for wind speeds from cut-in to cut-out are conducted. The rotor efficiency is given from the ratio of actual input power over the ideal input power. Input power is defined as the product of the Aerodynamic torque on the

rotor, times the rotor speed. For the efficiency plots shown below the ideal Input power is calculated according to the steady state characteristics of the wind turbine. Then a full set of runs is conducted and the bin method is used in order to sort the actual input power data into wind speed groups. The full efficiency envelopes for wind turbulences of 5%, and 10% are presented in figures 6 and 7. It is obvious from the plots that the efficiency is almost at the value of one, with one being the theoretical maximum efficiency.

In the Weibull distribution the wind speed and its variations are described by the probability density function and cumulative distribution which reveals the annual energy capture.

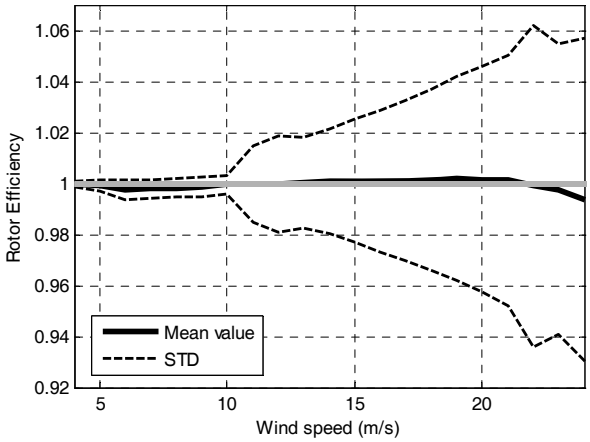

Figure 7: Efficiency for 10% turbulent wind

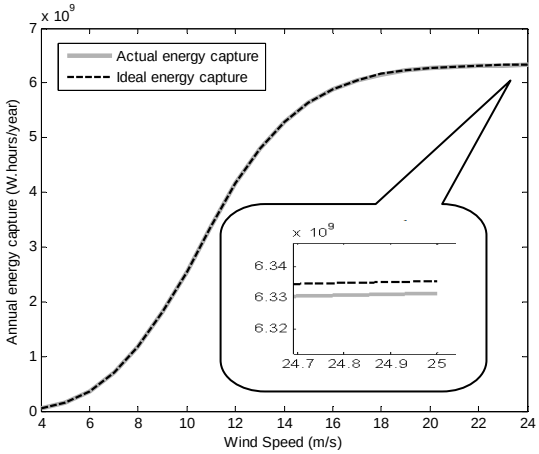

Figure 8: Annual energy capture curve

Once the Weibull probability distribution is calculated for a specific site, it is multiplied by the mean values of the input power values for each wind speed obtained from the simulation, giving the annual energy distribution of the specific site. The annual distributions considered here are for two sites with annual mean wind speeds of 7.5m/s and 8.5m/s and a shape factor of *k=2*. The annual energy capture of the wind turbine assessed, is given by the integration of the product of the mean of the input power values, times the probability distribution and is shown in figure 8. The ratio of the end values of the actual over the ideal annual energy capture curve, give out the percentage of the annual efficiency of the rotor of the wind turbine. The results for turbulences of 5%, 10% and 15% are presented altogether in the two tables given below.

Table 1: Aerodynamic efficiency results for a mean wind speed of 7.5m/s for different turbulence and different controller gains

Turbulence (%)	Controller Gain	Aerodynamic efficiency (%)
5%	0.2	99.75%
	0.1753	99.93%
	0.15	99.79%
	0.12	99.33%
10%	0.2	99.68%
	0.1753	99.87%
	0.15	99.74%
	0.12	99.29%
15%	0.2	99.57%
	0.1753	99.77%
	0.15	99.66%
	0.12	99.22%

Table 2: Aerodynamic efficiency results for a mean wind speed of 8.5m/s for different turbulence and different controller gains

Turbulence (%)	Controller Gain	Aerodynamic efficiency (%)
5%	0.2	99.79%
	0.1753	99.93%
	0.15	99.82%
	0.12	99.46%
10%	0.2	99.70%
	0.1753	99.88%
	0.15	99.78%
	0.12	99.42%
15%	0.2	99.62%
	0.1753	99.79%
	0.15	99.71%
	0.12	99.30%

The results from the aerodynamic assessment are significant as they reveal almost no energy losses if the operating strategy of the wind turbine is chosen carefully. Changing the

operating strategy will result in losses in energy capture as shown in figure 10. By choosing the optimum controller gain it is observed from figure 9, that the wind turbine operates as desired and from Table 1 & 2, a 99.93% of rotor efficiency is the result of this case. When using a slightly different controller gain, see figure 10, an obvious deviation in the tracking of the ideal curve is recorded.

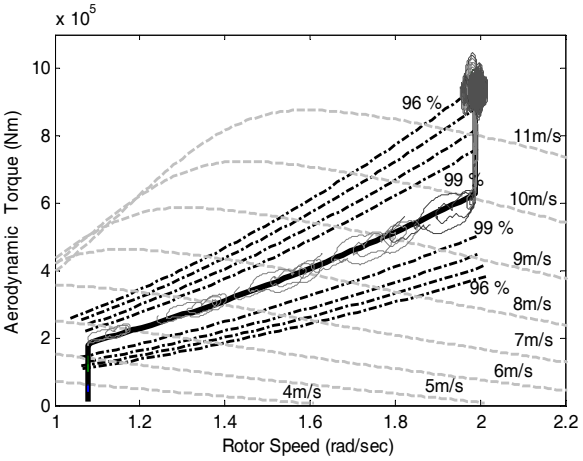

Figure 9: Actual Vs Ideal Operating Strategy for optimum controller gain

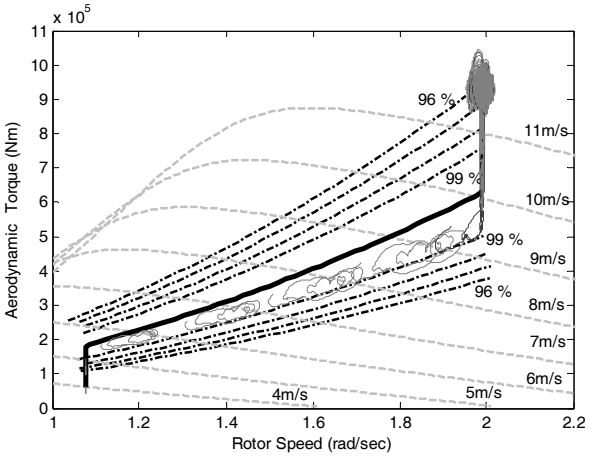

Figure 10: Actual Vs Ideal Operating Strategy with 0.15 controller gain

4 CONCLUSIONS

A thorough analysis of a Simulink simulation, validated against Bladed, of a large wind turbine is presented in this paper using spatially filtered wind speed as an input in order to assess its energy capture. The assessment is done by using a classic control approach for the operation of the wind turbine, and the results reveal that there is little dependence on the control method used. More dependence is on the operating strategy adopted and how close the wind turbine is operating on this strategy.

BIBLIOGRAPHY

[1] Simoes J.D., Bose B.K., Spiegel R.J., *Fuzzy Logic Based Intelligent Control of a Variable Speed Cage Machine Wind Generation System*, IEEE Transactions on Power Electronics, Vol. 12, No. 1, Jan 1997.

[2] Galdi V., Piccolo A., Siano P., *Exploiting maximum energy from variable speed wind power generation systems by using an adaptive Takagi–Sugeno–Kang fuzzy model,* Energy Conversion and Management, 413-421, 2009.

[3] Iyasere E., Salah M., Dawson D., and Wagner J., *Nonlinear Robust Control to Maximize Energy Capture in a Variable Speed Wind Turbine*, American Control Conference, Washington, USA, June 2008.

[4] Hui L., Shi K. L., and McLaren P. G., *Neural-Network-Based Sensorless Maximum Wind Energy Capture With Compensated Power Coefficient*, IEEE Transactions on industry applications, Vol.41, No.6, November/ December 2005.

[5] Leithead W.E., Rogers M.C.M, *Drive-Train Characteristics of Constant Speed HAWT's: Part I – Representation by Simple Dynamic Models*, Wind Engineering, Vol. 20, No. 3, 1996.

[6] Leithead W.E., Rogers M.C.M, *Drive-Train Characteristics of Constant Speed HAWT's: Part II – Simple Characterisation of Dynamics,* Vol. 20, No. 3, 1996.

Power Limitation at high wind speeds for a variable speed stall-regulated fixed pitch wind turbine

Rosmin, N [1], Watson, S.J [2], Thomson, M[3]

[1] Loughborough University, United Kingdom, [2] Loughborough University United Kingdom

ABSTRACT

This paper deals with power regulation for a fixed pitch stall-regulated variable speed wind energy conversion system. The power limitation in the stall region is the main topic of this paper where in this region the rotor/generator speed control activity is characterized by non-minimum phase behaviour. Here, a simple and effective control algorithm is used. A proportional integral (PI) controller was used to control the power and the generator speed. Results show that such a proportional integral (PI) controller is not good enough to accurately track rated power at the required rotational speed corresponding to the wind speed variation above the rated wind speed.

KEYWORDS

Variable speed, stall-regulated, fixed pitch, power limitation.

1 INTRODUCTION

In general, a variable speed stall-regulated wind turbine has 3 main different operating regions: Below, Intermediate and Above wind speed [1]. At above rated wind speed , the power system is designed to limit the power captured in the wind by changing the rotor speed [2]. This working region is the most demanding in relation to wind turbine control. In a fixed pitch, variable speed, stall-regulated wind turbine, power regulation above rated wind speed is particularly challenging where no alteration of turbine blade pitch angle is available in order to reduce the power output. In such a turbine, the only way how to keep the power at a constant value is by reducing the power coefficient by reducing the rotor speed so that the tip speed ratio can be operated between its minimum and its optimum value.

2 DESCRIPTION OF THE MODEL

2.1 Wind Turbine Model

Figure 1 shows the Simulink model used in this work to simulate a stall-regulated, variable-speed, wind turbine system. In this work, the operation of the variable-speed, stall-regulated,

wind turbine equipped with a squirrel-cage induction generator (SCIG) is examined. The value of power coefficient, C_p is calculated by using Equation (1), whereas the tip speed ratio, λ is computed by using Equation (2). Equation (3) then is used to calculate the aerodynamic torque, T_{aero} [3-4].

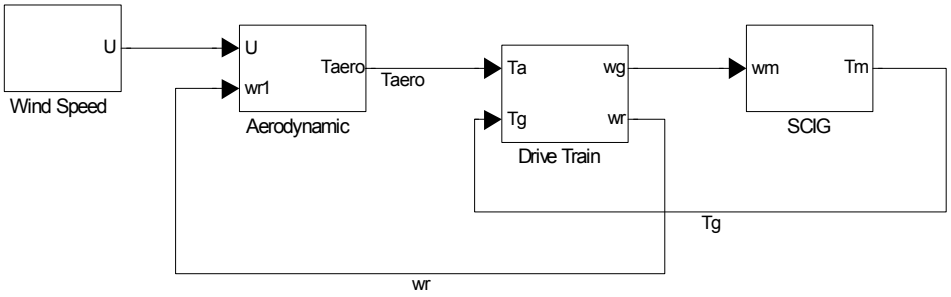

Figure 1: Wind turbine system

$$C_p = 3.964305\ e^{-5}\lambda^6 - 1.631763\ e^{-3}\lambda^5 + 2.672766\ e^{-2}\lambda^4 - 2.201691\ e^{-1}\lambda^3 + 9.253232\ e^{-1}\lambda^2 - 1.702488\ \lambda^1 + 1.136978 \quad (1)$$

$$\lambda = \frac{\omega_r R}{U} \quad (2)$$

$$T_{aero} = \frac{1}{2}\rho\pi R^2 U^3 \frac{C_p}{\omega_r} \quad (3)$$

where ω_r = rotor speed, R =blade radius, U = wind speed, ρ is air density.

2.2 Control Objective and Control Algorithm

The main objective of this study is to keep the generated electrical power at the rated value at 25kW when wind speed reaches 10m/s up until 20 m/s. A simple control algorithm used to achieve this goal is shown in Figure 3. It consists of two nested loops [3-4]. The inner loop demands a generator torque and the outer loop demands the generator speed. A PI controller is used in the both these control loops [4-5].

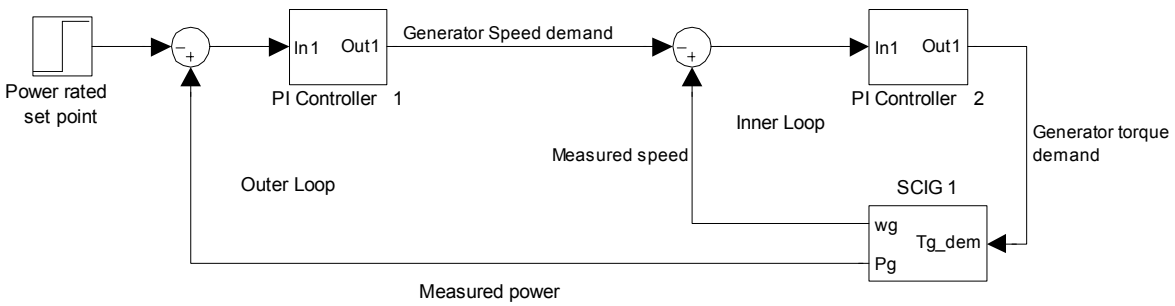

Figure 3: A simple contol algorithm for a variable-speed fixed pitch wind turbine

3 RESULTS

3.1 Simulation Results

Figure 4(a) represents the wind speed time series which was modelled by using Equation (4) from reference [6] .

$$U_{t+1} = rU_t + (1-r)(\overline{U}) + \varepsilon_t \quad (4)$$

where U_{t+1t} = Wind speed at time $t+1$, U_t = Wind speed at time t,

$\overline{U}$ = Desired mean value, r = Autocorrelation at unit lag, ε = Gaussian noise.

From Figure 4(b) and (c), it can be seen that by using PI controllers, the power coefficient can be reduced and the tip speed ratio can be controlled to be operated in the range between λ_{min} and λ_{opt}. λ_{min} is the minimum allowed value of tip speed ratio while λ_{opt} is the value of the tip speed ratio when power coefficient reach the maximum peak value. Tip speed ratio can be calculated by The values for λ_{min} and λ_{opt} for this turbine are equal to 1.8 and 5.75, respectively. Λ can be calculated by multiplying the rotor speed with the blade radius However, from the result in Figure 4(d), the demanded generator power is not kept at a constant value during the high wind speed fluctuations. The generator speed and the torque demand is shown in Figure 4(e) and 4(f). These demanded values are obtained from the output results of the first and second controller, respectively.

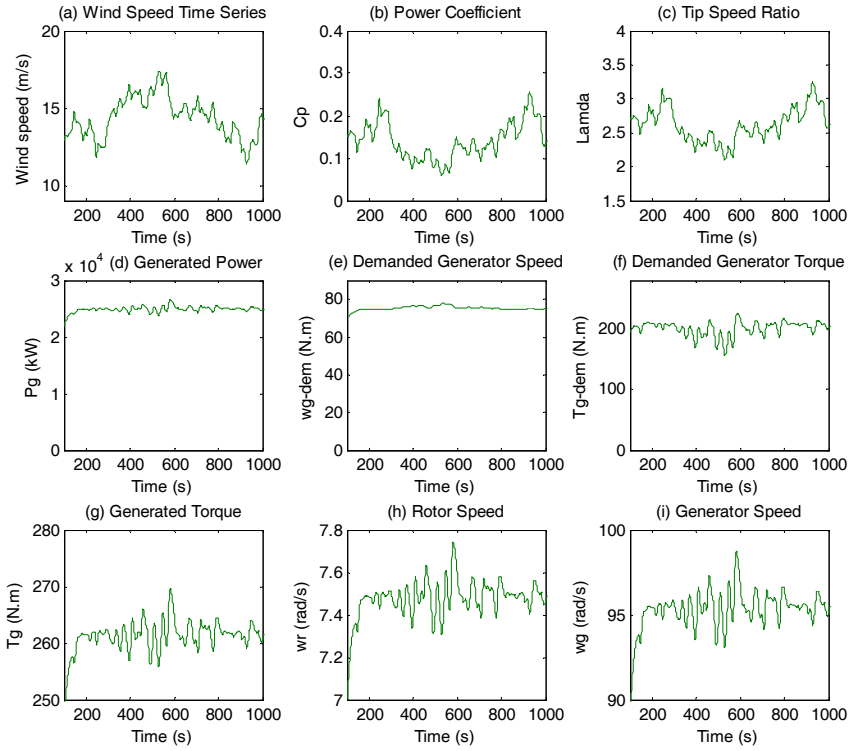

Figure 4: The results of (a) wind speed, (b) Power coefficient, (c) Tip speed ratio, (d) Generated power (e) Demanded generator speed, (f) Demanded Torque , (g) Generator torque, (h) Rotor speed, (i) Generator speed.

Even though they cannot limit the power at a constant value, the PI controllers are be able to reduce the generated torque below the permitted value as illustrated in Figure 4(g). By inspection of the results for the rotor speed and generator speed in Figure 4(h) and 4(g), it can be seen that the rotational speed changes in proportional to the wind speed variation. The rotor speed and the generator speed vary also, showing the impact of the variable speed concept as shown in Figure 4(h) and 4(i).

4 CONCLUSIONS

This paper shows some preliminary results of using classical PI control in order to limit the power above rated wind speed. Results show that a PI controller is good in reducing the generated torque from its maximum limit but it is not good enough to regulate the rotor speed in order to track the demanded value when dealing with the large variations of wind speed. In the future, work will be concentrated on how to improve the response of turbine's rotor speed. The rotor speed is expected can changing the speed corresponding to the wind speed variation, in the permitted range ($7.2 < \omega_r < 91.8 rad/s$).

BIBLIOGRAPHY

[1] Bianchi, F.D., Mantz, R. J., Battista, H.D, Wind Turbine Control System: Principles, Modelling and Gain Scheduling Design. 2007: Springer-Verlag London Limited.

[2] Battista, H.D., Performance analysis of a variable structure controller for power regulation of WECS operating in the stall region, Int. Journal of Energy Research, Vol.25, 2001, 1345-1357.

[3] Perahia, J and Nayar, C.V. Simulation of a fixed pitch wind turbine powered induction generator in EMTP, Int. Journal of Electrical Engineering Education, Vol.31, 1994, 362-374.

[4] Ekelund, T. Speed Control Wind Turbines in the Stall Region, Proceedings of the Third IEEE Conference on Control Applications, Vol.1, 1994.

[5] Burton,T., Sharpe, D.,Jenkins, N., Bossanyi, E. Wind Energy handbook, Wiley, 2001.

[6] CREST MSc Flexible & Distance Learning Series. Wind Power 2: Wind Statistics and structure, 2004, Loughborough University.

Active Flow Control for Noise Reduction and Performance Improvement of Future Generation Wind Turbines

Thorsten Lutz, Alexander Wolf

ABSTRACT

The aim of this Israeli-German cooperation between the universities of Tel-Aviv and Stuttgart is the application of active flow control (AFC) for trailing edge noise reduction of wind turbine blades. The noise reduction achieved by active flow control devices can lead to a higher acceptance of On-Shore facilities and/or a higher performance by increased rotating speed. The project concentrates on the reduction of the boundary layer induced trailing edge noise. Numerical and experimental investigations are performed to develop suitable AFC-devices. For the numerical investigations the RANS code (Reynolds Averaged Navier Stokes equations) FLOWer developed by the DLR is used. The results of the 2D RANS calculation are used to determine the trailing edge noise using the Rnoise code developed by the IAG by analysing the spectra of the pressure fluctuation.

KEYWORDS

Trailing edge noise reduction, active flow control, RANS

1 INTRODUCTION

The world's energy consumption is increasing fast and it will rise even more in the coming years. Wind energy will play an important role in fulfilling these requirements from a renewable source of Green energy. But this means a wider deployment of wind turbines and also a deployment closer to urban areas than what is done today. For this reason the noise annoyance caused by wind turbines must be reduced. There are several types of wind turbine aeroacoustic noise like:

- Turbulent boundary layer – trailing edge interaction noise
- Laminar boundary layer – vortex shedding noise
- Boundary layer separation noise
- Stall noise
- Trailing edge bluntness - vortex shedding noise
- Blade tip noise
- Inflow – blades interaction noise

Email: wolf@iag.uni-stuttgart.de

Investigations of two wind energy facilities [1] showed that the trailing edge noise seems to be the most dominant source of aeroacoustic noise. It is generated by the turbulence in the boundary layer which is scattered at the trailing edge of the turbine blade. The objective of the present collaborative study is to reduce the airfoil self-noise by using active flow control where the flow around the airfoil is affected by actuators. These actuators can, for example, blow additional air into the boundary layer. With such an actuator the boundary layer velocity profile and the thickness of the boundary layer can be affected. This will have an effect on the turbulence inside the boundary layer and therefore on the emitted trailing edge noise. During this project it shall be investigated how the boundary layer should be manipulated by the actuator to reduce the emitted noise and –based on this knowledge - which actuator is useful. But not only the noise must be regarded. The airfoil with active flow control device must also not produce more drag than the airfoil without active flow control. Of course a combined drag and noise reduction would be the optimal solution.

2 NUMERICAL INVESTIGATIONS

For the noise calculation the in-house code “Rnoise” developed by the IAG [2] was used. This code uses the numerical flow solution from the RANS solver FLOWer developed by the DLR (German Aerospace Center). For both studies the NACA64-418 airfoil was chosen, which is often used for wind turbine blades. For the noise calculation the boundary layer profile at the trailing edge is evaluated.

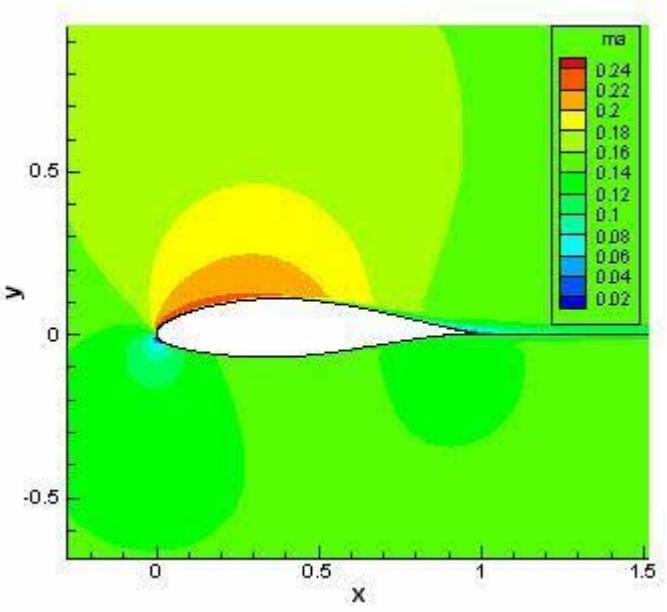

Figure 1: Field solution of FLOWer RANS-Simulation.

With the different parameters, which are delivered by the RANS analysis it is possible to determine the pressure fluctuation on the airfoil surface. Using the spectra of the pressure fluctuations on the surface it is then possible to calculate the far field noise. Calculations were done for a Mach number of 0.15, a Reynolds number of 3.378 million and a Cl of 0.905. The used Turbulence model was Wilcox k-ω.

In the first study the parameters like wall normal distribution of turbulence kinetic energy k_T, dissipation rate ε, vertical correlation length scale Λ_2, the RMS value of the autocorrelation of the vertical fluctuation velocity $\langle u_2^2 \rangle$ and the velocity profile were modified by a constant parameter α. The modification of the latter included also a recalculation of the velocity gradient in wall normal direction. In this first study all parameters were changed separately. The physical interdependence of the several investigated parameters was not regarded. These studies were done to investigate the influence of each single parameter on the noise result.

The study was subdivided into three parts. In the first part only the near wall region of the velocity profile was modified. Secondly, the outer part was modified. Finally the whole velocity profile was changed. During these three investigations the velocity inside the boundary layer was reduced and increased using the 3rd order function.

In the second study a coupling of the before mentioned parameters was implemented in the code (called RnoiseAFC). Starting with a modification of the velocity profile the gradient was recalculated first. Secondly, the turbulence kinetic energy k_T was adapted using the ratio of the original and the recalculated velocity gradient. Also the specific dissipation rate ω had to be adapted in a similar way. The approach for the modification of both parameters was derived from Prandtl´s mixing length theory. All other parameters depend on the velocity gradient, the turbulence kinetic energy and the specific dissipation rate. For this reason no further modification was necessary.

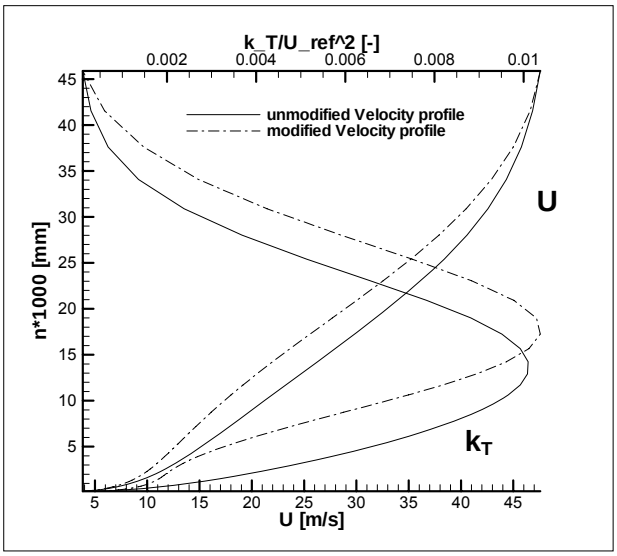

Figure 2: Boundary layer velocity profiles and corresponding k_T distributions

The mean velocity profile was modified by superposing the original velocity profile with a function of 3rd order. The region of influence and strength of the 3rd order function was controlled by boundary conditions.

Several velocity profiles were generated this way and a noise analyses was carried out. The changes of the new compared to the unmodified velocity profile were expressed by the

changes in the shape factor H_{12}. This factor is defined by the ratio of displacement thickness δ_1 to momentum thickness δ_2.

$$H_{12} = \frac{\delta_1}{\delta_2}$$

Figure 2 shows the original velocity profile along with an exemplary modified profile along with the corresponding k_T distributions. It can be easily seen that reducing the velocity inside the boundary layer reduces the turbulence kinetic energy close to the wall. This leads to a noise reduction. On figure 3 the noise contribution from the suction side of the airfoil is shown for different H_{12} values. The noise is represented by the overall sound pressure level L_P. The observers distance and the wetted length of the trailing edge were set to one meter. Please note that a velocity increase leads to a reduction of H_{12} and a decrease of the velocity increases the H_{12} value. The two plots show very well that a velocity increase always causes a noise increase. A velocity reduction usually reduces the noise, but for the suction side there is a H_{12} value where the noise level has a minimum (Fig. 4). For larger shape factors/lower velocities the emitted noise becomes louder again.

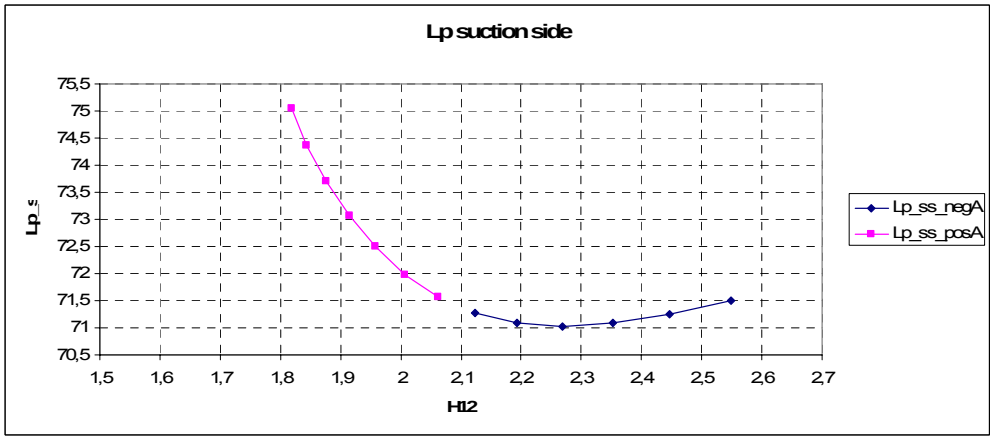

Figure 3: Lp-Results of airfoil suction side over shape factor H_{12}.

3 CONCLUSIONS

This paper deals with the reduction of trailing edge noise caused by the boundary layer turbulence using active flow control. It is investigated how the shape of the boundary layer profile must be affected to achieve noise reduction. This knowledge will be used to choose a suitable active flow control device. Further investigations are necessary to find an “optimal” solution depending on emitted noise and drag.

BIBLIOGRAPHY

[1] S. Oerlemans, M. Fisher, T. Maeder, K. Kögler, ”Reduction of Wind Turbine Noise using Optimized Airfoils and Trailing-Edge Serrations”, AIAA 2008-2819

[2] M. Kamruzzaman, Th. Lutz, A. Herrig und E. Krämer, „RANS Based Prediction of Airfoil Trailing Edge Far-Field Noise: Impact of Isotropic & Ansiotropic Turbulence”, AIAA Paper, AIAA-2008-2867-685

Presentation will be done by

- Oral presentation only

Extreme Response for Wind Turbines

Henrik Stensgaard Toft [1], John Dalsgaard Sørensen [1,2]

[1] Department of Civil Engineering, Aalborg University, Denmark

[2] Wind Energy Division, Risø-DTU, Denmark

ABSTRACT

The characteristic load on wind turbines during operation are among others dependent on the mean wind speed, the turbulence intensity and type and settings of the control system. The characteristic load during operation is normally estimated by statistical extrapolation of a limited number of simulated 10min time series of the response according to the wind turbine standard IEC 61400-1. However, this method assumes that the individual 10min time series and the extracted peaks from the time series are independent. In the present paper is this assumption investigated based on field measurements and a new method for estimating the characteristic load based on field measurements is proposed.

KEYWORDS

Wind Turbines, Load Extrapolation, Field Measurements.

1 INTRODUCTION

The methods for estimating the characteristic load on wind turbine during operation have been widely discussed within the wind turbine industry in the last years. In the wind turbine standard IEC 61400-1 3.edition 2005 [1] it is recommended that the characteristic load is determined by statistical extrapolation of simulated 10min time series of the wind turbine response during operation. This method is based on [2] and uses the Peak Over Threshold (POT) method for extracting the peaks from the simulated time series. Other methods for calculating the characteristic load and extracting the peaks are proposed in [3;4].

The load extrapolation method according to IEC 61400-1 is based on the assumption that the peaks extracted by the POT method and the individual 10 min time series are independent. The assumption about independence of the peaks has been studied in [4] and it was found that the correlation was weak. Since the extreme load is dependent on the mean wind speed, the turbulence intensity and the type and settings of the control system the correlation in the wind turbine response must be dependent on the correlation for these parameters.

In [5;6] has a correlation length in the range of 48-60 hours been used for the mean wind speed. Correlation in turbulence has been studied in [7] leading to a correlation length in the range of 10-20 seconds. For the control system the correlation will be dependent on how fast the wind turbine can e.g. pitch the blade or in other ways reduce the loads on the structural components. The correlation length for the control system will typically be in the range of a few seconds if the control system is active. The correlation length for the wind turbine response and thereby the extreme load is for this reason a combination of very different time scales.

2 STORM WIND SPEED

For normal civil engineering structures the extreme load occurs for the extreme wind speeds. However, for wind turbines the extreme load often occurs close to the nominal wind speed (typically U_{nom} = 15m/s) or the cut-out wind speed (typically U_{out} = 25m/s). In the following is a storm wind speed defined from which the extreme load can occur. In figure 1 is the mean wind speed and maximum flap bending moment for each 10min time series given for a pitch controlled wind turbine.

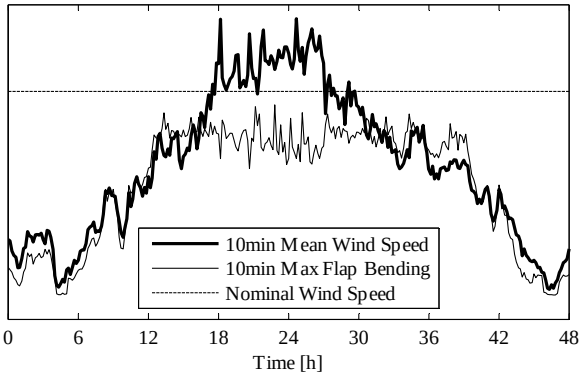

Figure 1: Mean wind speed and max flap bending for each 10min time series. Pitch controlled wind turbine.

From figure 1 it is seen that the maximum flap bending moment follows the mean wind speed closely for low wind speeds. However, at mean wind speeds close to the nominal wind speed the flap bending moment seems to reach a constant level. In order to avoid the non critical response at the small mean wind speeds in the extrapolation procedure is a storm wind speed defined. The storm wind speed is the smallest mean wind speed where the response can start to become critical. Based on figure 1 is the storm wind speed defined as the smallest mean wind speed where a gust can reach the nominal wind speed:

$$U_{storm} = U_{nom} - k_p \sigma_1 \quad (1)$$

where the turbulence is assumed to be a Gaussian process and the peak factor is assumed to be k_p = 3.5 as for the wind pressure. The standard deviation of the turbulence is given by [1]:

$$\sigma_1 = I_{ref}\left(0.75U_{storm} + c\right) \tag{2}$$

where I_{ref} is the reference turbulence intensity at 15 m/s and c = 3.8m/s is a constant. All wind speeds are specified at hub height.

3 LOAD EFFECT EXTRAPOLATION FOR FIELD MEASUREMENTS

Based on the definition of a storm wind speed given in the previous section a time series of field measurement can be reduced to a series of independent storms from which the extreme response can be extracted, see e.g. [8] where similar approach have been used for waves. From the extracted extremes a distribution for the extreme response can be obtained. In the present paper is a 3-parameter Weibull distribution fitted to the 25-30 largest extremes in order to ignore the smallest extremes and still have a representative dataset.

$$F_{response}\left(l \mid S\right) = 1 - \exp\left(-\left(\frac{l-\gamma}{\beta}\right)^{\alpha}\right) \qquad l \geq \gamma \tag{3}$$

where S indicates a storm and α, β, γ are parameters in the distribution function which is fitted using the Maximum-Likelihood Method in order to take the statistical uncertainty into account. The characteristic load during operation with a recurrence period on T_r years can then be calculated for the probability:

$$F_{response}\left(l_c \mid S\right) = 1 - \frac{1}{\lambda T_r} \tag{4}$$

where λ is the number of data per year used for fitting the distribution function. If the statistical uncertainty is taken into account the distribution function can be solved for the probability in (4) using FORM (First Order Reliability Method), see e.g. [9].

4 NUMERICAL EXAMPLE

In the present section is the characteristic load with and without statistical uncertainty calculated using the method in IEC 61400-1 and the method based on independent storms presented in the present paper. The dataset available for a stall controlled wind turbine contains 52 days of complete measurements and the results are given in table 1. A similar comparison should be performed for a pitch controlled wind turbine.

Table 1: Characteristic flap bending moment, with and without statistical uncertainty.

Method	Characteristic load	
	without stat. unc.	with stat. unc.
IEC 61400-1	1.000	1.037
Storms	1.106	1.348

It is seen from table 1 that the characteristic load calculated based on independent storms gives a higher characteristic load than obtained by the method used in IEC 61400-1. The limited dataset leads to a high statistical uncertainty.

5 CONCLUSIONS

In the present paper is a new method for estimating the characteristic loads on wind turbines proposed. The method is based on field measurements of the wind turbine response which is divided into independent storms. The characteristic load is determined by extrapolation of the largest response in each storm. In a numerical example is the characteristic load calculated for a stall controlled wind turbine using the method in IEC 61400-1 and the method based on independent storms. The difference between the characteristic loads could indicate that the local extremes and the individual 10min time series not are independent.

6 ACKNOWLEDGEMENT

The work presented in this paper is part of the project “Probabilistic design of wind turbines” supported by the Danish Research Agency, grant no. 2104-05-0075. The financial support is greatly appreciated.

BIBLIOGRAPHY

[1] IEC 61400-1. Wind turbines - Part1: Design requirements. 3rd edition. 2005.

[2] Moriarty PJ, Holley WE, Butterfield S. Effect of turbulence variation on extreme loads prediction for wind turbines. Journal of Solar Energy Engineering-Transactions of the Asme 2002 Nov;124(4):387-95.

[3] Peeringa JM. Extrapolation of extreme responses of a multi megawatt wind turbine. 2003. Report No.: ECN-C-03-131.

[4] Ragan P, Manuel L. Statistical extrapolation methods for estimating wind turbine extreme loads. Journal of Solar Energy Engineering-Transactions of the Asme 2008 Aug;130(3).

[5] Coles SG, Walshaw D. Directional Modeling of Extreme Wind Speeds. Applied Statistics-Journal of the Royal Statistical Society Series C 1994;43(1):139-57.

[6] Cook NJ. Towards Better Estimation of Extreme Winds. Journal of Wind Engineering and Industrial Aerodynamics 1982;9(3):295-323.

[7] Dyrbye CD, Hansen SO. Wind Loads on Structures. Wiley; 1996.

[8] Soares CG, Scotto MG. Application of the r largest-order statistics for long-term predictions of significant wave height. Coastal Engineering 2004 Aug;51(5-6):387-94.

[9] Madsen HO, Krenk S, Lind NC. Methods of Structural Safety. Dover Publications, Inc.; 2006.

SESSION 4 – PART B

Wednesday, 30.09.2009

4:00PM

A Study of Aerofoil Geometries on Post-stall Performance at Low Reynolds Number

Supakit Worasinchai[1)], Grant Ingram[2)], Robert Dominy[3)]

School of Engineering, Durham University, United Kingdom

ABSTRACT

The aerodynamic performance of aerofoils depends on many factors such as Reynolds number, angle of attack, and particularly their geometries, especially in the near stall region. This investigation of aerofoil geometry was performed numerically using NACA 4 digits series aerofoils by variation of maximum camber, position of maximum camber and maximum thickness. It was found that the increase of maximum camber and maximum thickness can improve post-stall performance as can the position of maximum camber if it is located near the leading edge of aerofoil.

KEYWORDS

Post-stall, Aerofoils, Low Reynolds number, Camber, Thickness

1 INTRODUCTION

Small-scale wind turbines often operate in areas having low wind speed. In this circumstance, the ability to self-start and operate is vitally important. For self-starting, it was found that root section of these small turbines plays an important role [1]. However, this root section operates with low Re and high angle of attack at standstill. To improve the starting performance, the understanding of aerodynamic characteristics at this condition is essential. The results from experiments on aerofoils at low Re are available in the literature [2-3]. These tests were conducted at board range of angle of attack but higher Re. Ostowari and Naik [2] showed that thicker aerofoils have milder stall characteristics. Unfortunately, their work was limited to NACA44XX series and only the effect of thickness can be observed. In the study presented here, the effects of maximum camber, position of maximum camber, and maximum thickness were all numerically modelled using NACA 4 digits series aerofoils.

Numerical modelling

Numerical modelling was performed using the Fluent CFD software. The computational domain is shown in Figure 1. Parameters of simulation in validation are shown in table 1.

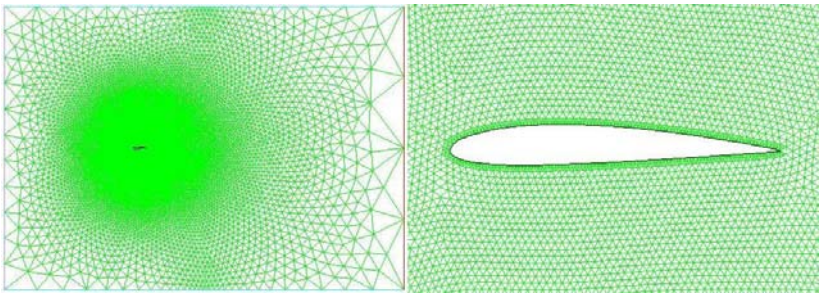

Figure 1: Computational domain and close-up of aerofoil

Table 1: Parameters of simulation

Number of cells	~60,000
Turbulence model	Realizable k-e model
Wall function	Enhanced-wall treatment
Model	Steady (0-15) and unsteady (20-90)

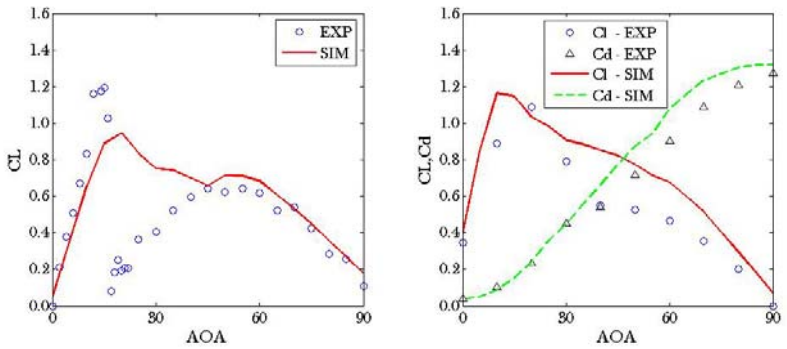

(a) **(b)**

Figure 2: CL and Cd comparison (a) NACA0018 at Re of 193,625 (b) NACA4412 at Re of 208,000

The results for CL and Cd are presented in Figure 2 together with experimental measurements from Crone [4] and Rainbird [5]. It can be seen from Figure 2a that the prediction of CL agrees well with that of experiment in pre-stall and deep-stall regions. Difference can be seen in the post-stall as experimental CL reduces suddenly while a smooth transition is seen in simulation result. It is believed that sudden reduction is due to non-uniformity of air flow in the test section [4]. Figure 2b showed that the simulation can capture the trend of lift and drag curves. Nevertheless, some differences are also found. These differences are due to inaccuracies of aerofoil surface manufacturing [5]. With these two comparisons, even though some differences can be seen, it is apparent that the simulation can be used to study the effect of aerofoil geometry with confidence.

2 RESULT

A Reynolds number of 90,000 was chosen to be a representative Re normally encountered by root section of small turbines and consequently a laminar model was adapted for all simulations. The effect of maximum thickness, maximum camber and position of maximum camber can be seen in Figure 3.

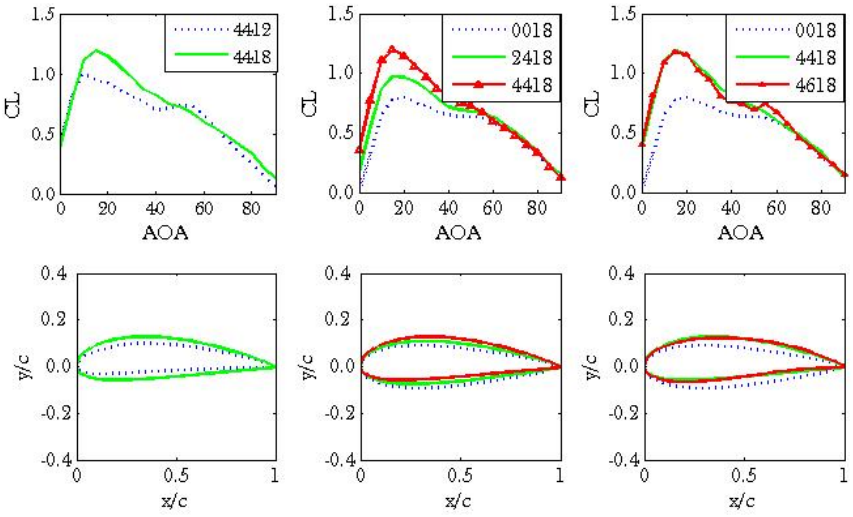

(a) (b) (c)

Figure 3: (a) thickness effect (b) camber effect (c) position-of-max-camber effect

It is clear that thickness can promote improved post-stall characteristics as it makes the flow around the leading edge smoother and more attached. This results in higher maximum lift and better stall behaviour (Fig.3a). It can also be seen from Fig.3b that the increase of camber can improve lift coefficient and also results in higher lift in the stall region. Figure 3c shows that position of maximum camber does not have great effect on post-stall but better performance can be seen if this position is located near leading edge of aerofoils, as seen in higher CL after the stall point. It is also worth noting that the drag coefficients from the simulation are almost identical (Fig. 4).

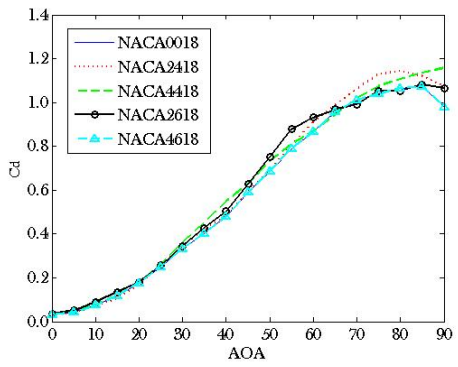

The difference between drag coefficients can be seen in pre-stall region that both skin-friction drag and pressure drag are important. Nevertheless, in post-stall region, drag coefficients from all simulations are comparable. This is because at stall the effect of friction is less important than pressure drag caused by the unsteady wake.

Figure 4: Drag coefficients

In order to see the overall picture of this post-stall performance, lift coefficients from the stall point to 60 angle of attack are averaged and shown as a function of maximum camber, position of maximum camber, and thickness in Fig. 5. It is apparent that thicker aerofoil has higher average lift coefficient as seen in Fig. 5. Furthermore, in each figure, camber aerofoils (represented in inclined surface) can achieve higher average CL. However, it can be observed that the position of maximum camber does not have a great effect on post-stall performance as shown in nearly parallel lines along camber-position axis. It is worth noting

that the amount of shift of inclined surface in Fig.5b is larger than that of Fig.5a. This can be seen as the combination effect of thickness and camber on aerofoil performance.

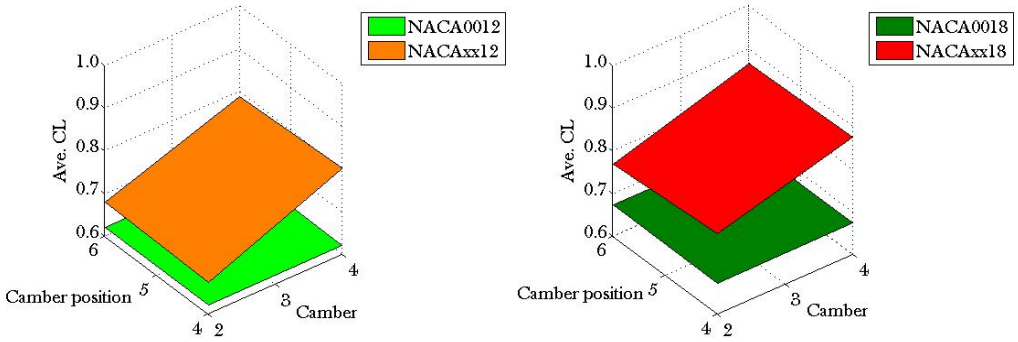

(a) (b)

Figure 5: Average lift coefficients as a function of maximum camber, position of maximum camber, and thickness

3 CONCLUSIONS

It can be seen from the simulation results that maximum camber, position of maximum camber, and maximum thickness have significant effects on aerofoil post-stall performance. The increase of maximum camber and maximum thickness can delay separation which results in milder stall while the position of maximum camber does not have profound effect on post-stall performance but a small improvement can be seen if it is located near the leading edge of aerofoil.

BIBLIOGRAPHY

[1] Wright, A.G., and Wood, D.H. 'The Starting and Low Wind Speed Behaviour of a Small Horizontal Axis Turbine,' Journal of Wind Engineering and Industrial Aerodynamics, Vol.92, pp.1265-1279, 2004.

[2] Ostowari, C., and Naik, D. 'Post stall studies of untwisted Varying Aspect Ratio Blades with NACA44XX series Airfoil Sections – Part II,' Wind Engineering, Vol.9, No. 3, 1985.

[3] Sheldahl, R.E., and Klimes, P.C. 'Aerodynamic Characteristics of Seven Symmetrical Airfoil Sections through 180-Degree Angle of Attack for Use in Aerodynamic Analysis of Vertical Axis Wind Turbines,' Energy Report, Sandia National laboratories, March 1981.

[4] Crone, B. 'The Aerodynamic Development of a Vertical Axis Wind Turbine,' MEng Thesis, School of Engineering, The University of Durham, April 2009.

[5] Rainbird, J. The Aerodynamic Development of a Vertical Axis Wind Turbine, MEng Thesis, School of Engineering, The University of Durham, April 2007.

Optimisation design of wind turbine blades based on CHC algorithm

Long Wang and Tongguang Wang

College of Aerospace Engineering

Nanjing University of Aeronautics and Astronautics

29 Yudao Street, Nanjing, 210016, China

ABSTRACT

The application of an improved genetic algorithms-CHC algorithm for design of horizontal axis wind turbine blades is presented in this paper. This algorithm is combined with the classical Wilson method and the blade element/momentum theory, taking the maximum power coefficient in a given wind speed and the maximum annual power output as the optimisation targets, respectively. It also uses linear weighted method, coupling the constraints of power output. As an example, a 1.5MW wind turbine blade is designed. The results show that the maximisation of the annual power output is more suitable for the design of a stall-regulated horizontal axis wind turbine blade.

KEYWORDS

Wind Turbine, Blade, Optimisation, Genetic Algorithms, CHC Algorithm

1 INTRODUCTION

At present, the more mature theories for optimisation design of wind turbine blades are mainly based on blade element/momentum (BEM) Theory, such as Glauert method[1], Schmitz method[2], Wilson method[3]. It is usually conceived that Wilson method comprehensively considers the effect of wind turbine rotor loss and lift-drag ratio.

There are several optimisation algorithms, for example, deasible direction algorithm, simulated annealing algorithm, genetic algorithms, *etc*. The improved genetic algorithms, Cross generation heterogeneous recombination cataclysmic mutation (CHC) algorithm[4], is adopted as the optimisation algorithm in this paper, since the genetic algorithms can more easily deal with non-linear, multi-constraints and multi-objectives optimisation problems. The genetic algorithms are highly random and adaptive search algorithm, which just use encoding and fitness function to describe the complex issues and to obtain the optimal solution. For its application in wind turbine design, the constraints of chord length and twist angle can easily be solved in the genetic algorithms.

2 THE MATHEMATICAL MODELS

2.1 CHC Algorithm combined with the Wilson method

The modified Wilson method takes the maximum local power coefficients of the key cross-sections in a given wind speed as the optimisation target. To obtain fitness function needed by the CHC algorithm, the penalty function is combined with objective function appropriately.

Fitness function:

$$F(a,b) = e^{f} \tag{1}$$

Where, $f = 4(1-a)bF\lambda^2 - \sigma_i\left|(1+b)b\lambda^2 - a(1+aF)\right|$, σ_i is the penalty factor.

Constraints:

$$a_{\min} < a_i < a_{\max} \ , \ b_{\min} < b_i < b_{\max} \ , \ i = 1,2,3,\ldots,11 \tag{2}$$

2.2 CHC Algorithm combined the strip theory

The strip theory is widely used in the wind turbine aerodynamic calculations. The CHC-STRIP approach here comprehensively maximises the power coefficient and limits the wind turbine power output behind the rated wind speed. It uses CHC algorithm to seek the optimal solution in this situation.

Fitness function:

$$F(V) = a\left(\frac{P}{\frac{1}{2}\rho A V^3} \right)^2 + (1-a)\left(\frac{1}{3}\sum_{14}^{17}\left(1-\left(\frac{P(V)-P}{P}\right) \right)^2 \right. \tag{3}$$

Constraints:

$$\theta_{\max} > \theta_3 > \theta_4 > \ldots > \theta_{11} > \theta_{\min} \ , \ c_{\max} > c_3 > c_4 > \ldots > c_{11} > c_{\min} \tag{4}$$

2.3 CHC Algorithm combined with maximum annual power generation

The annual generation capacity is one of the most important targets to measure the performance of the wind turbine. This method, MAX APG, which takes the BEM as the calculation model, maximises the annual power generation and limits the wind turbine power output behind the rated wind speed.

Fitness function:

$$F(V) = a\left(\frac{\int_6^{20} P(V) f(V) dV}{\int_6^{20} P(V)_{\max} f(V) dV} \right)^2 + (1-a)\left(\frac{1}{3}\sum_{14}^{17}\left(1-\left(\frac{P(V)-P}{P}\right) \right)^2 \right. \tag{5}$$

Constraints:

$$\theta_{\max} > \theta_3 > \theta_4 > \ldots > \theta_{11} > \theta_{\min} \ , \ c_{\max} > c_3 > c_4 > \ldots > c_{11} > c_{\min} \tag{6}$$

3 1.5MW BLADE OPTIMISATION DESIGN

As the Weibull distribution function of wind field is given, and the requirements of design power is met, CHC-Wilson method, CHC-STRIP method and MAX APG method are used

respectively to optimal design of the 1.5MW wind turbine blades. The overall parameters of the wind rotor are listed in table 1.

Table 1: 1.5MW wind rotor parameters

Parameters	Value	Parameters	Value
Rated Power	1.5 MW	Diameter	70 m
Rotational Speed	20 rpm	Design Wind Speed	13 m/s
Cut-in speed	4 m/s	Cut-out speed	20 m/s
Airfoil	LS(1)-0421	Number of Blades	3

Shown in figure 1 are the design results of the chord length and twist angle distribution of the 1.5MW blade using CHC algorithm combined with CHC-Wilson method, CHC-STRIP method and MAX APG method, respectively. The results from the CHC-Wilson method are significantly larger. This is because, in the process of optimisation design, only the maximum Cp of the wind is ensured, the constraints of the chord length and twist angle as well as power output limit are not considered. The power curves are shown in Figure 2, where the result from the CHC-Wilson method is not presented due to power overshoot at high wind speeds. It can be seen that, by adding a restriction of power output, the Cp value from CHC-STRIP method does not exceed that from the MAX APG method when the wind speed equals to the design wind speed 13m/s. The calculated energy production from the MAX APG method is increased by 4.1% compared to the CHC-STRIP method.

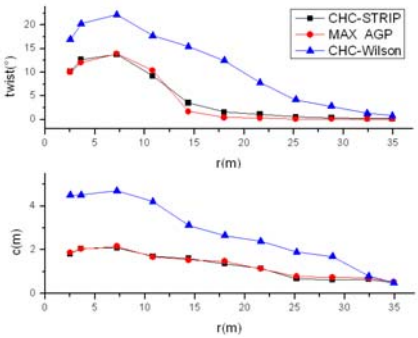

Figure 1: Chord and twist

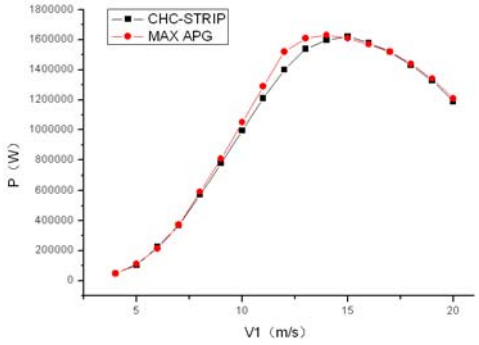

Figure 2: Power curve

To meet the demand of manufacture for blades, an 8-order Bezier curve fitting is used for blade layout smoothing as showed in Figure 3. The power curve in Figure 4 shows that the power excess appears after the smoothing, illustrating that the smoothing just following the optimisation design process might not be suitable under some circumstance. Therefore, the 8-order Bezier curve fitting for gene of the CHC algorithm is adopted before the optimisation process. Using this method, the optimal chord length and twist angle are obtained, shown in Figure 5. In this way, the power excess has disappeared when the wind speed exceed the designed wind speed, as demonstrated in Figure 6, while the calculated energy production is still increased by 3.8% compared to the value from the CHC-STRIP method.

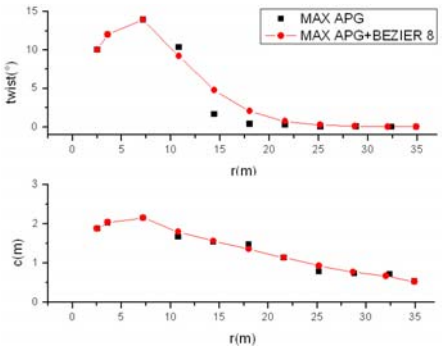

Figure 3: Chord and twist

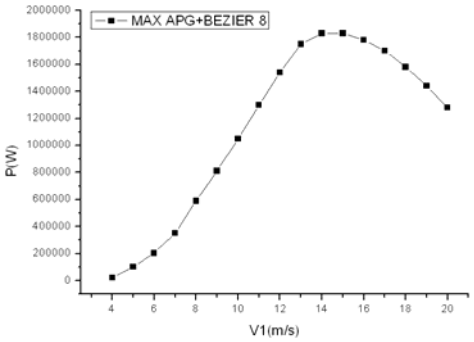

Figure 4: Power curve

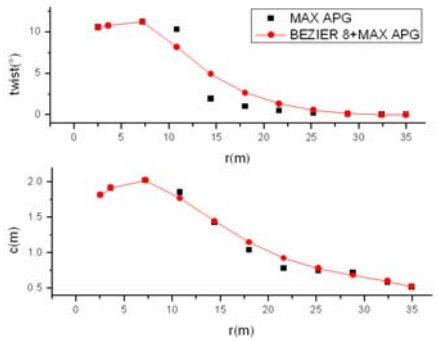

Figure 5: Chord and twist

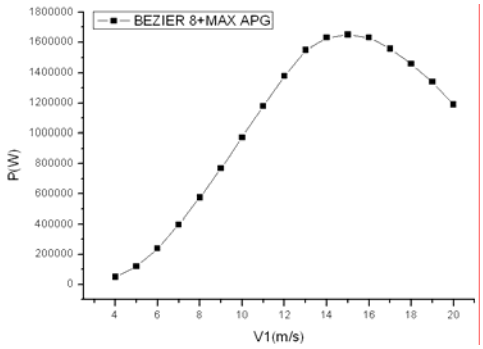

Figure 6: Power curve

4 CONCLUSIONS

The aerodynamic optimisation design for wind turbine blades has been investigated based on the CHC algorithm with the Wilson method, the strip theory and the maximum annual power generation. The genetic algorithm can be a good solution to the aerodynamic design of wind turbine blades, in which non-linear, multi-variables, multi-objectives optimisation is required. Taking the maximum annual power generation as the optimisation target, the CHC algorithm can improve the wind turbine blade design result.

5 ACKNOWLEDGEMENTS

This work was funded by the National Basic Research Program of China (973 Program) under Grant Number 2007CB714600.

BIBLIOGRAPHY

[1] Glauert,H., Airplane Propellers, Aerodynamic Theory(ed.W.F.Durand), Div.L,1943, Vol.

[2] Spera D A.Wind Turbine Technology[M]. Newyork: ASME Press, 1994.

[3] Wilson, R.E.and Lissaman, P.B.S., Applied Aerodynamics of Wind Power Machines, Oregon State Univ. Report NSF/RA/N-74113, July 1974.

[4] D.H.Wood, Dual Purpose Design of Small Wind Turbine Blades, Wind Engineering Volume 28, NO. 5, 2004 PP 511–528.

[5] P.J.Darrow, A.Wright and K.E.Johnson, Wind Turbine Control Design to Reduce Capital Costs, 47th AIAA Aerospace Sciences Meeting, 5 - 8 January 2009, Florida.

Dynamic Lift Measurement under Turbulent Conditions

Jörge Schneemann[1)], Pascal Knebel[1)], Michael Hölling[1)] and Joachim Peinke[1)]

[1)] ForWind - University of Oldenburg, Germany

ABSTRACT

We present dynamic lift measurements on a FX 79-W-151A airfoil under laminar and turbulent inflow. Turbulence was generated by a grid installed at the nozzle of the wind tunnel. Strain gauge sensors were used to measure lift and drag forces directly on the mounting of the airfoil. The pressure distribution on the wind tunnel walls measured by a set of 80 pressure sensors was used to calculate the lift coefficient. Thus we were able to obtain lift in two completely different ways at the same time. Mean lift curves were plotted. First results show a good agreement of the two different measured lift coefficients.

KEYWORDS

airfoil, dynamic lift, dynamic stall, turbulence, grid

1 INTRODUCTION

Most data about different airfoils available are static lift curves measured in laminar flow. Practically airfoils, or as an application the blades of a wind turbine almost never experience laminar inflow due to the surface roughness of the ground and are never flown against with a constant angle of attack (AoA) due to the increasing windspeed with increasing altitude. In both cases dynamic effects like dynamic stall take place. A major difference between static and dynamic lift is the raised maximum lift coefficient and fast changes of lift in the dynamic case. This leads to higher and fast changing loads on wind turbine blades which are not well known yet.

There are few studies dealing with dynamic effects on airfoils while pitching the foil in laminar flow (i.e. Ramsey et al., 1995; Sheng et al., 2009; Wolken-Möhlmann et al., 2007) and even less studies using turbulent inflow (Amandolèse and Széchényi, 2004). Larsen (2005) gives an overview about numerical dynamic stall models. The effect of alternating loads on wind turbines influenced by atmospheric turbulence was studied by Mücke et al. (2009).

Our goal was to arrange a system that allows us to measure dynamic effects on different airfoils under laminar and turbulent flow. The method of obtaining lift via measuring the pressure distribution on the wind tunnel walls set up by Bohlen (2005) works well for laminar

conditions, but there was no reference data to check it for turbulent conditions. So strain gauge based sensors were installed to be able to measure lift in two different ways at the same time.

2 METHODS

All lift measurements were performed in the closed loop wind tunnel of Oldenburg University with it's 1.0 m x 0.8 m x 2.0 m closed test section using a vertically mounted aluminium milled FX 79-W-151A airfoil with a chordlength of c=0.2 m. The typical wind velocity was about v≈50 m/s which led to Reynolds numbers of Re≈700,000. Lift coefficients were obtained in two different ways:

- The pressure distribution on the wind tunnel walls was measured using 80 pressure sensors. 40 sensors were placed on the wind tunnel wall opposite of the suction side of the foil with an interval of 5 cm between each other. The same setup was installed counterpart of the pressure side of the foil. c_L was calculated with

$$c_L = \frac{(p_p - p_s)}{q} \frac{L}{c} \eta \quad . \tag{1}$$

Hereby (p_p-p_s) is the difference between the over all pressure of the pressure- and suction side of the foil, q the dynamic pressure of the inflow, L the length of the wind tunnel walls (the space between 40 pressure sensors of one wall) and η = 0.94 the so called Althaus factor correcting the finite length the pressure distribution is measured on.

- The airfoil was mounted between two strain gauge based force sensors measuring lift and drag forces (perpendicular and parallel to the inflow). The lift coefficient c_L was obtained from

$$c_L = \frac{F_L}{q A} \quad , \tag{2}$$

where F_L is the lift force and A is the area of the airfoil.

All sensor signals were sampled with a frequency of f=1 kHz and calibrated after the measurements. Data analysis was performed with MATLAB. The signals of four pressure sensors were replaced by the average data of the neighbour channels because of apparently malfunctioning.

Turbulence was generated using a grid mounted on the nozzle of the wind tunnel. The mesh widths was 5cm and the blockage was 25%.

3 RESULTS

3.1 Static lift curves with laminar inflow

The measured time series for each AoA were averaged, and static lift curves were plotted. Figure 1 shows lift curves obtained from force- and wall pressure measurement. Additionally static data from Stuttgarter Profilkatalog by Althaus and Wortmann (1981) is plotted as reference. All curves show quite good agreement for AoA's smaller than 5°, for higher AoA's the force method slightly overestimates the lift. Maximum lift is faintly delayed.

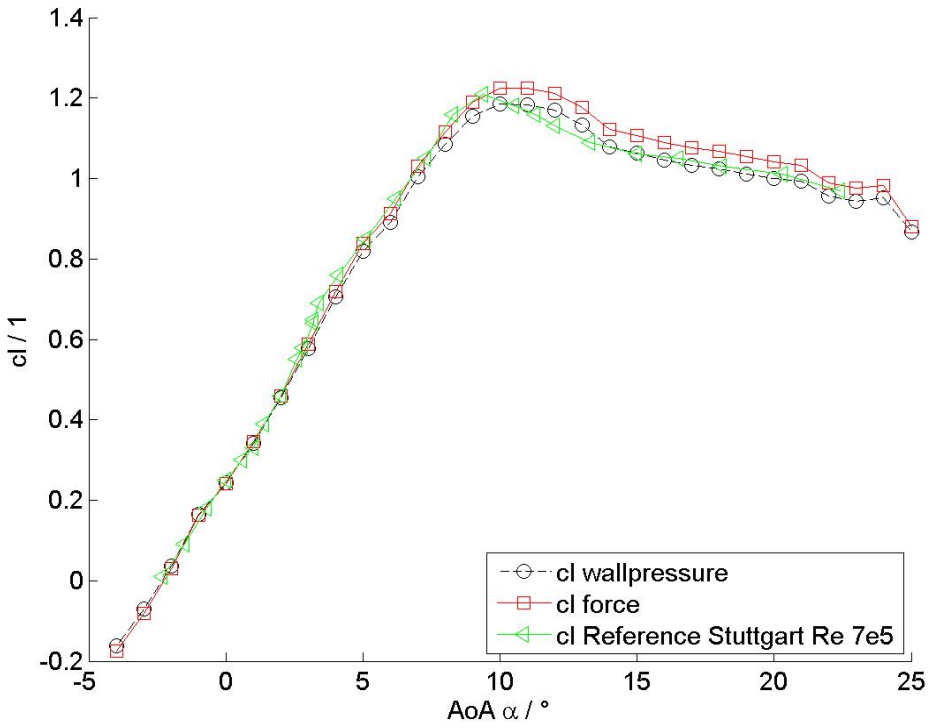

Figure 1: Mean lift curves: Black curve calculated from wall pressure, red curve is obtained from force measurement (both averaged over 10 s), green curve taken from Stuttgarter Profilkatalog by Althaus and Wortmann (1981)

3.2 Lift curves with turbulent inflow

In figure 2 time averaged lift for three different angles of attack is shown together with the reference. Curves measured under turbulent inflow generated by a 5 cm mashed grid is plotted as well as curves obtained under laminar inflow. Both used measuring techniques show good agreement in laminar and turbulent case. The overestimation of the force measurement is even smaller for the turbulent case. Under turbulent inflow lift is smaller for AoA's of 5° and 10° and higher for 22° than under laminar inflow.

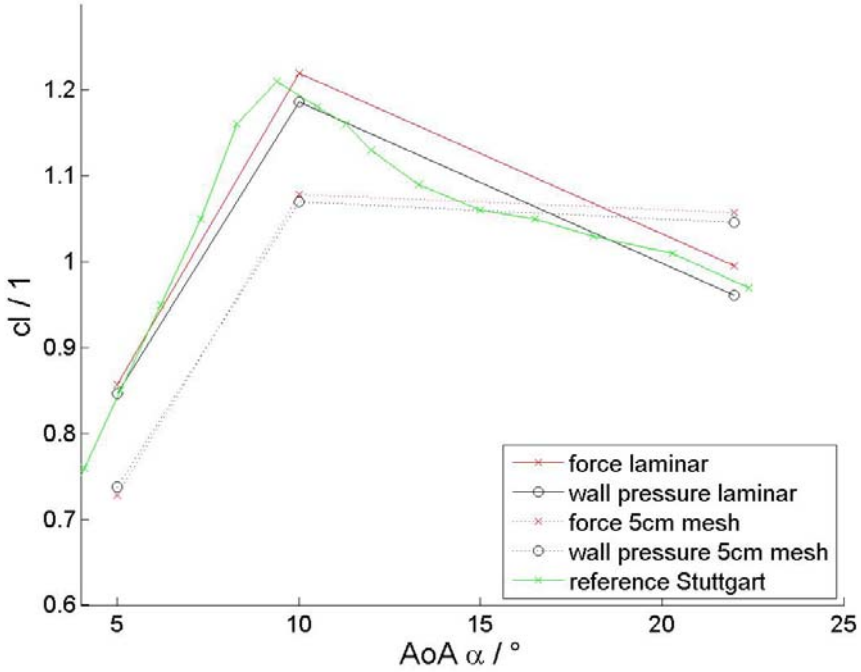

Figure 2: Wall pressure measurement and force measurement under laminar (solid lines) and turbulent (dotted lines) conditions. Every point is an average off a 120 s time signal.

4 CONCLUSIONS

The static lift data obtained from wall pressure and force measurements show really good agreement. For AoA's of 5° and above the force measurement seems to overestimate lift and shows an offset to the wall pressure data and the reference. Both curves run almost parallel, so we could assume the same effect is measured. The slightly delayed maximum lift compared to the reference might result out of small differences of the used airfoils and the finish of their surfaces.

Under turbulent conditions the wall pressure method still leads to the same averaged lift curves as the force measurement. As expected the lift under turbulent conditions is smaller at low AoAs but higher at large AoAs. The higher lift in the stall region of the foil could be explained with dynamic effects. Higher lifts in the stall region were obtained by Amandolèse and Széchényi (2004) for a *NACA 63$_4$_421* airfoil under turbulent conditions.

BIBLIOGRAPHY

- D. Althaus and F. X. Wortmann. Stuttgarter Profilkatalog I. Vieweg (1981).
- X. Amandolèse and E. Széchényi. Experimental study of the effect of turbulence on a section model blade oscillating in stall. Wind Energy, Band 7(4):Seiten 267– 282 (2004). doi:10.1002/we.137.
- T. Bohlen. Dynamische Auftriebsüberhöhung von Flügelprofilen. Diplomarbeit, Carl von Ossietzky Universität Oldenburg (2005).
- J. W. Larsen. Nonlinear Dynamics of Wind Turbine Wings. Dissertation, Aalborg University (2005).
- T. Mücke, D. Kleinhans and J. Peinke. Atmospheric turbulence and their influence on the alternating loads on wind turbines (2009).
- R. R. Ramsey, M. Hoffman and G. Gregorek. Effects of Grit Roughness and Pitch Oszillations on the S809 Airfoil. Technischer Bericht (1995).
- W. Sheng, R. A. M. Galbraith and F. N. Coton. On the S809 Airfoils Unsteady Aerodynamic Characteristics. WIND ENERGY (2009).
- G. Wolken-Möhlmann, P. Knebel, S. Barth and J. Peinke. Dynamic lift measurements on a FX-79-W-151A airfoil via pressure distribution on the wind tunnel walls. Journal of Physics: Conference Series, Band 75:Seite 012026 (7pp) (2007).

A CFD Investigation of the Near-Blade Local Flow Angle

Sugoi Gomez-Iradi [1+2], George N. Barakos [1] and Xabier Munduate [2]

[1] The University of Liverpool, Liverpool, United Kingdom
[2] The National Renewable Energy Centre (CENER), Spain

ABSTRACT

Compressible CFD methods for the analysis of horizontal axis wind turbines may become popular as the trend towards large-diameter rotors for off-shore wind turbines continues. The operational requirements of these rotors result in relatively high tip Mach numbers (of the order of 0.3 at sea-level conditions) and even higher local Mach numbers near the suction side of the blade.
The majority of the methods employed nowadays to calculate the loads of the blades and consequently the power of the wind turbine are based on BEM and need the incidence at each section of the blade in order to estimate the aerodynamic loads. In this paper, the NREL UAE Phase VI wind turbine is considered and an attempt is made to utilise the measured local flow angles (LFA) for comparisons CFD. Results from isolated rotors are also compared with computations for a complete wind turbine, highlighting the influence of the tower on the rotor aerodynamics.

KEYWORDS

Local flow angle, NREL UAE Phase VI. Rotor/tower interaction.

1 INTRODUCTION

Despite their recent success in several areas, CFD solvers still need validation against experimental or field data. Field data obtained using instrumented turbines offer more realistic conditions than tunnel measurements due to variations in inflow and associated turbulence, in addition to a full-scale geometry. However, uncertainties regarding in-field measurements make wind tunnel data more suitable for initial validation of CFD solvers. Further, wind tunnels offer carefully controlled conditions and refined measurement techniques not available on wind turbine farms. The review paper of Vermeer et al. [1] catalogues all experiments related to wind turbines measurements, prior to 2003. The categorisation by Vermeer et al. [1] considered wind turbine size, test conditions and type of measured data, amongst others. From this work [1], it appears that the most comprehensive experiment for CFD validation was carried out in the NREL UEA Phase VI wind tunnel [2] campaign. This is supported by the extensive use of this set of experiments by many researches [3-5]. The main measured quantity was the chord-wise pressure distribution [2] at five span-wise blade sections. A total of 22 pressure transducers were placed in each chord-wise section. The geometric characteristics of the two bladed upwind rotor configuration include 3° pitch at the tip, 0° of cone angle and 0° of yaw angle. The S809 aerofoil section [6] was used from 25% of the blade radius to the tip. Unfortunately, there were not any wake measurements, which could further enhance the value of these experiments and the fidelity of the CFD validation. In this direction, the MEXICO project [7] experiments look promising for validation purposes since they offer PIV measurements of the wake, unfortunately, the data is not in the public domain yet.
The definition of the blade geometry of the Phase VI experiments provided the coordinates of the employed S809 section, the tapper of the blade, as well as, the twist distribution and the blade pitch. The tip and root sections were not defined in a unique way, and the authors [8] have made an attempt to quantify their effect. It was found that the pitch and aspect ratio of

the blade have much stronger influence on the aerodynamic loading than the exact shape of the root attachment and tip cup. For that work, isolated rotor cases were considered (no tower and no nacelle) and the planform used for validation is shown in Figure 1.
No much research related to NREL UAE Phase VI campaign local flow angles (LFA) has been published. Some work has been published by DUT [9-11], where an in-house free wake vortex method was employed to calculate the angle of attack of several sections for non yawed and yawed flows. Kuik et al. [9] reported that the flow near a rotor is rather complicated and affected by the lift of the blade and the wake formation downwind of the rotor plane. The latter in combination with the finite span have in general a small influence on the local inflow angle in contrast to the up-wash caused by the lift. The Biot-Savart law can be used as a correction for the induced angle. Sant et al. [10] used the derived aerofoil data in a BEM code to predict the low speed shaft torque and the blade root flap/edge moments. They conclude that reasonably good agreement was achieved in these results when compared with those derived from the pressure measurements. Sant et al. [11] also shown that using a free wake vortex model, it was possible to derive the unsteady angle of attack distributions from knowledge of the aerodynamic normal and tangential forces acting on the blades of a yawed rotor. For that purpose 5, 10 and 15m/s cases at 30° of yaw angle were used. In order to calculate inflow correction curves, a 3D Lifting-Surface Inflow Correction Method (LSIM) was developed [12] with the aid of a vortex-panel code at University of Illinois at Urbana-Champaign. Comparison of the new method with 2D methods suggested that, due to the 3D geometry at the root and 3D flow effects at inboard stations, the 2D wind tunnel method of correction currently in use at NREL over-predicts the up-wash at pre-stall angles of attack and under-predicts up-wash at post-stall angles of attack. Madsen et al. [13] presented a comparison [13] between the EllipSys3D N-S solver, and the HAWC and HAWC3D methods that are based on the actuator disc concept. That work focussed on experiments at 7m/s and 45° yaw case. They reported that the agreement between the experimental data and the LFA calculated with EllipSys3D was generally good, although some deviations could be observed for thr inboards stations. Both HAWC and HAWC3D underestimated systematically the LFA due to the influence of up-wash. Johansen et al. [14] presented a method of determining the local angle of attack. The method was based on determining the disturbed axial velocity in the rotor plane and was called the reduced axial velocity method.
The present work is motivated by the established trend towards increased diameter HAWTs. This trend brings the design engineers near the edge of their knowledge envelope and creates an opportunity for CFD methods to be used as an economic alternative to wind tunnel and field experimentation. The Wind Multi-Block solver [5,16] has been used in this work to investigate the predictive capability of CFD and provide insight in the obtained flow angle measurements. The Wind Multi-Block CFD solver (WMB) employed for this work has been validated [2] against the NREL UAE Phase VI wind tunnel experimental data. Once confidence in the method was established, calculations were carried out for the complete NREL UAE Phase VI wind turbine. A sliding grid technique [15] has been employed in order to compute the rotating blades and spinner, the fixed nacelle and tower using a CFD mesh of 7 million cells [16]. The computations were compared with experimental local flow angles.

2 LOCAL FLOW ANGLE

The LFA study is presented in the following subsections. First of all, a relation between 3D and 2D LFA, as well as, incidence angle has been studied.
Then, the LFA & SFA obtained for the isolated cases at different wind speeds will be shown. Finally, the influence of the tower on the rotor aerodynamics through LFA comparison will close this section. Notice that for all computations the experimental probes were not modelled in CFD, which could have some influence especially at in-boards stations.

2.1 2D: S809 aerofoil

In order to find a relation between the 2D and 3D computations, identical sections have been

taken for both cases. In 3D, the loads and the LFA of four sections were extracted at 51%R, 67%R, 84%R and 91%R. For 2D, in order to recreate similar condition the local Reynolds number of each of the sections was selected. Sectionals loads were then compared at the same normal coefficient (CN) values. In order to get as close value as possible to the 3D case, the incidence used for 2D computations was varied. The obtained CFD data had to be processed the same way as the experiments. To this end, the CFD pressure was extracted at the locations of the pressure transducers shown in Figure 1. Then the CN was obtained with the Equation 1 for the 2D and 3D cases.

$$C_N = \sum_{i=1}^{n} \frac{P[i][m+1] + P[i][m]}{2} * (x[i][m+1] - x[i][m]) \quad (1)$$

Table 1 shows the direct relation between the 2D and 3D LFA. It is significant that for 5m/s case, the difference for the same loads from 3D LFA and 2D incidence is of 3.7-3.9°. For the 7m/s case this differences increases to 3.25-4.85°. And for 10m/s case, this difference becomes almost constant like for the 5m/s case oscillating the values between 7° and 7.4°.

2.2 Non yawed flow in isolated Rotor

To extract the LFA from CFD, values from a small area around the location of the probe were used. Different circular sections extracted from the flow-field demonstrated that extraction circle radii between 0.01 and 0.2 chords had no significant variation (less than 1%).

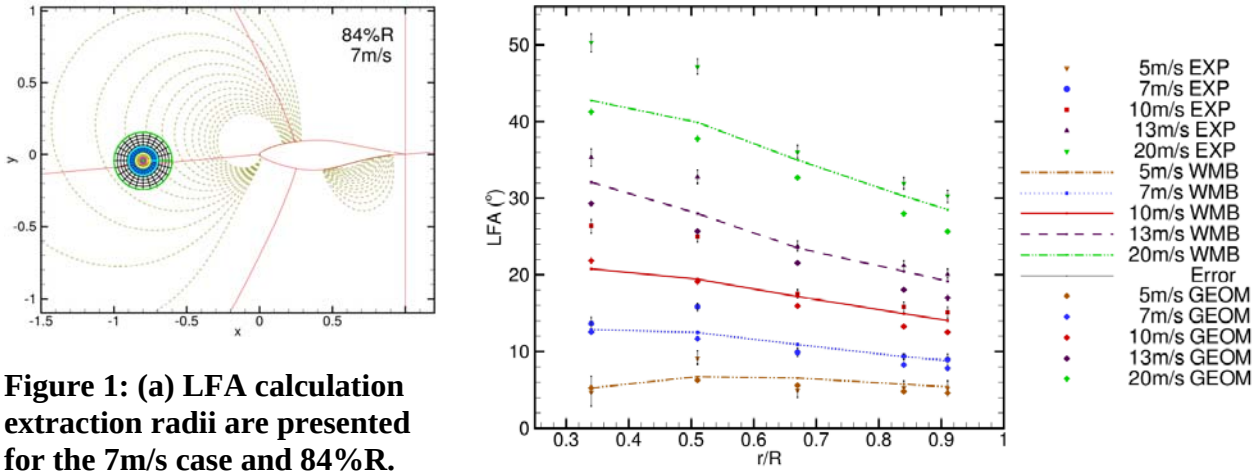

Figure 1: (a) LFA calculation extraction radii are presented for the 7m/s case and 84%R. (b) LFA for five different wind speeds along the span of the blade (5, 7, 10, 13 & 20m/s).

The LFA results are shown in Figure 1, and as can be observed, the agreement towards the tip is good overall. This was expected since the outboard station surface pressure coefficient predictions were also good [8]. Inboards, the first two stations are under-predicted, except for the low or moderate wind speeds, where the flow was still attached at these sections. There, the agreement at 34%R is also good. Remarkably, near the mid-span of the blade, at 51%R station, the agreement between the computations and experiments for all wind cases is poor. These large differences in flow angles are not fully understood since the surface pressure coefficients agree well for attached flow cases at 46.6%R station [8].

The differences between local flow angles for 2D and 3D computations can be used as an estimate of the down-wash seen by the 3D blade. At 5m/s, this approximate down-wash appears to be almost uniform along the span of the blade, as can be seen in Table 1. The LFA difference has a similar trend for wind speeds between 5 and 10m/s, while the effect increases on the last three span-wise stations as the blade tip is approached. The relatively high values at 51%R station could be explained by the root vortex formation at 25%R of the blade and the span-wise flow due to the high twist of that region. The analysed wind speeds (5-10m/s) involve attached and partially stalled flows. At 13m/s, where the flow stalls, the differences between 2D and 3D LFA increase considerably. On the other hand, the

difference of the AoA used for the 2D computations and the measured LFA, decreases for outboard span-wise stations as well as with the reduction of the free-stream velocity. This trend is, however, not followed by the 13m/s case, where similar differences as for 10m/s case are listed in Table 1.

Table 1: LFA for 2D & 3D cases with similar CN at four different wind speeds.

Wind Speed (m/s)	Span-wise Station	CFD	C_N	LFA (°)	Incidence (°)	$\Delta_{(LFA_{3D})-Incidence}$ (°)	Downwash (LFA_{3D}-LFA_{2D}) (°)
5m/s	51%R	2D	0.4205	4.2	2.40	1.80	2.50
		3D	0.4269	6.7	-	-	
	67%R	2D	0.4476	4.5	2.60	1.90	2.00
		3D	0.4486	6.5	-	-	
	84%R	2D	0.4158	4.0	2.30	1.70	2.00
		3D	0.4120	6.0	-	-	
	91%R	2D	0.3580	3.3	1.80	1.50	2.30
		3D	0.3598	5.6	-	-	
7m/s	51%R	2D	0.9489	11.5	7.25	4.25	1.00
		3D	0.9495	12.5	-	-	
	67%R	2D	0.8467	10.5	6.65	3.85	0.40
		3D	0.8514	10.9	-	-	
	84%R	2D	0.6991	8.2	5.10	3.10	1.10
		3D	0.7088	9.3	-	-	
	91%R	2D	0.6033	6.6	3.95	2.65	2.20
		3D	0.6042	8.8	-	-	
10m/s	51%R	2D	1.2828	17.0	11.20	5.80	1.50
		3D	1.2862	19.5	-	-	
	67%R	2D	1.1867	15.3	9.90	5.40	1.90
		3D	1.1893	17.2	-	-	
	84%R	2D	1.0228	12.6	8.00	4.60	2.40
		3D	1.0219	15.0	-	-	
	91%R	2D	0.8855	10.6	6.60	4.00	3.40
		3D	0.8823	14.0	-	-	
13m/s	51%R	2D	1.1217	14.2	9.10	5.10	13.80
		3D	1.1213	28.0	-	-	
	67%R	2D	1.0597	13.2	8.40	4.80	10.40
		3D	1.0552	23.6	-	-	
	84%R	2D	0.9856	12.0	7.60	4.40	7.50
		3D	0.9840	20.5	-	-	
	91%R	2D	0.8964	10.7	6.70	4.00	8.50
		3D	0.8975	19.2	-	-	

2.3 Full wind turbine

The trend of the experiments is well captured at all span-wise stations. The agreement between experiments and computations is good and shows the capability of the CFD as a predictive tool for full wind turbine analyses. The differences at the 51%R station may be due to some error in experimental data acquisition system and/or calculation, since the shape and the amplitude of the LFA variations are well captured. The magnitude, however, is under-predicted by almost 4°.

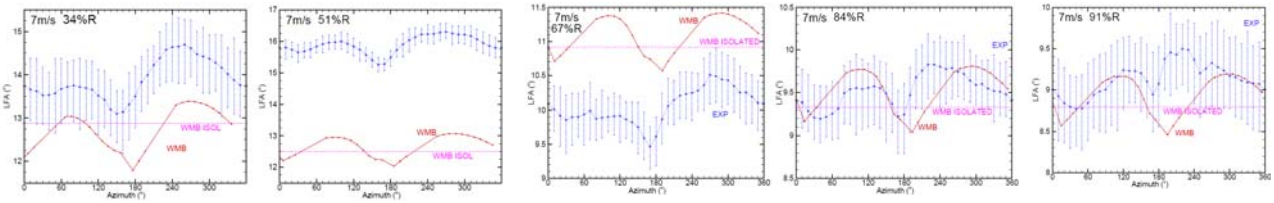

Figure 2: Comparisons of LFA between experiments, the isolated rotor and full wind turbine configuration at 7m/s case.

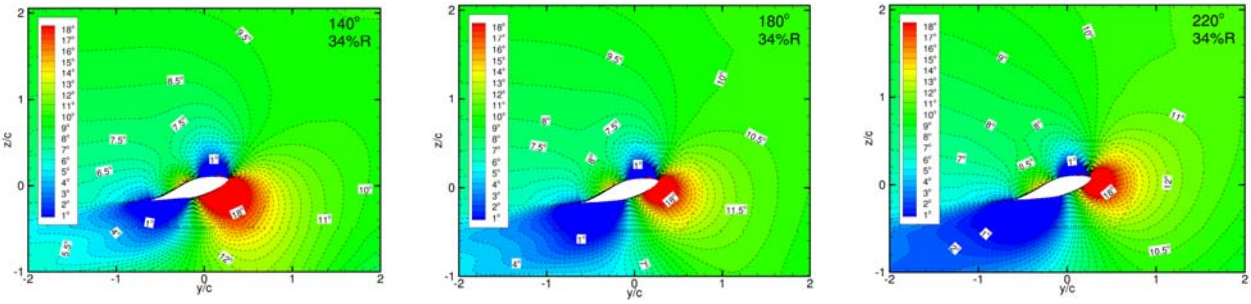

Figure 3: LFA at three azimuth positions (140°, 180° & 220°) for the 34%R and full wind turbine configuration at 7m/s case.

3 CONCLUSIONS AND FUTURE WORK

The results of the local and span-wise flow angles obtained with CFD can provide insight in the wind-turbine flow and can be used as input, for simpler engineering methods like BEM.

To improve the accuracy of the obtained prediction, the flow angle probes should be modelled and computed with CFD, especially where the velocity ratio between the inflow and local velocity due to rotation is small. Alternatively, less intrusive measurement techniques for flow angle measurements are could be employed. The obtained results show that CFD has adequate resolution to provide the details of the flow. The analysis of the data is, however, difficult since the 3D results contain no explicit information about flow incidence. Comparison with 2D data is, however, possible and provides valuable insight in the quantification of the blade down-wash along the span of the blades.
In the future, the work will focus on further analysis of this flow in an attempt to derive reduced models for the trend of the local flow angle that could be used in conjunction with simpler aerodynamic tools, like BEM.

Acknowledgements

The financial support of this project by the National Centre of Renewable Energy of Spain (CENER) is gratefully acknowledged as well as the release of the NREL data though the Annex XX consortium. The authors are also grateful to the DEISA consortium (www.deisa.eu), co-funded through the EU FP6 project RI-031513 and the FP7 project RI-222919, for support within the DEISA extreme computing initiative.

BIBLIOGRAPHY

[1] L.J. Vermeer, J.N. Sørensen, and A. Crespo, Wind Turbine Wake Aerodynamics, Progress in Aerospace Sciences, 39(6-7):467–510, 2003. DOI:10.1016/S0376-0421(03)00078-2.
[2] M.M. Hand, D.A. Simms, L.J. Fingersh, D.W. Jager, J.R. Cotrell, S. Schreck, and S.M. Larwood, Unsteady Aerodynamics Experiment Phase VI: Wind Tunnel Test Configurations and Available Data Campaigns, Technical Report TP-500-29955, NREL, December 2001.
[3] S. Schmitz and J.-J. Chattot, A Parallelized Coupled Navier-Stokes/Vortex-Panel Solver, Journal of Solar Energy Engineering, 127(4):475–487, 2005. DOI:10.1115/1.2035707.
[4] N.N. Sørensen, J.A. Michelsen, and S. Schreck, Navier-Stokes Predictions of the NREL Phase VI Rotor in the NASA Ames 80 ft x 120 ft Wind Tunnel, Wind Energy, 5(2-3):151–169, 2002.
[5] E.P.N. Duque, M.D. Burklund, and W. Johnson, Navier-Stokes and Comprehensive Analysis Performance Predictions of the NREL Phase VI Experiment, Journal of Solar Energy Engineering, 125(4):457–467, 2003. DOI:10.1115/1.1624088.
[6] D.M. Somers, Design and Experimental Results for the S809 Airfoil, SR-440-6918, NREL, 1997.
[7] H. Snel, J.G. Schepers, and B. Montgomerie, The MEXICO project (Model Experiments in Controlled Conditions): The database and first results of data processing and interpretation, DOI:10.1088/1742-6596/75/1/012014, The Science of Making Torque from Wind, DTU, 28-31, 2007.
[8] S. Gomez-Iradi and G. Barakos, Computational Fluid Dynamics Investigation of Some Wind Turbine Rotor Design Parameters, Proceedings of the Institution of Mechanical Engineers, Part A: Journal of Power and Energy, 222(5):455–470, 2008. DOI:10.1243/09576509JPE526.
[9] G.A.M. van Kuik, R.P.J.O.M. van Rooij, and H. Imamura, Analysis of the UAE Phase VI Wind Tunnel Results in the Non-Yawed Flow, 2003 EWEC, Madrid, June 2003.
[10] T. Sant, G. van Kuik, and G.J.W. van Bussel, Estimating the Angle of Attack from Blade Pressure Measurements on the NREL Phase VI Rotor Using a Free Axial Conditions, Journal of Wind Energy, 9:549–577, 2006. DOI:10.1017/we.201.
[11] T. Sant, G. van Kuik, and G.J.W. van Bussel, Estimating the Angle of Attack from Blade Pressure Measurements on the National Renewable Energy Laboratory Phase VI Rotor Using a Free Wake Vortex Model: Yawed Conditions, Journal of Wind Energy, 2008. DOI:10.1002/we.280.
[12] J. Whale, C.J. Fisichella, and M.S. Selig, Correcting Inflow Measurements from Wind Turbines Using a Lifting-Surface Code, Journal of Solar Energy Engineering, 122(4):196–202, 2000.
[13] H. Madsen, N.N. Sørensen, and S. Schreck, Yaw Aerodynamics Analysed with Three Codes in Comparison with Experiment, AIAA paper 2003-519, 41st AIAA, Reno, Nevada, 6-9 January 2003.
[14] J. Johansen and N.N. Sørensen, Aerofoil Characteristics from 3D CFD Rotor Computations, Wind Energy, 7(4):283–294, 2004. DOI:10.1002/we.127.
[15] R. Steijl, G. Barakos, and K. Badcock, A Framework for CFD Analysis of Helicopter Rotors in Hover and Forward Flight, International Journal for Numerical Methods in Fluids, 51(8):819–847, 2006.
[16] S. Gomez-Iradi, R. Steijl and G.N. Barakos, Development and Validation of a CFD Technique for the Aerodynamic Analysis of HAWT, Journal of Solar Energy Engineering, 131(3), 2009. DOI: 10.1115/1.3139144.

CFD Modeling of a Straight Blade Vertical Axis Wind Turbine (SB-VAWT)

K M Almohammadi[1)], L Ma[1)], D B Ingham[1)], M Pourkashanian[1)]

[1)] Centre for CFD, The University of Leeds, United Kingdom

ABSTRACT

In the last few decades, the consumption of energy has been significantly increased. As energy sources in the world are being depleted, wind energy becomes one of the most promising and reliable sources of energy. In this paper a 2-D straight blade vertical axis wind turbine is analyzed using Fluent in order to compare its performance at different modeling characteristics. A sliding mesh technique is used in the analysis and the performance is measured by the power coefficient. The convergence is assessed by the torque profile and it is found that there is a significant effect of the tip speed ratio on the turbine performance.

KEYWORDS

Straight-Blade Vertical Axis Wind Turbine (SB-VAWT), Turbulence Modelling, Sliding mesh.

1 INTRODUCTION

As energy sources in the world are being depleted, wind energy has become one of the most promising and reliable sources of energy. It can be extracted using either Horizontal Axis Wind Turbine (HAWT) or Vertical Axis Wind Turbine (VAWT) that transform some of this energy into other useful forms, such as electrical energy or mechanical energy. One of the main attractive attributes of the vertical type of wind turbine is that it is not affected by the changes in the wind direction, i.e. it does not need to be adjusted to the wind direction.

Due to the rapid progress in technology, computational schemes have become more efficient and reliable. The new facilities and advanced PCs have allowed researchers to change and modify the models for better understanding of the turbulence analysis. In this paper we determine and examine the performance of a straight-blade vertical axis wind turbine by simulating the flow around three airfoils using a CFD simulation.

2 CFD TURBULENCE MODELLING

2.1 Straight Blade Vertical Axis Wind Turbine Design

The three airfoils of the turbine are a NACA0018 airfoil with a chord length of 0.27 m. The mesh near the airfoil is generated as a structured mesh, whereas it is unstructured elsewhere in the domain as explained in figure 1 and 2.

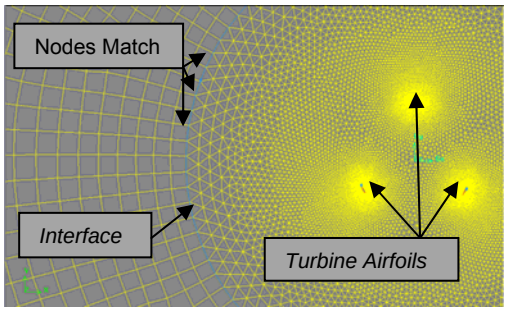

Figure 1. 2-D VAWT mesh illustration.

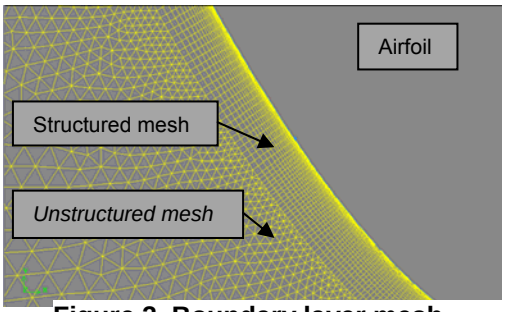

Figure 2. Boundary layer mesh.

An upwind speed is selected to be 12.5 m/s and the tip speed ratio is fixed at 3.75. The straight blade vertical axis wind turbine in the study runs in a relatively low Reynolds number range (< [10] 16) and therefore the tendency of separation is high. As a result, the analysis of the forces around the airfoils requires more consideration, especially near the airfoil wall[3]. The forces should be analyzed up to the wall surface and the effect of the molecular viscosity in the eddies must be included in the selected model. It is very important to adjust the distance of the nodes in the first row of the mesh around the airfoil. This distance is represented by a non-dimensional quantity, known as y^+. These nodes must be located in the log layer of the wall boundary in order to predict the velocity profile which can be non-dimensionally calculated using the equation

$$u^+ = \frac{1}{k}\ln y^+ + c \qquad (2.1)$$

where k and c are constants. It is known that if y^+ lies in the buffer region then the performance prediction would not be reliable due the complexity of the flow in the transition phase [4]. For that reason, two values of y^+, namely 3.7 and 0.5, are adjusted in two different simulations.

For the purpose of the analysis, 2-dimensional double precision Fluent is selected, and the sliding mesh technique is applied between the rotating and fixed circle interfaces. The iteration is stopped and the solution is converged when all iterated quantities achieve a residual of less than 10^{-5}.

2.2 Turbulence Models

There are many turbulence models available to be used. However, none of them is universally applicable. The choice of the turbulence model depends on many factors, such as: the accuracy required for the physics of the problem, computational power available, etc. Three turbulence models are applied for the same mesh in order to assess the prediction differences. These models are the RNG-K-ε, Spalart-Allmaras and K-ω SST. The formulation of this model makes it reliable for low Reynolds number applications and account for separa-

tion. The reason for this is that the constants in the transport equations become functions of the local

Reynolds number [4]. It is found that 200 time steps per rotation are enough for a good performance analysis.

3 RESULTS AND DISCUSSIONS

The prediction of the power coefficient for the RNG-K-ε , Spalart-Allmaras and K-ω SST models are 0.38, 0.379, and 0.413, respectively. It is clear from figure 3 that the power coefficients differ by about 8 %. All K-ε models are known to under predict near wall flows, and this explain the lower power coefficient obtained. It is clear that the power coefficients for the Spalart-Allmaras and RNG-K-ε models are very close (0.3 %). The possible explanation for this is that the mesh near the wall is not sufficient for the Spalart-Allmaras model and the wall function is applied as RNG-K-ε .

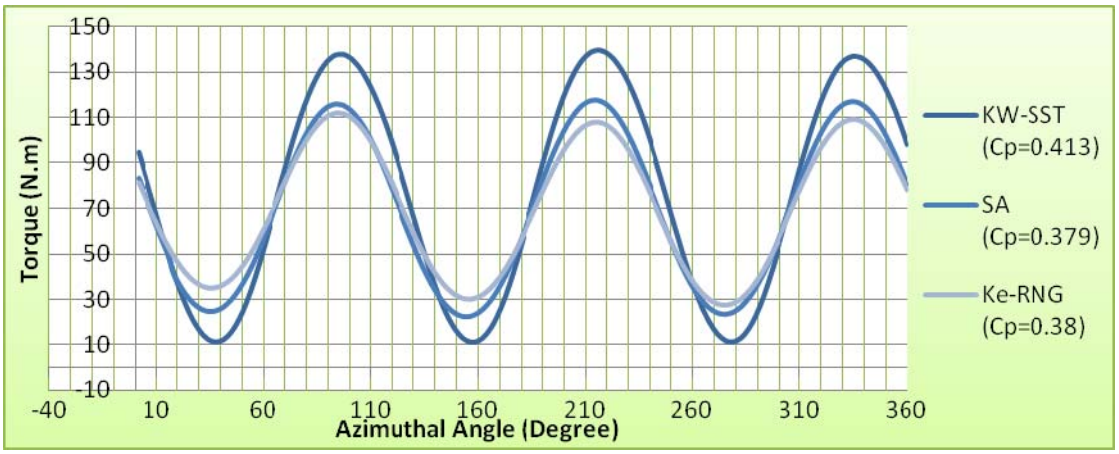

Figure 3. Torque profile for different turbulence models.

These models are capable of capturing the vortex shedding and secondary flows around the airfoils, as shown in figure 4.

	K-ω sst	RNG-K-ε	Spalart-Allmaras
Vortex structure	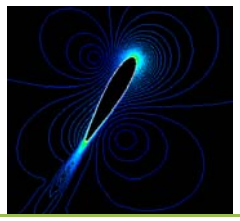	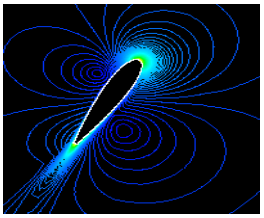	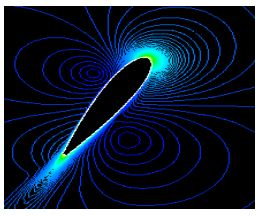

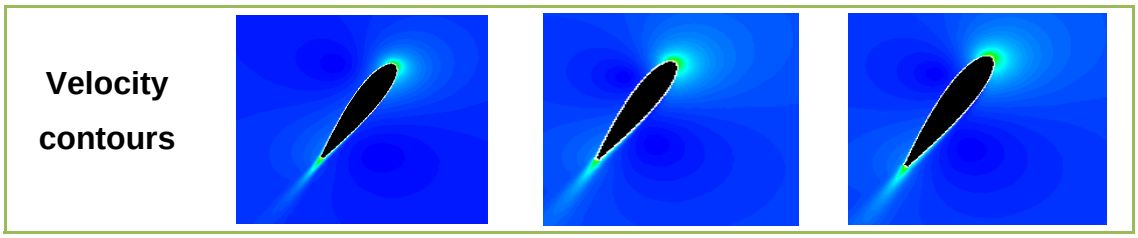

Figure 4. Veltocity contours and vortex structure for different turbulence modes for blade 2.

Figure 5 compares the results obtained for different values of y^+. Both mesh structures and all other factors are the same except for the value of y^+. The power coefficient when $y^+ = 3.7$ is 0.413 whereas it is 0.431 when $y^+ = 0.5$ and this difference is relatively low. The possible reason for this is that by reducing the distance of the first node from the wall will result in the power coefficient being enhanced.

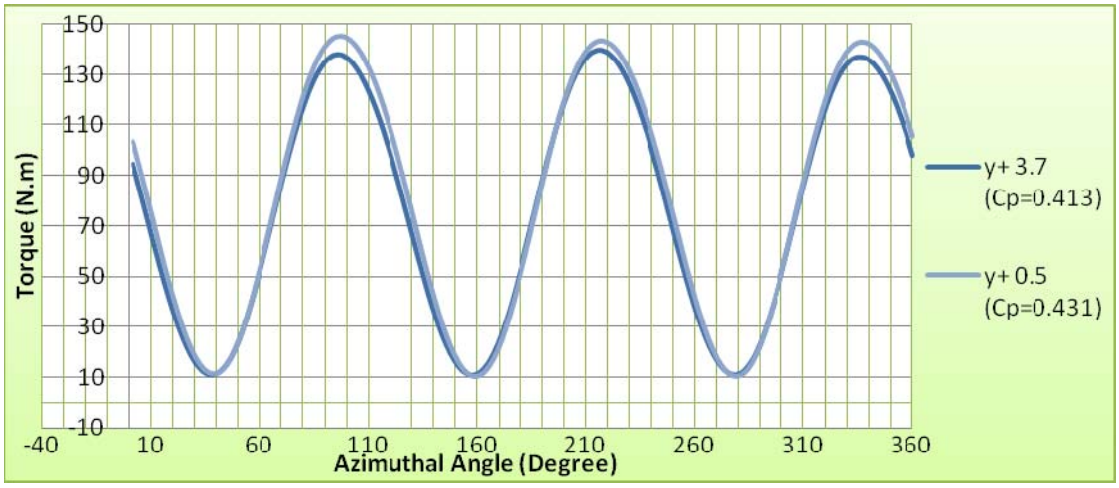

Figure 5. Torque profile for different values of y+.

4 CONCLUSIONS

The results show that the RNG-K-ε, Spalart-Allmaras and K-ω SST models are capable of predicting the straight blade vertical axis wind turbine performance. There is good agreement in the overall power coefficient. Also, it is clear from the analysis that there are no significant effects when using the mesh with $y^+ < 3.7$ and applying the K-ω SST. This may save a substantial amount of computational power and time.

However, the effect of the turbine rotor and bars connecting the blades to the rotor are not considered in this analysis. This should be accounted for in the future work since it may substantially affect the overall turbine performance. The RNG-K-ε and Spalart-Allmaras models should be assessed for $y^+ < 3.7$ to check if they behave as in the K-ω SST model.

ACKNOLEDGEMENT

Khaled M. Almohammadi would like to express his gratitude to Taibah University, Kingdom of Saudi Arabia supporting him to perform the work presented in this paper.

BIBLIOGRAPHY

[1] M. Islam, “Analysis of Fixed-Pitch Straight-Bladed VAWT with Asymmetric Airfoils,” Doctoral Dissertation, Mechanical Engineering, University of Windsor, Canda, 2008.

[2] M. Hansen, and D. S řensen, “CFD model for vertical axis wind turbine,” *ORBIT,* vol. 2007, pp. 2006, 2008.

[3] F. Fluent, “6.3 User’s Guide,” *Lebanon, New Hampshire (USA) Fluent Inc*, 2006.

SESSION 5

Thursday, 01.10.2009

9:00AM

Modal Analysis and Optimization of a Tubular Tower

Ruitao Peng[1)], Xiongwei Liu[2)]

[1)] University of Central Lancashire, UK, [2)] University of Central Lancashire, UK

ABSTRACT

The inherent dynamic characteristics of the tower have a significant impact on the dynamic performance of the wind turbine. In order to design an economic alternative tower for a commercial wind turbine, the design was based on a modal analysis performed by applying appropriately chosen various materials and geometries. And by identifying suitable finite element models of towers, inherent frequencies and vibration modes were calculated and optimized. The results show that the design of the tower meets the design specifications.

KEYWORDS

Tower, modal analysis.

1 INTRODUCTION

For a wind turbine, the tower must have sufficient strength and rigidity to sustain the weight of the turbine and the aerodynamic forces on the rotor and the tower. The inherent dynamic characteristics of the tower have a significant impact on the dynamic performance of the wind turbine **Error! Reference source not found.**.

In order to ensure the normal operation of the wind turbine, the inherent vibration characteristics of the turbine and tower should be matched properly to avoid the occurrence of resonance phenomenon. Given the material properties and geometrical shape of a commercial tower [2], several alternative designs were proposed by applying different materials and thicknesses. Consequently, modal analyses were carried out by using finite element method, and an alternative design was optimized to meet the design specifications.

2 ON THE FINITE ELEMENT MODEL OF THE TOWER

2.1 The Original Geometric Structure

The tubular tower has a total height of 33.1724 m and is formed as a truncated cone with an external diameter of 3.4725 m at the base and 2.0384 m at the top (Fig. 1). The tower consists of 5 sections with 5 shell thickness respectively in the height direction, noted as Sections A, B, C, D and E. The shell thickness ranges from 11.1125 mm at the base to 6.35 mm at the top. According to the structural characteristics of the tower, 8-node doubly curved

thick shell elements of reduced integration (S8R) are chosen to mesh the structure. An FE model is established after making some simplifying assumptions [3] (Fig. 2), including: 1) the tower is simplified as a 3D thin cylinder structure with fixed base and unrestricted top, 2) the position of mass center of the turbine is located at the top center of the tower. The material of the original tower is A36, which will be substituted by the material named Q 235 and 16Mn (shown in Table 1).This paper aims to design an alternative tower which has approximate natural frequencies to the original commercial one.

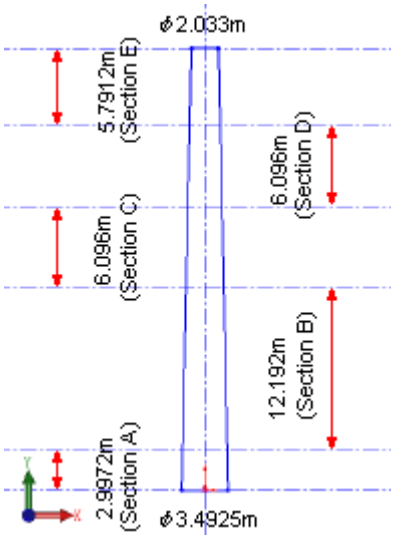

Figure 1: Sketch of the Tower Structure

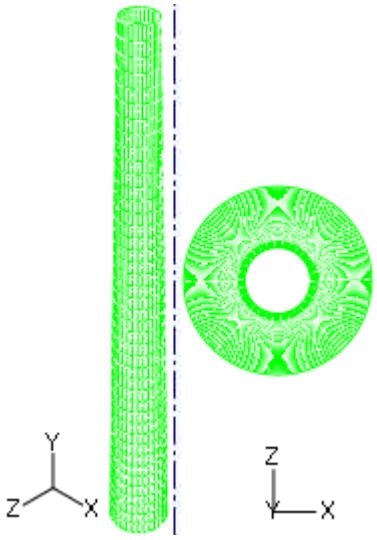

Figure 2: Finite Element Model of the Tower

Table 1: Physical Properties of the Tower Materials [2]

Material	Density [kg/m^3]	Young's Modulus [MPa]	Poisson's Ratio
A36	7880	196~206	0.24~0.27
Q235	7850	196~206	0.24~0.28
16Mn	7900	206	0.25~0.3

2.2 The Design Schemes

There are many factors which may affect the natural frequencies of the tower. It is perceived that the weight is inversely proportional to the natural frequency, and the stiffness is proportional to the natural frequency. In order to optimize the tower structure, different materials and shell thickness were combined, as shown in Table 2. From the cost point of view, the thickness of Section A, B, C and D will be set as 12 mm; 10 mm, 10 mm and 8 mm respectively, and the thickness of Section E will be increased from 6.5 mm to 8 mm.

Table 2: Design Schemes of the Tower

Design No.	Material	Section Thickness [mm]				
		A	B	C	D	E
1	Q235	12	10	10	8	6.5
2	Q235	12	10	10	8	7
3	Q235	12	10	10	8	8
4	16Mn	12	10	10	8	6.5
5	16Mn	12	10	10	8	7
6	16Mn	12	10	10	8	8

3 THE MODAL ANALYSIS AND DISCUSSION

A modal analysis module was used to perform eigenvalue extraction to calculate the natural frequencies and corresponding mode shapes of the tower, and eigenvalues are requested using the Lanczos eigenvalue solver. Since we only care about the low-level modes, the first 5 modes were extracted [4]. The first five eigenvalues of the tower, as computed by the above FE models, are listed in Table 3. It's shown that not only the first two modes, but also the third and fourth modes have the same natural frequency in all the designs. The same mode is a result of periodical symmetry of the structure, and they have the same shape, just deformed in two perpendicular planes.

Design 0 represents the original design of the tower, the tower from Design No. 1 to No. 6 stand for our design alternatives. According to the calculated results in Table 3, compared with the other five designs, the first 5 frequencies of Design No. 2 are very close to that of the original tower and it's chosen to be the selected optimal design. The corresponding eigenmodes in Design 0 and Design 2 are shown in Fig.3 and Fig.4 respectively. While the fifth eigenmode is manifested as whirly expansion, however the others manifested as bent vibrations.

Table 3: Calculated Natural Frequencies of the Tower

Design No.	Material	Natural Frequency [Hz]				
		1st mode	2nd mode	3rd mode	4th mode	5th mode
0	A36	3.8685	3.8685	16.828	16.828	34.986
1	Q235	3.9359	3.9359	16.905	16.905	35.297
2	Q235	3.8680	3.8680	16.721	16.721	35.036
3	Q235	3.7418	3.7418	16.401	16.401	34.524
4	16Mn	3.9714	3.9714	17.050	17.050	35.410
5	16Mn	3.8030	3.8030	16.864	16.864	35.148
6	16Mn	3.7757	3.7757	16.541	16.541	34.634

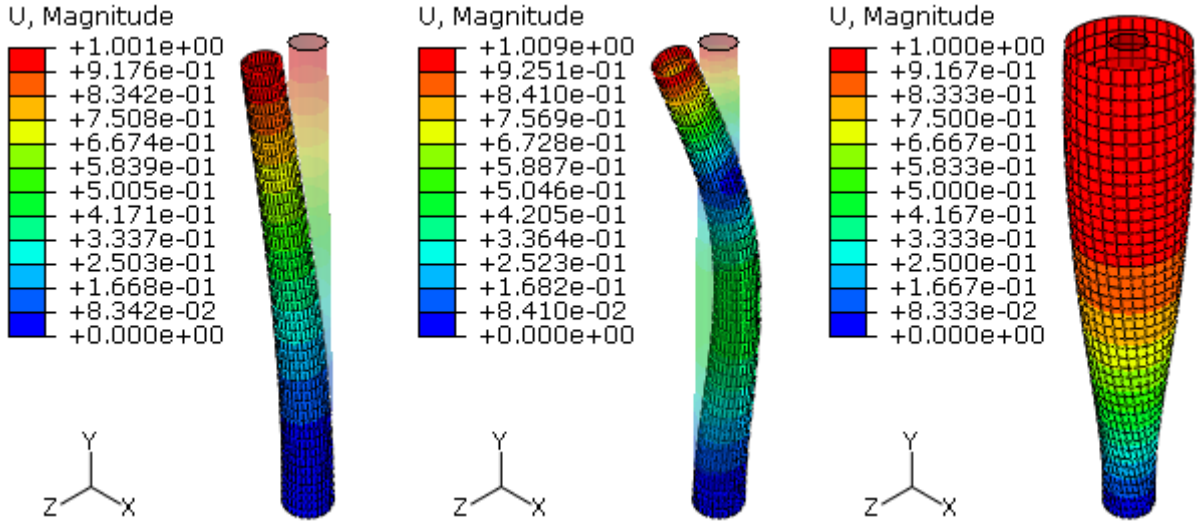

a) 1st and 2nd eigenmodes a) 3rd and 4th eigenmodes a) 5th eigenmode

Figure 3: The First Five Eigenmodes of the Original Tower

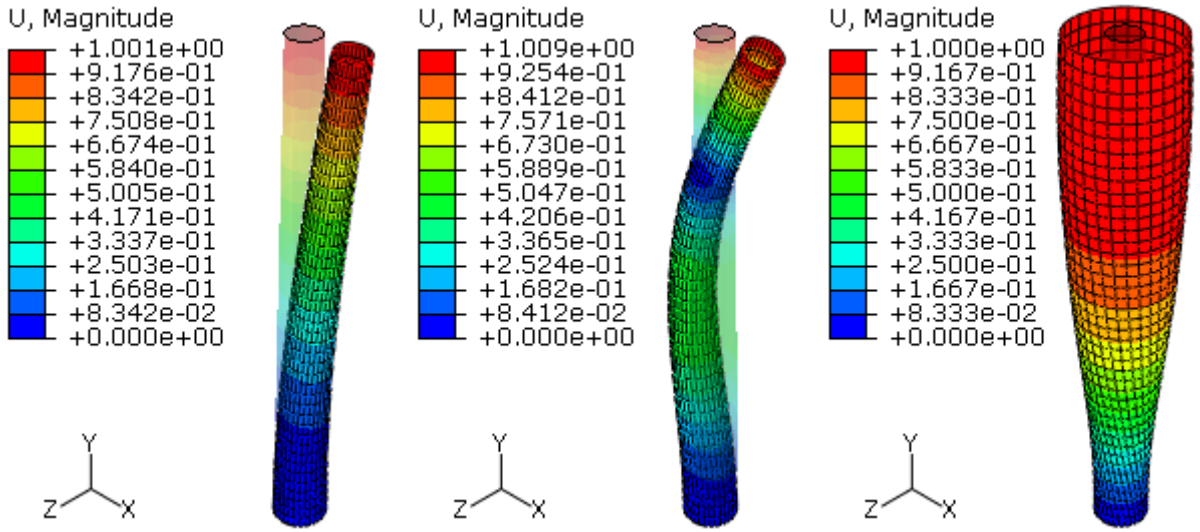

a) 1st and 2nd eigenmodes a) 3rd and 4th eigenmodes a) 5th eigenmode

Figure 4: The First Five Eigenmodes of the Tower in Design No.2

4 CONCLUSIONS

This paper addresses the design of an economic alternative tower for a commercial wind turbine, and modal analysis and optimization were carried out for several design alternatives via FEA.

1) The natural frequency of first eigenmode is much larger than the operating frequency of 0.94Hz, and there's no possibility of resonance.

2) By optimizing the material and the section thickness, an economic alternative tower can be designed to meet the design specifications.

3) The 8-node shell element is a suitable element type to mesh the tubular tower.

BIBLIOGRAPHY

[1] Erich Hau. Wind turbines-Foundamentals, Technologies, Applications and Economics(2nd edition). Springer, April 2005.

[2] Huang Shanqiu, Lu Ping. Model analysis of the tower for wind turbine zone Z-40. ACTA Energiae Solaris Sinica, Vol.22, No.2 April 2001.

[3] P.E. Uysa.; et al.: Optimisation of a steel tower for a wind turbine structure. Engineering Structures, 29 (2007):1337–1342.

[4] N. Bazeos.; et al.: Static, seismic and stability analyses of a prototype wind turbine steel tower. Engineering Structures, 24 (2002):1015–1025.

A NOVEL FLOATING OFFSHORE WIND TURBINE CONCEPT

Luca Vita[1)]

[1)] Wind Energy Division, Risø DTU, Roskilde, Denmark

ABSTRACT

The growth of the offshore market for wind turbines addresses the challenge to design wind turbines specifically for offshore condition and not necessarily using on-shore technology. This paper deals with a new concept for floating offshore wind turbine, consisting of a vertical axis wind turbine and of a rotating floating foundation. The main purpose is to have a more cost-effective floating offshore design. The concept is particularly indicated for big MW sizes and for deep water. This new configuration seems to offer many advantages but it also addresses a considerable number of new technological challenges that need to be investigated.

KEYWORDS

Offshore, floating, vertical axis wind turbine, new concept, Darrieus

INTRODUCTION

Offshore wind energy sector is becoming more and more strategic and attractive for companies and demands for deeper water are increasing. Offshore wind energy plays a strategic role because of the vast wind resources and the limited on shore possibilities.

Several international research institutes are involved in research and optimization of wind energy systems for deep sea conditions. NREL in USA has investigated the future perspectives of floating offshore concepts [2], and they have developed their own numerical tools for horizontal axis offshore concepts [3,4]. TUDelft in Netherlands have also modeled floating offshore concepts [5]. NREL and TUDelft have developed their own concept based on a big tripod structure as a floating buoy. They estimate that in deep water (30-200m) this kind of basement structure is three times cheaper than the traditional gravity foundations. Risø DTU extended their HAWC2 code also to include floating constructions [6]. An overview of the different aeroelastic tools and concepts for offshore floating wind turbines is in [7].

Several commercial companies have developed floating offshore projects, such as StatoilHydro [8], Sway [9], BlueH [10], Ecopower [11] and Nova [12] (the last one use a vertical-axis rotor).

THE NEW CONCEPT

1.1 Description of the new concept

The concept has been presented and fully described for the first time at the EWEC 2009 conference in Marseille [1]. The main innovation consists of a rotating floating foundation that avoids the use of main bearings, Figure 1. The new concept is integrated in a wind turbine, and some specific technological solutions are proposed for the different components of the turbine:

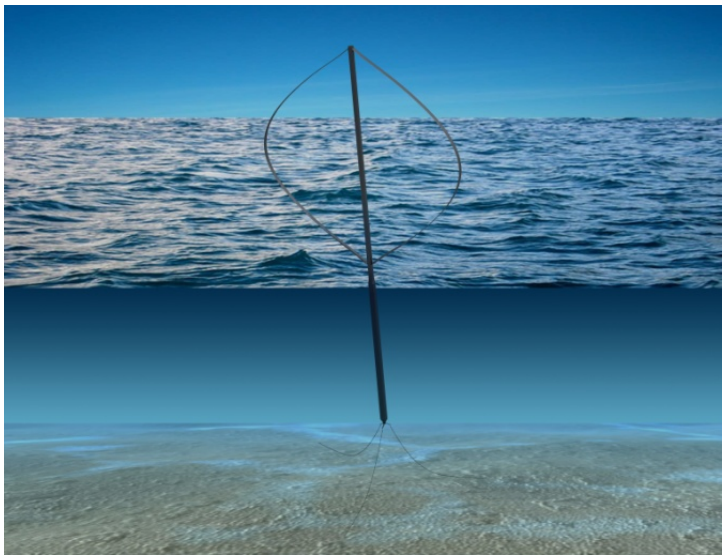

Figure 1 Artistic view of the new concept

- Rotor: Different technological solutions are possible but the vertical axis Darrieus rotor is, at the moment, the solution that suits best within the new concept.
- Blades: it is suggested to produce blades by GRP pultrusion to reduce the cost of a future industrial production
- Transmission systems: The concept gives the possibility to use several technological solutions on the shelf and permanent magnet generators suit particularly with the concept.
- Safety systems: A novel technological solution consisting of water brakes is thought.
- Control Systems: No pitch control is needed and the control is made by rpm control.
- Anchoring parts: The importance of this part is relevant in a floating structure and two or more rigid arms are placed at the bottom of the structure to absorb the torque.

The concept presents many advantages, some of them are:

- No pitch control neither yaw system
- The generator is placed into the bottom of the structure, moving down the barycentre of the whole structure (important for floating structure

- The concept is extremely simple and it is a great advantages for an industrial production and for an up-scale implementation
- Many possibilities are suitable for installation and for operation and maintenance

1.2 Preliminary dimensions

In the table1 and table2 are reported some preliminary data on the Darriues rotor and on the dimensions of the whole structure.

Table1 Darrieus Rotor Specifications

Size	2MW	20MW
Rotor Radius (m)	40	120
Rotor Height (m)	80	240
Chord (m)	2.5	11
Torque at rated power (N*m)	$1.4\ 10^6$	$5\ 10^7$
Thrust at rated power (N)	$2\ 10^5$	$2.5\ 10^6$
Rotational speed at rated power (rpm)	13.3	4.1

Table2 Structural Total Dimension

Size	2MW	20MW
Radius of the rotor structure (m)	2	3
Radius of the submerged part (m)	2.5	6.5
Thickness (m)	0.03	0.03
Total weight (tons)	2300	13000
Rotor length (m)	80	240
Total length (m)	161	345

CHALLENGES AND STUDIES

The new concept addresses several technological challenges.

The main ones regarding the hydrodynamic forces on the rotating foundation, in particular friction and Magnus effect. A literature survey has been made regarding these forces in order to implement a numerical model to couple to an aeroelastic code.

Some results about friction losses for a 2MW are reported in Figure2. The data are based on the formulas in 13.

The power losses due to friction depend from the radius and rotational speed. From Figure 2 is visible as the friction is more sensitive to the radius variation.

CONCLUSION

A new concept for floating offshore wind turbines is presented. The concept seems to offer many possibilities for a more cost effective wind energy production. Several technological challenges are addressed from the new design. The paper reports some structural dimensions along with some results on predicted power losses due to friction.

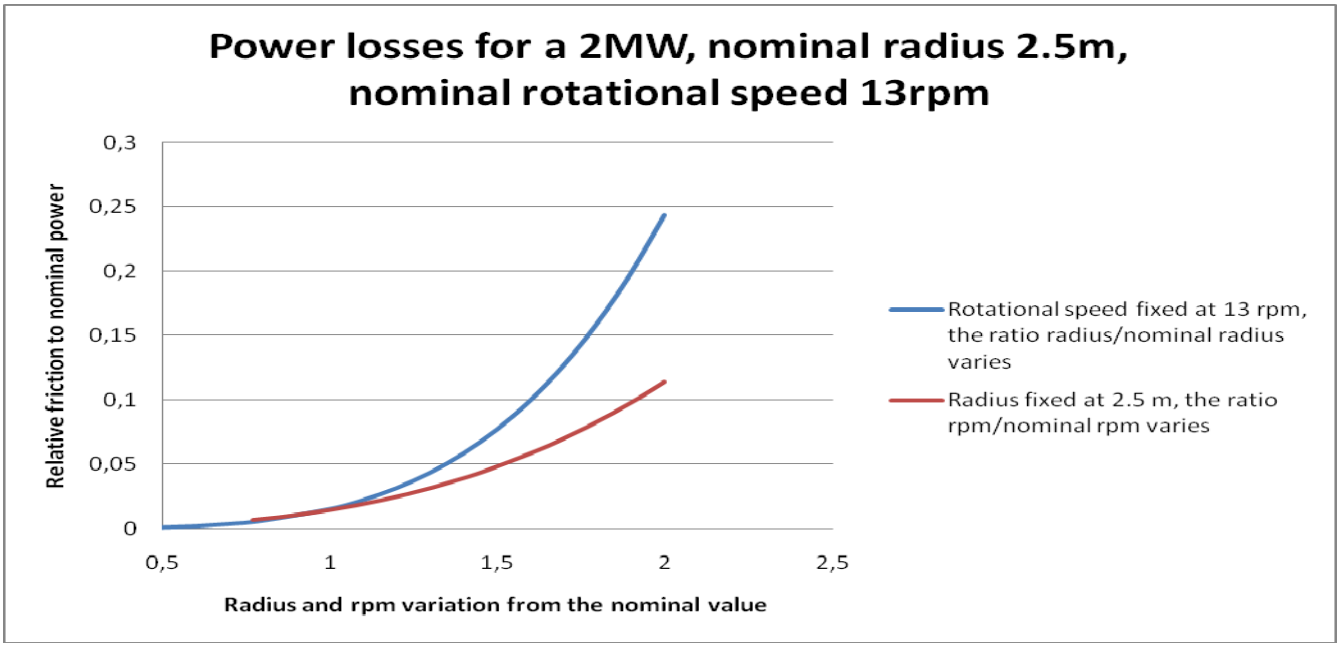

Figure 2 Power losses due to friction for variation of the radius and of the rotational speed

BIBLIOGRAPHY

[1] Vita L. Paulsen US, Pedersen TF, Madsen HA, Rasmussen F, «A novel Floating Offshore Wind Turbines Concept », EWEC2009, Marseille

[2] P.Sclavounos, S. Butterfield, W.Musial, J. Jonkman "Engineering challenges for floating offshore wind turbines", , NREL, US

[3] J. Jonkman, L.Buhl, "Development and Verification of a Fully Coupled Simulator for Offshore Wind Turbines", AIAA 2007, US

[4] J. Jonkman, L.Buhl, "Loads Analysis of a Floating Offshore Wind Turbine Using Fully Coupled Simulation", Windpower 2007, US

[5] Study of feasibility and boundary conditions for floating offshore wind turbines, ECN, MARINE, Lagerwey the Windmaster, TUD, TNO, December 2002

[6] T.J. Larsen and A.M. Hansen, "HAWC2, The user's manual", Risø-R-1597, 2008

[7] P. Passon et al., "OC3–Benchmark Exercise of Aero-elastic Offshore Wind Turbine Codes", , EAWE Special Topic Conference, Denmark 2007

[8] Hywind project : http://www.statoilhydro.com

[9] Sway website, http://www.sway.no/

[10] BlueH website, http://www.bluehgroup.com/

[11] Ecopower website, http://www.ecopowerusa.com/floatingTurbine.html

[12] Nova website, http://www.nova-project.co.uk/

[13] T.Theodersen, A.Regier, Experiments on drag of revolving disks, cylinders, and streamline rods at high speeds, American Committee for Aeronautics, 1946

Development of Design Methods and Requirements of Offshore Wind Turbines with Complex Support Structures

Daniel Kaufer

Endowed Chair of Wind Energy (SWE) at the Institute of Aircraft Design, Universität Stuttgart

Allmandring 5b, 70569 Stuttgart, Germany

ABSTRACT

The research project deals with the development of improved analysis tools for offshore wind turbines installed on deep water support structures. The main focus is the consideration of the wind turbine as a whole, with regards to the coupled interaction between aero- and hydrodynamic loading and motion of offshore wind turbines, including complex support structures. Such tools are commonly known as integrated analysis tools.

Validations will be based on code to code comparisons as well as on measurements from the first German offshore wind park *alpha ventus*. The research is part of the project 'Verification of offshore wind turbines' (OWEA).

KEYWORDS

Simulation, integrated method, aeroelastic, offshore, complex support structure

1 INTRODUCTION

Increasing sizes and water depths of modern offshore wind turbines (OWT) demand new support structure concepts. Today's sites for offshore wind farms reach water depth of up to 45m. The conventional structure, the monopile, is not cost-competitive in deeper water regions, because such dynamical soft support structures will become too heavy and thus expansive to resist extreme loadings. From the experiences of the oil and gas industry, lattice and braced structures have been identified to replace the monopile.

Such deep water conditions can be found along the German coast line in the North Sea, where recently the wind farm *alpha ventus* has begun installation. The wind turbines are installed at approximately 30m water depth. The difficulty is the design of proper support structures for large offshore wind turbines. There is a lack of appropriate analysis tools applied by industry which allow integrated simulations of offshore wind turbines mounted on multi-member support structures in a single calculation. Throughout different research projects, integrated analysis methods have been developed but not yet validated with field measurements to prove their exactness.

2 PROJECT DESCRIPTION

The thesis project launches in autumn 2008 at the University of Stuttgart and is part of the project 'Verification of offshore wind turbines' (OWEA) [1]. The OWEA project is a chance for a wide group of researchers to be part of an extensive measurement campaign. The thesis can be partitioned in five phases. Phase 1: developing an analysis method which allows integrated analysis under simultaneous aerodynamic and hydrodynamic loading; phase 2: plausibility checking of the method by code to code comparisons; phase 3: modelling and validating the REpower 5M and jacket support structure at the wind farm *alpha ventus*; phase 4: evaluating measurement data of *alpha ventus* and comparing measurements with simulations; phase 5: derivation of future design methods and requirements for offshore wind turbines.

A methodology has been developed and implemented which allows integrated simulations of the entire OWT [2]. For this purpose the well known wind turbine simulation tool Flex5 has been coupled to the finite element code POSEIDON [3] and coupling the industry tool ASAS(NL), developed by ANSYS®, is in progress. The basic idea is to include the Flex5 model in the finite element code under compliance of a proper sub-structuring technique. This results in a coupled set of equations of motions describing the OWT as a whole. Figure 1 illustrates the modelling approach. The equations are solved in the finite element code due to the capability of the 'infinite' number of degrees of freedom.

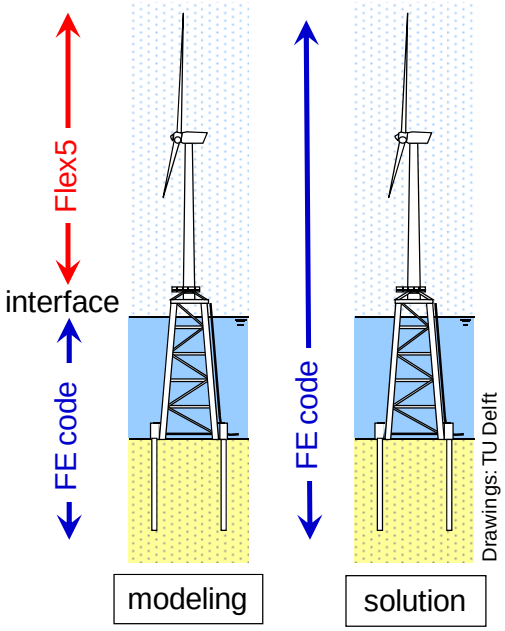

Figure 1: Sub-systems and coupling strategy

Plausibility checks with conventional simulation codes using very simple models and an OWT installed on a monopile have been performed. Comparisons with state of the art codes have been conducted in the project 'offshore code comparison collaboration' (OC3) within the IEA Wind Annex 23 [4]. The implemented coupling show very good agreement and looks very promising for future application in the OWEA project.

More detailed information about the methods and first results can be found in the bibliography.

3 CONCLUSIONS AND OUTLOOK

This paper describes briefly the planned procedure of the thesis. First objectives have been achieved already such as the development, implementation and validation of an integrated analysis tool. The next important phase is pending, as the installation of OWT's at *alpha ventus* is in progress and the measurement campaign may start at the end of this year. Sophisticated models of the REpower 5M and its jacket support structure have to be built and validated. Finally the evaluation of measurements and comparisons between measurements and simulation can be started.

ACKNOWLEDGEMENTS

The presented work is funded by the German Federal Ministry for the Environment, Nature Conservation and Nuclear Safety (BMU). The OWEA project number is 0327696A.

RAVE
RESEARCH AT ALPHA VENTUS
Eine Forschungsinitiative des Bundesumweltministeriums

BIBLIOGRAPHY

[1] Kühn, M.; et al.: Joint Technology Development for Offshore Wind Turbines – The OWEA Project at „*alpha ventus*“, conference paper, DEWEK 2008, Bremen

[2] Kaufer, D.; et al.: Integrated analysis of the dynamics of offshore wind turbines with arbitrary support structures, conference paper, EWEC 2009, Marseille

[3] Böker, C.: Load simulation and local dynamics of support structures for offshore wind turbines, dissertation, Institute for Steel Construction, Leibniz Universität Hannover, 2009

[4] Nichols, J.; et al.: Offshore Code Comparison Collaboration within IEA Wind Annex XXIII: Phase III Results, Regarding Tripod Support Structure Modeling. In 47th AIAA Aerospace Sciences Meeting. Garrad Hassan & Partners Limited (GH), 2008

Advanced Aerodynamic and Aero-Elastic Analysis of Wind Turbines with coupled MBS/CFD

Denis Matha

Endowed Chair of Wind Energy (SWE) at the Institute of Aircraft Design, Universität Stuttgart

Allmandring 5b, 70569 Stuttgart, Germany

ABSTRACT

The research objective is the analysis of complex fluid-structure interactions on wind turbines, leading to a better understanding of the underlying physics and the effects on the complete system regarding loads, rotor design and system performance. Special emphasis is put on fluid-blade aeroelastic interaction of large offshore wind turbines.

An aeroelastic CFD-MBS simulation tool for wind turbines is utilized and further improved, based on the coupled non-linear multibody simulation (MBS) SIMPACK and a computational fluid dynamics (CFD) code. The results should be compared with measurement data at the wind farm *alpha ventus* in the North Sea.

KEYWORDS

CFD, MBS, aeroelastics, fluid-structure, rotor, blade, offshore, numerical,

1 PROJECT DESCRIPTION

In the industrial design process of large wind turbines a fundamental change is in the offing on how the complete wind turbine system is being simulated. Currently, only simplified, inflexible aerodynamic and structural models with a fixed set of degrees of freedom are used. Validation and calibration is still primarily based on empirical data and detailed numerical analysis of single components.

In the future, advanced aerodynamic models based on CFD, coupled with multi-body and finite element simulation codes will be applied to directly simulate the complex dynamics of a wind turbine and in addition allow the flexibility to choose an appropriate degree of sophistication of the model. These advanced simulation tools will provide more detailed insight in the dynamic behavior of the complete system and will reduce the uncertainties related to blade dynamics since they overcome the limitations of current aerodynamic and

structural codes. These limitations are becoming increasingly important regarding the development of larger turbines and blades with fast individual pitch and the expected increased platform and turbine motions associated with new offshore developments (fixed bottom & floating). Additionally, possibilities to improve simpler aerodynamic and structural models with data derived from the more sophisticated CFD/MBS simulations will also be investigated. The results will also be used to provide more understanding into the blade design process.

The presented Ph.D. project has been started in June 2009. It is advancing the works ([1], [2], [3]) of S. Hauptmann at the Endowed Chair of Wind Energy (SWE) and S. Streiner at the Institute for Aerodynamics and Gasdynamics (IAG), both conducted at the University of Stuttgart. This close collaboration between the SWE and IAG will be continued by K. Meister and the author.

BIBLIOGRAPHY

[1] Hauptmann, S., Kaufer, D., Kühn, M., *"Wind Turbine Simulation Using a Coupled Free Wake and Multibody System Code"*, DEWEK08, Bremen, November 2008

[2] Hauptmann, S. et al.: *"Aero-elastic Simulation of a Wind Turbine and Drive Train Resonance Analysis Using the Multi-Body Simulation Code SIMPACK"* , DEWEK, Bremen, Nov 2006

[3] Streiner, S. and Krämer, E.: *"Aeroelastic Analysis of Wind Turbines Applying 3D CFD Computational Results"*, 2007 J. Phys.: Conf. Ser. 75

Urban Wind Energy

Christina Beller

Risø DTU, Denmark

ABSTRACT

My PhD project is to examine the application of wind energy in the built environment. This work is part of the determination of wind resources, present in terrain spiked with obstacles. To get familiar with the CFD (Computational Fluid Dynamics) solver EllipSys, simple test-cases, already examined by others, were conducted. A simple rectangular box with 64x64x64 cells was defined as computational domain. The boundary conditions were simple kept to inflow, outflow and wall. The Reynolds-Averaged Navier-Stokes (RANS) turbulence model was applied to three different roughness heights, $z_{0,1}$=0.001m, $z_{0,2}$=0.050m, $z_{0,3}$=0.500m, and the results in terms of stream-wise velocity profile, turbulent kinetic energy and turbulence intensity compared to each other and against the known logarithmic boundary profile- satisfactorily. The meaning is to implement an obstacle in a second step and scan the surrounding for advisable positions for appropriate wind turbines.

KEYWORDS

CFD, RANS, boundary layer, buildings aerodynamics

1 INTRODUCTION

Wind in very complex terrain, let's say a city, is interesting for wind engineers when it comes to loads on building structures, where they mostly examine the pressure distribution on the structure surface and not necessarily the flow field itself. Environmental research and the military have been investigating the propagation and dispersion of pollutants with big field tests, but also CFD simulations. I want to analyse the wind flow to produce energy locally. Here, my first approach is wind over flat terrain with different roughness heights.

2 SETTINGS

In the following, the input for the EllipSys code, set up in RANS mode, are announced. Flow over flat terrain was simulated for three different roughness heights, $z_{0,1}$=0.001m, $z_{0,2}$=0.050m and $z_{0,3}$=0.500m. In a second run, boundary conditions (BC) were toggled for the case with a roughness height of $z_{0,3}$=0.500m.

2.1 Computational domain

The computational domain is a simple box of 64x64x64 cells with the dimensions 5000mx1000mx1000m. The smallest cell-size located at the ground is 0.01m high for run1 and 0.001m for run2 (Figure 1).

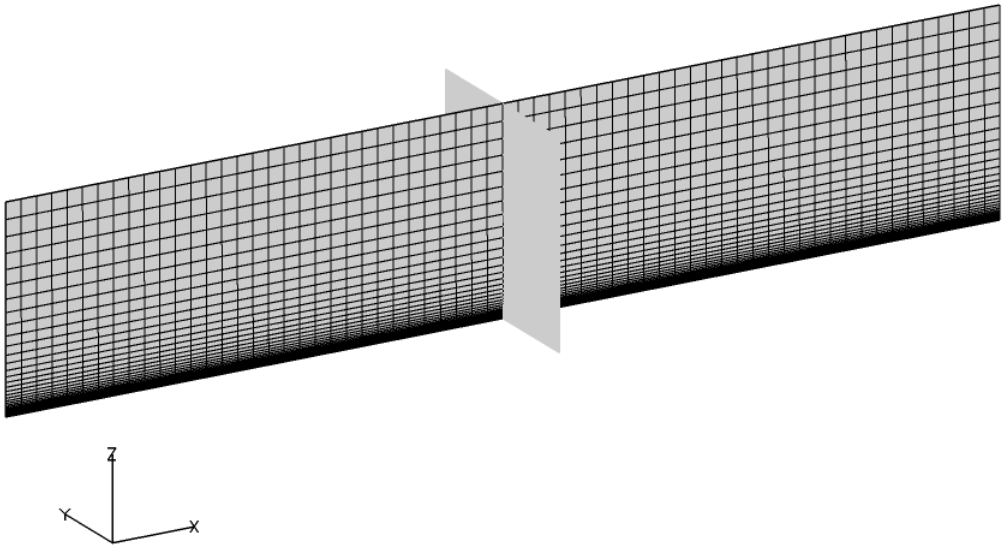

Figure 1: Grid of the computational domain with y-z plane at x=2500m

2.2 Boundary conditions

run1: Inflow is defined at the *yz(x=0m)*-plane and at the *xy(z=1000m)*-plane. The sides, *xz(y=0m)*-plane and *xz(y=1000m)*-plane, are set as symmetric boundaries, meaning that parameters can evolve, but no mass crosses the domain at these planes. Plane *yz(x=5000m)* is defined as outflow. The bottom, *xy(z=0m)*, is defined as wall and constitutes therewith the base of this parameter study.

run2: Here, the inflow is only at the *yz(x=0m)*-plane. The top plane, *xy(z=1000m)*, is changed from inflow to symmetric boundary.

For both runs a logarithmic velocity profile is given at the inflows with

$$u(z) = \frac{u_*}{\kappa} \ln\left(\frac{z}{z_0}\right). \qquad \textbf{(Equ. 1)}$$

The von Karman constant was set to κ=0.4. With that and the chosen roughness heights $z_{0,1}$=0.001m, $z_{0,1}$=0.050m and $z_{0,1}$=0.500m, the condition of $u(z)$=10m/s wind velocity at z=10m height for all three wind profiles, the friction velocities were found to be $u_{*,1}$=0.434m/s, $u_{*,2}$=0.755m/s and $u_{*,3}$=1.335m/s.

3 RESULTS

In computational fluid dynamical simulations the interesting part is how the flow field develops with given boundary conditions. In more complex problems one might have a measuring mast or kind of remote sensing device to tell about the incoming wind profile. To check the dependent development, a few other point-wise measurements are needed. In this case here, the wind profile shall be maintained over the whole domain, since there are no obstacles.

3.1 Run1

As expected, the derivative $\partial u / \partial z$ close to the wall is higher for lower roughness, than for higher roughness (see Figure 2, left column). Downstream the domain the profile is maintained, plotted for the positions *x*=0m, *x*=2500m and *x*=4999m. The turbulent kinetic energy (*tke*) should remain constant with the run1 BC (see Figure 2, middle column). Anyway, the graphs show changing *tke* profiles downstream, especially for increasing roughness heights, the numerical error grows.

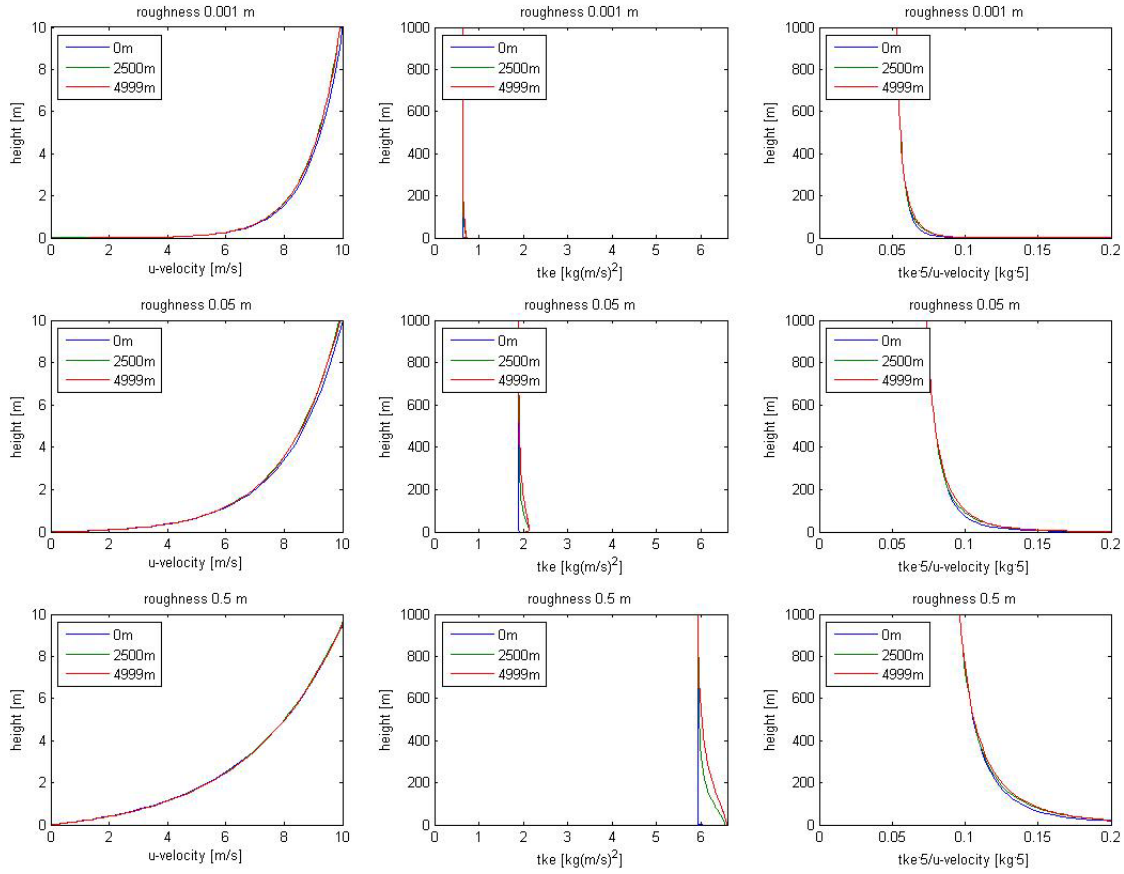

Figure 2: Run1 -top to bottom: plots for roughness heights z_0=0.001m; 0.050m; 0.500m -left to right: plots of stream-wise velocity, *tke*, turbulence intensity at *x*=0m; 2500m; 4999m

3.2 Run2

Seen in run1, *tke* remains almost constant. The constant value for *tke* is only an initial setting, coupled to the constant logarithmic velocity profile. Here comes the second BC set result where *tke* was free to develop over the whole length and height (see Figure 3).

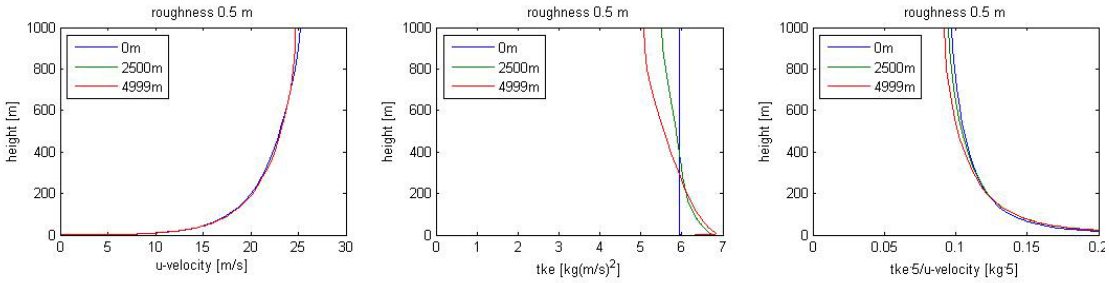

Figure 3: Run2 –roughness height $z_{0,3}$=0.500m; left to right: plots of stream-wise velocity, *tke*, turbulence intensity at *x*=0m; 2500m; 4999m

4 CONCLUSIONS

Parameter studies were conducted to control the setting of the CFD tool EllipSys. The wind profiles were satisfyingly following the request of a logarithmic profile. To change the constant *tke* profile to a more realistic one, the BCs were changed accordingly and with a second run the results were also satisfying for *tke*. This work states a starting point for more advanced simulations, where solid obstacles are going to be inserted in the flow field (see Figure 4) in order to scan the wind energy potential, resulting from the obstacles influences.

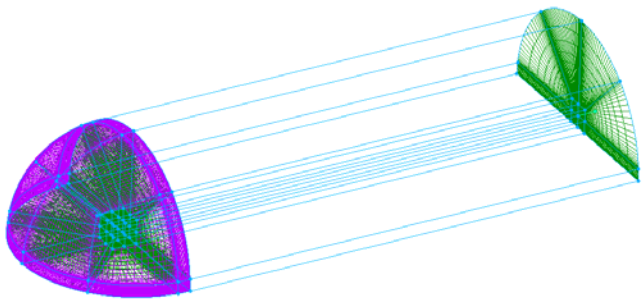

Figure 4: Computational domain to investigate obstacles influences on wind energy potential

BIBLIOGRAFY

[1] W K George; *Lectures in Turbulence for the 21st Century*; DTU Lecture notes, 2009

[2] R S Stull; *An Introduction to Boundary Layer Meteorology*; Kluwer Academic Publishers, 1988 Netherlands

Computational Fluid Dynamics (CFD) Modelling Of Wind Flow in and Around Forest Canopies.

Scott Wylie, Simon Watson

Centre for Renewable Energy Systems Technology, Department of Electronic and Electrical Engineering, Loughborough University, Leicestershire, LE11 3TU, United Kingdom.

ABSTRACT

Using the well known k-ε turbulence model [1], a CFD study has been carried out and compared to a wind tunnel study to assess its accuracy in modelling wind flow through and around a forest canopy. Adding additional source and sink terms to the turbulence model, has been common practice when taking into account the effect of trees on the approaching wind field. This research is looking at four different sets of closure coefficients, which define the source and sink terms, to see which can most accurately simulate the wind tunnel study.

KEYWORDS

Forest Canopy, Turbulence Modelling, Computational Fluid Dynamics.

1 INTRODUCTION

Utilising the framework of the well known k-ε turbulence model, many researchers have proposed modifications to predict canopy influences on approaching wind flows. The difference in these models is how they define the additional source and sink terms of the transport equations for turbulence kinetic energy (TKE), k, and its dissipation rate, ε. Equations 1 and 2 show the mathematical definition of these source/sink terms.

$$S_k = \rho C_d A(z)\left(\beta_P |U|^3 - \beta_D |U| k\right) \qquad \textbf{Equation 1}$$

$$S_\varepsilon = \rho C_d A(z) \frac{\varepsilon}{k}\left(C_{\varepsilon 4} |U|^3 - C_{\varepsilon 5} |U| \varepsilon\right) \qquad \textbf{Equation 2}$$

Where ρ is the density of air, C_d is the canopy drag coefficient (0.2 for this work), A(z) is the Leaf Area Density (LAD) of the canopy, k is the TKE, ε is the turbulence dissipation rate, and $|U|$ is the modulus of the wind speed. β_p, β_d, $C_{\varepsilon 4}$, and $C_{\varepsilon 5}$ are constants. In this work, a CFD study will be carried out to try and simulate flow through a forest canopy, using different combinations of the above mentioned constants. The results from the CFD study have been

validated against a wind tunnel study [2] to see which set-up produces the most accurate representation of the wind tunnel study.

Table 1.Summary Closure Coefficients

Canopy model	Scheme 1 [3, 4]	Scheme 2 [5]	Scheme 3 [6]	Scheme 4 [7]
β_p	1.0	1.0	1.0	1.0
β_d	5.1	4.0	0	4.0
$C_{\varepsilon 4}$	0.9	1.5	1.95	1.5
$C_{\varepsilon 5}$	0.9	1.5	0	0.6

2 CFD

The simulations for this work were done using the Reynolds Averaged Navier-Stokes (RANS) equations implemented in the commercial CFD software ANSYS CFX 12. ANSYS CFX is based on a coupled solver for mass and momentum and uses an algebraic multi-grid algorithm for convergence acceleration. Utilising the k – ε turbulence model, the vertical velocity variation can be plotted and compared with measured data.

2.1 Simulation Setup

The forest canopy was modelled as a simple rectangular volume, contained inside a larger rectangular volume. The forest was simulated as a porous domain, allowing air to pass through it, with its LAD profile shown in figure 1, taken from [8]. To cut down on computational time, only half the forest canopy was modelled; by assuming a plane of symmetry along the boundary through the centre of the geometry.

The forest canopy has a half width of 3m, a height of 7.5m, and a depth of 5.6m. The inlet of the domain has a half-width and half-height of 50m. The flow domain extends 100m from the inlet. The upstream face of the canopy was 200m downstream of the inlet. The flow domain was large enough so that its walls would not influence with the flow close to and around the forest canopy.

So that the solver can reach a suitable solution, it is necessary to apply appropriate boundary conditions to the domain and the geometry. A free slip boundary condition was implemented at the top and side walls of the domain. A logarithmic wind profile was applied to the inlet of the domain with a zero differential pressure at the outlet. Values for k and ε were defined manually at the inlet of the domain, as were the source and sink terms for canopy. The

ground surface had a no slip wall condition applied, with its roughness (equivalent sand grain roughness) set to 30 times that of the aerodynamic roughness length, [8, 9].

An unstructured tetrahedral mesh was used close to and inside the forest canopy, to ensure that the greatest changes in flow and pressure would be picked up accurately by the solver. Close to the inlet, outlet, and above the canopy section a swept mesh was used. This better resolves the undisturbed wind flow, parallel to the canopy, seen in these areas of the domain.

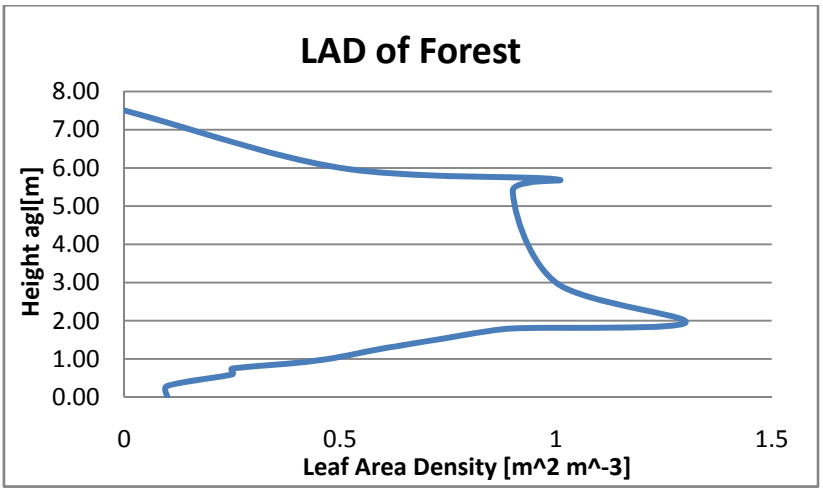

Figure 12: LAD of Forest in Simulations

3 RESULTS AND ANALYSIS

The vertical velocity profiles at various horizontal distances were compared with wind tunnel measurements from [2].Table 2 shows a comparison, in percentage difference, between the wind tunnel data and the simulation setup in scheme 7, as the errors for this scheme are the smallest.

Table 2. Percentage difference between wind tunnel data and simulation scheme 7

	x/h						
	-1	-0.5	0.5	1	3	6	10
z/h							
0.2	0.16%	0.47%	20.63%	27.12%	-39.45%	-386.12%	-1353.54%
0.4	-19.80%	-31.93%	10.96%	0.87%	-140.24%	-859.86%	-2277.66%
0.5	-23.97%	-39.25%	-103.82%	-74.08%	-301.92%	-1177.41%	-1577.71%
0.6	-26.52%	-38.64%	-105.71%	-75.46%	-442.47%	-932.17%	-1542.12%
0.8	-19.61%	-31.03%	-21.02%	-96.54%	-344.13%	-356.25%	-355.24%
0.9	-17.91%	-26.03%	-6.82%	-92.54%	-200.03%	-238.21%	-160.53%
1	-20.85%	-16.65%	-2.61%	-12.85%	-132.11%	-160.41%	-116.12%
1.1	-17.60%	-17.04%	-2.57%	2.92%	-87.36%	-115.77%	-82.82%
1.2	-15.59%	-12.80%	-5.39%	2.90%	-56.74%	-80.04%	-68.62%
1.3	-15.65%	-12.71%	-6.84%	4.05%	-37.80%	-68.11%	-59.49%

1.5	-10.51%	-8.24%	-7.41%	-3.48%	3.84%	-37.49%	-45.35%
1.7	-10.62%	-11.25%	-3.70%	-5.00%	5.08%	-8.97%	-29.10%
1.9	-8.81%	-6.53%	-3.17%	-1.60%	7.49%	4.97%	-13.15%
2	-12.40%	-5.33%	-3.19%	-1.79%	8.17%	5.14%	-12.30%
6	8.01%	14.55%	12.40%	13.06%	14.66%	15.94%	14.57%

A negative percentage difference shows an overestimation in wind speed by the simulation and a positive difference an underestimation.

4 CONCLUSIONS

The setup used in this work has identified the advantage of using the k-ε turbulence model to predict wind flow through and around forest canopies, using the modifications outlined in [3-7]. There are some large differences between the wind tunnel data and the simulations but qualitatively speaking the trends are similar. The differences in wind speed magnitude could be for a number of reasons like, for instance, mesh sensitivity or the difference in inlet profile from the wind tunnel to the simulations. All of these issues should, and will, be investigated further to try and make the CFD simulations as accurate as possible.

BIBLIOGRAPHY

[1] B. E. Launder, D. E. Spalding DE. "*Mathematical models of turbulence*", Academic Press, 1972.

[2] A. P. Morse, B. A. Gardiner, B. J. Marshall. *"Mechanisms Controlling Turbulence Development Across A Forest Edge",* Boundary-Layer Meteorology, 103:227-251, 2002.

[3] G. G. Katul, L. Mahrt, D. Poggi, C. Sanz. *"One- and Two-Equation Models for Canopy Turbulence",* Boundary-Layer Meteorology, 113:81-109, 2004.

[4] C. Sanz. *"A Note on k-ε Modelling on a Vegetation Canopy", Boundary-Layer Meteorology, 108:191-197, 2003.*

[5] R. S. Green. "*Modelling Turbulent Air Flow in a Stand of Widely-Spaced Trees", Phoenics Journal, 5:294-312, 1992.*

[6] U. Svensson, H. Haggkvist. *"A Two-Equation Turbulence Model for Canopy Flows",* Journal of Wind Engineering and Industrial Aerodynamics, 35:201-211, 1990.

[7] J. Liu, J. M. Chen, T. A. Black, M. D. Novak. *"E-ε Modelling of Turbulent Air Flow Downwind of a Model Forest Edge",* Boundary-Layer Meteorology, 72:21-44, 1998.

[8] B. D. Amiro, *"Comparison of Turbulence Statistics within Three Boreal Forest Canopies"*, Boundary Layer Meteorology, 51: 99-121, 1990.

[9] M. White, *"Viscous Fluid Flow"*, McGraw-Hill, 1979.

[10] H. Schlichting, *"Boundary Layer Theory"*, McGraw-Hill, 1979.

SESSION 6 – PART A

Thursday, 01.10.2009

9:45AM

Compensating gear plays in the pitch actuation system of a wind turbine

Jungchul Choi

ISET, Germany

ABSTRACT

Torque peak due to gear play reduces reliability in a pitch actuation system. Gear play will be an important issue in large wind turbines with individual pitch controllers. Gear play can be prevented by the use of two motors instead of one. Controllers are designed to optimize mechanical characters of the pitch actuation system, which will include external loads, nonlinear friction, and disturbance. The ways to distribute torque into two pitch motors are studied and tested.

KEYWORDS

Gear play, pitch actuation system, wind turbine

1 INTRODUCTION

If the kinetic energy in wind is too large, the pitch angle of wind turbine blades has to be adjusted in order to limit generator torques and speed. Electric motors in combination with planetary gears are usually used to rotate the blades around their pitch axes. Gear play in a planetary gear and a geared ring-pinion cause torque peaks, which increase fatigue and diminish machine's life time.

Gear play in a wind turbine has not been an important issue as yet. However, currently developing large scale wind turbines require an individual pitch controller, which influences the aerodynamic forces acting on the individual rotor blades [1]. Individual pitch controller changes blades' pitch angles much more frequently and quickly than currently used collective pitch controller. Thus gear play may not be ignored and a compensating tool for gear play should be developed.

2 SIMULATION OF THE COMPENSATING TOOL

2.1 Design a tool for compensating gear plays

A way to compensate the gear play is putting two pitch motors instead of one at a blade root. Torques of the two motors act in opposite directions. If the sum of the torques is zero, blade

jchoi@iset. uni-kassel.de

stays with tension in a position. Brake is not necessary. If the sum is not zero, blade rotates around pitch axis in the direction where the absolute value is bigger.

In case of emergency, the pitch angle can be changed very quickly by acting torques of both motors in a same direction. Since torque peaks due to the gear play are not important any more, bigger tolerance is allowed and production cost is saved [2]. But the new system requires one more motor and gear, which leads more cost.

2.2 Simulation of the design

- Pitch actuation system (See Figure 1):

The two-motor pitch actuation system is tested first with simulation program, Matlab/Simulink®. The components in the pitch actuation system are grouped into two parts. One is motor and gear, pinion and ring are contained in the other part. The motor and gear part is modelled as 1 mass-spring-damper with gear play, whereas the pinion and ring part owns only 1 mass and damper. Gear play in pinion-ring is transferred to the motor and gear part and the spring coefficient of the pinion and ring part is neglected because the part is very stiff as compared with the motor-gear part.

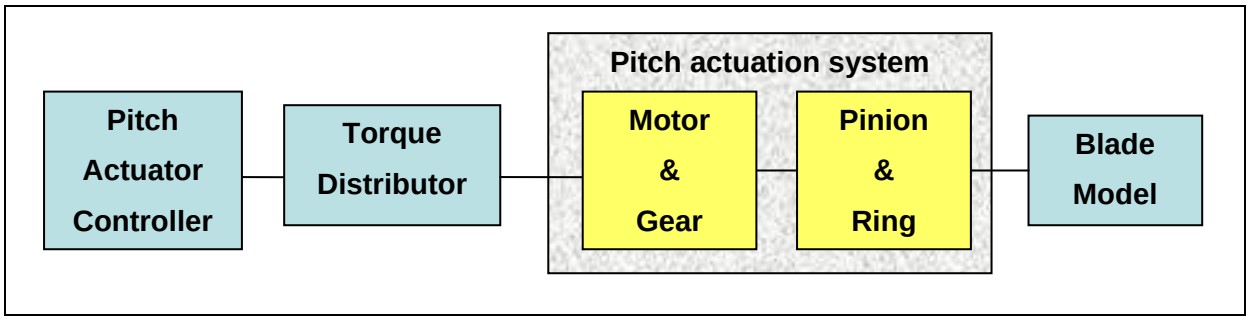

Figure 1: simulation model for a pitch actuation system

- Blade model:

A blade is modelled as 1 mass-spring-damper. This approach is useful since we can get the parameters easily from the modal analysis of the blade data. In the first step, effects of aerodynamic force, gravity, and centrifugal force on the moment of inertia and friction are not considered.

- Pitch actuator controller:

A classical PID-controller with anti-windup is adopted first. When forces on blades, nonlinear friction, and external disturbance are added later, PID-controller cannot control the nonlinearities any more, so that a controller adaptive to nonlinear systems should be designed.

- Torque distributor:

Calculated torque out of the controller is distributed into the two pitch motors. Three kinds of distributors are devised to keep tensions between two pinions (See Figure 2). The braking torques, those are the torque differences when the torque sum is zero, of the three distributors are designed to be identical. Later, the braking torque will be adjusted continuously according to turbulence intensity.

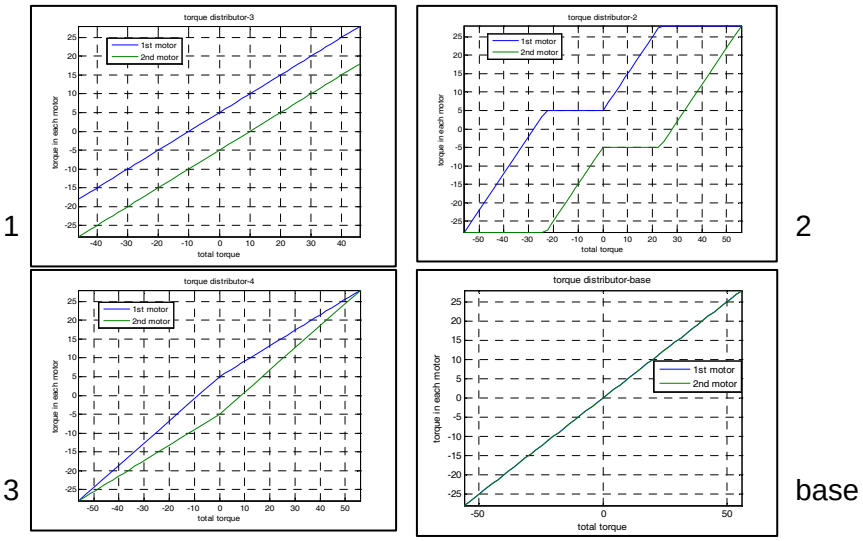

Figure 2: 3 kinds of torque distributor and torque distributor-base

2.3 Simulation results

Three torque distributors and a comparison model are tested. As I set the reference pitch angle as a sine function of 0.33Hz and 20° amplitude, input torque of ring-pinion part are shown in Figure 3. Torque distributor-1,3, and base pass a point where the torque of one motor is zero, so that their graphs have torque peaks. Thus torque distributor-2 is proved to be more secure than others.

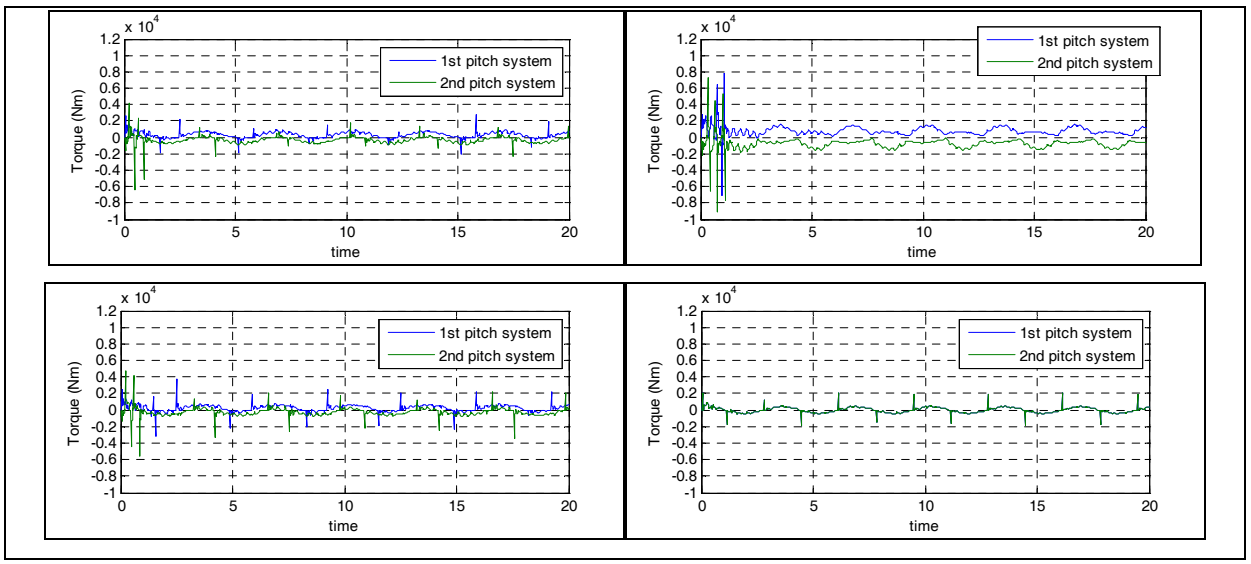

Figure 3: simulation results of torque distributor-1,2,3, and base

3 HIL-TESTING RIG FOR THE COMPENSATING TOOL

The design is investigated with a hardware-in-the-loop (HIL) testing rig, which mainly consists of 4 motors and a ring (See Figure 4). Two motors are pitch actuators and the rest simulate loads on a blade root. The testing rig is connected to PC via inverters and a CAN bus. The parameters of the model, i.e. mass, damper, spring, and a gear play are determined with experiments. Mass is calculated from the slope and the torque when the motor rotates reversely. Torque at a constant motor speed is used for estimating a friction coefficient. Spring coefficient is gained from different angles at different torque.

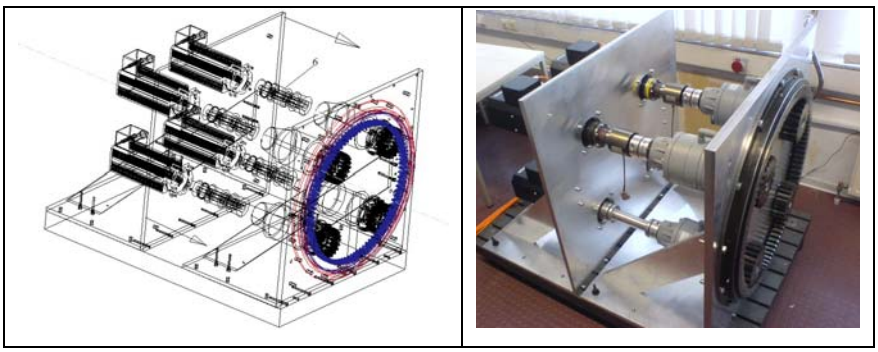

Figure 4: the testing rig

4 CONCLUSIONS

Torque peak due to gear play causes damage on a machine. Gear play can be compensated by two motors which hold a blade with tension. Dynamic mechanical characteristics of a pitch actuation system are optimized with a classical controller now and a controller for a nonlinear system later. Loads on the blade, nonlinear friction, and a disturbance will be added and tested with both simulation and experiment.

BIBLIOGRAPHY

[1] Geyler, M., Caselitz, P., Individual blade pitch control design for load reduction on large wind turbines, EWEC 2007, Milan, Italy, May 2007

[2] Hackl, Matthias: Robert Bosch GmbH, Offenlegungsschrift, DE 197 54 258 A 1**,** Deutsches Patent- und Markenamt

"Primary and Secondary Frequency Control with Wind Farms"

Author:
Dipl.-Ing. Alejandro J. Gesino
Energy Meteorology and Wind Power Management
R&D Division Energy Economy and Grid Operation
ISET e.V.

First supervisor:
Prof. Dr.-Ing. Siegfried Heier
Wind Power Technology
Faculty of Electrical Engineering/Computer Science
Dept. Power Supply Systems
University of Kassel

ABSTRACT

As a result of high penetration levels of wind power into the European grids, and also expecting that these levels will be even higher in the coming years, wind power is being requested by TSOs to meet the same grid stability functionality and grid codes requirements as conventional power plants, including balancing procedures and frequency regulation facilities.

The aim of this PhD is to determine how wind farms could contribute with primary and secondary power reserve. Based on the Wind farm Cluster structure developed at ISET e.V. in Germany, usual TSOs procedures for reserve power management are being considered and needed updates for wind power proposed. Prequalification rules for wind farms are also being analyzed as a fundamental part of the PhD main concept.

Keywords

Frequency control, reserve power, control strategies, prequalification rules for wind power.

Introduction

Transmission and distribution system frequency deviations are caused by unexpected unbalances between generation and demand, and are of particular concern in systems where the ratio of potential variation caused by fluctuating wind in relation to the amount of generated energy in total is high. These deviations could activate a significant share of primary power reserves. A further increase of these phenomena, for example due to high wind power penetration into the grids, could create frequency deviations large enough to activate the complete available primary power reserves reducing the security margins for frequency control and putting into question the adequacy of primary reserves to limit frequency variations, and secondary reserves to restore frequency variations. Up to now an

Dipl.-Ing. Alejandro J. Gesino: agesino@iset.uni-kassel.de

adequate frequency control[1] depends on conventional generation resources made available by generation companies to TSOs for this specific porpoise [1].

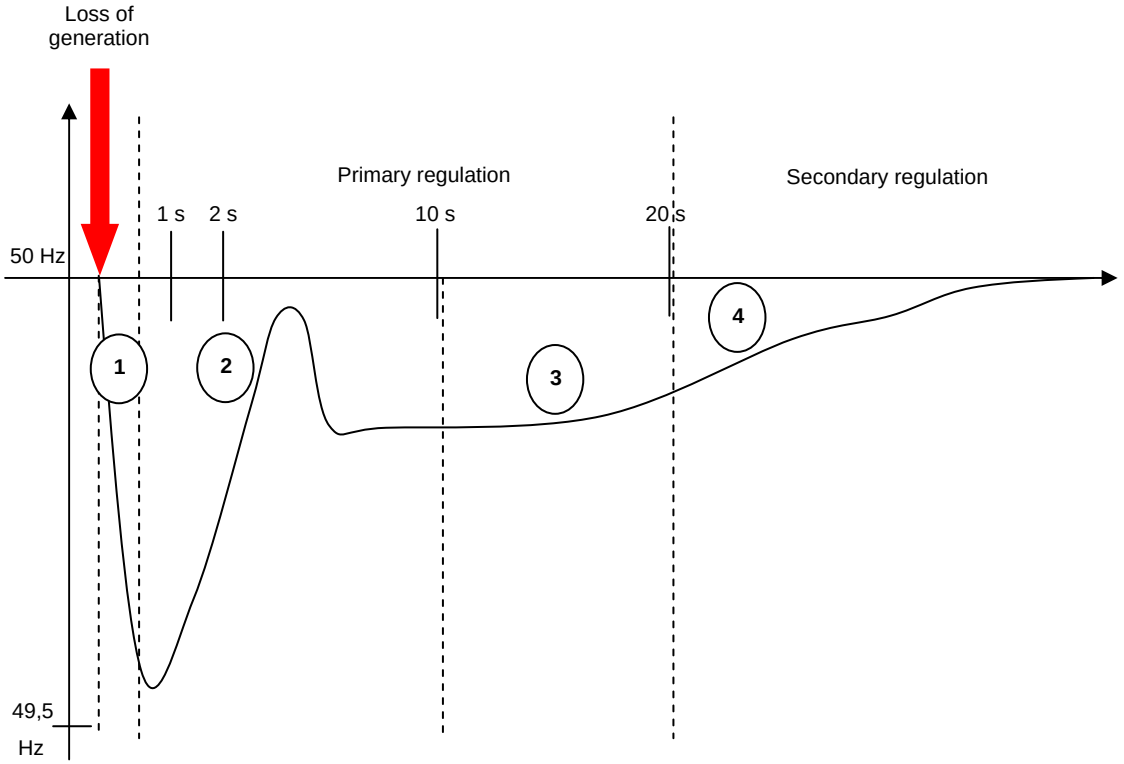

Figure 1 – Under frequency event due to a generation loss.

Frequency control with wind power

In order to address frequency control with wind power [2], different scenarios are proposed to be analyzed. Each of them is based on the install capacity relation "conventional generation-wind power". This relation by each scenario will be from 100% conventional generation and 0% wind power, to an ideal scenario of 100% of wind power. In between these two extremes are located the current EU targets for 2010, 2020 and 2030 regarding wind power development (onshore and offshore).

Conventional generation	100%	90%	85%	80%	60%	40%	20%	0%
Wind Power generation	0%	10%	15%	20%	40%	60%	80%	100%

Table 1 - Wind power installs capacity scenarios to be analyzed

One of the key issues in order to address frequency control with wind power is that the needed volume of wind power reserve for each control zone should be dynamically calculated in an accurate way by the TSO. By each control zone it should be considered that there are grid nodes and below each grid

[1] Control actions are performed in different successive steps, each with different characteristics and qualities and all depending on each other:
Primary control: starts within seconds as a joint action of all undertakings involved.
Secondary control: replaces primary control after minutes and is put into action by the responsible undertakings/TSO only.
Tertiary control: frees secondary control by re-scheduling generation and is put into action by the responsible undertakings/TSOs.

Dipl.-Ing. Alejandro J. Gesino: agesino@iset.uni-kassel.de

node wind farms are operating. Each wind farm has its own short and long term forecast with their confidence intervals and its own real time values regarding active and reactive power production. By each node in a given control zone, it must to be calculated the available power reserve according to the needs of the TSO.

The definition of “Wind Farm Cluster” [4] is a logical aggregation of geographical distributed wind farms under a given node. The “Wind Farm Cluster” structure is a fundamental element of the solutions for all previously mentioned issues. Such a structure allows TSOs to control several distributed wind farms operating under a given node as a big power plant, requesting to them frequency control, among other ancillary services.

Aim of this PhD

The aim of this PhD is to demonstrate that Wind Farms are able to contribute with primary and secondary frequency control, by providing the needed reserve power requested by the TSOs.

Through an analysis of the ancillary services which currently are being requested at wind farm level in the most advanced wind power countries in the world, and considering the new structure of Wind Farm Clusters developed at ISET e.V. as a natural evolution for wind power management structures [3] a concept for primary and secondary frequency control with Wind Farms will be developed and tested in both, simulation and real test fields scenarios.

Over frequency and under frequency events will be addressed as well. Frequency response procedures with Wind Farms will be developed and analyzed considering primary and secondary power reserve provision, taking into consideration the needed quick response time. It will be also analyzed which control strategy could better provide the needed power reserve according to the frequency event which could occur.

In case of an under frequency event happens, reserve active power should be injected into the grid contributing with the system stabilization. In order for the Wind Farms to be able to do so, they should be targeted during normal operation time with a certain value of active power to be reduced and known as an available reserve power by the system operator.

How to dynamically fulfill the TSOs needs concerning the needed volumes of primary and secondary power reserve and the optimization of these values in order to minimize looses, are going to be issues also addressed in this PhD.

In case of an upper frequency event occurs, active power should be curtailed according to the frequency variation. Control strategies to address this issue with Wind Farms will be also developed in this PhD, considering that each of them could be curtailed with different wind power volumes at

Dipl.-Ing. Alejandro J. Gesino: agesino@iset.uni-kassel.de

different moments. How to contribute to balance a system with wind power after an upper frequency event, minimizing losses and fulfilling with the needed grid time response requirements, will be addressed through the development of control strategies. The influence of available wind power forecasts and their uncertainties [5] is also going to be considered.

Bibliography

[1] UCTE AD-HOC Group, "Frequency quality investigation", Final report, 30th August 2008.

[2] Jonathan Horne, "Wind Farms Can provide Frequency Response – Experience of Great Britain Transmission System Operator", 7th International Workshop on Large Scale Integration of Wind Power and on Transmission Networks for Offshore Wind Farms, Madrid 26 – 27 May 2008.

[3] K. Rohrig, B. Lange, A. Gesino, M. Wolff, R. Mackensen, J. Dobschinsk, A. Wessel, M. Braun, C. Quintero, J. L.. Mata, R. Pestana, "Wind Power Plant Capabilities – Operate Wind Farms like Conventional Power Plants", European Wind Energy Conference 2009, Marseille, France, 16 – 19 March 2009.

[4] K. Rohrig, A. Gesino, R. Mackensen, M. Wolff, B. Lange, C. Quintero "Wind farm Cluster Management System", XV Energie Symposium, Fachhochschule Stralsund, Stralsund November 6 – 11th 2008.

[5] K. Rohrig, "Online-monitoring and prediction of wind power in German transmission system operation centres", World Wind Energy Conference, Cape Town, South Africa, 2003.

Biography

Alejandro J. Gesino (32) is working at Fraunhofer IWES since May 2007 in the area Energy Meteorology and Wind Power Management of the R&D Division Energy Economy and Grid Operation. Born in Mar del Plata, Argentina in 1977, graduated as Informatics Engineer (2005) and specialized in Germany at post degree level in Wind Energy and Hydrogen production and manipulation, Eng. Gesino's current main R&D interests are related wind power integration into electrical grids, Wind Farm Cluster concept design and implementation and control strategies for active and reactive power control with Wind Farm Clusters. Mr. Gesino is also PhD Student at the University of Kassel researching about "Primary and Secondary Frequency Control with Wind Farms".

Dipl.-Ing. Alejandro J. Gesino: agesino@iset.uni-kassel.de

Hybrid HVDC Transmission Systems for Offshore Wind Farms

Raymundo E. Torres [1], Tore Undeland[1], Marta Molinas[1]

[1] Norwegian University of Science and Technology, Norway

ABSTRACT

This work investigates the using of hybrid HVDC transmission systems, comprising a Voltage Source Converter (VSC) and a Current Source Converter (CSC), for Offshore Wind Farms. The paper describes the model and the control strategies proposed for this system. The hybrid model is implemented using PSCAD simulations to illustrate the proposed solution.

KEYWORDS

Hybrid HVDC, VSC, CSC.

1 INTRODUCTION

HVDC transmission may be the only feasible option for connection of a wind farm if the distance exceeds 100–150 km [1]. There are two different HVDC transmission technologies, i.e. Voltage Source Converter (VSC) using controllable switches like IGBTs and current source converter (CSC) or line-commutated (LCC) converter using partially controllable switches like thyristors [1]. CSC have been widely using for HVDC because can be used at very high power levels and have less losses compared with VSC , however when the AC system connected to the CSC is weak, difficulties to operate, as frequent commutation failure, are presented [2]. VSC have attracted more attention due to beneficial features such as: (i) active and reactive power exchange that can be controlled independently; (ii) no commutation failure problem; (iii) no communications required between two stations [1]. However VSC are defenceless against DC faults. The Hybrid HVDC option pretends to combined advantages of both, while CSC can handle high power levels the VSC can give more flexibility to the wind farm, and compensates their drawbacks to obtain the best economical and technical results, the VSC overcomes the problems of the CSC to feed a weak AC system while CSC can help in the protection of the system [2]. In spite of the above mentioned advantages, the Hybrid HVDC cannot reverse the power flow easily however for offshore applications only one power flow direction is required.

There have been other studies for Hybrid HVDC, in [2] is proposed a configuration and a controller for Hybrid HVDC, in [3] is proposed this configuration for Offshore Wind Farms.

2 HYBRID HVDC

The Hybrid HVDC configuration is shown in Fig. 1; VSCs are connected to the wind turbines all together in the same DC bus. The onshore CSC makes the connection with AC grid. It is expected that VSCs can handle the active and reactive power, while is expected to exploit the great capacity of the CSC.

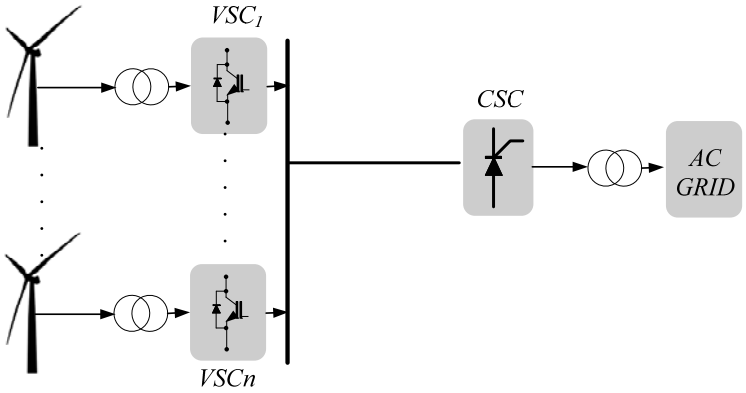

Fig. 1 Configuration of Hybrid HVDC for Offshore wind farms

2.1 System Description

The Fig. 2 shown the scheme of VSC connected with CSC through the equivalent model of a DC line. Based on this scheme, the model of the system in d-q synchronous reference frame to the VSC is

$$L\frac{di_{Sdq}}{dt} = v_{Sdq} - Ri_{Sdq} - u_{dq} + \omega LJi_{Sdq}$$

$$C\frac{dv_{C1}}{dt} = i_{dq}{}^{T}u_{dq} - i_{DC1}$$

Where the vector i_{Sdq} represents the line currents (d-q coordinates), v_{Sdq} represents line voltages, u_{dq} is the control input, v_{C1} is the voltage in the DC line and i_{DC1} is the DC current in the DC link.

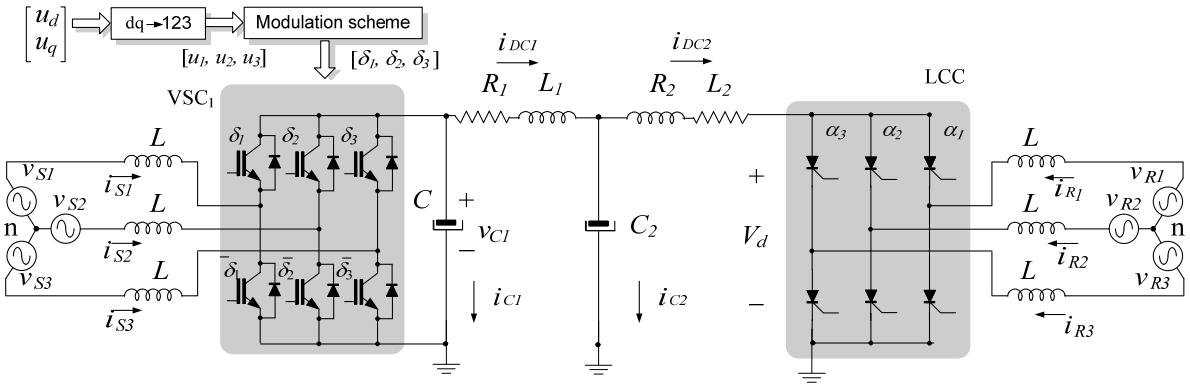

Fig. 2 Scheme of the Hybrid HVDC

While to the model of the CSC is

$$V_d = \frac{3\sqrt{2}}{\pi}E(\cos\gamma - \cos(\gamma + u))$$

Where the vector V_q represent DC voltage in Dc link, E is rms of line to-line voltage, γ is the extinction angle and u is the commutation angle.

2.2 Control Design

Based on the model, the controller shown in the Fig. 3 is chosen to VSC. This control scheme can regulate both d and q component of the line currents in order to control the active and reactive power, at the same time the DC current is controlled.

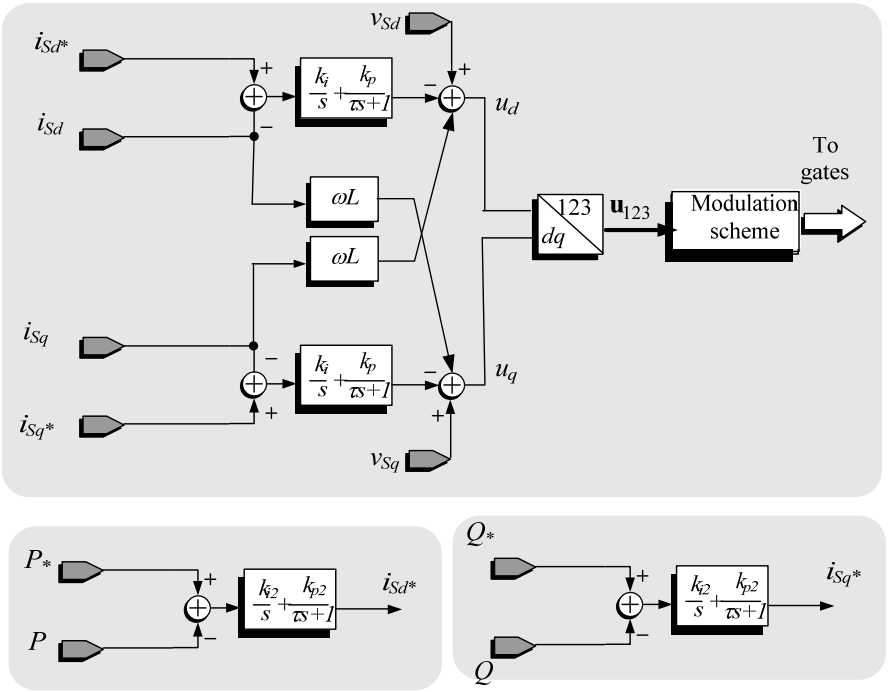

Fig 3. Block diagram of the VSC controller

For the CSC is proposed the PI controller which is shown in the Fig.4 This PI scheme can regulate the DC voltage toward its reference.

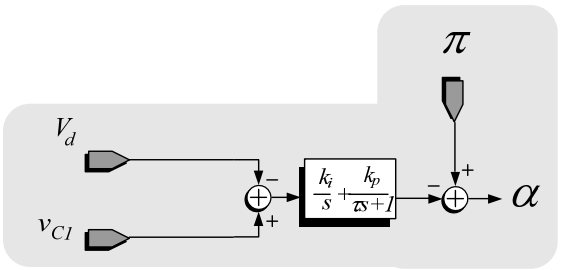

Fig.4 PI controller for the CSC

3 SIMULATION RESULT

The proposed controller was simulated using PSCAD, and using the parameters of the CIGRE model benchmark. Fig. 5 shows that active and reactive power are regulated to their references. The Fig 6.shows that DC voltage is regulated by the PI controller proposed.

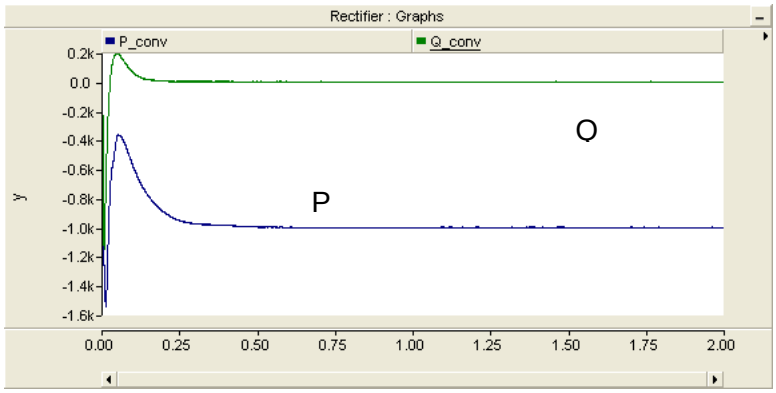

Fig. 5 Time response of the active and reactive power (KW)

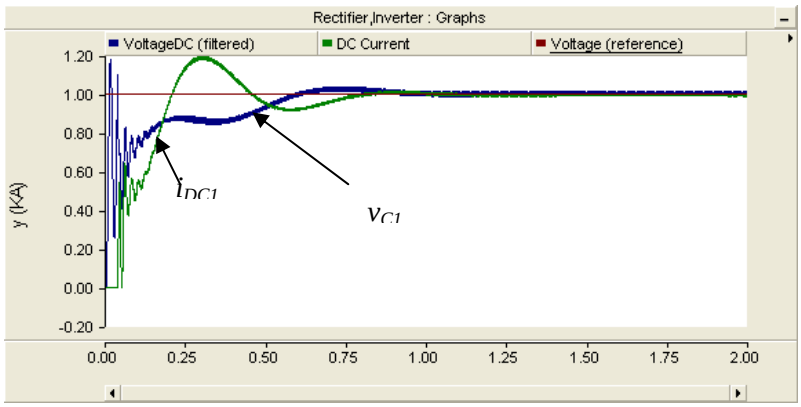

Fig. 6 Time response of DC Voltage and DC current (p.u.)

4 CONCLUSIONS

In this paper, a controller for a hybrid HVDC is proposed. A vector controller is proposed to regulate the active and reactive power and the DC current indirectly by means of the currents of the AC grid in d-q reference frame, while a PI controller is proposed to regulate the DC voltage in the DC link. Some simulations results have shown the performance of the proposed controller.

BIBLIOGRAPHY

[1] L Xu and B.R. Andersen. Grid Connection of Large Offshore Wind Farms using HVDC. Wind Energy, 9: 371-382,2006.

[2] Z. Zhao and M.R. Iravani Application of GTO Voltage Source Inverter in a Hybrid HVDC Link, 9 ; 369-375 ; 1994.

[3] W.Pan ,Y. Chang and H. Chen. Hybrid Multi-Terminal HVDC System for Large Scale Wind Power. Power Systems Conference Exposition PSCE 2006, 755-759,2006.

Numerical study of the performance of rooftop size VAWTs

S Wang[1 2)], L Ma[1)], DB Ingham[1)], M Pourkashanian[1)] , Z Tao[2)]

[1)] Centre for CFD, The University of Leeds, United Kingdom

[2)] School of Jet Propulsion, Beijing University of Aeronautics and Astronautics, China

ABSTRACT

This paper presents a 2D numerical investigation into the aerodynamic performance of a rooftop size straight-bladed Vertical Axis Wind Turbine (VAWT) with a NACA 0022 aerofoil. The aerodynamic interactions between different components of the VAWT, the effects of pitch angle and the position of the strut-blade joint on the performance of the wind turbine have been investigated using the Unsteady Reynolds-Averaged Navier-Stokes (URANS) method.

KEYWORDS

Vertical Axis Wind Turbine (VAWT), Aerodynamics, URANS, Sliding mesh, NACA0022

1 INTRODUCTION

Generating power from wind is emerging as one of the fastest growing sectors in power generation industry in recent years. For applications in urban areas, small scale rooftop size VAWTs are experiencing a renewed interest due to their several advantages over the Horizontal Axis Wind Turbines (HAWTs), such as the independence of the wind direction, achieving the maximum power coefficient at low rotational velocity, and low noise levels [1]. Nevertheless, VAWTs suffer from several complex aerodynamic problems that limit the achievement of their best performance, of which the strong aerodynamic interactions between different components have important impacts on the performance of such type of wind turbine.
The application of CFD techniques can provide detailed information of the flow around the turbine blades and across the turbine. With the rapid increase in computing power, it is an emerging subject to use advanced CFD models to simulate the flow phenomena associated with VAWTs [1] and this paper aims to report some findings from the numerical investigations.

2 CFD SIMULATIONS

2.1 CFD techniques

For the time being, the URANS method is still the work horse for solving such complex unsteady flows as those involved in VAWTs, because of its robustness, economy and reason-

able accuracy compared with more advanced but usually computationally costly CFD techniques, such as LES and DES. For the straight-bladed wind turbine studied, we performed a 2D URANS simulation with the *RNG* $k-\varepsilon$ turbulence model, in order to achieve a preliminary assessment of the performance of the wind turbine.

2.2 Computational setup

The blade of the turbine simulated is a NACA0022 airfoil with a chord length of 0.2 m. The diameter of the turbine is 2.5 m. We use the configuration as detailed in [1] as a baseline case in which the blade pitch angle is zero and the turbine shaft is ignored. Then a series of models with different shaft diameters or pitch angle have been simulated so as to investigate the effects of the turbine shaft, pitch angle and the position of the strut-blade joint on the aerodynamic performances of the turbine.

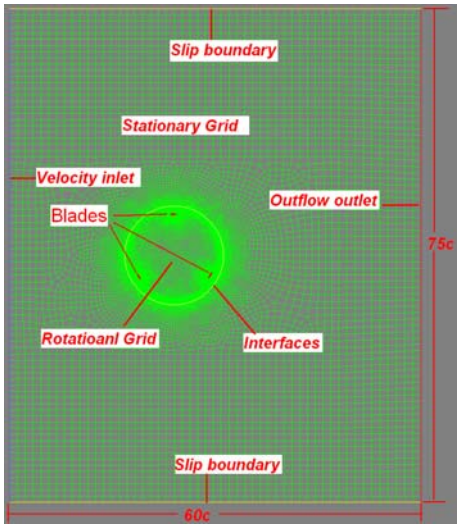

Figure 1: Computational setup

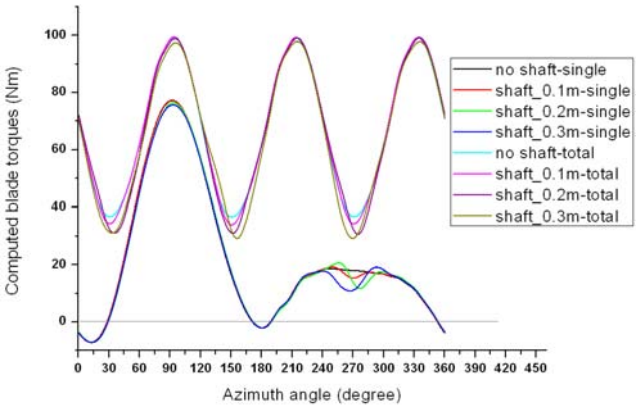

Figure 2: Comparison between the computed torques for various geometrical configurations

The sliding mesh technique has been used to model the movement of the blades, as shown in Figure 1. The turbine rotates counter clockwise with a tip speed ratio of 3 at a constant wind speed of 12 m/s. The wind is modelled to enter the computational domain from left and exit from the right. The domain consists of two parts, a *Rotational Grid* which rotates with the same angular velocity as the wind turbine and a *Stationary Grid* which is stationary. The non-equilibrium wall function is employed to account for the severe boundary layer separations that are expected near the blade surface. It is found that 1,000 time steps for one revolution is fine enough to obtain time-dependence solutions.

3 RESULTS AND DISCUSSIONS

Figure 2 shows the computed instantaneous aerodynamic torques exerted on an individual blade and the total torque produced by the turbine. The azimuth angle is defined to be zero

when the blade is just at the due north position as shown in Figure 4. The predicted performances are in a good agreement with the work of [3, 4]. The dynamic stall phenomena expected such as leading edge separation and trailing edge rolling up, is also captured, see Figure 3. It appears that the URANS method with *RNG* $k-\varepsilon$ model can capture the basic flow features and produce a reasonable prediction to the turbine performances.

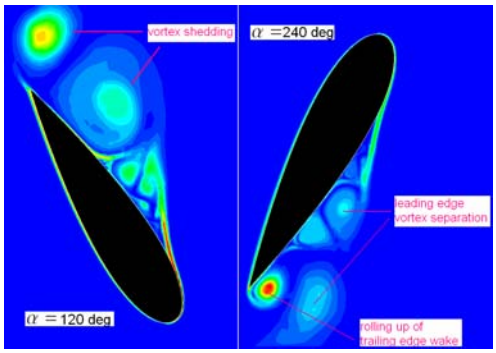

Figure 3: Vorticity contours near the blades

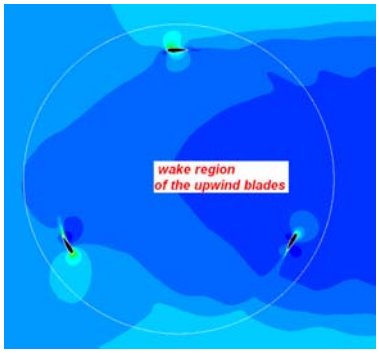

Figure 4: Velocity contours near the turbine

3.1 Aerodynamic interactions between turbine components

Firstly, it can be seen clearly from Figure 2 that, in all the cases, the torque generated by the blade, when it is travelling in the downwind phase, i.e. $180^\circ < \alpha < 360^\circ$, is much lower than that generated while the blade travelling in the upwind phase, i.e. $0^\circ < \alpha < 180^\circ$. This reflects a strong aerodynamic effect of the upwind blade on the downwind blade and can be confirmed by examining the fluid velocity field, see Figure 4. It can be seen that the downwind blades are completely covered by the low velocity wake flow of the upwind blade, or even by its own wake if operating at a high tip speed ratio [3].

Secondly, the effect of the turbine shaft on the downwind blades is captured in form of a Kármán vortex street behind the shaft. In Figure 2, the computed torque, both with and without the shafts, overlap in the upwind semi-circle. However, for the downwind semi-circle, the torque curve without the shafts is comparatively smooth while those with shafts have small ripples. Also it is found that the strength of the ripples grows as the diameter of the shafts increases, see Figure 5. Nevertheless, it appears that the effects of the shafts are not very strong in the studied cases.

3.2 The effect of the pitch angle and the position of the strut-blade joint

With the purpose of investigating the effect of pitch angle on the performance of the VAWT, a case with a pitch angle of 2-degree is simulated. It can be seen from Figure 6 that in the upwind phase, the performance of the turbine with a 2-degree pitch angle is smaller than that without pitch angle, but in the downwind phase, the situation reverses. From Figure 5, the averaged total torque of the turbine with the pitch angle is larger than those without pitch.

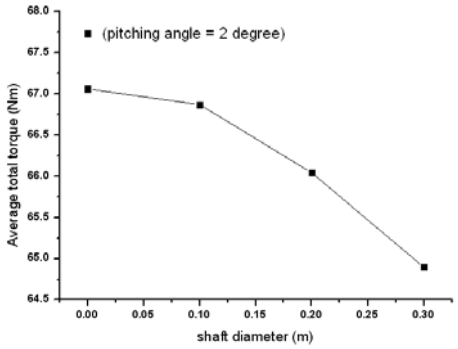

Figure 5: Averaged total torques for different shaft diameters and pitch angles

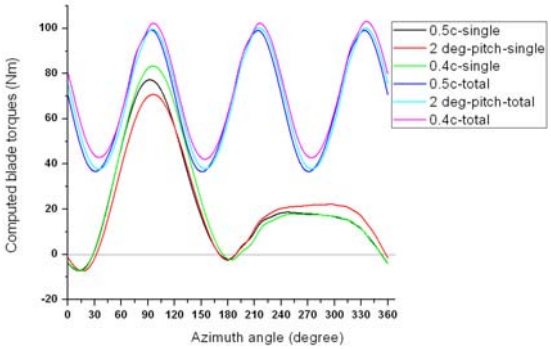

Figure 6: Comparison between the computed torques for $x_j = 0.4c$ and $x_j = 0.5c$

The distance of the position of the strut-blade joint from the leading edge, x_j, is a design parameter for the VAWTs. Therefore, a $x_j = 0.4c$ configuration is simulated to compare with the baseline configuration in which $x_j = 0.5c$. It can be seen from Figure 6 that the performance of the turbine with $x_j = 0.5c$ is better than that with $x_j = 0.4c$. In order to determine the best position of the strut-blade joint, more research with different x_j for different working conditions needs to be performed.

4 CONCLUSIONS

The results show that the URANS method with the *RNG* $k-\varepsilon$ model can predict basic flow feature and present a reasonable assessment of the turbine performances. The wake flow of the windward blades has a strong adverse effect on aerodynamic performances of the leeward blades in the operation condition studied. A moderate influence of the turbine shaft to the performance is discovered and it is found to be related to the shaft diameter. And the pitch angle, as well as the position of the strut-blade joint, also can influence the performances, although in the present cases the effects are not significant.

BIBLIOGRAPHY

[1] Hamada. K ; et al.: Unsteady Flow Simulation and Dynamic Stall around Vertical Axis Wind Turbine Blades. 46th AIAA Aerospace Sciences Meeting and Exhibit, Reno, Nevada, January 2008.

[2] Paraschivoiu. I: Wind turbine design: with emphasis on Darrieus concept. Polytechnic International Press, Canada, 2002.

[3] Lida. A ; et al.: Numerical Simulation of Unsteady Flow and Aerodynamic Performance of Vertical Axis Wind Turbines with LES. 16th Australasian Fluid Mechanics Conference, Australia, December 2007.

[4] Vittecoq. P, et al.: The aerodynamic forces for a Darrieus rotor with straight blades : wind tunnel measurements. J. Wind Eng. Ind. Aerodyn. Vol. 15, 1983.

SESSION 6 – PART B

Thursday, 01.10.2009

9:45AM

Direct Numerical Simulations of a Heaving Airfoil Using Spectral/HP Elements Method

Medjroubi W.[1) 2)], **Stoevesandt B.**[1) 2)] **and Peinke J.** [1) 2)]

[1)] ForWind, Germany [2)] University of Oldenburg, Germany

ABSTRACT

We consider the numerical simulation of the flow around a motionless and a heaving airfoil. The numerical method used is a high order method and a moving frame of reference for the airfoil motion. The effects of increasing the mean incidence and of the airfoil motion are investigated.

KEYWORDS

Direct numerical simulations, heaving airfoils, unsteady flows, dynamic stall.

1 INTRODUCTION

Wind turbines operation conditions are characterized by turbulent and direction-varying wind. Those conditions trigger unsteadiness which are associated with dynamic stall. This latter phenomenon is characterized by boundary-layer growth, detachment and re-attachment, making it challenging to understand and simulate numerically. The effects of varying the mean incidence and the frequency of oscillations on the flow and particularly on the aerodynamical coefficients are investigated.

2 NUMERICAL APPROACH

2.1 The numerical method

The numerical method used is based on both spectral methods and finite element methods. The physical domain is decomposed into small sub-domains or elements and the solution is approximated in every sub-domain using high-order polynomials (Jacobi polynomials) [1].

2.2 The airfoil motion

The motion of the airfoil is enabled using a moving-frame of reference method. The Navier-Stokes equations are written in a moving-frame of reference and a structural equation is derived to account for the airfoil motion [2].

2.3 The simulation code

2.4 The numerical code used is the NekTar code which uses the Galerkin and discontinuous Galerkin formulations and high-order trial basis [3].

3 SIMULATIONS

The numerical simulations are 2D simulations for a NACA12 profile at moderate Reynolds numbers ($Re < 10^5$) and at moderate to high mean incidences ($0° \leq \alpha_{mean} \leq 20°$). An unstructured grid composed of 4000 elements is used for the simulations.

3.1 Motionless airfoil:

Figure 1 represents the vorticity contours at selected times at Re=1600 and a mean incidence $\alpha_{mean}=12°$. The white colour indicates positive vorticity, the black colour negative vorticity and grey regions have almost zero vorticity.

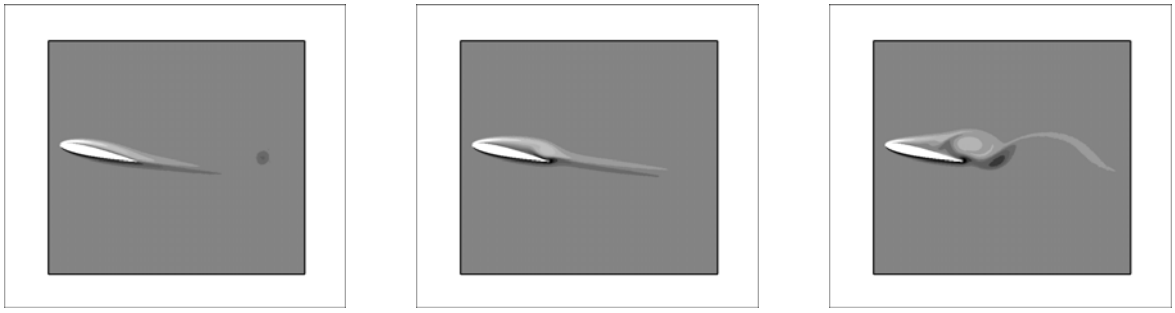

t=1.8 t=3 t=6

Fig.1: Vorticity contours at (a) t=1.8, (b) t=3 and (c) t=6 for a fixed airfoil at Re=1600 and mean incidence $\alpha_{mean}=12°$.

At t=1.8 a negative vortex is already shed in the wake while the flow at the upper-surface of the airfoil is still attached. At t=3 the upper-surface flow detaches and rolls at the trailing edge forming a positive vortex. This latter is be shed along with a negative vortex at t=6. Figure 2 represents vorticity contours at at Re=1600 and a mean incidence $\alpha_{mean}=20°$.

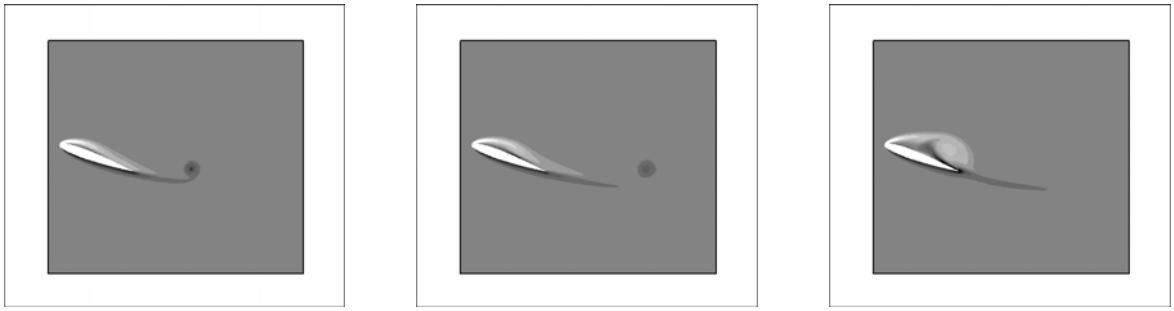

t=1.8 t=3 t=6

Fig.2: Vorticity contours at (a) t=1.8, (b) t=3 and (c) t=6 for a fixed airfoil at Re=1600 and mean incidence α_{mean}=20°.

Compared to the case at α_{mean}=20° the flow is delayed [3], following the same developments as in the previous case. In Figure 3 the lift and drag coefficients are plotted for the simulations at α_{mean}=12° and α_{mean}=20° for comparison.

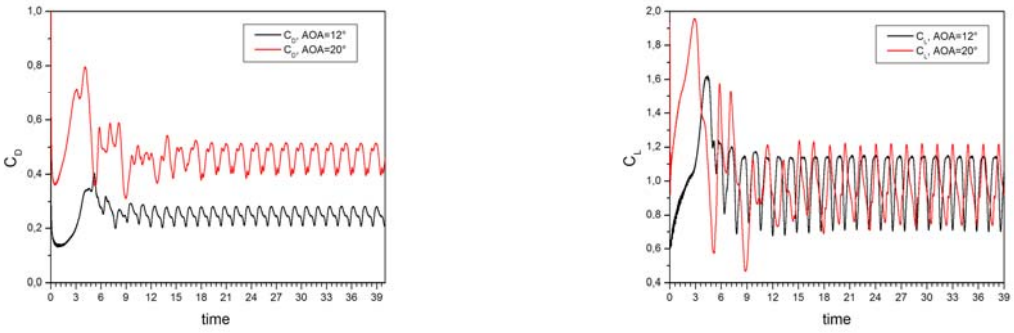

Drag coefficient Lift coefficient

Fig.3: Drag and lift coefficients at Re=1600 at mean incidences α_{mean}=12° and α_{mean}=20°.

Increasing the mean incidence results in an increase for both the lift and drag coefficients.

3.2 Heaving airfoil:

The airfoil is heaving with non-dimensional frequency and amplitude of oscillations of 0.3184 and 0.01; respectively. Figure 4 represents the velocity contours for the mean incidence α_{mean}=12° at Re=4500.

t=1.8 t = 3 t = 6

Fig.4: Vorticity contours at (a) t=1.8, (b) t=3 and (c) t=6 for a heaving airfoil at f=0.3184, a=0.01, Re=4500 and mean incidence α_{mean}=12°.

Compared to the motionless case (at Re=4500 and α_{mean}=12°, not presented here) the boundary layer separation is more important and occurs earlier. The motion of the airfoil is also visible in the near wake and it influences the process of vortex shedding. Figure 5 represents the comparison of the aerodynamical coefficients for the motionless and the heaving airfoil. It is clear that the lift and drag coefficients increased dramatically when the airfoil is forced to oscillate [3].

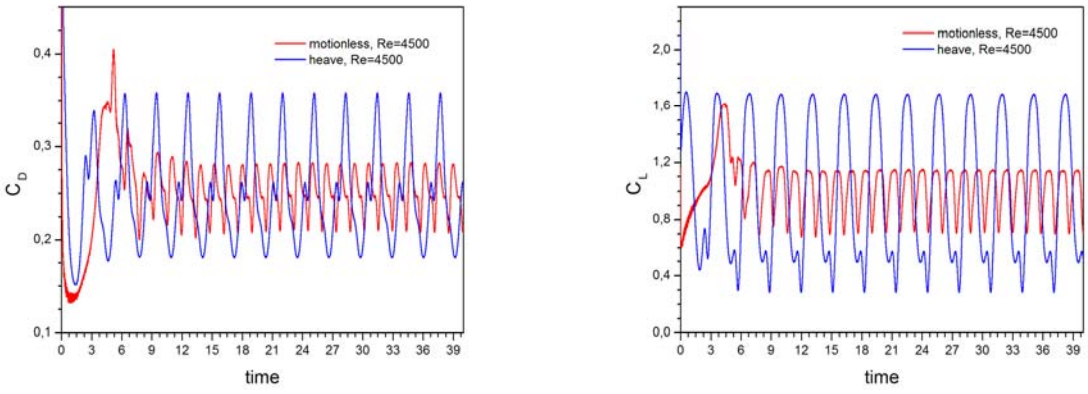

C_D C_L

Fig.5: Drag and lift coefficients at Re=4500 for a motionless and a heaving airfoil at f=0.3184, a=0.01. The mean incidence is α_{mean}=12° for the two cases.

CONCLUSION

The flow around a motionless and a heaving airfoil was successfully simulated using a high-order numerical method. The simulations were validated against previously published results. Increasing the mean incidence for the motionless airfoil increases the values of the aerodynamical coefficients. The same result is observed when setting the airfoil in a sinusoidal heaving motion.

BIBLIOGRAPHY

[1] Sherwin, S.J. & Karniadakis, G. E.: Spectral/hp Element Methods for Computational Fluid Dynamics, Oxford University Press, 1995.

[2] Li, L., Sherwin, S. J., Bearman, P. W., Jan. 2002. A moving frame of reference algorithm for fluid/structure interaction of rotating and translating bodies. International Journal for Numerical Methods in Fluids 38, 187–206.

[3] Akbari, M. H., Price, S. J., Aug. 2000. Simulation of the flow over elliptic airfoils oscillating at large angles of attack. Journal of Fluids and Structures 14, 757–777.

Please indicate whether you wish to present your paper by

Oral presentation only

Poster only (posters should be printed and brought to Durham by the participant)

Both oral presentation and poster

Structural Design of Large Future Wind Turbine Blades under Combined Loading

Zuzana Andrlová[1)], Kim Branner[1)]

[1)] Risø DTU, National Laboratory for Sustainable Energy, Denmark

ABSTRACT

The paper summarizes the design concept for very large wind turbine blades and review challenges which might be related to the upscaling of the blades to the length of 120 m. As the part of the initial study background data and the state of the art are briefly described. Later various design requirements and assumption are formed in order to define a geometrical outline for the 120 m long blade. Once the design criteria, geometry and aerodynamic properties of the blade are stated, the aeroelastic and structural analyses are the next step in the design process. This is requiring an interactive process usually conducted using numerical simulations. The application of combined load during structural analysis is discussed in order to provide realistic simulation of the operational and extreme load cases. The last part of the paper reviews the potential challenges expected during upscaling of the wind turbine blades.

KEYWORDS

Very Large Wind Turbines, Blade Design, Upscaling, Aeroelastic Analysis, Finite Element Analysis, Combined Loading.

1 INTRODUCTION

Issues as limited area of onshore sites in Europe, increasing demand for clean energy and the requirement of a higher energy output per turbine unit are currently the driving force in wind energy industry. Therefore the interest moves to the offshore wind turbines and wind farms. Thinking offshore, the environmental impact is lower, so it is the right region to take larger structures into consideration. The main motivation for increasing the size of wind turbines is that larger turbines have higher energy output per unit rotor area due to increased mean wind velocity with the height. The concentration of fewer but larger wind turbines on the most wind rich positions will be beneficial with respect to energy output, compared to a number of smaller turbines spread on larger and less favourable sites [1]. The purpose of

zuan@risoe.dtu.dk

the PhD project is to investigate, which structural and aeroelastic design challenges can be expected for blades of such a very large wind turbines. As offshore wind turbines are supposed to increase in size, the reference turbine for the project is expected to have a power output of 20 MW and the length of one blade to be 120 m.

2 THE DESIGN CONCEPT FOR 120 M BLADE

2.1 Background and state of the art

The optimal design of ever larger wind turbine blades is a constant challenge. The design process of blades for larger wind turbines is usually based on the approved concept of smaller blades. This approach can be in the case of very large blades inappropriate so innovative thinking is needed in this area. Integrated design is one of the current ideas how to improve the design process and performance of the rotor. Once the structural and aeroelastic analyses are considered at the same time, the iterative process is expected to bring significant results. However scaling of the current concepts is the first easy step to the better knowledge of the structure behaviour. Nowadays one of the biggest development intentions in the area of very large wind turbines is the EU project UpWind. The project looks towards the design of very large wind turbines (8-10MW), both onshore and offshore [2]. There is still a lot of discussion about various challenges and even feasibility of wind turbines of this size. Considering such enormous structure the crucial difficulties are expected in following areas: manufacturing, testing (replacement of the full scale test), transport, installation, operation and maintenance.

2.2 Design requirements and assumptions

Considering the future rotor blade to be twice longer than the longest one in these days, the challenges which were not important in the smaller scale become critical. Apposite examples are the wind shear and effect of Reynolds number changes, which have to be considered when talking about 120 m long blade, nearly 360 m tip height (the highest point of the rotor). As the reference turbine is expected to be placed offshore, the effect of the wave load and its combination with other loads should not be neglected. The development of the rotor blades in recent years shows that the blades became slender a more flexible. This tendency leads to intentionally prebended blades to prevent the tower collision during the operation. In this case the large displacement at the tip of the blade leads to the non linear effects that have to be considered during analyses. The fatigue caused by increase in the weight of the blade,

and thus selfweight loads, is expected to be one of the essential issues of very large blade design. Materials as carbon, wood or bamboo could be employed to decrease the weight, as well as new concepts of the blade structure. Significant weight reduction together with increased buckling capacity offers for example use of new sandwich elements in the primary structure of large wind turbines (main spar), more details in [1].

2.3 Structural and aeroelastic analyses

The structural analysis of the wind turbine blades is currently often performed using finite element method. As the blade structure is very complex due to the use of composite and sandwich materials and limited computational capacity, various concepts and simplification are used. The blade is usually modelled by layered shell, layered solid or combination of these elements. As the layered shell elements are inaccurate with respect to torsional stiffness determination and shear stress due to torsional loading, layred solid elements are recommended for more accurate models [4]. Next step to the detailed structural analysis is the sophisticated application of the real loads to the model. The global and local behaviour of the model should be validated over experimental results to ensure obtained response corresponds to the reality. The finite element model is generally too detailed, so the multibody based formulation is one of the possibilities of aeroelastic analysis of the wind turbine. The aeroelastic code HAWC2 developed at Risø DTU considers the blades and other parts of wind turbine as a finite number of 3D Timoshenko beam elements. These beam elements must accurately represent all of the mechanical properties of the full blade. The constitutive matrix can be obtained by the Beam Property Extraction Method [5] that determines displacements and rotations of each beam element by applying six different load cases.

2.4 Combined load

The wind turbine blade is loaded by three types of loads: aerodynamic load caused by wind field, the inertial load due to blades acceleration or deceleration and the sinusoidal gravitational load which acts with frequency corresponding to the rotation of the wind turbine and thus increases the fatigue loading. Nowadays the blades are mostly only tested for two separate load cases, flapwise and edgewise bending. The application of combined load during the tests is expected to improve the simulation of the real operational and extreme loads. The FE modelling can be improved by use of more advanced methods of applying the aerodynamic loading (pressure distribution over full model) instead of the simplified load

application (lift and drag force on each cross-section). The loads are than applied in a manner which accurately simulates the way loads are applied in operation. Generally is expected that new load cases may become important when the blades grow in size and flexibility.

3 CONCLUSIONS

As initial step of the PhD project study on changes in aeroelastic and structural behaviour of the wind turbine blade when scaled from 34 m to 120 m length is going to be performed. As the design concept will remain the same, some issues are expected to be critical. The gravitational load increases cubically with the rotor diameter, the large composite and sandwich panels are more sensitive to buckling, profile changes during operation could significantly influence the energy output and flutter will need to be considered.

BIBLIOGRAPHY

[1] Bergreen, C., et al.: Application and Analysis of Sandwich Elements in the Primary Structure of Large Wind Turbine Blades, Journal of Sandwich Structures and Materials, Vol. 9 – November 2007.

[2] www.upwind.eu

[3] Knill, T.: The Application of Aeroelastic Analysis Output Load Distributions to Finite Element Models of Wind, Wind Engineering, Vol. 29, No. 2, 2005.

[4] Laird, D., et al.: Finite Element Modeling of Wind Turbine Blades, Sandia Report, 2005.

[5] Malcolm, D.J., Laird, D.L.: Identification and Use of Blade Physical Properties, Sandia Report, 2005.

ACKNOWLEDGEMENTS

The PhD project is supported by Danish Energy Agency through the Energy Technology Development and Demonstration Programme (EUDP 2008), DTU Mechanical Engineering and Risø DTU. The support is gratefully acknowledged.

A Case Study of a 10kW Horizontal Axis Wind Turbine Blade Design

Xinzi Tang[1)], Xiongwei Liu[2)]

[1)] University of Central Lancashire, UK, [2)] University of Central Lancashire, UK

ABSTRACT

Determination of the blade aerodynamic shape with a chord and twist distribution at a specified design tip speed ratio where the blade has a maximum power coefficient is the main task of the blade design. The aerofoil aerodynamic characteristics and the rotor specifications are highly important for the wind turbine power performance, which depends on the match between the site's wind resource, the rotor and the generator. This paper addresses a case study of a 10kW wind turbine rotor blade design considering an existing generator and a site-specific wind speed distribution. The design process and the power performance prediction are presented.

KEYWORDS

Blade design; Horizontal axis wind turbine, Power performance, Site-specific.

1 INTRODUCTION

Wind turbine technology has become a hot issue as renewable energy guarantees environment-friendly and sustainable energy supply. The power performance of a wind turbine depends on the match between the site's wind resource, the rotor and the generator. In order to maximum the annual power output, the aerofoil aerodynamic characteristics and rotor specifications should be carefully considered in the design process. In this paper, the key rotor specifications are discussed with regards to an existing generator and a site-specific wind speed distribution. The aerodynamic optimal blade shape design and power performance estimation are implemented based on the blade element momentum (BEM) theory [1, 2, 3]. Finally the blade geometry and the predicted power curve are presented for maximum power coefficient control purpose.

2 DESIGN CONSTRAINS

2.1 Wind speed distribution

The local wind speed distribution is the first consideration of erecting a wind turbine. Wind speed Weibull distribution is widely accepted for describing the wind resource, the probability density function of which is defined as:

$$f(v)=\left(\frac{k}{c}\right)\cdot\left(\frac{v}{c}\right)\cdot\exp\left[-\left(\frac{v}{c}\right)^{k}\right] \quad (1)$$

Here, v is the wind speed, k is the shape parameter, and c is the scale parameter. Considering some wind farm in northern part of Britain, a shape parameter of 2.1 and a scale parameter of 6.89 is used, and the annual wind speed distribution is shown in Figure 1. The mean wind speed is found to be 6.1m/s from Equation 2.

$$V_{mean}=\int v f_{weibull}(v)dv \quad (2)$$

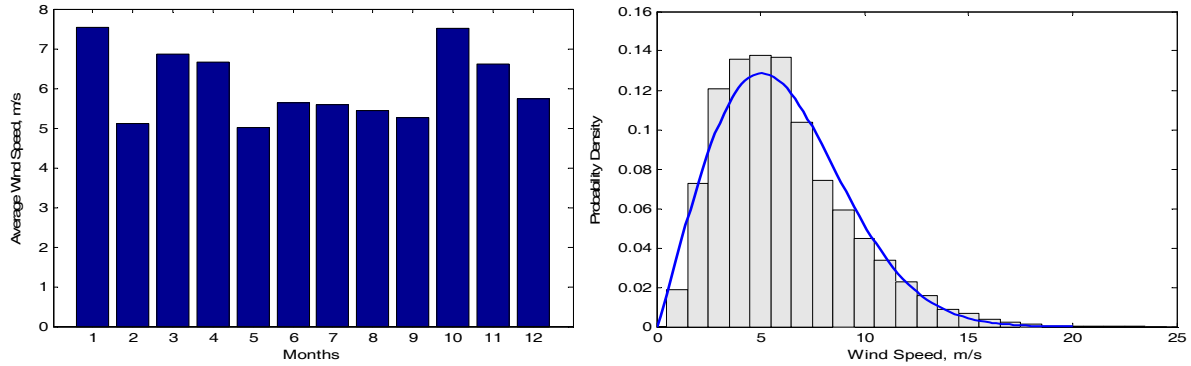

Figure 1: Annual Wind Speed Distribution

Considering maximum annual power output, it is better choose a rated wind speed which is close to the annual mean wind speed of 6.1m/s, but it is also worth emphasizing that a lower rated wind speed means a larger rotor, which causes an increase in cost. The rated wind speed is finally chosen according to the rated tip speed ratio in 3.2.

2.2 An existing generator

Due to economical reason, the turbine rotor is designed for an existing generator that is a permanent magnet synchronous alternator, rated power 10kW at the speed of 150 RPM.

3 ROTOR SPECIFICATIONS

3.1 Aerofoil type

Aerofoil for HAWT is often designed to be used at low attack angle, where the ratio of lift to drag coefficient is very high. A general aviation aerofoil shape is NACA series, and dedicated aerofoil shapes used in modern wind turbines are: S8, FFA-W, RisØ-A1, DU and etc. DU93-w-210 has been widely used in some European wind turbines, which has a max ratio of lift to drag coefficient of 118 and max lift coefficient of 1.39 at Reynolds of one million, and is chosen in our case. It has been found in some applications that more than one aerofoil shape can be used, but this may add to uncertainties in the design process, and in our design case only one aerofoil is used from root to tip except for the short root transition area.

3.2 Basic parameters

The power extracted by the rotor from the wind is given as Equation (3), from which the rotor radius can be estimated.

$$P = 0.5 C_p \rho V_r^3 \pi R^2 \quad (3)$$

Note here, P is the mechanical power but not the electrical power, Cp is the aerodynamic power coefficient, Vr is the rated wind speed, ρ is the air density, r is the rotor radius. Assuming the alternator efficiency of 84%, the rated power of the rotor in our case is about 11620W rather than 10kW. Obviously, as the rotor radius increases, the power output increases. But it is not a good idea to expand the rotor radius so as to increase the power output as expansion of the rotor radius will result in higher cost. Due to structure reason with an existing tower, our rotor radius is not allowed to exceed 5m. The rotor diameter is selected to be 9m with a first estimated aerodynamic efficiency of 0.45 and a rated wind speed of 9 m/s.

The optimal design tip speed ratio for DU93-w-210 aerofoil locates around 10 according to Yurduseva method [3], and the maximum efficiency at the tip speed ratio of 5 to 8 does not vary sharply from a first estimation. Note the tip speed ratio at rated wind speed as λ_{rated}, the optimal design tip speed ratio λ_{design} should be equal to or larger than λ_{rated} to avoid sharp decrease of speed. Having a rotor radius of 4.5 m, a generator of 10 kW and 150 RPM, we can calculate λ_{rated}, Vr and Cp. And remember, Cp cannot be larger than 0.593(Betz limits). From a first estimation, tip speed ratio of 8 is selected to be the best match where Cp is about 0.45 for DU93-w-210. The rated wind speed is then calculated from Equation (4).

$$\lambda = \frac{\omega R}{V_r} \quad (4)$$

Where ω is the rotor speed, R is the rotor radius and Vr is the rated wind speed.

The basic parameters of our wind turbine are listed in Table 1.

Table 1: Rotor Specifications

Parameters	Value
Power [W]	10000
Wind Velocity [m/s]	8.8
Number of Blades	3
Optimal Tip Speed Ratio	8
Air Density [kg/m3]	1.2
Rotor Radius [m]	4.5
Generator Rated Speed[RPM]	150
Aerofoil	DU93W210

4 BLADE GEOMETRY AND POWER PERFORMANCE

With the above specifications, the geometry of the blade is obtained based on the BEM theory, which has a maximum twist of 26.5° and a maximum chord of 0.489m. The blade geometry is shown in Figure 2. The Cp was predicted using the following equation and a computer program was coded to calculate:

$$C_p = (8/\lambda^2)\int_{\lambda_h}^{\lambda} F\lambda_r^3 a'(1-a)\left[1-(C_d/C_l)\cot\varphi\right]d\lambda_r \qquad (5)$$

Here C_l and C_d are the lift and drag coefficients, λ is the tip speed ratio, λ_h and λ_r are the local speed ratios at hub (root) and at position r/R, φ is the angle of relative wind, a is the axial induction factor, a' is the tangential induction factor and F is the tip loss factor. The maximum Cp is found at the tip speed ratio of 8, which is about 0.445. For maximum Cp control purpose, the corresponding rotor power output versus different wind speeds are shown in Figure 3.

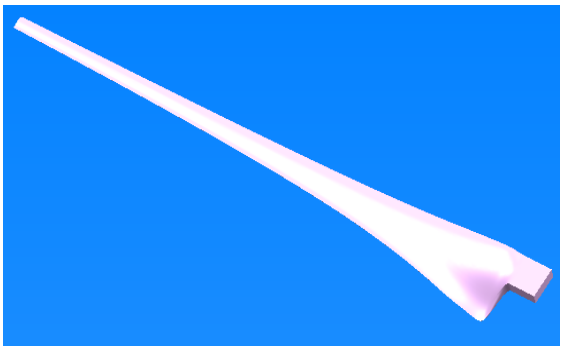

Figure 2: Blade Geometry

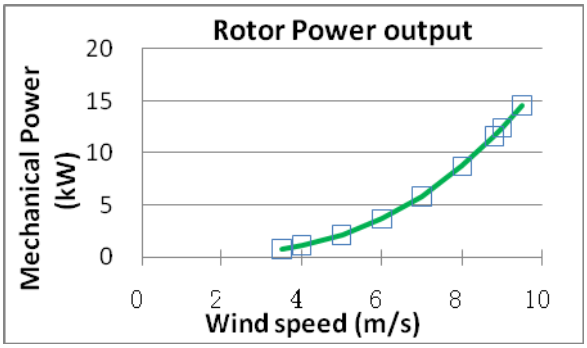

Figure3: Power Performance Prediction

5 CONCLUSIONS

A case study of a 10kW horizontal axis wind turbine blade design has been carried out with an existing generator and a site-specific wind speed resource. With a mean wind speed of 6.1m/s and a generator of 10kW and 150RPM, a rotor of 4.5m radius and the DU93-w-210 aerofoil has been applied. It has been predicted to be with a power coefficient of 0.445 at the tip speed ratio of 8 based on the BEM theory. A further structure analysis and testing will be developed in the future.

BIBLIOGRAPHY

[1] Li, H. and Chen, Z., "Design optimization and site matching of direct-drive permanent magnet wind power generator systems," Renewable Energy, vol. 34, no. 4, pp. 1175-1184, 2009

[2] Benini, E. and Toffolo, A., "Optimal design of horizontal-axis wind turbines using blade-element theory and evolutionary computation," Journal of Solar Energy Engineering-Transactions of the Asme, vol. 124, no. 4, pp. 357-363, 2002

[3] Manwell, J., "Wind energy explained: theory, design and application," John Wiley & Sons Inc, pp. 83-138, 2002

[4] Yurduseva, M. A., Atab, R., and Çetin, N. S., "Assessment of optimum tip speed ratio in wind turbines using artificial neural networks," Energy, no. 31, pp. 2153-2161, 2006

Wind turbine blade vibration at standstill conditions

Witold Skrzypinski[1)], Mac Gaunaa[2)]

[1)] Ph.D. student, Risø DTU, Denmark [2)] Senior Scientist, Risø DTU, Denmark

ABSTRACT

This paper deals with estimating whether the assumption of quasisteady aerodynamics in deep stall in present aeroelastic codes has an effect on prediction of the edgewise vibrations usually observed in deep stall in these codes. Some light is shed on this issue by computing chordwise damping ratio of a 2-D 3-DOF elastically mounted airfoil, both with quasisteady aerodynamics and with an imposed time lag in the aerodynamic response. Such model shows that the introduction of lag in the aerodynamic response of a vibrating airfoil significantly increases the amount of chordwise damping in deep stall, which indicates that present aeroelastic codes may overpredict deep-stall edgewise vibration.

KEYWORDS

Aerodynamics, aeroelasticity, dynamic stall, deep stall, edgewise vibration, blade vibration

1 INTRODUCTION

Since the introduction of computational models for the dynamic aeroelastic response of wind turbines, specific problems have necessitated evolution of sub-models, such as the so called dynamic stall models [i,ii] that model the dynamic aerodynamic response from the onset of separation until the flow over the airfoil is fully separated. Applying the existing aeroelastic tools to investigate the dynamic response of wind turbines in standstill has indicated that under certain conditions, the edgewise vibrational mode of wind turbine blades is negatively damped, leading to very big fatigue loads or even failure. Since the unstable regions occur for angles of attack far from normal operation, in deep stall, where the underlying aerodynamic coefficients are uncertain, it was initially assumed that the problem existed only in computations. In recent years, however, turbine failures at standstill conditions reported from the industry spurred new analytic and numeric investigations [iii,iv]. The investigations in [iii,iv] concluded that the standard aerodynamics existing in aeroelastic codes for deep stall is effectively quasi-steady. On the other hand, it is not known how far the quasi-steady approximation is from what occurs in real life. In this paper, some light is shed on how the aerodynamic damping is sensitive to time lag in the aerodynamic response. This is achieved by imposing different amounts of lag in the aerodynamic response of a nonlinear 2-D 3-DOF model of an elastically mounted airfoil, subjected to onset flow at different angles of attack,

and by computing the damping ratio of the vibrations of the aeroelastic system in the chordwise direction.

2 MODEL DESCRIPTION

2.1 Structural model

The structural model used here was originally presented by Buhl *et al* [v]:

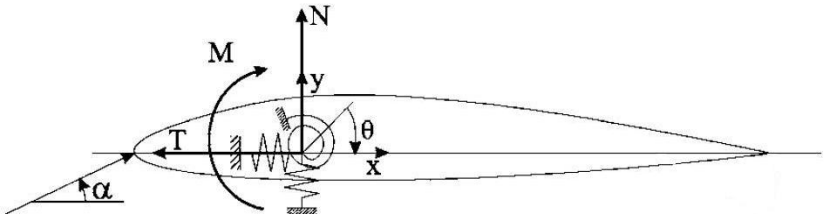

Figure 1: 2-D 3-DOF model, reproduced from Buhl *et al* [v]

where *T* and *N* are the chordwise and normal-to-chord aerodynamic force components, *M* is the aerodynamic moment, α is the angle between the chord and the onset flow, *x*, *y* and *θ* are degrees of freedom of 2-D the elastic system with linear stiffness and damping.

2.2 Aerodynamic model

The aerodynamic drag and moment exerted on the airfoil by the onset flow remain quasisteady in the model. However, the lift is governed by a dynamic stall model similar to the one presented in [ii]. The dynamic lift coefficient is calculated as the static lift coefficient at an effective angle of attack:

$$C_L^{Dyn} = C_L^{St}(\alpha_E) \qquad (1)$$

where the effective angle of attack – which is the angle between the airfoil's chord and a line representing the disturbed airflow relative to the airfoil – is calculated as:

$$\alpha_E = \alpha_{3/4}(1 - A1 - A2) + x_1 + x_2 \qquad (2)$$

where $\alpha_{3/4}$ is the angle of attack as observed at the three-quarter chord, A_1 and A_2 are the first half of the parameters defined in the description of the aerodynamic time lag, and x_1 and x_2 are state-variables governed by the differential equations:

$$\dot{x}_i + T_u^{-1} b_i x_i = b_i A_i T_u^{-1} \alpha_{3/4} \qquad i = 1,2 \qquad (3)$$

where b_i are the second half of the parameters used for defining the aerodynamic time lag, and

$$T_u = c/2V_{rel} \qquad (4)$$

where *c* is chord length and V_{rel} is airflow velocity relative to the airfoil.

3 PARAMETERS, MODEL VALIDATION AND RESULTS

3.1 The choice of parameters

The choice of parameters – namely: A_1, A_2, b_1, b_2 – characterizes a specific temporal behavior of the aerodynamic model. Such a choice is visualized by plotting the unit response function, defined as:

$$\varphi = 1 - A_1 e^{-b_1 s} - A_2 e^{-b_2 s} \qquad (5)$$

where s is non-dimensional time, $\frac{2}{c}\int_0^t V_{rel} dt$. The choice of three parameter sets made here is presented below, together with the respective response functions:

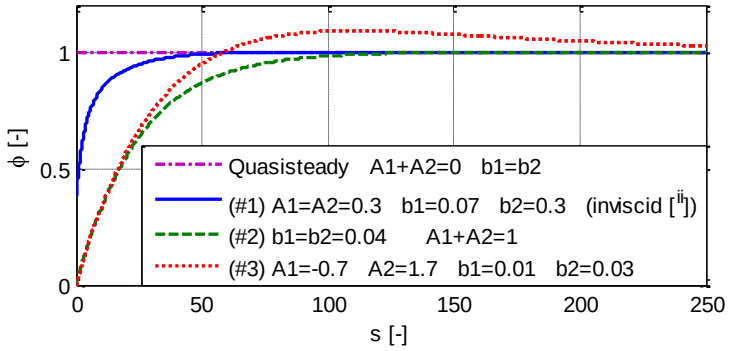

Figure 2: Response functions characteristic for the three sets of dynamic parameters

The first response function is an approximate representation of a thin airfoil's inviscid response [ii], and is therefore expected to be faster than the response function needed for an airfoil in deep stall. The aeroelastic behavior, including also damping characteristics, for the full nonlinear 3-DOF aeroelastic system depends on the aforementioned response functions. Therefore, the next chapter presents the dependence of the damping ratio of the chordwise vibrations on the choice of the response function parameters and compares the results obtained using a quasisteady aerodynamic response.

3.2 Model validation and presentation of results

The model is validated by comparing the chordwise damping ratio obtained using the quasisteady aerodynamic response with the damping ratio from the analytical linearized 1-DOF quasisteady model presented in [iii]. This comparison is shown in Figure 3 along with the damping ratios characteristic for the aerodynamic response functions presented above. It is observed that the results of the present model compare well with the analytical model, thus validating the present implementation. The main finding from the comparison of the QS response and the other response functions is that even for the case #1 – where the response is as fast as for inviscid flow – most of the regions with negatively damped vibration vanish. The effect is even more pronounced for cases #2 and #3. This, together with the fact that the standard aerodynamics existing in aeroelastic codes for deep stall is effectively quasi-steady,

indicates that these aeroelastic codes may overpredict vibration in deep stall. One should also remember that it is reasonable to suspect that the aerodynamic response in deep stall – where the flow is massively separated – is presumably slower than for attached inviscid flow, i.e. in case #1. The next step of the current work is to investigate whether the present aerodynamic model can be used to describe the main unsteady aerodynamic response in deep stall and, if so, find one or more sets of parameters for the response function that can be used for prediction of standstill response of wind turbines.

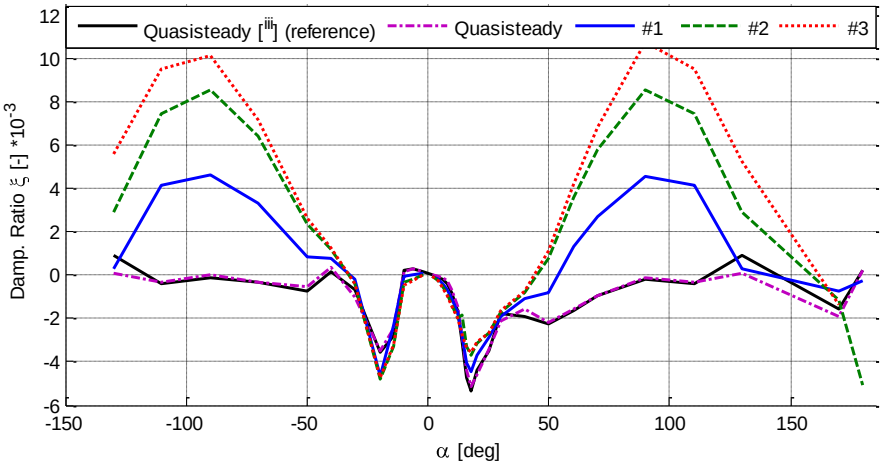

Figure 3: Damping ratios of the quasisteady and lagged models

4 CONCLUSIONS

This paper deals with estimating whether the assumption of quasisteady aerodynamics in deep stall in present aeroelastic codes might affect prediction of edgewise vibration in deep stall in these codes. The present findings indicate that the introduction of lag in the aerodynamic response of a vibrating airfoil significantly increases the amount of damping in deep stall. This indicates that present aeroelastic codes – characterized by the potentially inaccurate assumption of quasisteady aerodynamics in deep stall – may overpredict the edgewise vibrations in deep stall seen in simulations of standstill response of wind turbines.

BIBLIOGRAPHY

[i] Øye, Stig: *Dynamic stall simulated as time lag of separation*, in: Proceedings of the EWEC, Thessaloniki, Greece, Oct. 1994.
[ii] Hansen, Morten; Gaunaa, Mac and Aagard-Madsen; Helge: *Beddoes-Leishman type dynamic stall model in state-space and indicial formulations*. Risø-R-1354(EN) (2004) 40 p.
[iii] Gaunaa, Mac; Larsen, Torben J.: *Stilstandslaster;* chapter in ”Forskning i Aeroelasticitet” 2002, ed. Christian Bak, Risø-R-1434(DA) in Danish, Risø DTU National Laboratory for Sustainable Energy
[iv] Buhl, Thomas: *Edgewise vibration in stand still*, chapter in “Research in Aeroelasticity EFP-2006”, ed. Christian Bak, Risø-R-1611.
[v] Buhl, Thomas; Gaunaa, Mac; Bak, Christian: *Potential Load Reduction Using Airfoils with Variable Trailing Edge Geometry,* Journal of Solar Energy Engineering, Nov. 2005, Vol. 127

SESSION 7

Thursday, 01.10.2009

10:45AM

Nonlinear Model Predictive Control of Wind Turbines

L. C. Henriksen A[1)], N. K. Poulsen[2)]

[1)] Risø DTU, Denmark, [2)] DTU Informatics, Denmark

ABSTRACT

The work presented in this paper describes a proposal of how to implement nonlinear model predictive control of wind turbines. The control problem for the entire wind speed range is comprised into one constrained optimization problem. This integrated control problem is different from previous work of the author, where the overall control problem was divided into of a subset of control problems, depending on wind speed.

KEYWORDS

Nonlinear Model Predictive Control, Constraints, Pitch and Generator Torque Control

1 INTRODUCTION

The never-ending pursuits of making wind turbines last longer or using less material in their construction necessitates the need for improvement of control strategies, sensors and fault detection schemes. In this work the focus is on control strategies. A candidate control strategy is Model Predictive Control (MPC), typically based on linear models of the plant to be controlled. MPC offers the ability to handle constraints and is used to honor the constraints on the actuators, i.e. pitch angle and -rate and torque and –rate. MPC has previously been investigated with application on wind turbines in [1,2]. Usually actuators are designed such that velocity constraints are hardly ever encountered and as results the benefit of MPC is arguably questionable. MPC can however also be implemented using nonlinear models, enabling optimal nonlinear control of nonlinear plants and promising superior performance within a model-based control design framework. In this paper the preliminary work of constructing a suitable Nonlinear MPC method is presented.

2 OBJECTIVE FOR CONTROL OF WIND TURBINES

Nonlinear Model Prediction Control seeks to minimize an objective function within a prediction horizon where t_0 is the current time and t_f is the final time of the prediction horizon. The objective function of the control problem is given as

$$\min_{[]} \|x(t_f)\|_Q^2 + \int_{t_0}^{t_f} \|h(x(t), u(t))\|_{W_z}^2 + \|r - y_r(x(t), u(t))\|_{W_r}^2 \, dt \quad (1)$$

subject to the constraints

$$f(x(t), u(t)) - \dot{x}(t) = 0, \qquad t \in [t_0, t_f] \quad (2)$$

(3)

$$c(x(t), u(t)) \leq 0, \qquad t \in [t_0, t_f[$$

The nonlinear ordinary differential equations of the simplified wind turbine model are described by eq. (2). Eq. (3) describes constraints, such as pitch angle, pitch rate etc. The actual control problem also includes soft constraints, but these have been excluded here to keep the expression simple. It should be noted that for practical reasons it is necessary to reformulate the infinite dimensional continuous-time problem into a finite dimensional problem with a finite number of discrete time steps.

The cost function eq. (1) contains different terms: The final time term $x(t_f)$ aims to give infinite horizon stabilization properties and the linear quadratic regulator weight matrix Q is calculated under the assumption of a linear unconstrained model. The dynamic term h includes various velocity and acceleration terms that should be minimized according to the weighting matrix W_x. The reference tracking term $r - y_r$ includes generator power and –speed, which should be as close to their nominal values as the given wind speed permits in order to maximize power production. A steady state optimization of the control problem over wide range of wind speeds shows that below rated wind speed, the optimal solution gives a unique generator speed and pitch angle, while above rated wind speed multiple solutions giving the nominal power production exist. It is thus necessary to enforce that the generator speed should be driven towards it nominal value when above rated wind speeds. The weighting matrix W_r should be constructed in way that reflects this need.

3 PRACTICAL ISSUES

The implemented algorithm is based on a trust-region optimization algorithm [3]. Currently typical computation times are in the order of seconds when in fact the time available is only the sample time, which is in the order milliseconds. The problem of inadequate computation speed renders any real world application of the control algorithm infeasible until the algorithm has been significantly improved or is implemented on faster hardware.

BIBLIOGRAPHY

[1] Trainelli, L., Sirchi, W., Savini, B., Croce, A., and Bottasso, C. L., “Aero-servo-elastic modeling and control of wind turbines using finite-element multibody procedures,” Multibody System Dynamics, Vol. 16, No. 3, 2006, pp. 291–308.

[2] Henriksen, L. C., “Model Predictive Control of a Wind Turbine with Constraints,” EWEC2008 Online Conference Proceedings, 2008.

[3] Nocedal, J; Wright, S J: Numerical Optimization, Second Edition, Springer 2006.

Data-driven control for wind turbines with smart rotors

Gijs van der Veen[1)], Jan-Willem van Wingerden[1)], Michel Verhaegen[1)]

[1)] Delft Center for Systems and Control, Delft, The Netherlands

ABSTRACT

Active control of blade deflections is becoming more and more important for the wind energy community. Comparing traditional stall controlled turbines with today's individual pitch controlled turbines we see that loads can be reduced, leading to lighter or larger turbines.
A relatively novel concept is to use a number of control devices that locally change the aerodynamic forces on the wind turbine blade. The success of distributed load reduction greatly depends on the sensors that measure the loads and a controller that processes the measured signals and generates the actuation signals. In this project we focus on the development and validation of time-varying control methodologies, and investigate how much performance can be improved compared to state-of-the-art designs and how it depends on the number of actuators and sensors we use.

KEYWORDS

Data-driven control, smart rotors, modal control, robust control

1 INTRODUCTION

Active control is becoming more and more important for the wind energy community. If we compare the `old' stall controlled turbines with today's individual pitch controlled turbines we see that the loads can be reduced, leading to lighter or larger turbines. However, limited actuator bandwidth and component fatigue impose constraints on the pitch system. Due to the increasing size and cost of wind turbines and the limitations of individual pitch control, control engineering is becoming a critical enabling technology. New control concepts are necessary which can deal with the distributed nature of turbulence, and guarantee an economic lifetime of at least 20 years for the next generation of offshore wind turbines (diameter over 150 meters).

One novel concept is to use a number of control devices that locally change the aerodynamics forces on the wind turbine blade. The success of distributed load reduction greatly depends on the selection of appropriate sensors that measure the loads, and a controller that processes the measured signals and generates the actuation signals. In this

project we focus on the development and validation of time-varying control methodologies (such as Model Based Gain Scheduled Robust Control or Data Driven Robust Control), and investigate how much performance can be improved compared to classical time-invariant state-of-the-art-designs. One of the key performance metrics will be the reduction of fatigue-critical loads such as blade root moment. Furthermore, we investigate how the optimal performance depends on the number of actuators and sensors we use (Individual Pitch Control vs. 'Smart' rotor).

2 PROOF OF CONCEPT AND BEYOND

The potential of using deformable trailing edges to locally influence the aerodynamics loads on wind turbine blades has been demonstrated by several research groups. See e.g. [1], [2]. Many of the available studies focussed on single input-single-output control designs to investigate the achievable load reductions (Figure 1), predominantly in terms of blade root moments. These proofs of concept stimulate further research into full-span rotor blades with one or more trailing edge devices. Issues will be raised as:

- What are optimal locations to change the aerodynamic loads locally?
- Which sensors provide the most relevant signals to achieve load reductions?
- What are the most suitable controlled variables to achieve the desired load reduction goals?

Figure 1: The adaptive blade used in [1] to demonstrate the potential of active load reduction

The earlier proofs of concept stimulate a thorough investigation into multivariable control. In this case, multiple sensor inputs and multiple actuator outputs need to be integrated in a multivariable control design. A study of the blade mode shapes, combined with the aerodynamic interactions, will provide fundamental insight into the dynamics and what the key locations are along the blade for sensing and actuation.

3 CONTROLLER DESIGN

Inevitably, the distributed control of wind turbine blades will require processing a sizable amount of signals, converting inputs to control outputs according to some control algorithm. Recent developments in data-driven control theory **Error! Reference source not found.** allow online identification of the relevant dynamics of the system. These dynamics vary with the operational condition of the turbine, most notably with rotational speed and wind speed. Connected with an optimal control law such as predictive control, there is an intrinsic level of fault tolerance and robustness. Alternatively, a fixed controller with gain scheduling may be designed to cover the (identified) operational conditions of the turbine.

One of the main challenges in this project will be to devise fast and efficient control algorithms by exploiting data structure. This is absolutely necessary to allow the algorithms to run real-time on present day hardware. The issue of computational complexity is still a considerable bottleneck with many of the modern control methods.

4 CONCLUSIONS

In this research we aim to develop systematic results for the control design of smart rotor blades. These results should include constructive methods for sensor and actuator placement to provide the greatest control authority. Additionally, suitable control techniques will be investigated that are streamlined enough to run on state-of-the-art hardware and possess the necessary robustness to deal with the varying nature of wind turbine dynamics across the operational conditions.

BIBLIOGRAPHY

[1] Van Wingerden, J.-W. et al.; On the proof of concept of a 'smart' wind turbine blade for load alleviation, Wind Energy, 2008.

[2] Andersen, P.B., et al.; Load Alleviation on Wind Turbine Blades using Variable Airfoil Geometry, Risø DTU, 2007.
Available at http://www.risoe.dk/rispubl/art/2007_96_paper.pdf.

[3] Van Wingerden, J.-W., Control of Wind Turbines with 'Smart' Rotors: Proof of Concept & LPV Subspace Identification, PhD thesis, Delft University of Technology, 2008.

Optimisation of Wind Turbine Rotor Using Cost of Energy as a Parameter and the effects of the Weibull Distribution

T.S.Yeow[1)], A. Cuerva [2)], J.Alvarez[3)], A. Munuera [4)]

E.T.S.I. Aeronáuticos, Universidad Politécnica de Madrid,Spain,

ABSTRACT

A study of determining the optimum radius size for a 3MW land based horizontal axis wind turbines was conducted using cost of energy production as a parameter to obtain the optimum value of rotor radius with corresponding rated velocity. The optimisation processes were found to be dependent of the Weibull distribution of potential sites. The results obtained shows that the combination of specific rotor radius and rated velocity can produce significant reduction in energy production costs. This supported the current need of optimisation for a specific wind farm. Wind farms with stringent noise limitation also benefits from customized wind turbine designs.

KEYWORDS

Cost of energy, Weibull distribution, Wind turbine rotor optimisation.

1 INTRODUCTION

Wind farm sites around the world has been observed to have almost similar wind distribution with similar characteristics of *c=7* and *k=2*. Most wind turbine manufacturers can be assumed to be designed their wind turbines based on these conditions with optimisation also focused on wind farm installations in these wind conditions. With the current competitive state of the industry, new design practices are pushing towards the lowest cost of energy production rather than low turbine cost. Therefore, it has become necessary for wind turbines to be optimised accordingly to individual wind farm sites. Though this design methodology is considered costly as wind turbines are built purposely for a chosen site, current market conditions can make this an economically viable option in the near future. These developments are the reasons that this work has been carried out. The work aims to achieve and show that customization of wind turbines to sites resource can give significant cost reduction in energy production.

2 METHODOLOGY

2.1 Model of the Wind Turbine Rotor

A generic design of a wind turbine is required. Utilising a wind turbine rotor design Matlab toolbox developed in Universidad Politécnica de Madrid, Spain, a 3MW rated wind turbine can easily be designed. By inputting known blade airfoil data and the desired chord wise airfoil distribution into the toolbox, a preliminary design of a turbine rotor can be obtained. While the toolbox is capable of aerodynamic optimisation, the objective of this work does not require that to be done.

Once the values of $C_{P\max}$ and λ_{op} are known, it is possible to obtain a value for the rotor radius, R with the corresponding rated velocity, V_N and the rotational speed ΩR. The following parameters are also necessary: efficiencies (mechanical and electrical) : η_M and

η_E, rotational speed limit due to noise limitation : ΩR_{NL} and technological limit for specific power rating based on existing turbines in the market : $SP_{\min}$ & $SP_{\max}$.

The model of the turbine rotor and the parameters used in this study are as follows: Blade = TESTBladeT1 with $\lambda_{op} = 7.9225$, $C_{P\max} = 0.5112$, $\theta_{op} = 0$ rad, $\eta_m = 0.95$, $\eta_e = 0.95$ and $P_N = 3000000\ W$. Operating conditions are set to: $V_{in} = 3\ m/s$, $V_{out} = 25\ m/s$, $NHY = 8760 hours/year$ and $\rho = 1.225\ kg/m^3$

2.2 Technological Limits Defined by Current Technological State

A study of existing wind turbines shows that most turbines exist in the range of $350 < SP < 550 W/m^2$. With the data available, we can obtain a minimum and maximum rotor radius for a given specific power rating.

$$R_{\min} = \left(\frac{P_N}{\pi SP_{\max}} \right)^{1/2} = 40.9306m \quad (1)$$

$$R_{\max} = \left(\frac{P_N}{\pi SP_{\min}} \right)^{1/2} = 57.8846m \quad (2)$$

The noise limitation on the maximum rotational speed allowed imposes a limitation to the rated velocity with the expression given by:

$$V_{N,NL} = \frac{\Omega R_{NL}}{\lambda_{op}} \quad (3)$$

This limitation can also be further imposed onto the relation between the radius of the rotor and the rated velocity. This gives an additional limitation onto the minimum radius allowable.

$$R_{NL} = \left(\frac{2P_N}{\rho \pi \eta_M \eta_E C_{Pmax}} \right)^{\frac{1}{2}} V_{N,NL}^{-\frac{3}{2}} \quad (4)$$

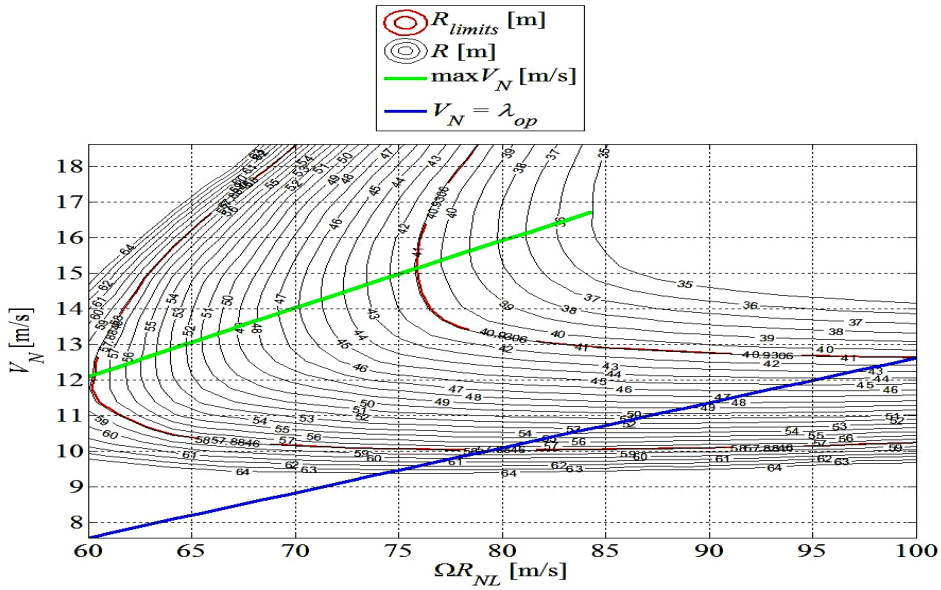

Figure 1 Design region bounded by technological limits ($R_{\min,SP}$ and $R_{\max,SP}$), blade tip speed limited by noise and $P_{\max}$ for rotor radius.

The relation between R, V_N and $V_{N,\Omega R_{NL}}$ is given by the following equation:

$$\frac{P_N}{\eta_E \eta_M \frac{1}{2}\rho\pi R^2 V_N^3} - C_P\left(\frac{\Omega R_{NL}}{V_N}, \theta_{C_{op}}\right) = 0 \tag{5}$$

The equation above defines a surface $f\left(R, \Omega R_{NL}, V_N\right) = 0$. Using the blade design used previously and maintaining the operating conditions, a surface can be generated as shown in Figure 1.

2.3 AEP Calculation

The wind resource of a particular site is dependent on many factors which are mainly geographical and seasonal wind patterns. These constant changing factors make it hard to have a constant wind resource data profile for year to year prediction. However, in predicting wind speed variations for a particular year, it is possible to represent in a probability distribution. The common practice is to use a Weibull distribution which has been found to give satisfying representation of the variation in hourly mean wind speed over a year. It is characterized by a scale parameter, *c* and a shape parameter, *k*, which describes the variation of the mean speed.

The probability density function of the Weibull distribution can be expressed as

$$f\left(U\right) = k\frac{U^{k-1}}{c^k}\exp\left(-\left(\frac{U}{c}\right)^k\right) \tag{6}$$

This allows for a specific site to be classified in terms of Weibull parameters c and k. Then the average wind speed V_{ave} can be calculated.

$$V_{ave} = \begin{cases} c\Gamma\left(1+\frac{1}{k}\right) \\ c\sqrt{\pi}/2 \text{ , if k} = 2 \end{cases} \tag{7}$$

To calculate the annual energy production, the power curve is combined with the Weibull distribution of the wind resource. This can be expressed as:

$$AEP = NHY \int_{V_{cut-in}}^{V_{cut-out}} P(v).p(v)\,dv \quad (8)$$

$P(v)$ power curve function

$p(v)$ wind distribution function

The total energy produced by the wind turbine over a period of a year can be obtained using this value of capacity factor with the assumption that the wind resource is known by its Weibull characteristics. The total annual energy is given by $AEP = f((\Omega R_{NL}, V_N, c, k)$ for a selected value of radius and blade tip speed limit due to noise, operating a corresponding rated velocity over the period of one year.

2.4 Cost of Energy Calculation

Fingersh, Hand & Laxson (2006) gives COE as the levelized cost of energy produced per kilowatt hour and is calculated by the following equation:

$$COE = \frac{(FCRxICC)}{AEP_{net}} + AOE \quad (9)$$

Where COE : levelized cost of energy ($/kWh), FCR : fixed charge rate (constant $)(1/yr), ICC : initial capital cost ($) and AEP_{net} : net annual energy production (kWh/yr), while

AOE = annual operating expenses

$$= \text{LLC} + \frac{(\text{O\&M} + \text{LRC})}{\text{AEP}_{\text{net}}}$$

Where LLC : land lease cost, O&M : levelized O&M cost & LRC : levelized replacement / overhaul cost

They developed the cost model as an update and more accurate model compared to Harrison and Jenkins (1993) model. The WindPACT cost model used scaling relationships developed during their WindPACT rotor study project. It is interesting to note though that both cost models shows that optimum rotor size is not particularly sensitive to the type of technology installed on the wind turbines. Also in maintaining the objective of this study of optimisation, it is deemed not necessary to consider different wind turbine technologies.

3 RESULTS

3.1 Case 1: c=7, k=2.5

The results are presented in contours of $COE = f(\Omega R, V_N, R, c, k)$ as can be seen below.

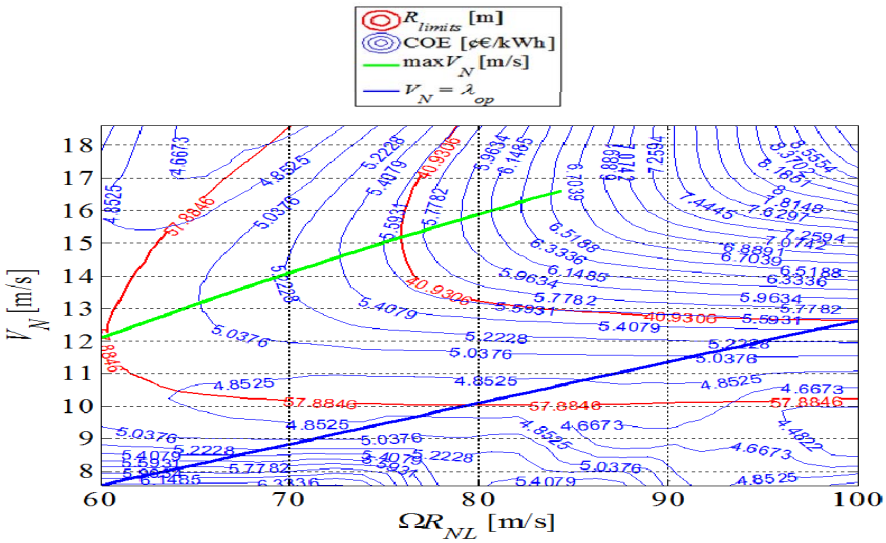

Figure 2 Cost of Energy for a given H/R and chosen technology options

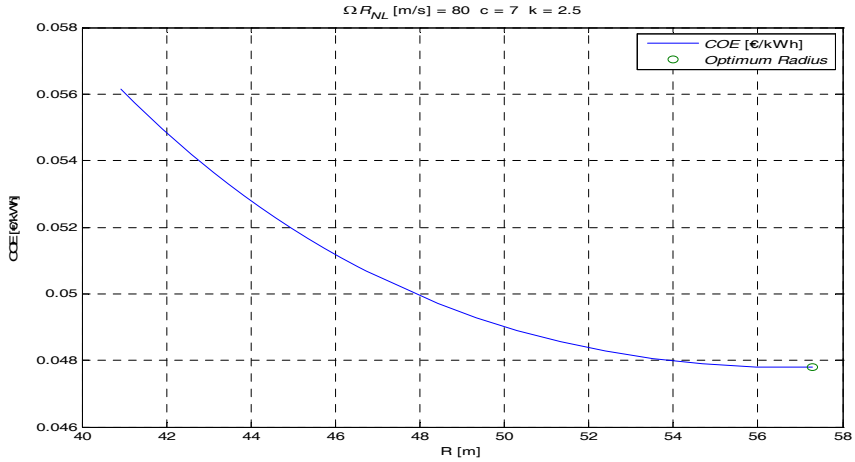

Figure 3 COE value versus Radius showing optimum radius for lowest COE.

Referring to Figure 2, the COE values are represented by the cutting lines in the figure. For a given value of blade tip speed limit due to noise, ΩR_{NL} it can be easily read from the figure the value COE with its corresponding radius. Naturally, it is assumed that the value COE would generally follow the behaviour of $P_{AVE}/P_N = g(\Omega R_{NL}, V_N)$ which is dictated by the AEP produced and the radius size. However, in the figure, it is obvious that COE are not only dependent on the AEP but instead is influenced by many factors such as rotor size and machine rating in scaling relationships.

This is apparent as seeing the minimum COE values are generally obtained from a larger set of rotor operating in rated velocity range of 10-11 m/s and lower ΩR_{NL} .

3.2 Case 1: c=10.5, k=2.5

In Figure 3, this region of minimum COE is given by smaller rotor diameters operating in higher rated velocity range of 11.5-12.5 m/s and higher ΩR_{NL} .

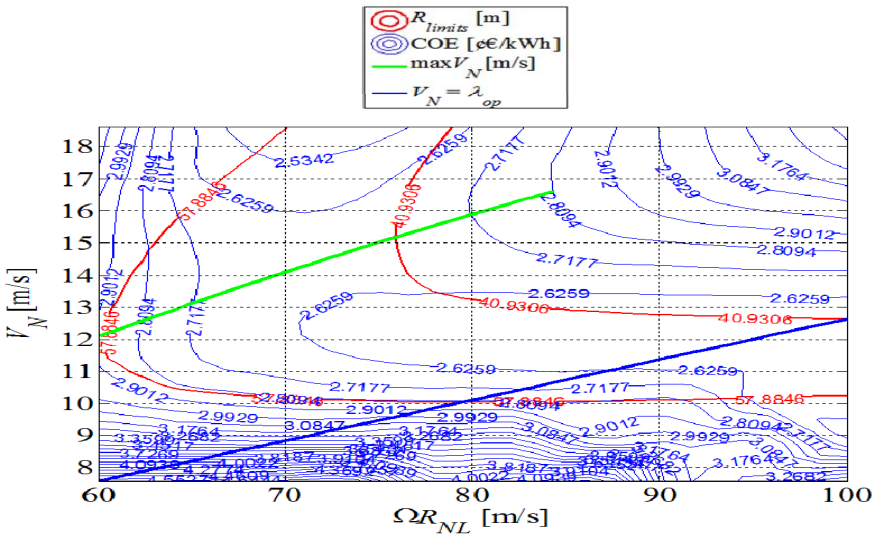

Figure 4 Cost of Energy for a given H/R and chosen technology options

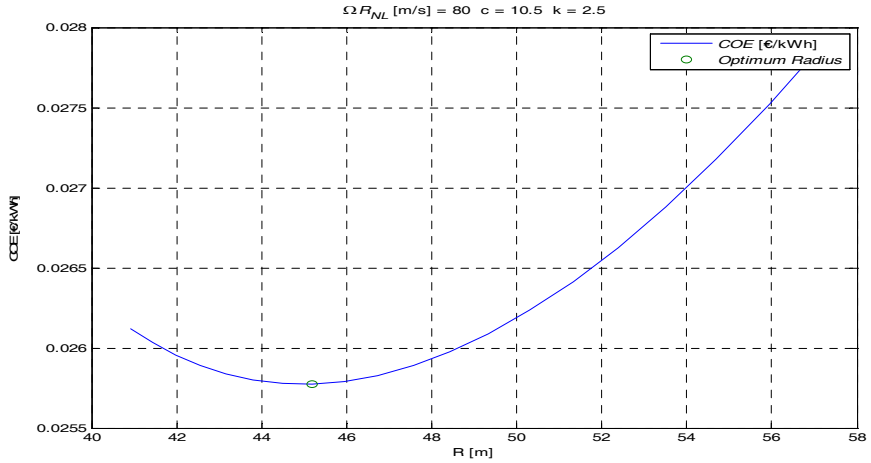

Figure 5 COE value versus Radius graph showing optimum radius for lowest COE.

For both cases having the same rotational speed limit due to noise, the optimum rotor radius for the lowest COE varies greatly. In the first case, the minimum value is not achieve within the limits while in the second case there is a clear minimum which represents the optimum rotor radius.

4 CONCLUSIONS

The paper proved that wind turbine rotor size can be optimised to achieve the lowest cost of energy production. The COE is proven to be a design parameter that can result in significant reductions. The potential of the total reduction coupled with optimisation in other aspects such as aerodynamics and material would eventually lead a very lean and efficient machine. Customization of wind turbines for selected wind farm sites will be a design practice worth considering in the future with the shown benefits in this work.

BIBLIOGRAPHY

[1] Burton, T., Sharp, D., Jenkins, N., Bossangi, E. *Wind Energy Handbook*, John Wiley & Sons Ltd. Publications, USA, 2001.

[2] Collecutt, G.R., Flay, R.G.J. *The Economic Optimisation of Horizontal Axis Wind Turbine Design*. Journal of Wind Engineering and Industrial Aerodynamics 61 (pg 87-97), Elsevier Science, 1996.

[3] Fingersh, L., Hand & Laxson, A. *Wind Turbine Design Cost and Scaling Model*, Technical Report NREL /TP-500-40566, 2006.
[4] Harrison, R., Hau, E., Snel, H. *Large Wind Turbines: Design and Economics*, John Wiley and Sons Chichester, 2000.
[5] Harrison, R., Jenkins, G., *Cost Modelling of Horizontal Axis Wind Turbines*. ETSU W/34/00170/REP. University of Sunderland, School of Environment, December 1993

Wind farm – fuel cell hybrid energy system for reducing power fluctuations in wind farms

J. E. Villena-Lapaz[1)], A. Vigueras-Rodríguez[1)], E. Gómez-Lázaro[1)], J. A. Fuentes-Moreno[2)], A. Molina-García[2)]

1) Renewable Energy Research Institute, University of Castilla la Mancha, Spain
2) Technical University of Cartagena, Spain

ABSTRACT

With the increasing production of wind power worldwide, power fluctuations have an impact on power system operation and costs. Power systems with high wind penetration give rise to concerns about the adverse effects of wind farms on power operations and their stability.

In order to reduce these power fluctuations, a simple wind farm-fuel cell stack hybrid power system has been proposed. Fluctuations are evaluated through ramp rates and reserve requirements in both systems: the wind farm and the wind farm-fuel cell hybrid system, and they are compared. The model proposed improves the behaviour of the system in terms of power fluctuations.

KEYWORDS

Power fluctuations, hybrid system, ramp limitation.

1 INTRODUCTION

Regarding the integration of wind energy in power systems with high wind penetration, the power fluctuations are a relevant issue that must be studied **Error! Reference source not found.**. The integration of the power produced by wind farms is evaluated through ramp rates and reserve requirements calculated as suggested by Parson et al. **Error! Reference source not found.**.

The ramp rates are calculated as the difference between the average power produced in one time interval and the previous one:

$$P_{ramp}(j) = \overline{P(j)} - \overline{P(j-1)} \quad (1)$$

The reserve requirements deal with the energy reserves that have to be allocated in advance, and so it quantifies the difference between the instantaneous power in the following interval and the averaged power at the current interval:

$$P_{res}(j) = P(j) + P_{min}(j-1) \quad (2)$$

Therefore these power ramp rates are the ramp requirements the electrical system would have to compensate, keeping constant the production. For instance, this can be done by regulating the other power plants with an opposite ramp.

The worst cases regarding the power system are the most negative ramp rates in the wind farm and the greatest reserve requirements, so the percentile 99% and 1% respectively, are used as a way of characterizing the integration difficulties.

In order to improve these indicators, a simple wind farm-fuel cell stack hybrid power system has been proposed.

2 SYSTEM DESCRIPTION

Using the wind farm aggregated simulator shown in **Error! Reference source not found.** and **Error! Reference source not found.**, several 2-hour series of available power have been simulated for average wind speeds which follow a Weibull distribution. The fuel cell produces energy to attenuate the variations in the power production of the wind farm. Thus, the power produced by the wind farm is averaged every two minutes, the total power produced by the hybrid system is calculated in real time as the sum of that value and the fuel cell power production, and the derivative in each point (every two minutes) of the total power is approximated, also in real time, using the two previous values and the one at that point itself. Finally, the power that the fuel cell will produce during the next two minutes is equal to the power produced during the previous interval minus the variation experimented by the system total production.

$$PT(j) = PWF(j) - PFC(j)$$

$$PFC(j) = PFC(j-1) + \Delta PT(j) = PFC(j-1) + k(3PT(j) + 4PT(j-1) - PT(j-2))$$

Where

$PT(j)$ is the total power produced by the hybrid system in the jth interval.

$PWF(j)$ is the power produced by the wind farm in the jth interval.

$PFC(j)$ is the power produced by the fuel cell in the jth interval.

$\Delta PT(j)$ Is the variation of the power produced by the hybrid system at the end of the jth interval.

and $\Delta PT(j) = 3PT(j) + 4PT(j-1) - PT(j-2)$ comes from the approximated derivative of a function using the two previous values: $f'(x) \approx \frac{3f(x) + 4f(x-h) - f(x-2h)}{2h}$

Interval size of two minutes has been considered because, according to **Error! Reference source not found.**, it's enough if compared with the time the fuel cell needs to reach the new level of power when a sudden change in demand occurs.

The fuel cell proposed in this model is always producing power between two values, thus avoiding the lack of time a real device needs to get restarted when it's stopped. In that way, the minimum power that the stack produces is been fixed to 0,05 pu (5% of the wind farm nominal power). Different maximum values of the power produced by the fuel cell, from about 0,4 pu to the minimum, 0,05 pu, have been set. The last case corresponds to a fuel cell that is always producing the same amount of power (0,05 pu).

In figure 1, an example of a 2-hour series of power is presented. The blue line corresponds to the power produced by the wind farm, averaged every two minutes. The variable nature of the wind causes fluctuations of this production, as one can see in the figure. From that variations, as explained above, the fuel cell power production is calculated in real time, and it is represented by a green line. Finally, the total amount of power produced by the wind farm-fuel cell stack hybrid system is drawn in red.

After that, one of the regulation techniques for smoothing the fluctuations of a wind farm is implemented **Error! Reference source not found.**. In this work, positive ramp limitation is applied to the 2-hour series of wind farm power. In the case of study the power losses associated with this regulation technique are 5%. This corresponds to a maximum slope of 4.7×10^{-3} pu / min **Error! Reference source not found.**. From the curtailed power produced by the wind farm, the fuel cell acts in order to compensate the fluctuations that exist despite the ramp limitation technique used, as detailed above. Finally, the total amount of energy produced by the hybrid system is analysed and compared again with the case in which the wind farm operates alone and no regulation is used.

In figure 3, an example of a 2-hour series of power is presented. Here, the black line represents the power produced by the wind farm when the positive ramp limitation is applied. The fluctuations of the power generated by the hybrid system, represented by a red line in figure 1 and figure 3, are perceptibly lower than those of the wind farm when operating alone.

Ramp rates and reserve requirements, and percentiles 99% and 1% respectively have been calculated for both the wind farm in one hand, and for the hybrid system proposed in the other hand, and they have been compared for different values of the fuel cell maximum production. In the case of no ramp limitation applied (figure 2), as expected, when the fuel cell produces a constant amount of energy, there is no improvement in neither the ramp rates nor the reserve requirements. As seen in the figure, from the point of view of power fluctuations, a fuel cell that produces a maximum of 25% of the wind farm nominal power would reduce power ramp rates by nearly 70%, and the reserve requirements by 60%.

Thus, taking a fuel cell capable of producing power between 5% and 10% of the wind farm nominal power, which is possible to implement in the Renewable Energy Research Institute laboratory, the improvement in the ramp rates is 18%, and in the reserve requirements, 14% approx. In the second case of study, with tamp limitation, ramp rates and reserve requirements, and percentiles 99% and 1% respectively have been calculated for both the wind farm without any curtailment in one hand, and for the hybrid system proposed in the other hand, and they have been compared. In this case, when the fuel cell produces a constant amount of energy, there is an improvement in either the ramp rates and the reserve requirements, due to the effect of the ramp limitation (see figure 4).

As seen in figure 4, a fuel cell that produces power between 0,05 pu and 0,1 pu, the improvement in both the ramp rates and the reserve requirements is over 21%.

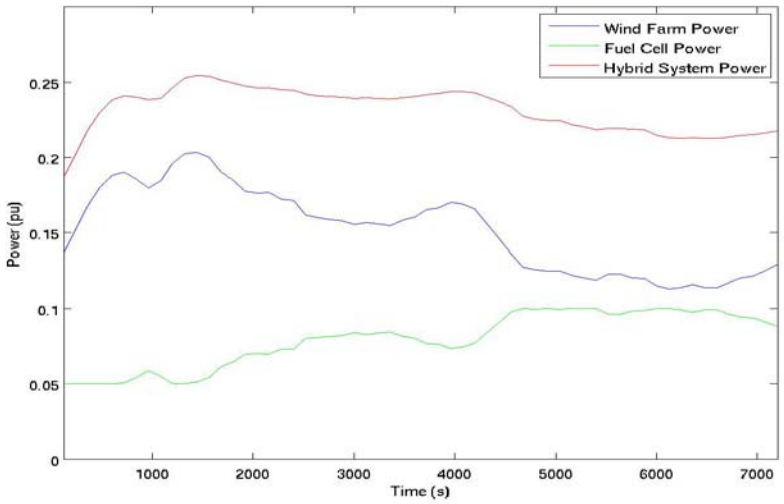

Figure 1: **Example of a 2-hour series power production of the wind farm, the fuel cell-stack and the hybrid system**

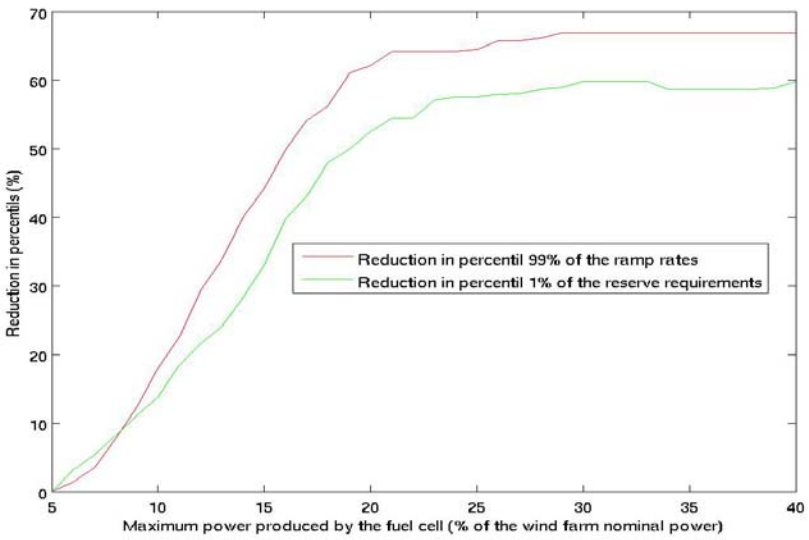

Figure 2: **Improvement in percentiles 99% or ramp rates and 1% of reserve requirements when reducing the maximum power produced by the fuel cell from 40% to 5% of the wind farm nominal power**

Figure 3: **Example of a 2-hours series power production of the wind farm, the fuel cell-stack and the hybrid system when positive ramp limitation is applied**

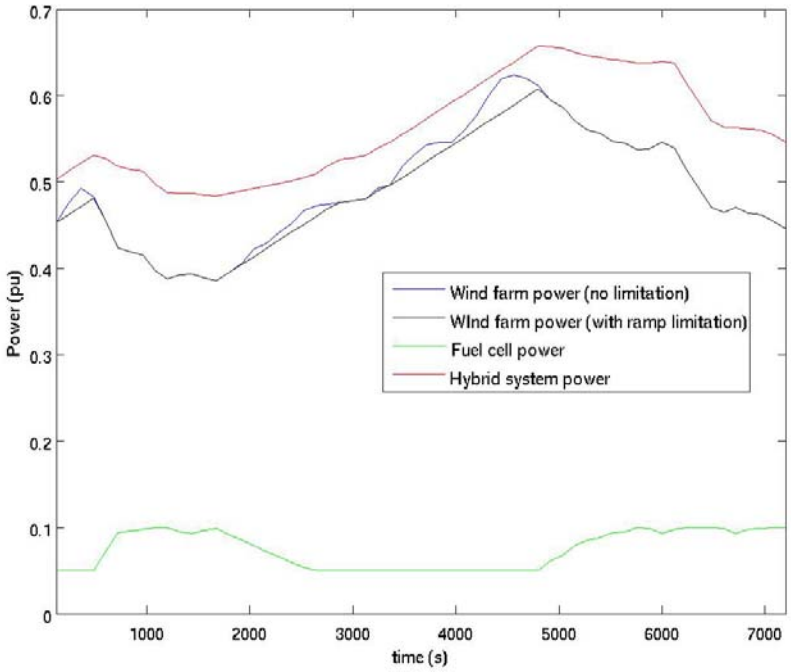

Figure **4: Improvement in percentiles 99% or ramp rates and 1% of reserve requirements when reducing the maximum power produced by the fuel cell from 40% to 5% of the wind farm nominal power, in the case in which ramp limitation has been applied to the wind farm power production**

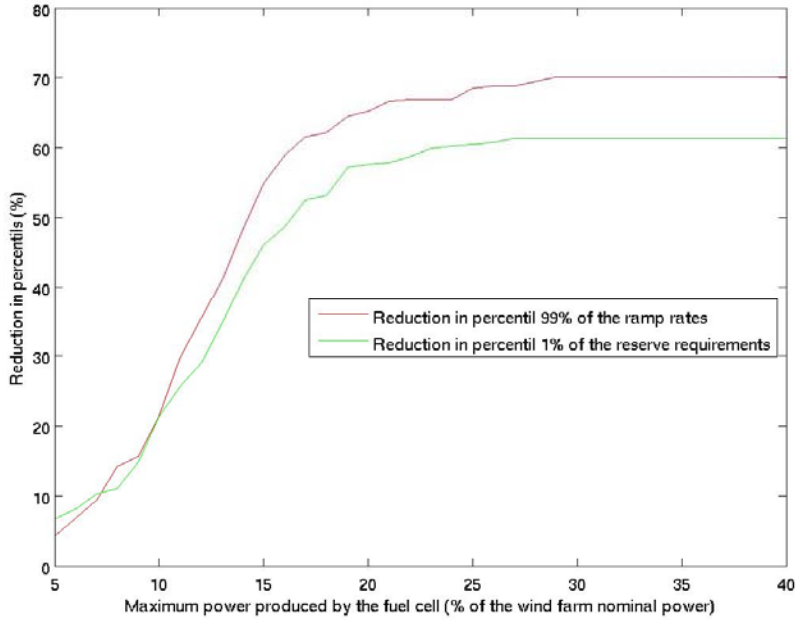

3 CONCLUSIONS

Studies of the power fluctuations of a wind farm-fuel cell hybrid power system have been carried out, comparing them with the wind farm-only system.

The model proposed enables the fuel cell to generate energy as a function of the total power variation in real time. As a consequence, power fluctuations, estimated trough ramp rates and reserve requirements, get considerably lower.

If ramp limitation is applied to the wind farm power production, the improvement is even higher. Moreover, since the fuel cells produces power depending on the fluctuations of the wind farm, and these are lower because of the ramp limitation, the variation in its production is lower too, which means better behaviour and easier implementation in a real device.

The authors in this paper have focused in power fluctuations, without taking into consideration efficiency aspects. For instance, infinite amounts of hydrogen are available, so the fuel cell can generate as much power as desired. Further studies will get closer to real cases, and some real experimentation will be carried out at the Renewable Energy Research Institute.

BIBLIOGRAPHY

[1] Akhmatov, V.; Kjaergaard, J. P. & Abildgaard, H. Announcement of the large offshore wind farm Horns Rev B and experience from prior projects in Denmark European Wind Energy Conference, 2004.

[2] Parson, B.; Milligan, M.; Zavadil, B.; Brooks, D.; Kirby, B.; Dragoon, K. & Caldwell, J. Grid Impacts of Wind Power: A summary of recent studies in the United States Wind Energy, 2004, 7, 87-108.

[3] P. Sørensen, N. Cutululis, A. Vigueras-Rodríguez, L. E. Jensen, J. Hjer- rild, M. H. Donovan, and H. Madsen. Power fluctuation from large wind farms. IEEE Transactions on Power Systems, 22(3):958–965, 2007. Special Section on Power System Perfomance Issues associated with Wind Energy.

[4] Vigueras-Rodríguez, A.; Sørensen, P.; Cutululis, N.; Viedma, A. & Donovan, M. H. Wind model for low frequency power fluctuations in offshore wind farms, Wind Energy, to appear.

[5] M.Y. El-Sharkh, A. Rahman , M.S. Alam, P.C. Byrne, A.A. Sakla, T. Thomas. A dynamic model for a stand-alone PEM fuel cell power plant for residential applications . Journal of Power Sources 138 (2004) 199–204

[6] Elfrakt System and Eltra. Wind turbines connected to grids with voltages above 100 kV: Technical regulation for the properties and the regulation of wind turbines. Technical report, registered with the Danish Energy Authority, 2004.

[7] Vigueras-Rodríguez, A. Modelling of the Power Fluctuations in Large Offshore Wind Farms . PhD, Universidad Politécnica de Cartagena.

Energy Preservation in the Numerical Calculation of Wind Turbine Wakes

B. Sanderse[1) 2)]

[1)] ECN, Energy Research Centre of the Netherlands; [2)] CWI, Dutch Centre for Mathematics and Computer Science

ABSTRACT

In order to calculate the wakes of wind turbines and their interaction in wind farms, the current state of the art is to solve the incompressible Navier-Stokes equations with a suitable turbulence model (e.g. a RANS or LES model), and with an actuator-type approximation of the wind turbine blades [4]. Especially in LES it is important that the numerical scheme used not only conserves first-order quantities as momentum but also second order quantities like kinetic energy [2]. The method of Harlow and Welch [1] posesses this property through the use of staggered grids, and has been used in so-called symmetry-preserving discretizations [6]. In such discretizations, sometimes called *mimetic*, the difference operators mimick the properties of the underlying differential operators. In this way the discrete kinetic energy can only change due to viscous dissipation, leading to a discretization that is stable on any grid.

We have tested a second-order and fourth-order symmetry-preserving discretization in two dimensions and have found that the inclusion of a body force, as presented in actuator-type formulations, is more straightforward then when using a colocated discretization like in [3]. Furthermore we have shown that accurate results can be obtained for a number of laminar flow benchmark test cases, including discrete energy conservation in case of unsteady flows.

These ideas of symmetry preservation and conservation are currently pursued in extending the method to turbulent flow. Instead of adapting the diffusive operator of the Navier-Stokes equations, as done in RANS computations, in our opinion it is more logical to model turbulence through approximations of the non-linear convective term, since this term is responsible for transferring energy from large to small scales of the flow. Convection-operator based turbulence models should then be constructed such that the symmetry and conservation properties are preserved [5]. Higher-order schemes will be necessary to avoid interference of the subgrid-scale model with truncation errors. The use of this approach for turbulent atmospheric flows is one of the topics of ongoing research.

KEYWORDS

sanderse@ecn.nl

Wind turbine wake, wind farm, Large Eddy Simulation, actuator line model, energy conservation, symmetry preserving discretization.

BIBLIOGRAPHY

[1] F.H. Harlow and J.E. Welch. Numerical calculation of time-dependent viscous incompressible flow of fluid with free surface. Physics of Fluids, 8:2182–9, 1965.

[2] K. Mahesh, G. Constantinescu, and P. Moin. A numerical method for large-eddy simulation in complex geometries. Journal of Computational Physics, 197:215–240, 2004.

[3] P.-E. Réthoré and N.N. Sørensen. Actuator disc model using a modified Rhie-Chow/SIMPLE pressure correction algorithm. Comparison with analytical solutions. In European Wind Energy Conference, Brussels, 2008.

[4] B. Sanderse. Aerodynamics of wind turbine wakes. Technical Report ECN-E–09-016, Energy Research Centre of the Netherlands, 2009, http://www.ecn.nl/publications/default.aspx?nr=ECN-E--09-016.

[5] R. Verstappen. On restraining the production of small scales of motion in a turbulent channel flow. Computers & Fluids, 37:887–897, 2008.

[6] R.W.C.P. Verstappen and A.E.P. Veldman. Symmetry-preserving discretization of turbulent flow. Journal of Computational Physics, 187:343–368, 2003.

Please note that all papers should be less than 4 pages.

No presentation intended.